



**NTNU – Trondheim**  
Norwegian University of  
Science and Technology

# Design and development of a Remotely Operated Vehicle for inspection of- and fish collection in Aquaculture Facilities

**Magnus Rogne Myklebost**

Mechanical Engineering

Submission date: June 2014

Supervisor: Nils Petter Vedvik, IPM

Co-supervisor: Frode Korneliussen, Argus Remote Systems

Norwegian University of Science and Technology  
Department of Engineering Design and Materials



# 1 PREFACE

This master thesis has been written the spring 2014 as part of the Mechanical Engineering master's programme at Department of Engineering Design and Materials (IPM), Norwegian University of Science and Technology (NTNU).

The project is a combination of a project thesis written the fall 2013 and this master's thesis. The project goal was to design and develop a Remotely Operated Vehicle (ROV) for the aquaculture industry. The project is funded by Argus Remote Systems, who will manufacture the final ROV. The ROV, which is named the Manta, will be used as a tool to inspect fish farming facilities and collect dead fish at the bottom of the net cages. Since this is a product development project, the time has mostly been spent on simulation based design using the Siemens NX 8,5 software. More than hundred 3D models have been created and evaluated, of which only half were used in the final design. Due to time and space limitations, only the most relevant of the finite element simulations will be presented. The assembly model is fairly detailed, but some components are not yet defined. All the prototyping work is conducted by the author unless otherwise specified.

The remaining development will be done during the fall of 2014, through cooperation between Inventas Bergen AS and Argus RS.

**The contents of this report is confidential until 15.06.2015**

## 1.1 ACKNOWLEDGEMENTS

I would like to thank **Nils Petter Vedvik**, who has been my excellent supervisor, for great support and interesting conversations throughout this project.

I would also like to thank **Bjørnar Vasenden** and the Inventas Bergen office for great assistance, ideas and suggestions, and taking the time to visit Argus RS with me.

I am also grateful for the assistance provided by **Børge Noddeland and Alexey Matveev** at SmartMotor, and **Robert Nilsen** at NTNU regarding the thruster design.

Moreover, I want to thank **Vidar Saue**, the inventor of the original Manta, for taking his time to answer my questions. I would also like to thank **Stein Mohn**, who had god input and many interesting and relevant stories on our first meeting.

Furthermore, I would like to express my gratitude to **Frode Korneliussen and Frederik Wendel** at Argus RS who have replied quickly and thoroughly to my questions and provided excellent guidance. Frederik Wendel has also done a magnificent job on the electromagnetic design of the thruster and the thruster prototype. There have been many great meetings at Argus' HQ at Laksevåg that lead to vital clarification, and new ideas and solutions.

Lastly, I want to thank my friends and family for all your great support.

This master's thesis concludes my 5 year education at NTNU and it has been a fantastic time of my life where I have learned a lot.



Magnus Rogne Myklebost, Trondheim, June 2014

## 1.2 ABSTRACT

A concept for a lightweight Remotely Operated Vehicle (ROV) named the Manta was designed for inspection of the net cages and collection of dead fish at aquaculture facilities. The current thesis presents the initial development and engineering design of the product, including requirements and need findings, material selection, technical solutions and design verification by the finite element method.

The Manta has a streamlined body with an internal cavity. Three vertical thrusters are mounted into thin wings on the exterior of the hull, and two horizontal thrusters are located inside the hull cavity. The ROV will use the suction through the hull created by the main thrusters to collect the dead fish into a rear-mounted net. Harsh environment and rough handling will require a robust design- and material selection.

The hull of the Manta has been designed and engineered based on the currently chosen components, which may be changed in the future. Based on the combination of easy manufacturing, good impact properties, low density and low cost, ABS plastic was selected as material for the hull. The hull design is based on 4 mm thick ABS plastic sheets manufactured by vacuum forming, with a total component weight equal to 6,6kg. The sections are joined together by adhesives and bolts. The estimated manufacturing cost of the hull is approximately 2000 NOK per unit including tool cost for 100 units.

The vertical thrusters, which are located in the wings, must have a low profile. A mechanical design of a so-called rim-driven thruster (RDT) has been developed and the current design has a predicted weight of 1,7kg. This is a design where the propeller is fitted permanent magnets on an outer ring instead of being powered by a centre axle. The resulting geometry has a significantly lower profile than conventional ROV thrusters, and a higher torque per length ratio. A thruster prototype and a special designed test rig for the prototype has been developed and manufactured at the IPM workshop. This test rig has been submitted to Argus for completion of their electromagnetic design.

Commercially available thrusters will be used for horizontal propulsion. These thrusters have to be streamlined since they are oriented parallel to the main direction of travel, as opposed to the vertical thrusters. The RMI 1000 thruster from RoboMarine Indonesia is the most relevant candidate, with a weight of 2kg and a 200N nominal thrust force.

The ROV now has an estimated total weight of 29kg, which is within the limits set by the requirements. The final weight may, however, differ slightly due to the uncertainties of the thrusters mass.



FIGURE 1: LATEST RIM-THRUSTER DESIGN (LEFT) AND FINAL ROV RENDERED WITH A TRANSLUCENT CASING (MIDDLE) AND RIG MOUNTED THRUSTER PROTOTYPE (RIGHT).

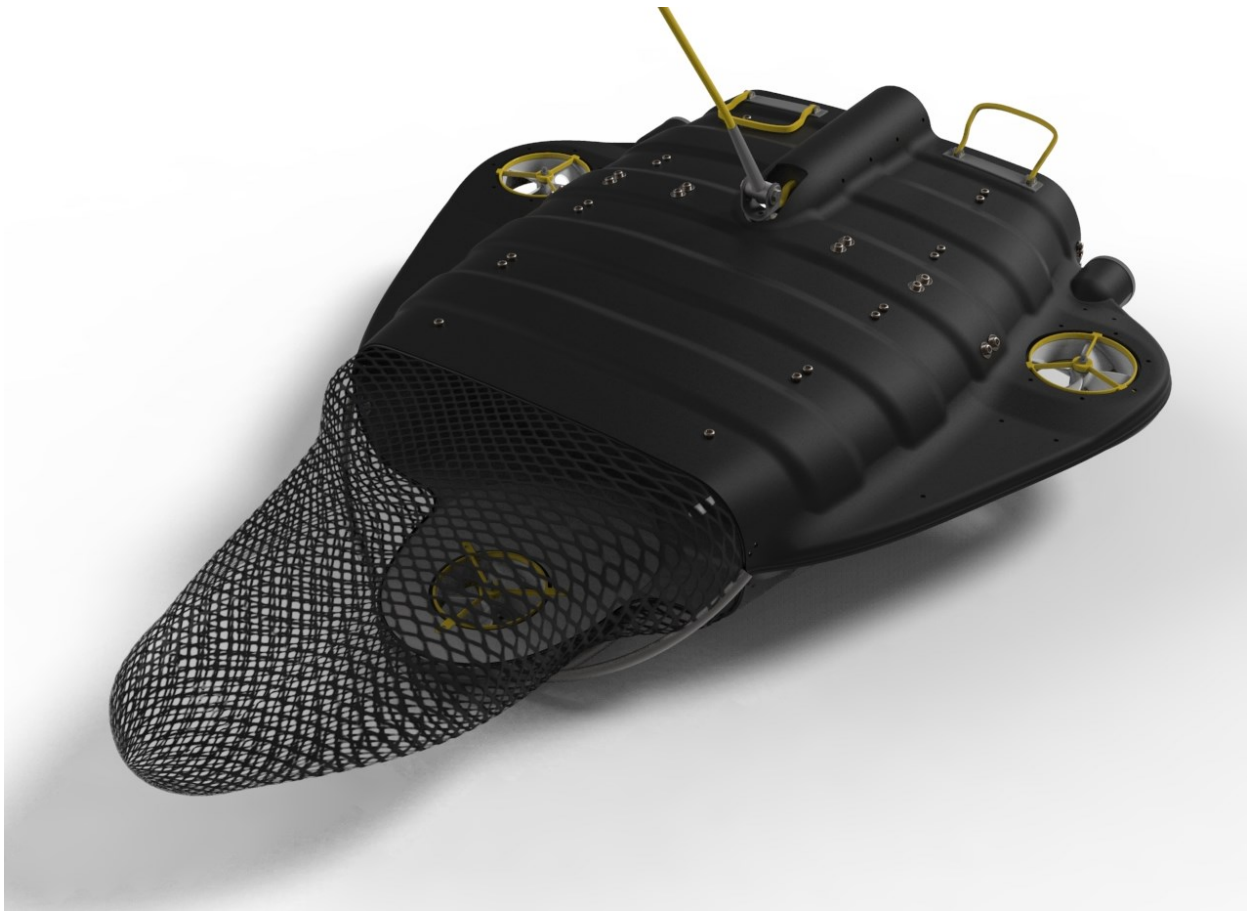


FIGURE 2: LATEST DESIGN

### 1.3 SAMMENDRAG NORSK

Denne masteroppgaven er en videreføring av høstens prosjektoppgave [1]. Målet med prosjektet var å utvikle en fjernstyrt undervannsfarkost (ROV) for inspeksjon av oppdrettsanlegg. ROVen, som har fått navnet *The Manta* skal også plukke opp død fisk på bunnen av merdene. Mantaen vil redusere belastningen på arbeidere i oppdrettsnæringen, ved å utføre oppgaver som er både risikofylte og kostbare, og gi muligheten for en mer lettvent og effektiv kontroll av anlegget. Formen på Mantaen er hul og mer strømlinjeformet enn en vanlig ROV. Dette gjør at den har mindre risiko for å henge seg fast eller skade merdene, går raskere gjennom vannet, og oppdraget blir utført på kortere tid. ROVen har montert to horisontalthruster i skrogets hulrom skaper kraft for fremdrift og suger død fisk inn i et nett som er montert bak på skroget. De tre vertikalthrusterne er lokalisert i tynne vinger på utsiden av skroget.

Designet av selve skroget er nesten helt ferdig. Kun detaljer rundt innfestning av motorer og nett mangler. Dette vil bli fullført når detaljene rundt disse komponentene er ferdig. Skroget er laget av 4 mm vakuumformede ABS-plater og er den bærende strukturen i ROVen. Formen er korrugert for å øke stivheten, og ved å ha en avstand på 6 mm mellom korrugeringstopp- og bunn i skroget økes stivheten med 45% med hensyn på løfting. Skroget produseres i to deler som festes sammen med lim og bolter. En rekke produsenter har blitt forespurt om pris på skroget, og prisen ser ut til å ligge på rundt 2000NOK per skrog inkludert verktøykostnader for 100 enheter.

Et mekanisk design for en *ringdrevet* thruster (RDT) som kan få plass i vingene på Mantaen har blitt utviklet. Dette er en motor hvor propellen har fått montert permanentmagneter på en ytre ring i stedet for å være drevet av en senteraksling. Dette gjør at motoren får et mye høyere moment i forhold til lengde og alle sårbare komponenter kan være totalt forseglet. Motorens geometri er også totalt forskjellig fra konvensjonelle ROV thrusterne. Typisk er disse lange og tynne, mens den nyutviklede thrusteren er svært flat. Ytre mål er ca 190x40mm, og estimert vekt ligger på 1,7kg. Det elektromagnetiske designet er det Argus RS som står for og de gjenværende detaljer avhenger av hvordan det elektromagnetiske designet til motoren blir. En prototype av RDTen og en spesialdesignet testtrigg for denne er utviklet og maskinert i IPMs verksted. Sammenstillingen er overlevert til Argus for ferdigstilling av elektromagnetisk design.

RMI 1000 thrusteren er den mest optimale horisontal-thrusteren som er funnet på markedet. Denne modellen veier 2kg, har en nominell skyvkraft på 200N og prisen er oppgitt til ca. 18 000 NOK per enhet.

Estimert vekt på ROVen slik designet er nå er ca. 29kg



FIGURE 3: SISTE DESIGN

## 1.4 MASTER THESIS PROBLEM TEXT

THE NORWEGIAN UNIVERSITY  
OF SCIENCE AND TECHNOLOGY  
DEPARTMENT OF ENGINEERING DESIGN  
AND MATERIALS

### MASTER THESIS SPRING 2014 FOR STUD.TECHN. MAGNUS MYKLEBOST

#### LIGHTWEIGHT DESIGN OF ROV FOR INSPECTION AND REMOVAL OF DEAD FISH

A Remotely operated vehicle (ROV) for subsea operation shall be developed. The ROV design shall emphasize lightweight solutions both for the structural components, propulsion and auxiliary equipment. Focused tasks are

- Design and engineering for manufacturing of main body
- Conceptual design of rim thrusters and their mechanical components
- Relevant prototyping and development of manufacturing processes

Three weeks after start of the thesis work, an A3 sheet illustrating the work is to be handed in. A template for this presentation is available on the IPM's web site under the menu "Masteroppgave" (<http://www.ntnu.no/ipm/masteroppgave>). This sheet should be updated one week before the Master's thesis is submitted.

Performing a risk assessment of the planned work is obligatory. Known main activities must be risk assessed before they start, and the form must be handed in within 3 weeks of receiving the problem text. The form must be signed by your supervisor. All projects are to be assessed, even theoretical and virtual. Risk assessment is a running activity, and must be carried out before starting any activity that might lead to injury to humans or damage to materials/equipment or the external environment. Copies of signed risk assessments should also be included as an appendix of the finished project report.

The thesis should include the signed problem text, and be written as a research report with summary both in English and Norwegian, conclusion, literature references, table of contents, etc. During preparation of the text, the candidate should make efforts to create a well arranged and well written report. To ease the evaluation of the thesis, it is important to cross-reference text, tables and figures. For evaluation of the work a thorough discussion of results is appreciated.

The thesis shall be submitted electronically via DAIM, NTNU's system for Digital Archiving and Submission of Master's thesis.



Torgeir Welo  
Head of Division



Nils Petter Vedvik  
Professor/Supervisor

## 1.5 TABLE OF CONTENTS

<b><u>1</u></b>	<b><u>PREFACE.....</u></b>	<b><u>I</u></b>
1.1	ACKNOWLEDGEMENTS.....	I
1.2	ABSTRACT.....	II
1.3	SAMMENDRAG NORSK.....	IV
1.4	MASTER THESIS PROBLEM TEXT.....	V
1.5	TABLE OF CONTENTS.....	VI
1.6	LIST OF TABLES.....	IX
1.7	TABLE OF FIGURES.....	IX
1.8	LIST OF ABBREVIATIONS.....	XIV
<b><u>2</u></b>	<b><u>INTRODUCTION.....</u></b>	<b><u>1</u></b>
2.1	THE PARTNERS.....	1
2.2	HISTORY.....	2
<b><u>3</u></b>	<b><u>REQUIREMENTS.....</u></b>	<b><u>3</u></b>
3.1	WEIGHT.....	3
3.2	SIZE.....	3
3.3	MANOEUVRABILITY.....	3
3.4	OPERATING ENVIRONMENTS.....	3
3.5	USER DEMAND SPECIFICATION.....	4
3.6	PRODUCT DEMAND SPECIFICATIONS.....	5
<b><u>4</u></b>	<b><u>MATERIAL SELECTION.....</u></b>	<b><u>6</u></b>
4.1	THERMOPLASTICS.....	6
4.2	THERMOSETTING POLYMERS.....	6
4.3	COMPOSITES.....	7
4.4	CHOSEN HULL MATERIAL.....	8
<b><u>5</u></b>	<b><u>DESIGN.....</u></b>	<b><u>9</u></b>
5.1	CONCEPT.....	11
5.2	MAIN HULL.....	12
5.2.1	MESH CONVERGENCE ANALYSIS.....	13
5.2.2	PLASTICS JOINING.....	17
5.2.3	HULL STRENGTH.....	21
5.3	ELECTRONICS PRESSURE VESSEL.....	24
5.3.1	MESH CONVERGENCE ANALYSIS ON BUCKLING CASE.....	25
5.4	THRUSTERS.....	27
5.4.1	BRUSHLESS MOTOR DESIGN.....	28

5.4.2	RIM-DRIVEN THRUSTER DESIGN .....	29
5.4.3	HORIZONTAL THRUSTERS .....	36
<b>5.5</b>	<b>LAMPS.....</b>	<b>38</b>
5.5.1	EMBEDDED DESIGN .....	39
5.5.2	DRY DESIGN .....	41
5.5.3	CREE XML-T6 DESIGN .....	42
5.5.4	CUSTOM LED RACK .....	45
<b>5.6</b>	<b>BUOYANCY UNITS .....</b>	<b>47</b>
<b>5.7</b>	<b>UMBILICAL LIFTING POINT .....</b>	<b>48</b>
5.7.1	LOAD DISTRIBUTION BRACKET .....	51
<b>5.8</b>	<b>LIFTING HANDLE .....</b>	<b>52</b>
<b>6</b>	<b><u>PROTOTYPING.....</u></b>	<b><u>54</u></b>
6.1	SMARTMOTOR STATOR BASED PROTOTYPE.....	55
6.2	BUSCK STATOR BASED PROTOTYPE.....	56
6.2.1	STATOR .....	56
6.2.2	ROTOR.....	60
6.3	THRUSTER TEST RIG .....	65
<b>7</b>	<b><u>MANUFACTURING.....</u></b>	<b><u>68</u></b>
7.1	MANUFACTURING THE HULL .....	68
<b>8</b>	<b><u>CONCLUSIONS AND FUTURE WORK.....</u></b>	<b><u>69</u></b>
8.1	FUTURE DESIGN TASKS.....	71
8.2	FUTURE SIMULATION REQUIREMENTS.....	71
8.3	FUTURE PROTOTYPING.....	71
8.4	FUTURE TESTING .....	71
<b>9</b>	<b><u>REFERENCES.....</u></b>	<b><u>72</u></b>
<b>10</b>	<b><u>APPENDIX A: MANUFACTURING COMPONENTS.....</u></b>	<b><u>75</u></b>
10.1	THERMOPLASTICS .....	75
10.2	FIBRE COMPOSITE LAMINATE.....	77
<b>11</b>	<b><u>APPENDIX B: MATERIAL COMPARISON .....</u></b>	<b><u>79</u></b>
11.1	COMPOSITE MATERIAL THEORY.....	79
11.1.1	LAMINATE .....	80
11.1.2	SANDWICH STRUCTURE.....	80
11.1.3	MATERIAL UTILIZATION .....	80
11.1.4	FAILURE IN COMPOSITES .....	81
11.1.5	MAXIMUM STRESS THEORY FOR COMPOSITES .....	82

11.2	INITIAL MATERIAL COMPARISON .....	82
11.3	MATERIAL COMPARISON BY FEM ANALYSIS .....	84
11.3.1	STRUCTURAL RESPONSE CRITERIA.....	84
11.4	FEA BASED MATERIAL COMPARISON ON SIMPLIFIED HULL.....	86
11.4.1	MATERIAL DATA USED IN THE FEA .....	86
<b>12</b>	<b><u>APPENDIX C: ILLUSTRATIONS OF FINAL DESIGN.....</u></b>	<b>90</b>
<b>13</b>	<b><u>APPENDIX D: EVOLUTION OF HULL DESIGN .....</u></b>	<b>95</b>
<b>14</b>	<b><u>APPENDIX E: ALTERNATIVE SYMMETRICAL HULL DESIGN .....</u></b>	<b>96</b>
<b>15</b>	<b><u>APPENDIX F: CORRUGATED VS SMOOTH HULL .....</u></b>	<b>97</b>
<b>16</b>	<b><u>APPENDIX G: ORIGINAL MANTA 505 BROCHURE.....</u></b>	<b>100</b>
<b>17</b>	<b><u>APPENDIX H: THRUSTER PROTOTYPE FEM ANALYSIS.....</u></b>	<b>101</b>
17.1	RIM PROPELLER FEA DETAILS.....	101
17.2	PROPELLER AXLE FEA DETAILS .....	103
<b>18</b>	<b><u>APPENDIX I: RIM-THRUSTER FEA DETAILS .....</u></b>	<b>105</b>
<b>19</b>	<b><u>APPENDIX J: ROV LIGHT FEA DETAILS .....</u></b>	<b>107</b>
<b>20</b>	<b><u>APPENDIX K: HULL SIMULATIONS.....</u></b>	<b>109</b>
20.1	REAR THRUSTER WING LOADING .....	112
<b>21</b>	<b><u>APPENDIX L: UMBILICAL LIFTING POINT .....</u></b>	<b>115</b>
21.1	UMBILICAL FIXTURE FEA RESULTS.....	115
21.2	UMBILICAL PIVOT FEA RESULTS .....	118
21.3	UMBILICAL LIFTING POINT MACHINE DRAWINGS (ORIGINALLY A3 SIZE) .....	120
<b>22</b>	<b><u>APPENDIX M: MACHINE DRAWINGS OF THRUSTER TEST RIG.....</u></b>	<b>123</b>
<b>23</b>	<b><u>APPENDIX N: MACHINE DRAWINGS OF COMPONENTS.....</u></b>	<b>131</b>
<b>24</b>	<b><u>APPENDIX O: RISK ASSESSMENT SHEET (NORWEGIAN) .....</u></b>	<b>136</b>

## 1.6 LIST OF TABLES

Table 1: User demand specification.....	4
Table 2: Product demand specification.....	5
Table 3: Mesh convergence test results from simplified hull .....	14
Table 4: Pros and cons with bolted hull joints.....	18
Table 5 Pros and cons with hot welded hull joints .....	18
Table 6: Pros and cons with solvent welded or adhesive hull joints .....	19
Table 7: Mesh convergence analysis on buckling of electronics pressure vessel.....	25
Table 8: Thermal properties of relevant materials for lamp assembly [7].....	40
Table 9: Thruster stator data .....	59
Table 10: Estimated cost of manufacturing hull .....	68
Table 11: Material comparison [50] .....	82
Table 12: Material comparison based on FEM analysis (geometry dependant).....	84
Table 13: Effect of sandwich core thickness .....	85

## 1.7 TABLE OF FIGURES

Figure 1: Latest rim-thruster design (left) and final ROV rendered with a translucent casing (middle) and rig mounted thruster prototype (right).....	II
Figure 2: Latest design.....	III
Figure 3: Siste design.....	IV
Figure 4: Norwegian aquaculture facility [2].....	1
Figure 5: Illustration Of Original Manta [37].....	2
Figure 6: Crystallinity [4] .....	6
Figure 7: Sandwich structure properties [5].....	7
Figure 8: Design process flow chart .....	9
Figure 9: The complete ASsembly in NX.....	10
Figure 10: Principle of a jet pump [42].....	11
Figure 11: Concept design .....	11
Figure 12: Concept design water flow .....	11
Figure 13: Smooth hull from project thesis [1].....	12
Figure 14: Corrugated hull.....	12
Figure 15: Mesh convergence analysis load state.....	13
Figure 16: 2,5mm Mesh boundary area stress .....	13
Figure 17: 3mm mesh - maximum elements.....	14
Figure 18: Mesh convergence analysis results graph .....	14

Figure 19: Comparison of 2,5mm and 3mm mesh .....	15
Figure 20: Displacement of Smooth simplified hull, Max is 142mm.....	16
Figure 21: Displacement of Corrugated simplified hull, max is 98mm .....	16
Figure 22: Heated tool welding [9].....	18
Figure 23: Recommended solvent- and adhesive plate joints (left).....	19
Figure 24: Hull section overlap.....	20
Figure 25: hull stress plot.....	21
Figure 26: Stress plot from rear thruster wing .....	22
Figure 27: Rear wing bumper .....	23
Figure 28: Section view of Electronics container with lens and end-cap .....	24
Figure 29: Mesh convergence graph.....	25
Figure 30: Displacement plot of mode 1 buckling of electronics pressure vessel.....	26
Figure 31: Typical ROV design [12] .....	27
Figure 32: Difference between conventional ROV thrusters and RDTs [15] [16].....	27
Figure 33: Windings in a 3-phase motor.....	28
Figure 34: Composite stator (left [15]) and slotted stator.....	28
Figure 35: Illustration of bearing friction .....	30
Figure 36: Early hub-less design with angular contact bearings on rotor flange.....	30
Figure 37: Secondary thruster concept .....	31
Figure 38: Thruster design - rendered with translucent components.....	32
Figure 39: Skewed stator .....	32
Figure 40: Rim-thruster internals.....	33
Figure 41: Grease flow (green) from propeller hub nipple.....	33
Figure 42: Rim-thruster hub (rendered translucent) .....	34
Figure 43: Stress plot of rotor hub (max 185,5MPa).....	34
Figure 44: Cylinder section magnet.....	35
Figure 45: RMI 1000 exterior 3d model [28] .....	36
Figure 46: Submertec ARS850 (left) next to a RMI 1000 (right).....	37
Figure 47: Conceptual thruster assembly .....	37
Figure 48: Deepwater lamps on an Argus ROV .....	38
Figure 49: ARgus' Custom made rectangular LED circuit board .....	38
Figure 50: Illustration of <i>embedded design</i> .....	39
Figure 51: Cross-section of typical LED [33].....	39
Figure 52: Normal LED (left) and a LED discolored due to chemical incompatibility (right) [33].....	40

Figure 53: 3D-model of Dry lamp design.....	41
Figure 54: Stress plot of lamp at 150m depth.....	41
Figure 55: 60° Lens (upper left), 20mm XML LED (top) and 16mm (bottom).....	42
Figure 56: Single led design .....	43
Figure 57: Section view of lamp.....	43
Figure 58: 3X CREE XML Design, total of 3000lumen .....	44
Figure 59: Cooling ribs .....	44
Figure 60: section view of casing .....	44
Figure 61: Custom LED rack with a total of 5600 lumens .....	45
Figure 62: 3 x 3 x 2 mm Osram LCWCQAR CC LED .....	45
Figure 63: 100 W led design.....	46
Figure 64: Section view of 100w LED .....	46
Figure 65: 100w LED with reflector, 120° lens and XML LED (below) for scale .....	46
Figure 66: Buoyancy unit locations in the hull.....	47
Figure 67: mAIN Buoyancy unit .....	47
Figure 68: Umbilical connection point seen from above.....	48
Figure 69: Umbilical Lifting Point .....	48
Figure 70: Load case on umbilical pivot (1500N distributed).....	49
Figure 71: Load case on umbilical fixture (2x750N bearing force) .....	49
Figure 72: Stress plot on umbilical pivot 1000x deformation (max 246MPa) .....	49
Figure 73: Umbilical fixture before (left) and after redesign – same load and mesh .....	50
Figure 74: Load distribution bracket.....	51
Figure 75: Mounted load distribution bracket .....	51
Figure 76: Concept flip up handle .....	52
Figure 77: Surface mounted handle from parts-express.com .....	52
Figure 78: The Manta (The 3d model of the salmon is courtesy of Magnus Skogsfjord).....	53
Figure 79: Smart motor actuator stator .....	55
Figure 80: Stator from Busck motor .....	56
Figure 81: Stator jig before and after mounting in the lathe.....	57
Figure 82: The stator in the jig before (above) and after diameter reduction .....	58
Figure 83: Skewing of the stator teeth .....	59
Figure 84: Thruster prototype rotor 3d model .....	60
Figure 85: Displacement plot of rim propeller .....	61
Figure 86: Stress plot of rim propeller.....	61
Figure 87: Stress plot of rim propeller,.....	62

Figure 88: Manufacturing the rotor iron .....	63
Figure 89: Finished Prototype rotor .....	64
Figure 90: Stator test rig assembly.....	65
Figure 91: Thruster in test rig without magnets and windings .....	66
Figure 92: Complete prototype thruster test rig.....	67
Figure 93: Complete prototype test rig .....	67
Figure 94: Final design .....	70
Figure 95: Rotational moulding process .....	75
Figure 96: Blow moulding process .....	75
Figure 97: Injection moulding process .....	76
Figure 98: Vacuum forming process [40].....	76
Figure 99: Resin transer moulding process.....	77
Figure 100: Hand layup of composites .....	77
Figure 101: Spray up process.....	77
Figure 102: Vacuum infusion layup [43].....	78
Figure 103: Planes of symmetry in an orthotropic material (left) and plane of isotropy in a transversely isotropic material (right) [44] .....	79
Figure 104: Fibre orientation in composites - From left: Unidirectional continous and discontinues, randomly oriented long and short fibre and weaved fabric [44].....	79
Figure 105: Illustration of a laminate [44].....	80
Figure 106: Sandwich structure properties [5].....	80
Figure 107: Failure in composites (fig 6.15 [48]).....	81
Figure 108: Local delamination around a drilled hole. [10] .....	81
Figure 109: Maximum stress criterion .....	82
Figure 110: Plate Thicknesses With Equal Weight .....	83
Figure 111: Load Distribution Used For Fem Material Comparison .....	84
Figure 112: Example of sandwich distribution.....	84
Figure 113: Alternative symmetrical hull .....	96
Figure 114: Corrugated (upper) and plane (lower) hull load state (shown on 10mm mesh)....	97
Figure 115: Resulting stress plot on corrugated (upper) and plane(lower) simplified hull .....	98
Figure 116: Resulting displacement on hull. (corrugated on top) .....	99
Figure 117: 2mm CTETRA(10) mesh .....	101
Figure 118: Propeller Load .....	101
Figure 119: Stress plot of the rotor .....	102
Figure 120: Displacement plot of the rotor.....	102
Figure 121: Axle mesh:.....	103

Figure 122: Axle Load state.....	103
Figure 123: Axle Stress plot: Max stress 407MPa.....	104
Figure 124: Displacement plot axle - 100x Deformation – Max displacement 0,048mm.....	104
Figure 125: Thruster hub mesh (1mm CTETRA(10)).....	105
Figure 126: Thruster hub load.....	105
Figure 127: Thruster hub displacement plot (max 0,437mm) .....	106
Figure 128: Thruster hub stress plot (max 185,5 MPa von mises) .....	106
Figure 129: Light assembly FEA mesh details .....	107
Figure 130: Light assembly FEA load details.....	107
Figure 131: Light assembly FEA displacement plot.....	108
Figure 132: Light assembly FEA stress plot.....	108
Figure 133: Hull FEA 6mm CTETRA(10) MESH.....	109
Figure 134: Hull load state.....	109
Figure 135: Hull displacement (max 135mm).....	110
Figure 136: Hull strain (max 0,022) .....	110
Figure 137: Hull low level Stress.....	111
Figure 138: Hull high level stress .....	111
Figure 139: 5mm CTETRA(10) Mesh on Lower hull .....	112
Figure 140: Upwards 500N force load case.....	112
Figure 141: Rear thruster wing displacement plot (1x deformation).....	113
Figure 142: Rear thruster wing stress plot .....	113
Figure 143: Inwards force load case (500N).....	114
Figure 144: Inwards load case stress plot .....	114
Figure 145: Umbilical fixture load case.....	115
Figure 146: Umbilical fixture mesh - 0,5mm CTETRA(10) elements .....	116
Figure 147: Stress plot from straight forwards force (left) and straight upwards force (right) .....	117
Figure 148: Displacement plot from straight forwards force (left) and straight upwards force (right) .....	117
Figure 149: Umbilical pivot Load data .....	118
Figure 150: Umbilical pivot mesh data – 0,5mm CTETRA(10) elements .....	118
Figure 151: Umbilical pivot stress plot (half section view).....	119
Figure 152: Umbilical pivot displacement plot 100x deformation (half section view).....	119

## 1.8 LIST OF ABBREVIATIONS

ABS	Acrylonitrile Butadiene Styrene (Thermoplastic)
CF	Carbon Fibre
CFRP	Carbon Fibre Reinforced Polymer
CRI	Colour Rendering Index
FEA	Finite Element Analysis
FEM	Finite Element Method
GFRP	Glass Fibre Reinforced Polymer
HCP	Hydraulic Crush Point in bar (Sandwich core foam)
HD	High Definition
IPM	Institute of Product development and Materials
KFRP	Kevlar Fibre Reinforced Polymer
LED	Light Emitting Diode
MSTRS	Maximum stress criterion value
PM	Permanent Magnet
PMDC	Permanent Magnet Direct Current
RDT	Rim-Driven Thruster
ROV	Remotely Operated Vehicle
RS	Remote Systems
RTM	Resin Transfer Moulding
UTS	Ultimate Tensile Strength

## 2 INTRODUCTION

The fish farming industry is in constant need of new solutions in order to improve working conditions for its employees, better fish health, reduce environment impact and increase efficiency. There is a large degree of manual labour with respect to inspection and maintenance of the net cages and removal of dead fish. The work at a fish farm is physically demanding as the equipment is heavy. The environment is often harsh and the manpower is limited. Maintaining acceptable working conditions for the divers is a challenge, and their service is an important expense. The net cages vary in depths, at some places reaching down to 90m. In Norway the net cages are typically between 10 and 30m deep. A characteristic Norwegian aquaculture facility is pictured in Figure 4.

A fish farmer could use remotely operated vehicles (ROVs) for a series of tasks. It is mandatory to inspect the net cages regularly and it is also smart in order to monitor fouling and problem zones, like developing holes. Also, in order to maintain a good fish health, collecting dead fish is critical, as dead fish on the bottom of the net could be a source of disease. These tasks can be combined with the use of a single ROV. The ROV operator can work safely inside and inspect the net while recording HD-video. Dead fish could be collected continuously through the inspection run.

Since this thesis contains the development of many parts of the ROV, I have chosen to first present the background and requirements for the ROV. Material selection for the hull will be explained. Finally, the design and prototyping work will be presented.

Throughout this thesis, the most relevant theory is presented where it is applied. More detailed theory, simulations and documentation are located in the appendix, and it is referred to in the text.



FIGURE 4: NORWEGIAN AQUACULTURE FACILITY [2]

### 2.1 THE PARTNERS

The partners cooperating in this project are NTNU, Argus Remote systems AS and Inventas AS. Inventas AS is a consultant firm with focus on design, product development and engineering. They work as a connecting link between me and the customers, who are a combination of Mohn Aqua AS and Argus Remote Systems AS. Inventas also provides guidance throughout the project, with special respect to the product development. Argus Remote Systems (RS) AS is a company who designs and manufactures ROVs for underwater inspection, oil- and gas industry and aquaculture. Mohn Aqua delivers equipment to aquaculture industry and they are the owners of the project.



## 2.2 HISTORY

The ROV is named *Manta* and there has been a predecessor with the same name and similar tasks. The original *Manta* is illustrated in Figure 5. It was an ROV for inspection and collection of dead fish in fish farms. It was built in the 1990s by Vidar Saue and some of the same people who run Argus RS today. It featured easy control and relative low price. Although not many Mantas were sold some people in the aquaculture industry still know the name. The *Manta* had a simple design with few parts. The “soap piece” shape with no protruding components had few problems with entanglement or getting stuck in the net. However the *Manta* had its cons as well. The hull was made out of rotation moulded plastic and was very heavy. The ROV weighed approximately 65 kg.

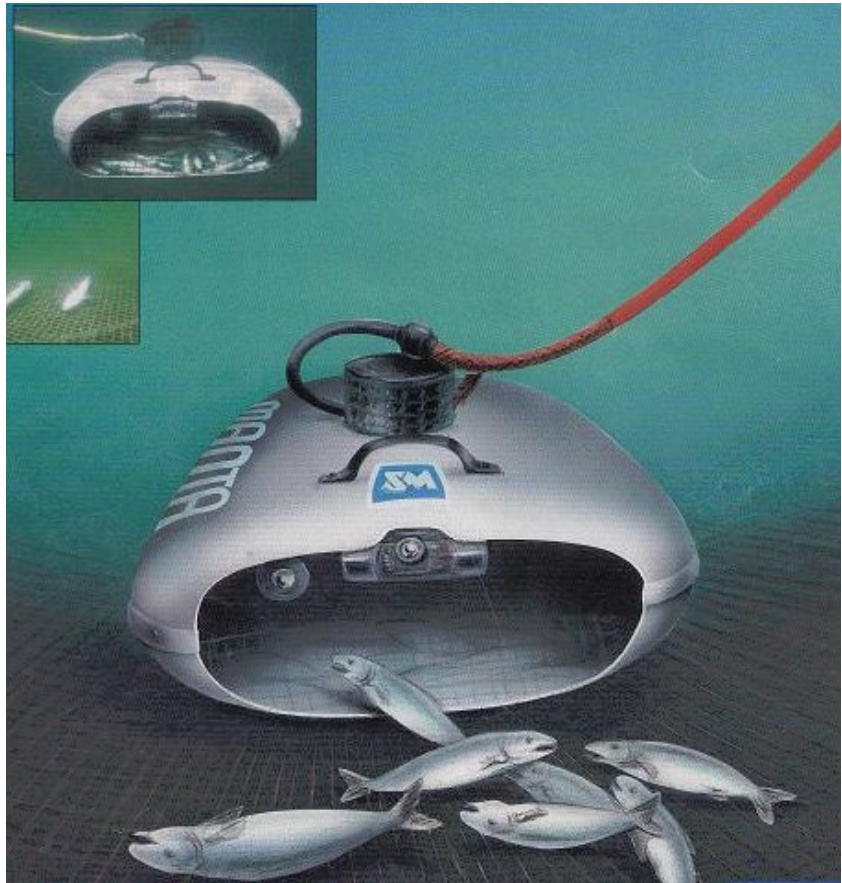


FIGURE 5: ILLUSTRATION OF ORIGINAL MANTA [37]

The rotational moulding process did not provide sufficient tolerances on the wall thickness. Some areas of the body had thicker walls than needed while others were thinner. The *thrusters* were unreliable because leaky seals made them prone to breakdowns. This model of the *Manta* only had three thrusters, which limited the controllability. There was also some customer feedback that suggested that it was a bit challenging to clean, as there were narrow, hard to access cavities that could hold bacteria, viruses or parasites.

No ROVs with similar design is known to exist on the market today.

### 3 REQUIREMENTS

In order to create a successful product, it is vital to investigate the requirements and customer needs. To sum up the basic requirements, the ROV has to be as light as possible, robust to withstand harsh environments, rough handling and cleaning, and must be able to both inspect the net and collect dead fish. It should be kept as simple as possible, in order to reduce the cost, maintenance requirement and limit the number of components that could fail.

Argus RS has close contact with the aquaculture industry through cooperation, meetings and fairs, and most of the following requirements are specified by Argus. These requirements were determined during the project thesis. [1]

#### 3.1 WEIGHT

A single operator has to be able to launch the ROV by hand. This is important to small facilities, where manpower is limited and installation of a crane is unfeasible. A low weight will also ease the transportation of the ROV, which can be done by small boats or standard vans. The weight is of major importance, and a main focus of this thesis will be to design a lightweight structure.

#### 3.2 SIZE

The ROV has to be easy to transport and store, which limits the size. The opening through the hull has to handle large salmon, which might be affected by rigor mortis (stiffness after death). Therefore a compromise was found during the first meeting with the partners of the project. The ROV should have a small enough footprint to fit on a standard EURO-pallet, which is 1200x800mm, but the orientation is not set. In other words it could be set vertically in a Styrofoam jig during transportation.

#### 3.3 MANOEUVRABILITY

The Manta must be easy to control and be able to move in all directions. It is required that the Manta is an efficient inspection tool and accurate fish collector. Argus RS has responsibility for the control engineering.

#### 3.4 OPERATING ENVIRONMENTS

The fish farms are open facilities at sea all over the world, from Chile to the Arctic. The temperatures can span from -20°C in the winter to 30°C in the summer. Especially the cold temperature is a challenge in combination with moisture, as the risk of frozen and jammed components is high. At sub-zero temperatures ROVs are typically lowered into the sea a couple of minutes before the motors are started, which allows the ice to thaw. The materials change properties along with the temperature. Many materials experience a ductile to brittle transition at a certain temperature, which has to be accounted for.

The Manta will operate in a corrosive environment, constantly exposed to a mix of salt water, air and moisture. The ROV might also be cleaned with chemicals to prevent spreading of salmon louse and diseases.

One must expect that operating errors will occur and that the ROV will be handled roughly. Examples of expected operator errors are dropping the ROV into the water from heights, dropping it onto the deck / ground, rough mechanical de-icing and hitting underwater objects like anchor chains.

All these points combined require a robust material selection. The requirements have been expressed in a user demand specification and quantified in a product demand specification. This summarizes what the development should focus on further.

### 3.5 USER DEMAND SPECIFICATION

The user demand specification in Table 1 describes in a qualitative way what the user expect the product to do. It divides the features into two categories, should or must. This way all parties of the project can have a common understanding of the priorities. The “should”-category are features to keep in mind and try to implement, but not absolutely vital if they are impractical due to other considerations.

<b>User demand specification</b>			
<b>Product: Manta ROV</b>		<b>Made by: MRM</b>	<b>Date: 11.09.2013</b>
<b>#</b>	<b>Description</b>	<b>Must</b>	<b>Should</b>
<b>Primary Users: Aquaculture Industry</b>			
<b>1. Functional requirements</b>			
	Accurate control	✓	
	Easy to control and navigate	✓	
	Easy to disassemble		✓
	Easy to change wear parts	✓	
	Good video quality and intuitive heads up display	✓	
	Easy to transport	✓	
	One man operable	✓	
	Ability to save video	✓	
	Ability to stream video over Wi-Fi		✓
	Standard spare parts (O-rings, bolts and nuts etc.)		✓
	Waterproof control box		✓
	Liftable by cable		✓
	Quick detachable net		✓
	Ability to save location (of for example a hole in the net)		✓
<b>2. Environmental requirements</b>			
	Weather resistant	✓	
	Will work in salt water (all temperatures)	✓	
	Will work in all air temperatures		✓
	Resistant to harsh cleaning	✓	
	Easy to clean	✓	
	Easy to maintain		✓
<b>3. Safety</b>			
	Emergency stop button	✓	
	No possibility of electrical shock	✓	
	Streamlined geometry to reduce risk of entanglement		✓
	Grid / bars to ensure no fish gets into the propellers	✓	

TABLE 1: USER DEMAND SPECIFICATION

### 3.6 PRODUCT DEMAND SPECIFICATIONS

The product demand specification in Table 2 is a quantitative specification that puts sizes on the most important requirements.

<b>Product demand specification</b>			
<b>Product: Manta ROV</b>	<b>Created by: MRM</b>	<b>Approved: YES</b>	<b>Date: 11.09.13</b>
<b>Description</b>			
<b>Level 1:</b>	<b>Level 2:</b>	<b>Unit</b>	<b>Value</b>
<b>Functional requirements</b>	Capacity	# fish	10
	Fish dimensions	mm (LxWxH)	600x150x200
	Fish weight	kg	5
	Weight of unit	kg	m < 32
	Length	mm	300 < L < 1000
	Width	mm	b < 1000
	Speed	m/s	>2
	Maximum operating depth	m	<100
<b>Environments</b>	Sea temperature	°C	-5 < T < 40
	Air temperature	°C	-20 < T < 50
	Wave heights	m	< 1
<b>Operational</b>	Running time	hours/day	< 16
	Running time between services	weeks	4
	Time between maintenance	hours	12
<b>Safety</b>	Emergency stop	switch	1 / operator
	Distance to emergency stop	m	< 1

TABLE 2: PRODUCT DEMAND SPECIFICATION

The quantitative requirements in Table 2 are not absolute. Deviations of up to 10% are allowed and expected.

The user- and product demand specification is approved by Argus.

## 4 MATERIAL SELECTION

Due to the focus on lightweight structures, the hull material should be as strong, stiff, and light as possible. ABS plastic was chosen for the hull during the previous project thesis [1] and that choice is considered in more detail here, and found to still be valid. Even though ABS is not considered to be very strong nor stiff, it has a low density and is easy to manufacture. Material for auxiliary components will be described during the design presentation.

Many materials have been considered for the hull, and the selection process was mainly conducted during the project thesis [1]. The different materials evaluated are described in chapter 11 along with more detailed theory. Manufacturing method for thermoplastics and composites are presented in chapter 10.1 and 10.2 respectively.

### 4.1 THERMOPLASTICS

A thermoplastic is a polymer material that has only secondary links between the molecule chains. This feature allows the material to become soft and mouldable when heated above a certain temperature. Thermoplastics are either amorphous, where molecule chains are randomly oriented, or semi-crystalline, where the molecule chains are oriented and tightly packed in the crystalline regions, illustrated in Figure 6. Polymers are rarely more than 50% crystalline, but materials with higher degrees of crystallinity exist. The degree of crystallinity typically effects hardness, wear, friction, and creep properties [3]. This comes from the fact that the molecules are closer and the intermolecular bonds therefore stronger. Examples of thermoplastics are ABS, polyethylene (PE), polypropylene (PP) and polycarbonate (PC). These materials allows for injection moulding or vacuum forming, by heating the plastic and then shaping it.

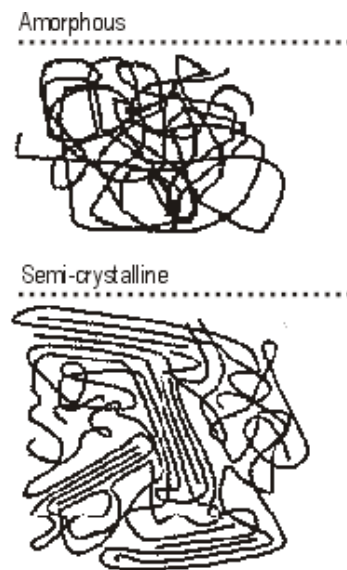


FIGURE 6: CRYSTALLINITY [4]

### 4.2 THERMOSETTING POLYMERS

A thermoset polymer is used where a high dimensional and thermal stability is required. The resin blend is also typically liquid at room temperature before hardening. This allows for easier manufacturing. The molecule chains of the polymer are cross-linked, which adds strength and stops creep. The cross linking also prevents the thermosetting polymer from being reshaped once cured (hence thermoset). A thermoset polymer is typically a mix of liquid resin and hardener, that when combined creates an irreversible reaction resulting in a solid polymer. The resulting solid can be considered as one big molecule. Examples of thermosetting polymers are polyesters, polyurethanes and epoxies. [3]

### 4.3 COMPOSITES

Composite materials combine features of different materials that often are useless separately. There are many kinds of composite materials, but in this thesis only fibre composites will be discussed. These consist of strong and stiff fibres, bonded together in a polymer matrix, creating a lightweight and strong material. Carbon fibre reinforced polymer (CFRP) is the most relevant composite material, due to its high strength and stiffness compared to weight.

The reasons for not choosing CFRP for hull material are material and manufacturing cost, durability and robustness. Details around composite manufacturing methods and theory are found in chapter 10.2 and 11.1 respectively.

When an even higher stiffness and strength to weight ratio is needed, a low density core material can be added to the centre of the laminate. The structure then defined as a sandwich structure.

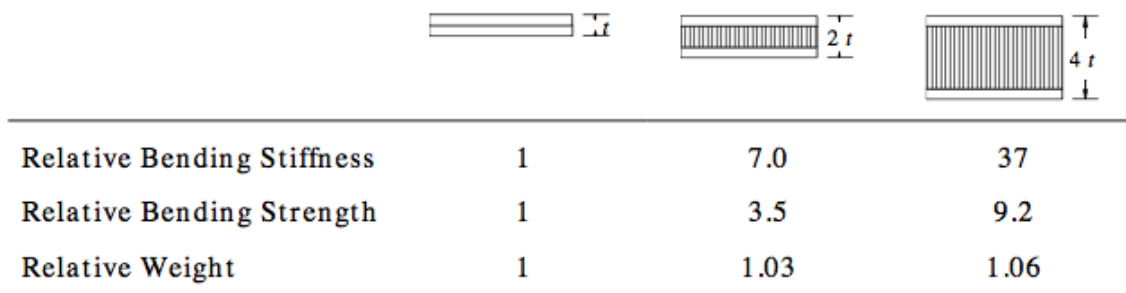


FIGURE 7: SANDWICH STRUCTURE PROPERTIES [5]

A sandwich structure uses a low density core to increase the second moment of inertia per weight significantly, by increasing the distance between the load carrying skins of the structure. The effect is displayed in Figure 7. The core could be made of closed cell foam, which will provide buoyancy to the hull. If the chosen material for the hull was CFRP, it would most likely be used in a sandwich structure. When manufacturing this sandwich, it is vital to eliminate internal cavities that could be affected by the external pressure.

One example of foam that could be used in the hull sandwich structure is Diab Divinycell [6]. The foam is designed for use as a buoyancy material and the different types of foams have different classifications referring to the hydraulic crush point (HCP). HCP30 foam has a crush point of 30 Bar, or 3MPa. Loading from the sandwich skins can require the use of stronger and stiffer foam (higher HCP value) than what is required from the hydrostatic pressure alone. This can be investigated by FEA.

There can be challenges with water entering the sandwich and degrading the material and structure, for instance by freezing. These challenges require special considerations when drilling holes in the structure or performing other modifications to the skin of the sandwich. It is normal for some matrix cracking of the skin material to occur, and this can also lead to water in the core material.

The structure can be therefor be made very light weight, but it is also less robust.

#### 4.4 CHOSEN HULL MATERIAL

The previously chosen hull material was ABS plastic.

ABS (Acrylonitrile Butadiene Styrene) plastic is a thermoplastic material that combines the rigidity and hardness of acrylonitrile and styrene with the soft and ductile butadiene rubber. The result is a tougher plastic, and the service temperature range is increased. Because of the polarity of the nitrile group, ABS plastic can be painted or glued, something that can be very challenging with thermoplastics like polyethylene or polypropylene. ABS plastic comes with many types of additives, most relevant for the hull is glass or carbon fibre filling. Adding 20% carbon fibres could increase the stiffness of the plastic from 2 GPa to 12 GPa and the ultimate tensile strength (UTS) from 40 MPa to 105 MPa, while the density only increases by 8%. Also glass fibre filling is highly relevant, and 20% added glass fibres gives approximately 90 MPa UTS and a Young's modulus (stiffness) of 6 GPa with a resulting density of 1,2 g/cm<sup>3</sup>. [7] Using fibre filling in the material does however wear more on the tools used for machining the hull and the material is more expensive, and this has to be taken into account. The fibres also wear on the sheet extrusion tools, so there are few manufacturers for fibre filled ABS. It could therefore be more relevant with a stronger (yet more expensive) plastic, like Polycarbonate.

ABS plastic:

- Low cost material and manufacturing equipment
- Fast and efficient manufacturing
- Durable, tough and robust
- Good adhesive properties
- Flexible (elongation at break: 50% [8])
- Low density (1,05g/cm<sup>3</sup> [7])
- Low strength and stiffness, which affects weight

ABS plastic is thus still the recommended choice of material. It is economical to manufacture and will be more durable than a composite laminate. Even though the ABS hull will weigh approximately twice as much as a CFRP hull, the difference is only ca. 3-4 kg, which is not much compared to the total weight of the ROV, which is ca. 30 kg. The hull weighs proximately 6,6 kg with 4mm thick ABS, which is the designed thickness.

Polycarbonate (PC) could be an alternative to ABS if more impact strength, strength, and stiffness are required. However, PC is generally more challenging to glue and in some cases it is susceptible to stress cracking [9]. PC could also be blended with the ABS plastic, increasing strength and stiffness to some extent.

## 5 DESIGN

The design of the different components is presented in this chapter. The most relevant simulation results are displayed where they are applied. This is done to better communicate the design choices. All simulation documentation is found in the appendix, and the relevant documentations are referred to throughout the chapter. When weight is discussed, it is the weight in air if not otherwise specified. The submersed weight is not relevant to the requirements, as the personnel will have to lift the ROV above the surface.

The design has been created in the Siemens NX 8,5 software, backed up by hand sketches. For new components, the requirements for strength, as well as geometrical requirements and ease of manufacturing and assembly were considered. Fast hand sketches visualizing different ways to satisfying the requirements were made, and suitable commercially available substitutes were sought after. Commercially available substitutes were evaluated by cost, how well they fitted the requirements, how they would affect the total design and how they would impact the total user experience. If there was no satisfactory commercially available product, or it was found feasible to design custom components, a geometric design was created. The geometry were been based on engineering knowledge and experience. The components were analysed using Siemens Nastran solver in NX 8,5 with SOL 101 Linear Statics –Global Constraints solutions [10] if not otherwise specified. If the component is sufficiently strong and stiff, it is added to the assembly. If there are large stress concentrations that could be avoided or any of the structural response requirements are not met, the part is redesigned and analysed again. The design process is displayed as a flow chart in Figure 8.

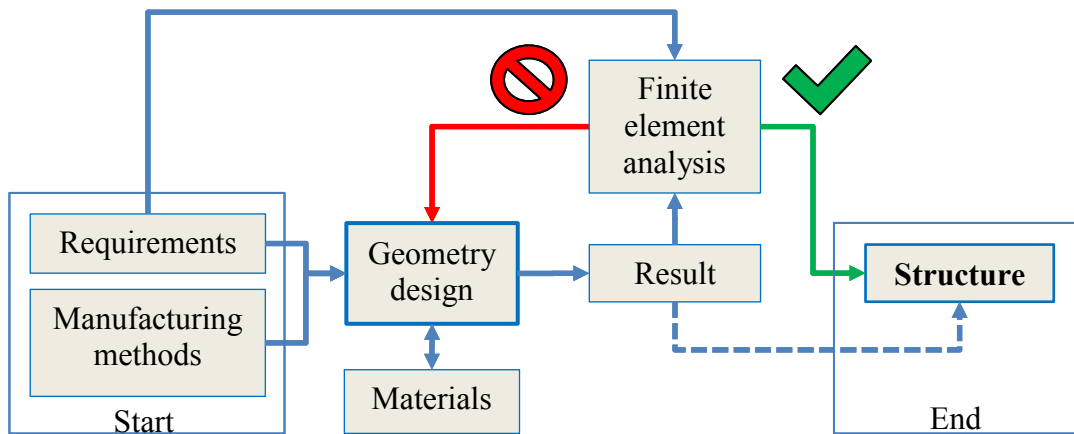


FIGURE 8: DESIGN PROCESS FLOW CHART

The modelling has been done using a combination of sheet and solid modelling. Some shapes and features lead to challenging design issues when using solid geometry, so surface modelling had to be used [10]. Since the hull has a complex shape, other components were designed using the hull part file, and linked to new part files. This was done in order to ensure perfect fit on a complex surface. The design is founded on engineering theory and confirmed by finite element simulations.

When evaluating the structural response and material utilization, the von Mises stress is compared to the yield strength of the material. The material is assumed to yield when the von Mises stress reaches the yield strength of the material. Material utilization is defined as the ratio between the von Mises stress and the yield strength of the material. Simplifications have been made to many of the analyses. This is done in order to save time, but there might be higher stresses located around the removed details. It can be argued that the von Mises yield criterion is inaccurate when used on plastics as the material could yield when only subjected to isostatic stresses. This has not been taken into account as the von Mises yield criterion is thought to be sufficiently accurate for these engineering purposes.

There are some uncertainties with respect to geometry and component selection, so a parametric design has been prioritised when possible. Parametric design is more time consuming to create, but it allows for easy changing model geometry through its key parameters. Parametric design is mainly used in the thrusters, but also for some of the electronic components.

The complete NX assembly is seen in Figure 9.

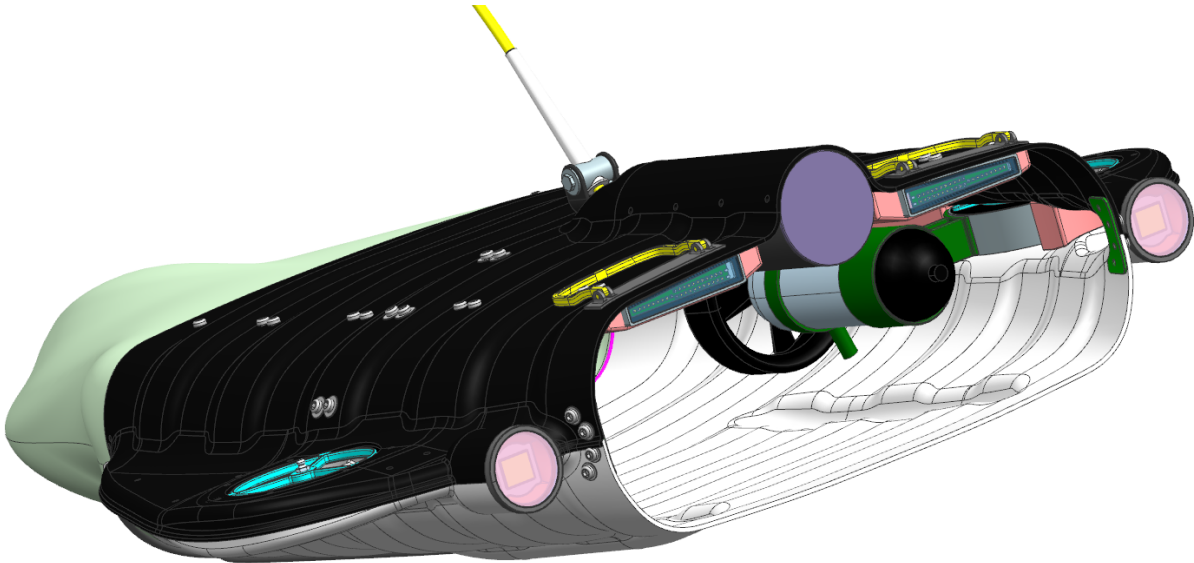


**FIGURE 9: THE COMPLETE ASSEMBLY IN NX**

The graphics has mostly been rendered in Luxion keyshot 4,3 due to its superior rendering quality compared to build in render tools in NX.

## 5.1 CONCEPT

The concept of the Manta is to utilize the main thrusters to create a flow of water through the hull cavity. This flow of water will suck any dead fish through the hull and into a net located at the rear of the ROV. The principle is just like a jet pump / ejector pump, which is illustrated in Figure 10. In this kind of pumps, a smaller flow at higher velocity creates a resulting larger flow with a lower velocity.

During the first meeting with the management and technical representatives from Argus RS, Mohn Drilling and Inventas AS some basic requirements were presented, and a 3D model, displayed in Figure 11 was quickly created. This first version of the model was made to better explain the principle and to demonstrate the concept. The suction concept is proven to work with the original Manta, where fish collection could be observed on the monitor during operation. Fish that were longer than the hull opening were oriented and guided through the hull cavity without problems.

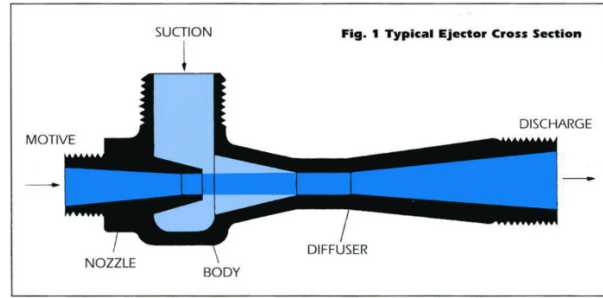


FIGURE 10: PRINCIPLE OF A JET PUMP [42]

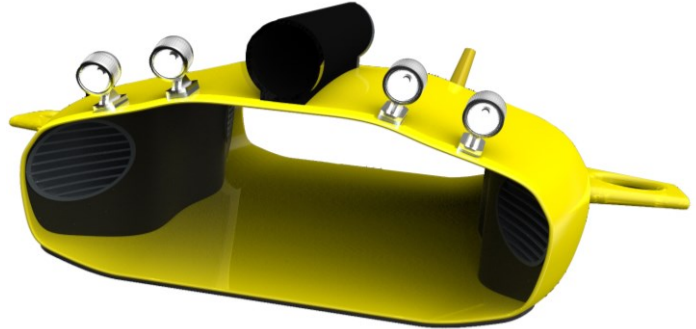


FIGURE 11: CONCEPT DESIGN

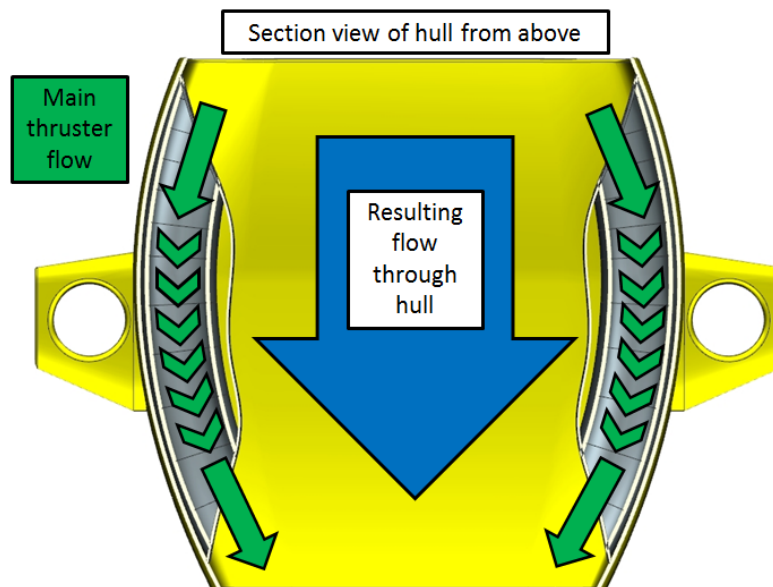


FIGURE 12: CONCEPT DESIGN WATER FLOW

On the Figure 12 the ejector pump principle is shown implemented on the Manta, and the flow is illustrated. The green arrows represent the water flow through the main thrusters and the blue flow sucks fish through the hull while the ROV is pushed forward. The flow goes through pipes in the early design because the original Manta had these. They were later removed because there was found no need for them.

## 5.2 MAIN HULL

The primary design objective for this thesis is the hull of the ROV. The hull is the largest component of the ROV, and all the components are mounted onto this structure. It also needs to protect important parts from impacts or accidental loads. The wings are primarily designed to protect the side thrusters from entanglement, but they also protect the side-thrusters from accidental loading. The hull is made symmetric about the vertical centre plane, and the wings are symmetric about two planes. This is done in order to simplify manufacturing of the hull itself and the components that will be mounted on or inside of it. The same thruster insert can therefore be fitted in both wings. The hull was first designed so it could be manufactured in two pieces by the same mould, but there were later added features to the hull that could not be mirrored. This includes rear thruster holder, mount for electronic cylinder and rails on the bottom. The early design with symmetric upper and lower hull can be seen in chapter 14.

The hull is very exposed the surroundings. Therefore a lot of effort is put into the design and material specification of the main hull. First of all, the geometry is curved in two directions. In combination with being corrugated, this creates a stiff geometry. Stiff hull geometry is wanted because some of the components are stiff, so if the hull flexes unwanted contact forces could occur. The ABS plastic used has a low material stiffness (Young's modulus) and that requires geometry stiffening in order to keep its shape during loading. The hull is designed for manufacturing by vacuum forming. That means both sections have a positive draft angle so they will not stick to the mould. Plexx AS [11], a plastics manufacturer, has confirmed that the design will work well with vacuum forming.

The hull that was designed in the project thesis that is displayed in Figure 13 [1] did not have any corrugation. After a revision early in this master thesis it was found that creating a corrugated surface with only 6mm offset distance, the simplified hull became approximately 45% stiffer with respect to lifting. The corrugated design, illustrated in Figure 14, will also improve stiffness with respect to accidental loads and bumps. The result is better protected internal components. The hull is made of 4mm ABS thermoplastic sheets, and the current design is estimated to weigh 6,6kg. The design will be explained in this chapter.



FIGURE 13: SMOOTH HULL FROM PROJECT THESIS [1]



FIGURE 14: CORRUGATED HULL

### 5.2.1 MESH CONVERGENCE ANALYSIS

When analysing the hull of the Manta, the CTETRA(10) 3D mesh has been used. It can be argued that the CTETRA(10) mesh might be too stiff when there is only one element in the thickness of the body. A mesh convergence test has been conducted on a simplified hull to analyse the element size's influence on displacement and stress. The CTETRA(10) mesh was used for consistency when detailed analysis of for instance adhesive or bolted connections would be performed.

The simplified corrugated hull was used for the study. The hull was sectioned in four parts, creating two 200mm wide centre sections and two side sections. These were later connected using mesh mating. The hull has a totally fixed constraint on the lower middle section and 500N upward force is applied to the upper middle section, see Figure 15. The interfered element size by NX is 15,1 mm.

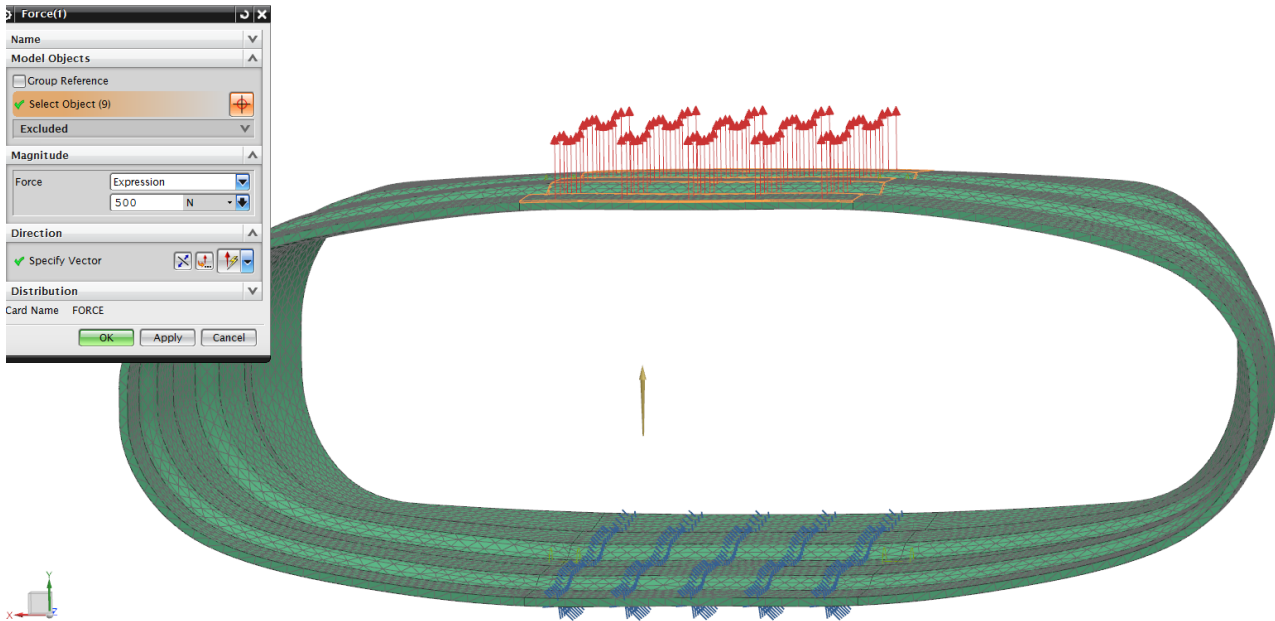


FIGURE 15: MESH CONVERGENCE ANALYSIS LOAD STATE

The rigid constrain resulted in maximum stress at the boundary areas to the fixed constraint, displayed in Figure 16. This kind of localization of stress is close to what is expected around stress concentrating geometry on the detailed hull. 2,5mm mesh was the finest mesh analysed due to hardware limitations.

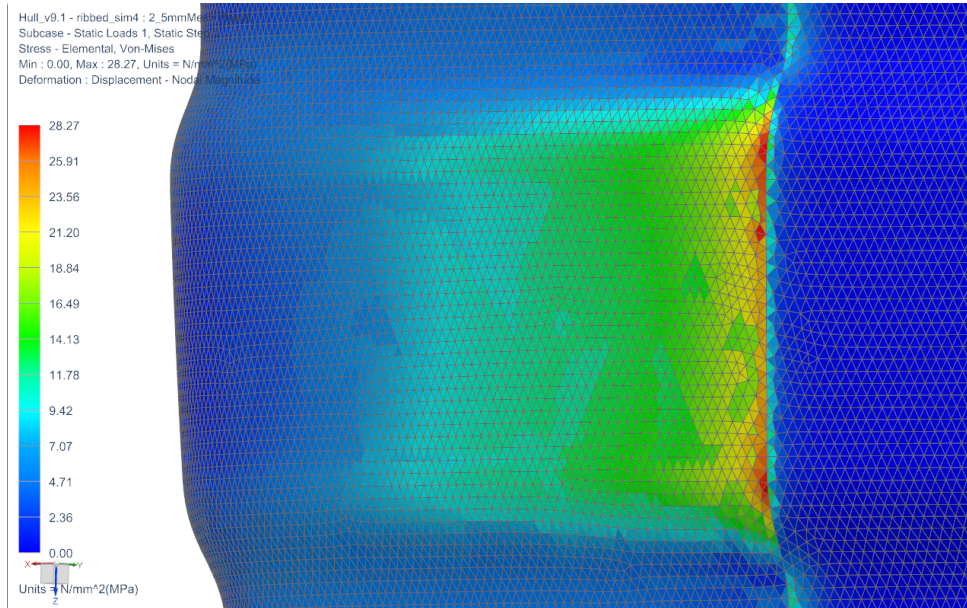


FIGURE 16: 2,5MM MESH BOUNDARY AREA STRESS

Element size [mm]	Number of elements	Displacement[mm]	Stress [MPa]	Stress AVG [MPa]
2,5	1 108 497	98,30	28,27	27,88
3	475 284	98,23	33,28	27,55
4	263 130	98,15	26,58	24,71
5	169 108	98,11	22,30	20,64
10	50 586	97,82	19,54	18,74
15	34 462	97,57	18,25	17,65

TABLE 3: MESH CONVERGENCE TEST RESULTS FROM SIMPLIFIED HULL

The *Stress AVG* column displays the average stress values of the 10 highest stressed elements. This is done in order to even out singularities that can occur at transition areas or stress concentrations.

In Figure 17 the 10 highest loaded elements in the 3mm mesh are identified. The difference from the element with the highest stress to the one with the 10th highest stress is 26%. This kind of singularities is evened out by using the average of the 10 elements with highest stress. In Table 3 this is referred to as *Stress AVG*. It is thought to represent the stress levels better than the single maximum value, which is called *Stress* in the same table. Therefore it is the data from the *Stress AVG* series that are used for the evaluation of the CTETRA(10) mesh convergence results. The element size impact on the results is displayed in Figure 18, below.

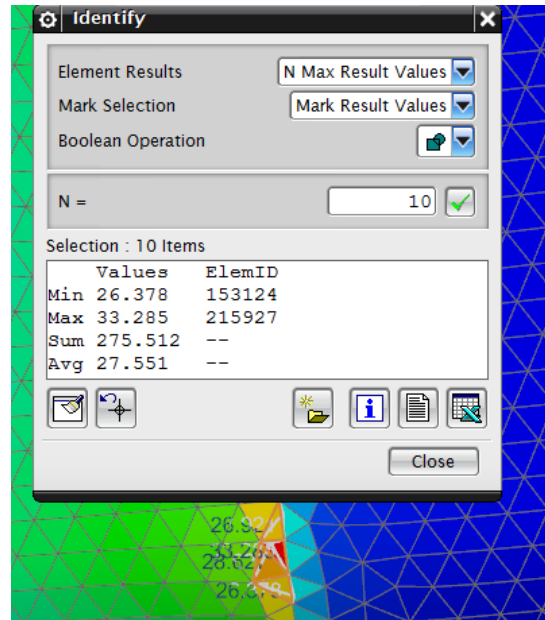


FIGURE 17: 3MM MESH - MAXIMUM ELEMENTS

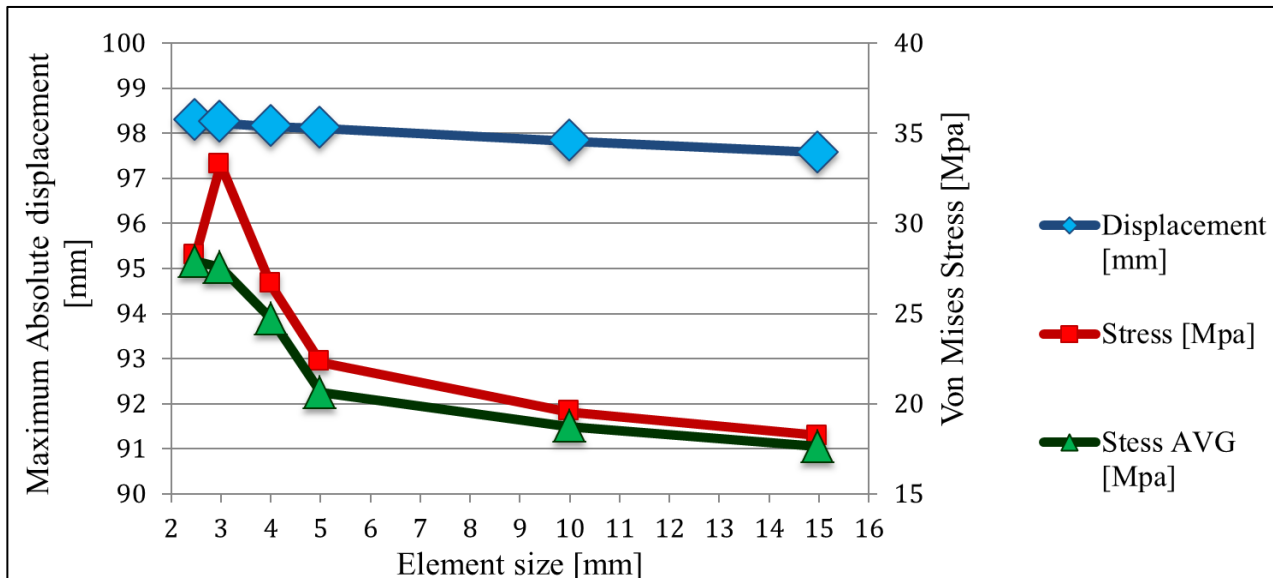


FIGURE 18: MESH CONVERGENCE ANALYSIS RESULTS GRAPH

The mesh convergence analysis results in Figure 18 indicates that CTETRA(10) elements are relatively accurate with respect to stiffness when used on this kind of structure. The difference between the displacement result when the number of elements are multiplied by 32, from 15mm elements to 2,5mm elements, is only **0,75%** on this geometry.

The stress at boundary areas or areas with high stress concentration increase when refining the mesh size. The *Stress AVG* series shows a converging trend when the element size is smaller than 3mm. At 3mm element size, parts of the structure had two elements in the thickness direction. On 2,5mm mesh the whole structure had two elements in the thickness direction.

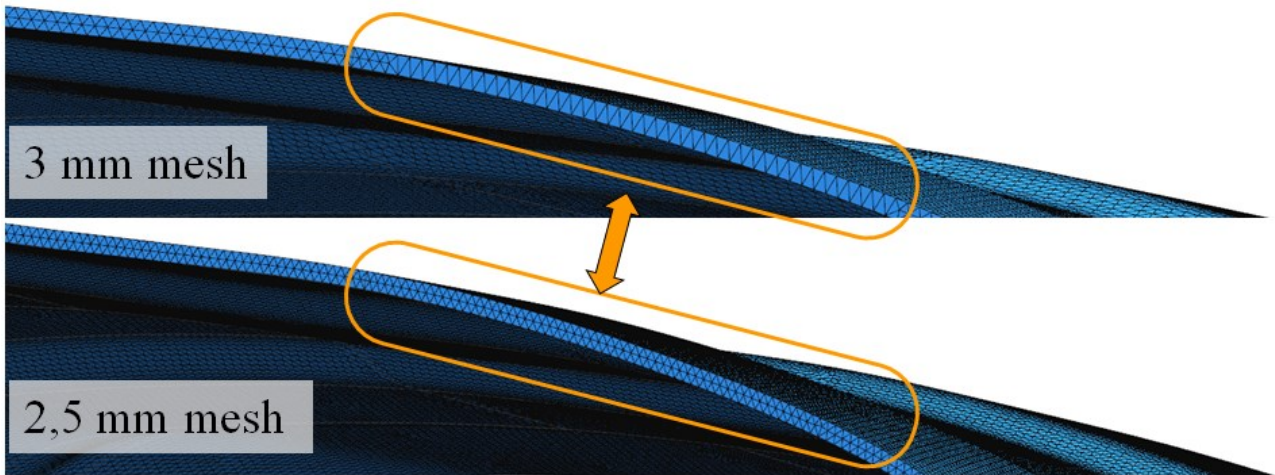


FIGURE 19: COMPARISON OF 2,5MM AND 3MM MESH

Regions in the 3mm mesh with only one element in the thickness direction can be seen in Figure 19, and the same region is shown have two elements in the thickness direction of the hull with the 2,5mm mesh.

The stress peak that occurred with the 3mm mesh is the result of a single element. This is evened out by using the average of the 10 highest stressed elements, *Stress AVG*.

From this analysis it can be argued that 3mm or finer mesh is suitable for this kind of geometry when performing a stress analysis. If the primary object of the analysis is displacement, a coarser mesh could be used, for instance 10mm.

If a mesh coarser than 3mm is used on the hull, one must expect that higher stresses can occur around stress concentrating geometry or boundary areas. This has to be taken into account when reviewing the results.

A simplified stiffness test was conducted to investigate what impact corrugation has on the stiffness of the geometry. An offset of 6mm from centre to centre of the corrugation was found to be a good compromise between stiffness, ease of manufacturing and visual appearance. The structure is 4mm ABS and it is loaded by 500N on the centre top and fixed on the bottom, the same load state as the mesh convergence analysis in chapter 5.2.1. The simplified hull had the same base shape, or general curvature as the hull, but did not have wings, skis or space for the electronic cylinder. This analysis is conducted as a comparative stiffness study. An element size of 2,5mm is used in the CTETRA(10) mesh. The displacement results from the smooth and corrugated simplified hull are displayed in Figure 20 and Figure 21 respectively.

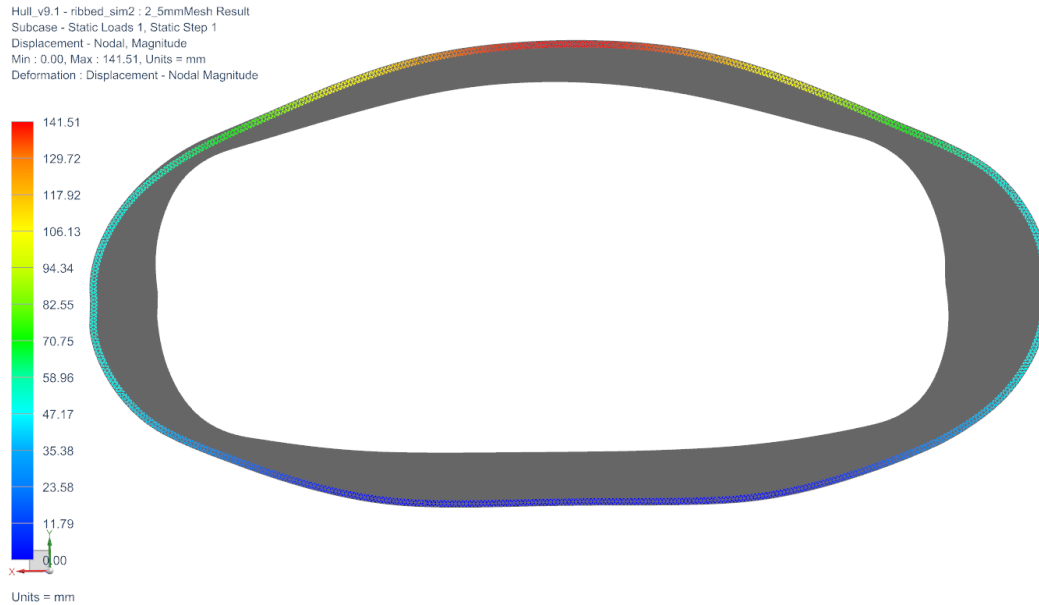


**FIGURE 20: DISPLACEMENT OF SMOOTH SIMPLIFIED HULL, MAX IS 142MM**

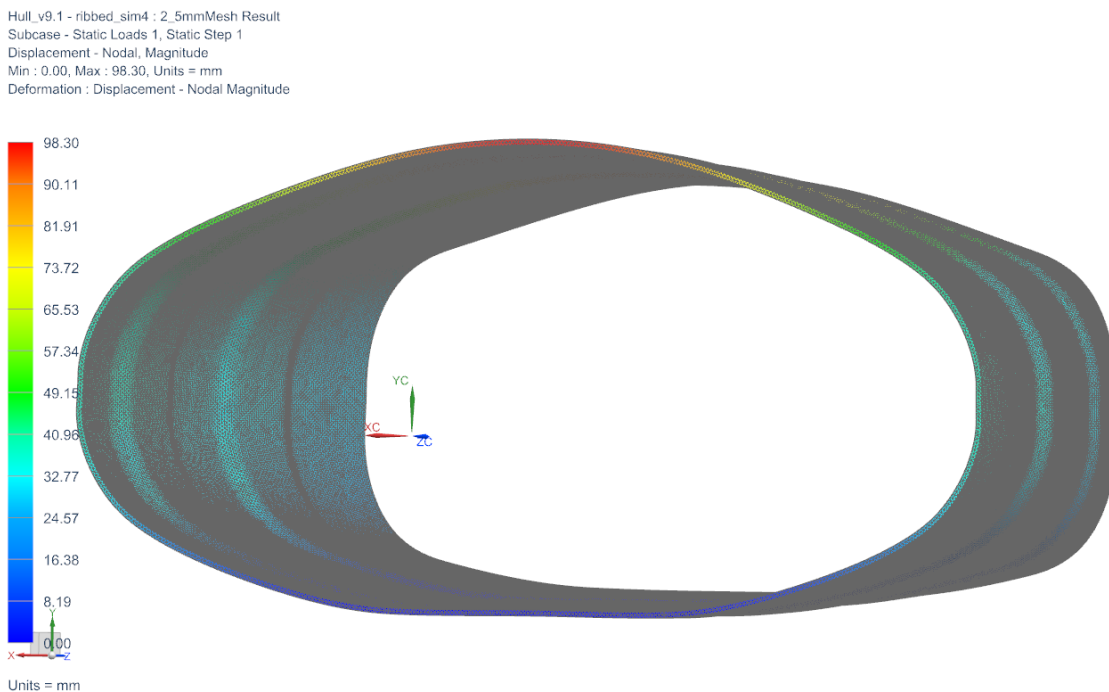


**FIGURE 21: DISPLACEMENT OF CORRUGATED SIMPLIFIED HULL, MAX IS 98MM**

The results show that the stiffness increase approximately 45% with respect to lifting. The details are found in Appendix F: Corrugated vs smooth hull.

### 5.2.2 PLASTICS JOINING

The hull is to be manufactured in two parts. The connection between these parts is an important detail, as significant forces are transferred through it, especially when the ROV is handled roughly. The connection should be strong, lightweight and cost as little as possible, both with respect to time, materials and tools.

There are two main groups of connectors; one is mechanical locking by for instance bolts, brackets or snap connections. The other group is to bond the two materials together by the use of adhesives, heat welding or solvent welding.

Adhesive and solvent welding should typically have specially designed joints that provide more contact area, because the joint is typically a bit weaker than the base material. The adhesive itself could however be stronger than the base material [9].

When designing the joint there are important design considerations to each connection that should be followed. In this chapter different joining techniques are explained and the most important design considerations are described.

### 5.2.2.1 BOLTED JOINTS

When designing bolted joints for plastics, it is important to keep the local stresses at a reasonable level. Compressive stresses are also better for the material than tensile stresses, which require flat washers to be used. Possible connection types could be flanged, joggled or bracket supported butt joints. Bolt pretension is an important aspect of a bolted joint. The pretension ensures that the load is transferred by friction at the joint surface rather than shear loading through the bolts. Thermoplastics experience creep, and the relaxation of polymers may lead to significant loss of the bolt pretension. This aspect requires special consideration when designing a bolted connection on a thermoplastic structure. The bolts in the hull may therefore require to be retightened after some time, which has to be included in the maintenance plan.

Positive aspects	Negative aspects
Reversible – the hull sections could be disassembled	Time consuming assembly
Requires few tools and equipment	Adds weight
Simple process - requires little knowledge / training	Bolts could protrude
Well known joint that is easy to control	Stress concentrations around the connection
	Connection has to be accessible

TABLE 4: PROS AND CONS WITH BOLTET HULL JOINTS

### 5.2.2.2 HOT WELDED JOINTS

Hot welded joints could be welded by many different techniques, here only the most relevant will be discussed. *Heated tool welding* uses a hot tool that is pressed against the connecting surfaces until they are proper softened or melted. The tool is then removed and the faces are pressed together, allowing the molten material to fuse together and solidify. The whole process is illustrated in Figure 22. The process creates a high quality welds economically once the equipment is purchased. The equipment does however represent a significant cost. [9]

The welding could also be conducted manually by a *hot air torch* or a *handheld extrusion tool*. The welding process is similar to welding of metal, and the joints are designed similarly. The equipment for hot air welding has a very low cost.

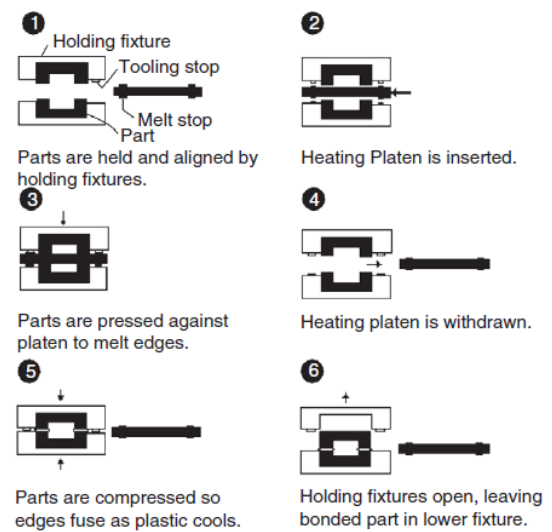


FIGURE 22: HEATED TOOL WELDING [9]

For extrusion welding it is more expensive but faster than hot air welding, and the weld quality is higher due to better controllability. The processes are however much more time consuming than heated tool welding. [9]

Positive aspects	Negative aspects
Lightweight, smooth and strong joint	Costly equipment for <i>heated tool welding</i>
Relative low stress concentration	Requires automation or trained personnel
Visually pleasing weld after treatment	High temperature can degrade the material
Welding can be integrated in the vacuum forming	Unwanted weld flash may be created

TABLE 5: PROS AND CONS WITH HOT WELDED HULL JOINTS

### 5.2.2.3 SOLVENT WELDED OR ADHESIVE JOINTS

The *solvent welding*- or *solvent cementing* process uses a solvent to fuse the material together. With solvent cementing, the solvent blend contains dissolved polymer, which improves the ability to fill voids and gaps. The solvent reduces the glass transition temperature of the material, creating a soft and sticky surface. The surfaces are then pressed together and held in place until the solvent has diffused out and the normal material properties have been reinstated. The diffusion is time consuming, typically taking many days. [9]

*Adhesive joints* are similar to solvent-cemented joints, but the adhesive is different from the base material. With adhesive joints, proper cleaning and surface treatment is vital. It is recommended to use a sandpaper or similar to grind down the surface, and then wash it with a non-destructive solvent. The curing time is typically shorter than solvent welds, where curing within a few seconds is possible.

Both the adhesive- and the solvent joint require some surface area to be efficient. If the wall thickness is small, the plate ends should overlap, creating a larger contact surface. This lowers the stress and ensures shear loading of the joint. Recommended joint designs are displayed in to the left in Figure 23. It is important to design the join with respect to load state. Generally, cleavage- and peeling loads should be avoided, Figure 23-(d) and (e) respectively [9].

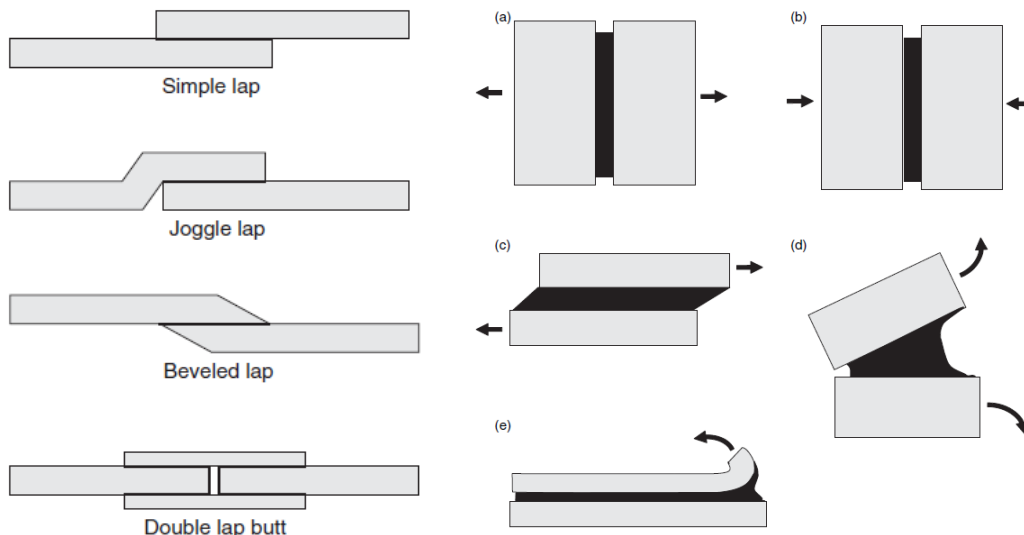


FIGURE 23: RECOMMENDED SOLVENT- AND ADHESIVE PLATE JOINTS (LEFT) AND DIFFERENT LOAD STATES OF A JOINT (RIGHT) [9]

Positive aspects	Negative aspects
Low stress concentration	Requires more surface area
Smooth joint	Not as strong as hot welds
Simple and relatively fast operation	The solvent cements are often hazardous
Requires little tools and equipment	Curing may increase cycle time

TABLE 6: PROS AND CONS WITH SOLVENT WELDED OR ADHESIVE HULL JOINTS

#### 5.2.2.4 SELECTED SOLUTION FOR HULL JOINING

The hull sections could be joined using several different methods, which all have positive and negative aspects. The joint is critical to the Manta, so it has to be tough and durable.

As discussed in chapter 5.2.2.3, using suitable adhesives creates a strong bond. The joint should however be designed specifically for gluing, which implies a sufficiently large contact area. It is also important that the materials and bonding agents are compatible. The load state of the joint is also important for a glued connection, as peeling and cleaving loads should be avoided. A joggled joint (overlap) has been designed for gluing these sections together.

Some manufacturers, like Plexx AS [11], have the machinery to vacuum form and hot weld the hull together in a combined process. This vastly reduces cycle time, however the tools costs twice as much as the standard vacuum mould and jig, but each hull gets 10-15% cheaper. This estimation does not include the cost of manual assembly, which will represent a substantial portion of the hull cost for other joint connection designs. If it is assumed that bolts, brackets and labour cost at least 200 NOK per hull, the required number of units is approximately 400 to break even compared to the typical tool and hull cost.

As for now, the designed way of joining the hull is a combination of bolts and glue. Thrusters and buoyancy units in the wings require through bolts, and these bolts plus bolts and brackets at the two hull openings will hold the hull together. The glue is added to relieve stress concentrations and as redundancy. The overlap of the hull and the bolt connection can be seen in Figure 24.

All the components can be removed from the hull without disconnecting the two hull sections. A permanent bond will therefore not violate the requirements.

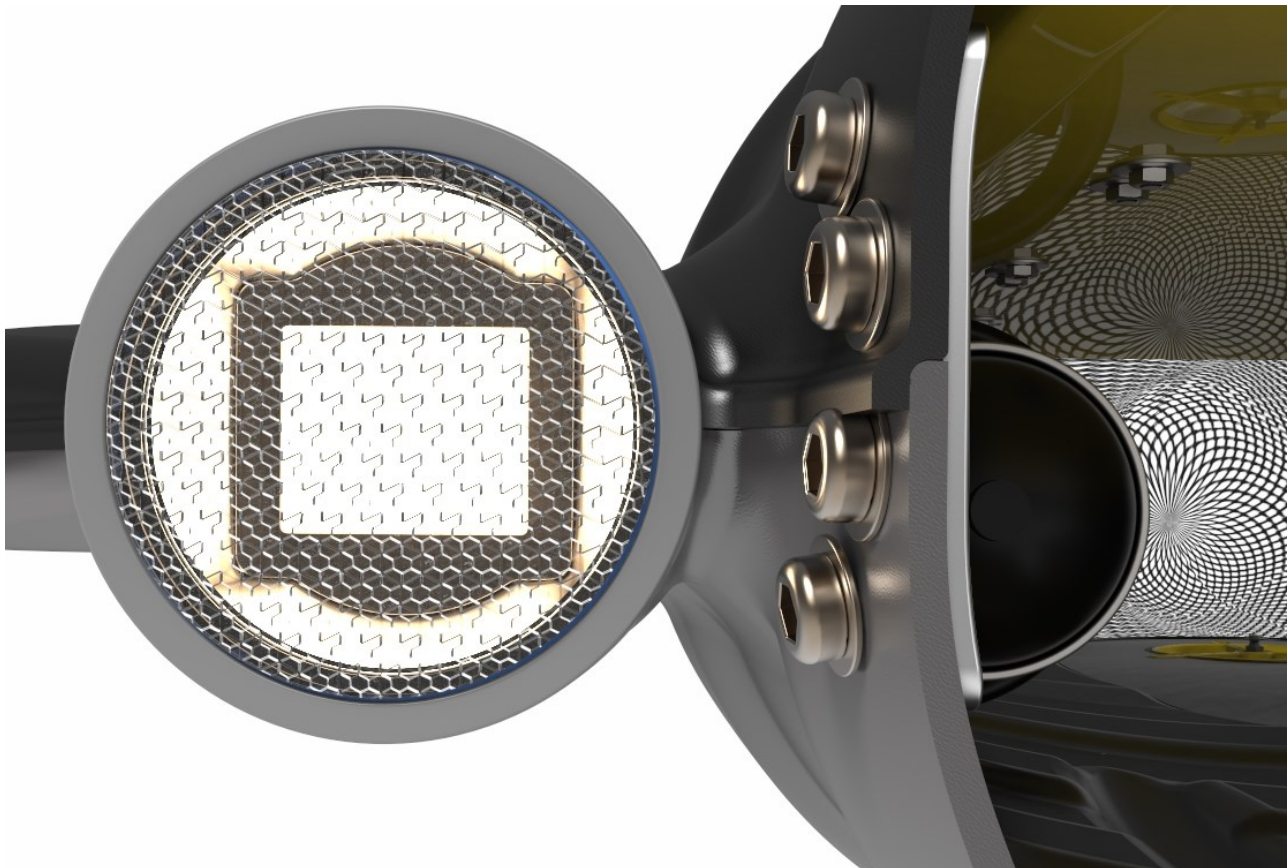


FIGURE 24: HULL SECTION OVERLAP

### 5.2.3 HULL STRENGTH

The hull has been analysed and modified several times in order to minimize stress concentrations and material use. This is done in order to reduce weight without getting a vulnerable structure.

Due to the size of the body, a coarser mesh than what is recommended from the mesh convergence analysis results in chapter 5.2.1 is used. The stresses at boundary areas or areas with stress concentrating geometry may therefore be higher than what is indicated from these results. This must be taken into account when evaluating the outcome.

Highly conservative loads are used in the analysis, where the applied umbilical lifting force of 1500N is 50% larger than the design load. The structure will only be loaded in this fashion if the operator loses power or control over the ROV. The most efficient way of getting the Manta to the surface will be to use the propulsion system rather than pulling the umbilical.

Hull\_v12\_ribbed\_sim1 : Copy of Solution 1 Result  
Subcase - Static Loads 1, Static Step 1  
Stress - Elemental, Von-Mises  
Min : 0.00, Max : 391.83, Units = N/mm<sup>2</sup>(MPa)  
Deformation : Displacement - Nodal Magnitude

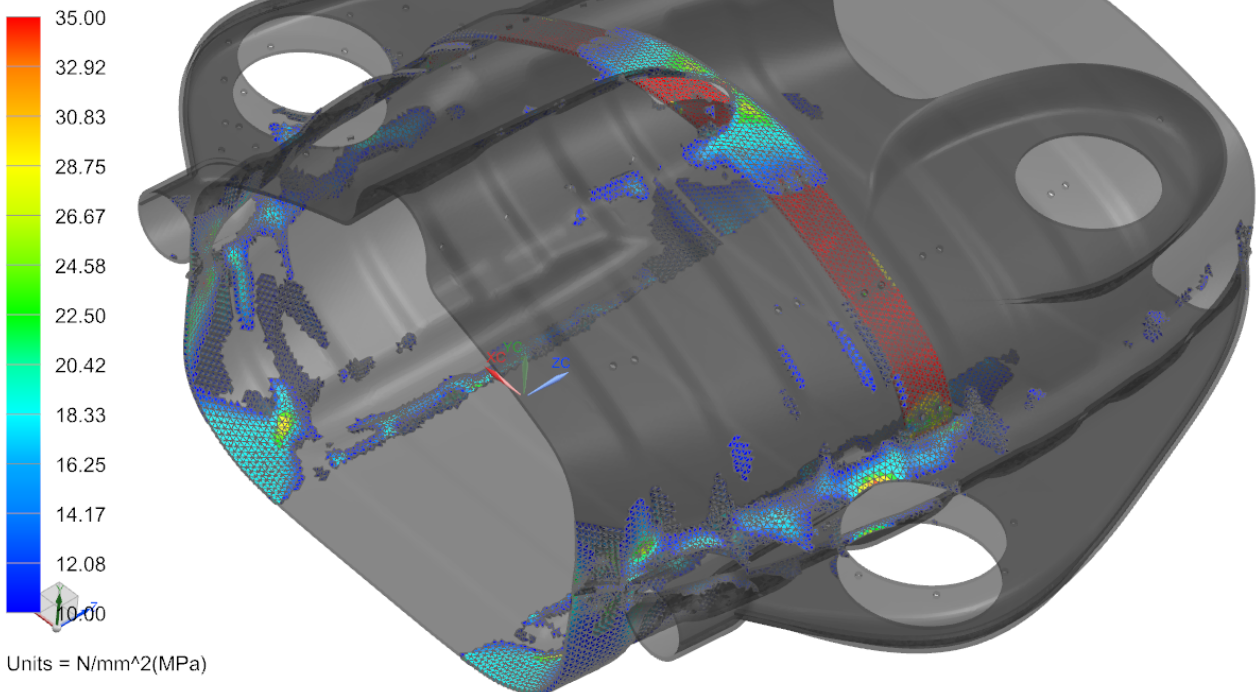


**FIGURE 25: HULL STRESS PLOT**

The 4mm ABS hull has been analysed with the aluminium load distribution bracket (see chapter 5.7.1). The mesh were 6mm CTETRA(10) for the whole assembly, and the two hull parts and the bracket were all glued together using standard surface-to-surface gluing [10].

Elements with stress below 10MPa are rendered transparent in Figure 25 for better overview of the situation. The stress level of 35 MPa is set to maximum to focus this plot on the hull, which has much lower stress levels than the aluminium load distribution bracket. Note that most of the structure has a von Mises stress below 10MPa.

From the plot in Figure 25 it can be seen that the stress levels of the hull are below the typical yield strength of ABS, which is about 35 MPa. Higher grades of ABS can have yield stress of up to 51 MPa [7]. The stresses at some areas, like the umbilical hole and thruster holes, are close to the yield strength. However, it is thought that the components that distributes loads and support the hull will lower the general stress around these areas. These components include thruster assemblies and buoyancy units. Due to the complexity of a complete assembly FEM analysis and due to the fact that the details of many components still are unknown, this type of analysis has not been conducted. Stress concentrations around features like bolted connection are not considered, and higher stresses may occur at these areas. This must be taken into account when reviewing the results.

Maximum displacement is 135mm, which is considerable. This value will most likely be substantially reduced by the support of the main buoyancy unit. The total result is therefore seen upon as satisfactory.

**Details around this analysis and other load scenarios concerning the hull are found in chapter 20: Appendix K: Hull simulations.**

The rear wing has been simulated using a 500N force. When applying an upwards force of 500N around the rear thruster hole, high stresses were found where the rear wing connects to the hull. Although the rear wing will be considerably supported by the upper lid and the thruster, the results indicate a need for a rear thruster bumper or other sort of support. These high loads could for instance come from dropping the Manta down hard on the deck or other dynamic loads. Thrust force from the rear thruster in operation will most likely be about 100N. The 500N magnitude can only come from accidental loading, in other words operator error. The load is set relatively high since no dynamic simulations have been performed. The load of 500N is considered to be conservative, since the Manta will weigh approximately 30kg.

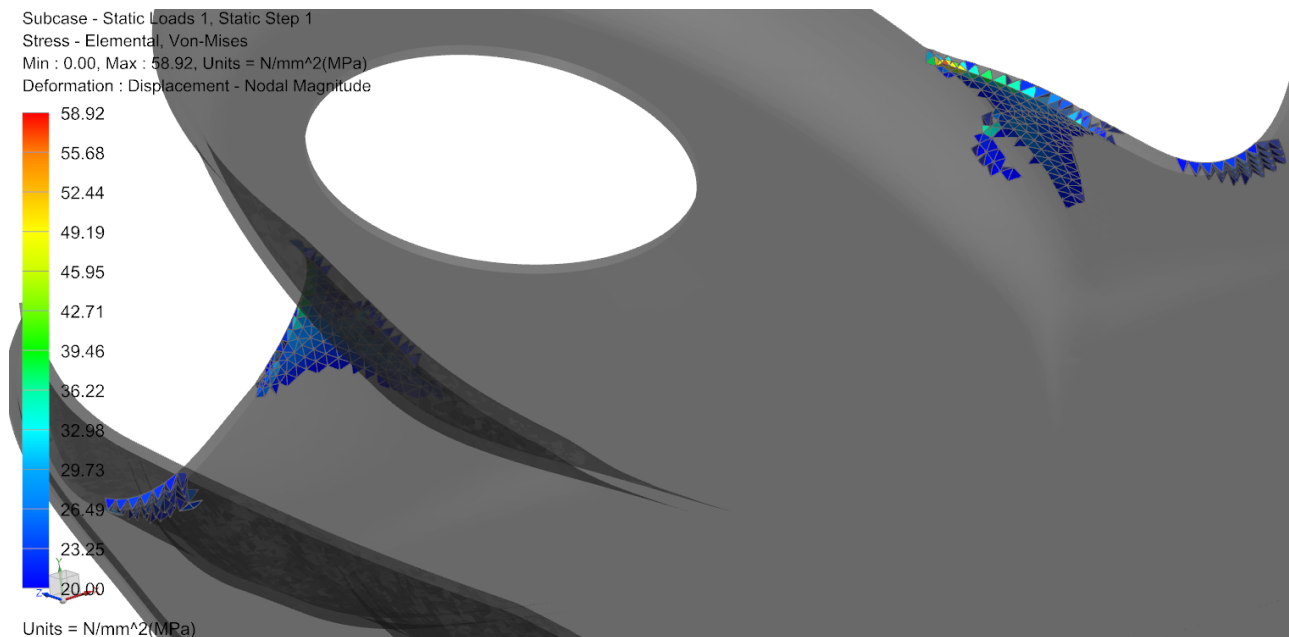


**FIGURE 26: STRESS PLOT FROM REAR THRUSTER WING**

Elements with stress below 20 are rendered transparent because they are considered unproblematic. The stress plot in Figure 26 shows stresses above yield strength, which is typically 35 MPa for ABS, at the outer surface of the rear wing. Since this is a linear elastic analysis, yielding is not accounted for. The material will yield and experience plastic deformation at the highest loaded areas. This will most likely damage the rear wing, especially over time. The stress is highly localized, which can be explained by a bad transition from the rear wing to the main body. The stresses can be reduced by using a larger radius on this transition. The highest loaded elements are located at a very sharp edge, which will be smoother in reality.

In order to protect the rear thruster wing, a simple design for a rear bumper has been developed. This bumper consists of three curved aluminium tubes, the lower one is  $\varnothing 16 \times 12 \text{mm}$  and the two side tubes are  $\varnothing 14 \times 10 \text{mm}$ . The weight of this structure is 390g and it is connected at the rear hull bracket and through the end of the rails. This bumper would take most of the force from hits to the rear wing and minimize deflection.

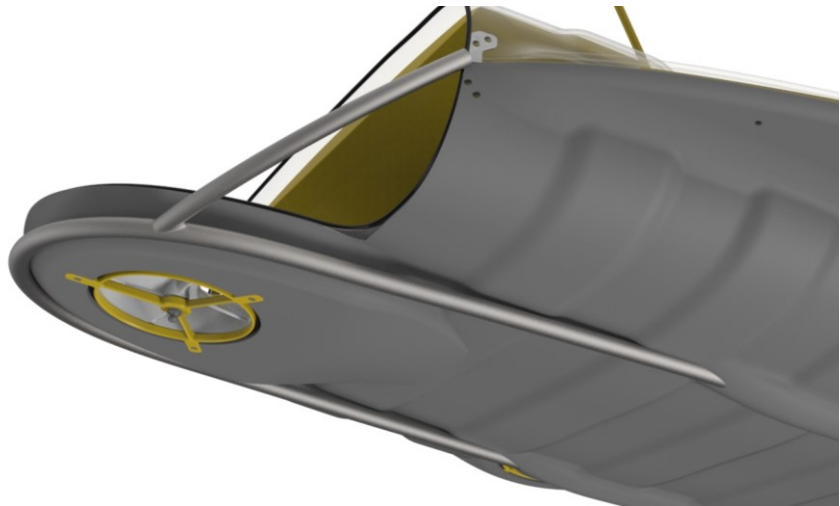


**FIGURE 27: REAR WING BUMPER**

One can argue that it is better to replace the hull if damaged, rather than adding a bumper which adds weight and costs money. The Manta hull cost approximately 1000 NOK excluding tools, and can be considered a wear part. The load is also considerably higher than what is expected by normal use. The need for a rear bumper must be decided by Argus RS, since loads of this magnitude has to be caused by operator error.

### 5.3 ELECTRONICS PRESSURE VESSEL

The electronic components, excluding lamps and thrusters, require a dry environment. In order to reduce complexity and ease assembly, all these components have been gathered in one pressure vessel. The container needs the integrity to withstand the hydrostatic pressure at a water depth of 100m. The pressure used in the analysis corresponds to 150m water depth, 1,5MPa. Since the cylinder is on the top of the ROV the buoyancy should be positive, which will result in more stable handling in the water. The current design weighs 850g and has a volume of two litres. That means that the weight of the internal components can be up to ca. 1100g and the cylinder would still be buoyant. The contents of this cylinder will amongst others be HD camera, sensors, power controls and main circuit board.

Argus RS has experience with using tubes made of CFRP, Aluminium and Titanium for pressure vessels. The power control units create a lot of excess heat inside this container, and if the heat is not removed the electronics will suffer or seals could fail due to high temperature or thermal expansion etc.

The cylinder will be made out of aluminium, which is a good compromise between material cost, machinability and thermal conductivity. Argus RS has good experiences with using aluminium in their already existing ROV solutions. The aluminium easily conducts the heat from the electronics that would be problematic in CFRP or thermoplastic cylinders. The lens is made out of PMMA due to optical properties and low cost.

The electronics container is subjected to exterior pressure; a load state that when combined with the thin-walled structure of the cylinder will most likely result in buckling if the pressure gets too high. This sudden failure is caused by the compressive stresses in the structure; stresses lower than the ultimate compressive strength of the material. The buckling is typically initiated by a local imperfection or concentrated load. Buckling is heavily influenced by geometry, and therefore FEA is needed for accurate results.

There will only be conducted a simple dimensioning of the cylinder as the components are unknown at this time. It is however assumed to be in the about  $\varnothing 100 \times L 250$ mm with a wall thickness of 3mm.. Heat sinks to the power control will be cut so that they match the inside of the cylinder perfectly. The contact surface between the power supply and pressure vessel will be applied heat sink paste to aid the heat transfer. In this way, the heat from the electronics will efficiently transfer to the cold seawater on the outside of the cylinder. A section view of the electronics container can be seen in Figure 28.



FIGURE 28: SECTION VIEW OF ELECTRONICS CONTAINER WITH LENS AND END-CAP

The pressure vessel cylinder has been analysed using the Nastran SOL 105 Linear Buckling solver in NX 8,5. This tube is thin-walled, and will experience exterior pressure, so buckling is the most important failure mode. Catastrophic buckling could happen if the cylinder has been dented or otherwise damaged before deep dives. Linear buckling analysis is considered to not be conservative, as the solution is based on perfectly elastic behaviour and perfect material. In real life, there are imperfections in the material and the structure that will lead to earlier buckling. Therefore, an eigenvalue of around 3 is required in combination with the standard safety factor of 1,5, where 100m design depth is dimensioned by using pressure equivalent to 150m depth. The safety factor is set relatively high because of wear and tear is expected, and this will reduce structural integrity.

The eigenvalue result tells us the ratio between buckling load and the current load, in other words how much the load could be multiplied before buckling occurs.

The cylinder has been simulated with both supported and free ends. Supported ends are more realistic, as the cylinder has end caps that would help against buckling, but to be safe the tube has been dimensioned from the case without end effects.

### 5.3.1 MESH CONVERGENCE ANALYSIS ON BUCKLING CASE

In this simulation, the tube was fixed at two nodes on one side and fixed radial movement at a single node the other side constrain rigid body movement. The constraints will not provide any support with respect to buckling. The outer pressure is set to 1,5MPa (15 Bars / 150m depth) and end forces of 11800N, representing the force from end caps with a diameter of 100mm. A mesh convergence test has been conducted in order to investigate the properties of the CTETRA(10) 3D tetrahedral mesh when used on thin-walled structures. Several element sizes were used. The largest element size used is 22,5mm which is the interfered size. The finest mesh had an element size of 1,25mm which gave three elements in the thickness direction in average. The results are displayed in Table 7 and Figure 29.

Element size [mm]	Number of elements	Displacement[mm]	Eigenvalue
22,5	2 633	1,184	3,733
10	5 011	1,174	2,869
5	20 400	1,174	2,698
3	55 054	1,071	2,683
2	150 298	1,215	2,684
1,5	313 189	1,162	2,679
1,25	728 576	1,223	<b>2,677</b>

TABLE 7: MESH CONVERGENCE ANALYSIS ON BUCKLING OF ELECTRONICS PRESSURE VESSEL

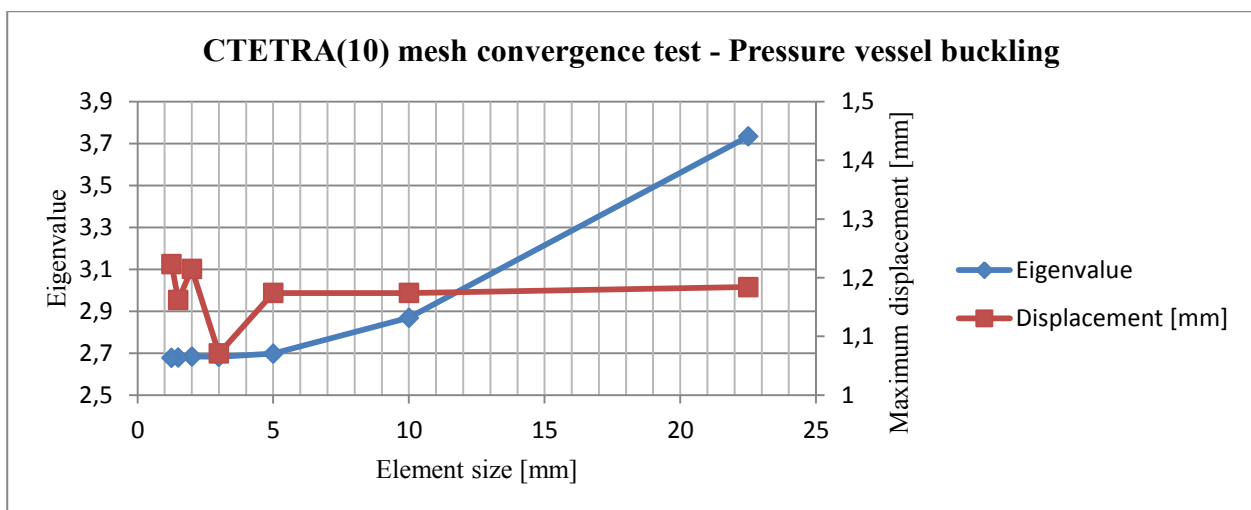


FIGURE 29: MESH CONVERGENCE GRAPH

From the results in Figure 29, it can be seen that the eigenvalue result converges to 2,7. A mesh with an element size of 5mm or smaller is thought to provide sufficient accuracy for buckling results. This is only an initial analysis to get an indication of the needed wall thickness of the cylinder. There are several simplifications to the structure, with no details on O-ring slots or connections. Further analysis is required when these details are set.

The results also show that the CTETRA(10) mesh displays some irregularities for thin-walled structures with respect to displacement. The displacement changes when the number of elements in the thickness direction changes. The deviations are however relatively small. The displacement result of the finest mesh is displayed in Figure 30.

Electronic\_cylinder\_sim1 : 1\_25mmMEsh Result  
Subcase - Buckling Method, Mode 1, Eigenvalue = 2.677e+000  
Displacement - Nodal, Magnitude  
Min : 0.000, Max : 1.223, Units = mm  
Deformation : Displacement - Nodal Magnitude

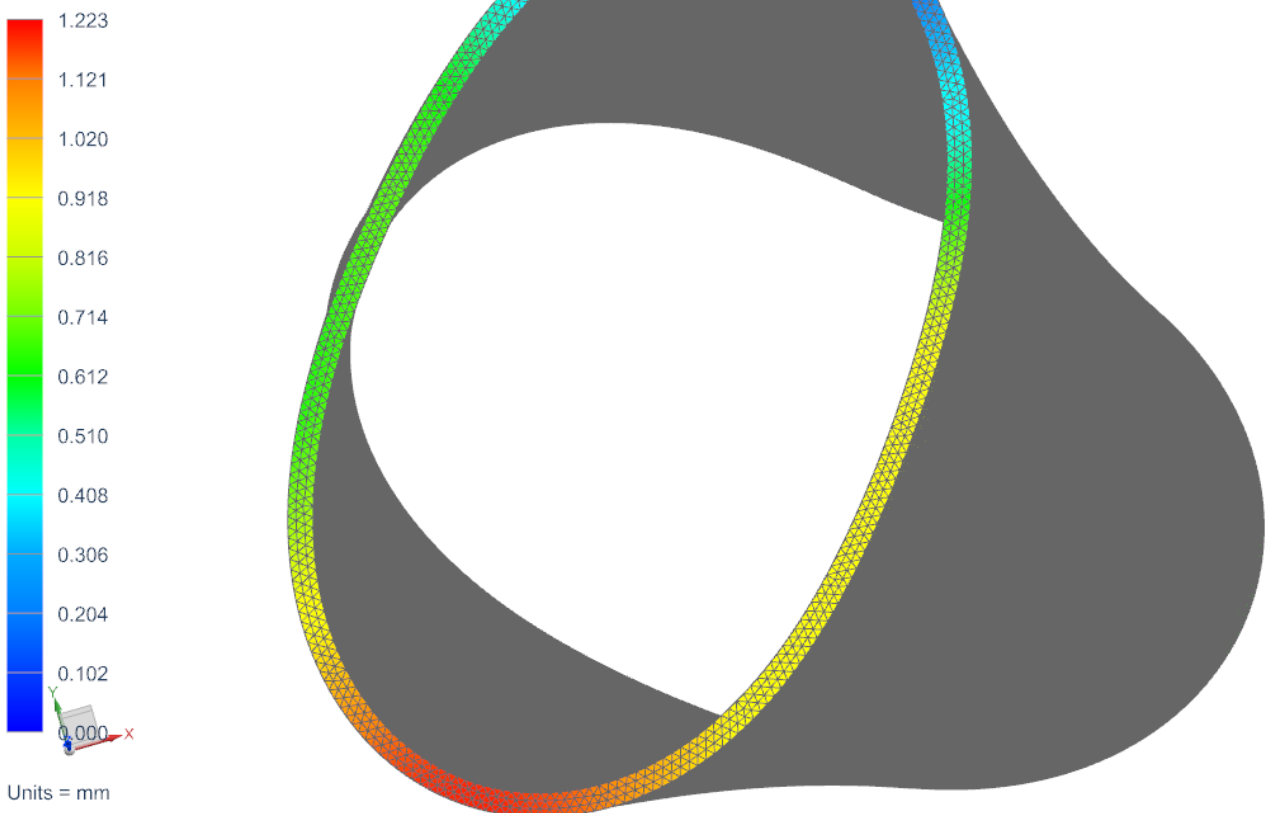


FIGURE 30: DISPLACEMENT PLOT OF MODE 1 BUCKLING OF ELECTRONICS PRESSURE VESSEL

Since the **eigenvalue result of 2,7** is based on a load case with no support from end caps and a relatively high safety factor, it is regarded as satisfactory. This must however only be viewed as an initial analysis of the macro geometry. The structure is simplified, as the internal components are not specified.

## 5.4 THRUSTERS

The thrusters are electrical motors with attached propellers, and they create the thrust force needed for an ROV's propulsion and orientation.

The thrusters are some of the most important components of an ROV. The Manta will feature three vertical and two horizontal thrusters. The propulsion is primarily provided by the two horizontal thrusters, whereas the three vertical thrusters position and orient the ROV.

During this initial phase of development, no flat thruster solutions that fit the Manta's needs were found. Typically an ROV is bulky, like Figure 31, and slow, so there is no need for a low profile thruster. A conventional ROV thruster is shown in Figure 32 to the left.

In the Manta, the three vertical thrusters have to have as *low profile* as possible, as they are located on the wings. As for any other component in the Manta, low weight is also very important.

A new trend in the ship industry is the use of rim-driven thrusters (RDT). In RDTs, like Figure 32 to the right, there is no need for a centre hub, and the magnets are located at the outside of the propeller, creating a large diameter motor with a low profile. This results in higher torque density per height [13]. The challenge is the bearings, often a combination of magnetic and hydrodynamic bearings is used [14]. It is important that the Manta is streamlined to be fast, so conventional thruster designs are not suitable for vertical thrusters. At this time, there were not found any small-scale flat RDTs that could fit the Manta's needs.

Since the design requires low profile vertical thrusters for the wings, it has been a goal to develop a concept for these. These flat rim-driven thrusters could also be sold separately if the design is a success.

For the horizontal thrust, commercially available solutions will be used. The horizontal thrusters do not have the same space- and geometry requirement as the vertical ones. Many conventional solutions could fit this need, so the horizontal thrusters will be selected mainly with respect to price, weight and thrust force.



FIGURE 31: TYPICAL ROV DESIGN [12]



FIGURE 32: DIFFERENCE BETWEEN CONVENTIONAL ROV THRUSTERS AND RDTs [15] [16]

#### 5.4.1 BRUSHLESS MOTOR DESIGN

The motors used in all the Manta's thrusters will be of the brushless permanent-magnet type. A brushless electromotor does not need any electrical contact between the rotor and the stator, which is the static part that contains the windings.

A brushless permanent magnet motor typically consists of a rotor with permanent magnets, a stator with windings, Hall Effect sensor(s) and a motor controller. The motor controller gets information about the rotor position from the Hall Effect sensor(s), and applies current to the correct sets of windings. This creates an *alignment* and a *repulsion torque*, by magnetically pulling and pushing the rotor respectively [17].

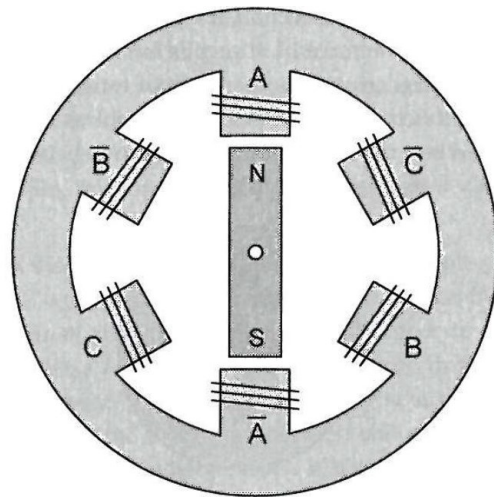


FIGURE 33: WINDINGS IN A 3-PHASE MOTOR

The simplified motor illustration in Figure 33 consists of three sets of windings, or three phases. This this motor's rotor only has two poles. The rotor magnet is aligned with A, as shown in Figure 33. To move the rotor clockwise in the simplest manner, the current could be applied to the windings C. This will create alignment torque, where the poles of the rotor magnet will be aligned to the opposite pole of the windings. One could combine this with simultaneously applying current in the opposite direction to B creating a repulsion torque. This repulsion is created by the magnetic poles of the windings push the same magnetic pole of the permanent magnet rotor. [17]

The *air gap* is the distance between the stator and the rotor, and a small air gap is generally better for the motor performance. A smaller air gap does however require tighter tolerances, which can be costly. The torque is also linearly related to the active length of the motor windings, in other words the stator lamination stack height. [18]



FIGURE 34: COMPOSITE STATOR (LEFT [15]) AND SLOTTED STATOR

The windings, which are coloured red to the right in Figure 34, and rotor magnets are in most motors mounted on a laminated steel structure. The illustration shows a slotted structure, which is the most common, but a slot-less structure is also possible.

A relative new technology is so-called ironless motors, which utilize a composite stator, displayed in Figure 34 to the left. The composite stator removes *cogging torque*, a jerky motion at lower speeds. The ironless design also creates high power- and torque density, smoothness and efficiency [19]. However, the design-RPM for this type of motor design is typically higher than what would be suitable for a larger diameter propeller in water.

These motors use neodymium permanent magnets, which are brittle and highly susceptible to corrosion. The corrosion properties are so poor because of the reactive contents and the complex microstructure of the magnets [20]. Because of this low corrosion resistance, the magnets are typically plated by metals like tin or nickel. Without this plating the magnets would soon flake or crumble in a corrosive environment. It is therefore very important to ensure that no abrasive wear or impact between stator and rotor occurs. The reason for using neodymium magnets is that they have the highest magnetic field density of permanent magnets, which enables a compact design [21].

## 5.4.2 RIM-DRIVEN THRUSTER DESIGN

In this chapter different designs for a rim-driven thruster will be presented. Basic theory about electric motors has been reviewed, but this is primarily a mechanical design. The work will be presented in chronological order, where the earliest designs comes first and the final design is introduced at the end.

### 5.4.2.1 BEARINGS

By studying existing rim-driven thrusters (RDTs) from Schottel [22], Brunvoll Thrusters [23] and Voith [24] it was found that most RDTs had a hub-less design. The rotors of these designs are supported by a combination of magnetic and hydrodynamic bearings.

Since the Mantas thrusters are much lighter and smaller than the ship thrusters, a simpler bearing technology can be used. The Manta operates in a corrosive environment, so standard stainless steel ball bearings could corrode if not maintained well. Maintenance should include flushing with fresh water and reapplying lubricant after operation. The earliest design had plastic bearings, as it was thought to be the best solution at the time.

It is unknown at this time if stainless steel ball bearings will be durable enough, because they will be exposed to seawater, abrasives and air. Ceramic ball bearings or plastic bearings (slide rings) are other alternatives. Materials used for the plastic bearings are typical phenolics, nylon, Teflon, POM, or ultra-high molecular weight polyethylene (UHMWPE) [25]. These materials have a low coefficient of friction in combination with being self-lubricating and resistant to chemicals and corrosion. Ceramic ball bearings are expensive compared to the stainless steel types. The chosen design at this time has stainless steel bearings, and prototype field testing will make sure these are up for the task before the product is launched.

### 5.4.2.2 COATINGS

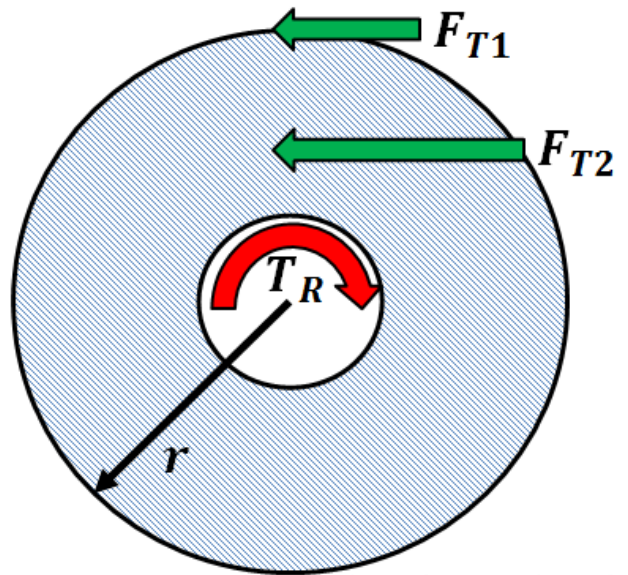
In order to shield the electronic components and vulnerable metal (magnets and stator stack) a good coating is vital. The coating has to be able to conduct heat away from the windings and withstand seawater and wear over time. Special motor coatings that conduct heat will be used, but the product details are not set at this time. Precisely embedding stators is known to be difficult, so some work has to be put into the coating design.

### 5.4.2.3 FIRST THRUSTER CONCEPT

The first vertical thruster concept had a propeller with 140mm diameter and the total height of the thruster is approximately 40mm.

Inspired by the existing ship thrusters, the first concept created had a hub-less design. Where in larger scale thrusters the rotor would be supported by hydrodynamic bearings, the design was simplified by using six plastic bearings in combination with the magnetic force. The bearings would roll on a 45 degree flange on the rotor, supporting both radial and axial forces. By using three bearings on each side, the load is more evenly distributed among the bearings and a less precise alignment is needed. The bearings are shown in Figure 36.

This bearing design was later changed because of the concern about wear and the fact that the resistance of these small diameter bearings would be far greater than a simple centre hub bearing. If it is assumed that the inner resisting torque ( $T_R$ ) is constant, a larger attack radius will require a lower tangential force ( $F_T$ ) to rotate the bearing, illustrated in Figure 35.



$$F_{T1} < F_{T2} \Leftrightarrow r(F_{T2}) < r(F_{T1})$$

FIGURE 35: ILLUSTRATION OF BEARING FRICTION

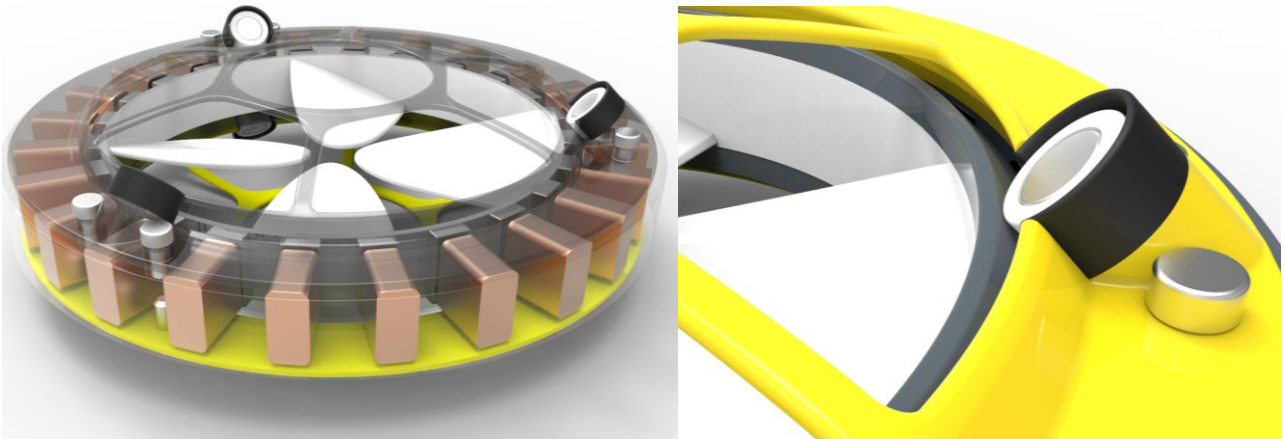


FIGURE 36: EARLY HUB-LESS DESIGN WITH ANGULAR CONTACT BEARINGS ON ROTOR FLANGE

Motor efficiency is dependent on the air gap between rotor and stator, where a smaller air gap improves torque. This bearing design will most likely require a larger air gap than a centre mounted ball bearing, because of the low precision that is expected from the roller bearings.

#### 5.4.2.4 SECOND THRUSTER CONCEPT

The second RDT concept features a single plastic bearing on each side of the rotor centre-axis, it is displayed in Figure 37. The bearings support both axial and radial loads. The bearings (opaque green) are located on a centre shaft that is fixed to the propeller / rotor. The conic outer shape ensures best possible concentricity to the stator. A stable and concentric rotor support is vital in order to minimize *air gap*, as discussed in chapter 5.4.1. If the rotor is allowed to vibrate or move radially, there is a risk of contact between the stator and rotor. This is highly unwanted, as it will wear the coatings and lead to corrosion and ultimately motor failure. The motor failure will typically come from short circuit, corrosion build-up or loosening of the magnets. It is therefore important to find an air gap that ensures minimal risk of particle abrasion and rotor / stator impact in combination with maximum torque and efficiency. Maintenance frequency must also be determined.



FIGURE 37: SECONDARY THRUSTER CONCEPT

This concept features a simple propeller with 24 magnets oriented as 12 poles. This means that two magnets simulate one pole, as they are oriented N-N-S-S-N-N-S-S and so on. The stator and windings are completely embedded in plastic in order to minimize corrosion. The plastic coating must be as thin as possible in order to conduct heat and minimize weight and air gap.

The rotor is supported by CFRP frames and plastic bearings. The rotor fixture could also be made out of aluminium, which could reduce cost. The main contributors to the weight of the thrusters are the magnets, the windings plus the stator- and rotor steel lamellas.

The second thruster concept was also purely a mechanical concept, made with only basic understanding of how a brushless motor works.

#### 5.4.2.5 THIRD THRUSTER CONCEPT

The third thruster concept is based on the second concept and what was learned from the test rig mounted prototype. In the third RDT concept, several details have been changed. This includes bearings, bearing hub and stator. The new design is presented in Figure 38, rendered with translucent casing for a better view of the internals. In this design the stator is skewed, which is seen in Figure 39. This reduces the cogging and thereby lowers the minimum operating speed.

This thruster has 24 magnets on the rotor, and the propeller diameter is 124mm. The total height of the thruster is 46mm without the grease nipple, and the casing height is 38mm.

The bearing hub will be machined out of an 8mm thick plate of 7075-T6 or similar grade aluminium. The thruster is expected by Argus to have maximum of 200N thrust force. Most likely, the thrust will be about 100N. The design thrust force is set to 200N to be safe. The radial load is harder to predict, as it is heavily influenced by how well centred and balanced the rotor is. During the assembly, a maximum magnetic load of about 750N is expected, but in the simulations 1000N radial bearing force is applied on each hub. Radial operating design load is set to 400N. The load assumptions are thought to be highly conservative.



**FIGURE 38: THRUSTER DESIGN - RENDERED WITHH TRANSLUCENT COMPONENTS**



**FIGURE 39: SKEWED STATOR**

The bearings are closed inside the hub, and a grease nipple is mounted on the top, demonstrated in Figure 40 and Figure 41. This way, biodegradable grease could be pumped through the bearing housing, pushing out old grease.

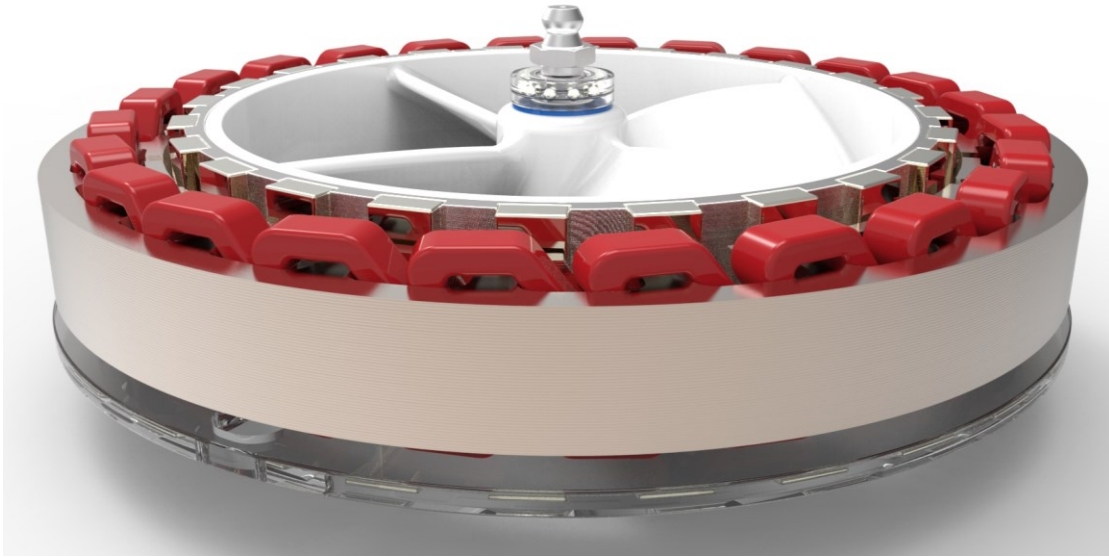


FIGURE 40: RIM-THRUSTER INTERNALS

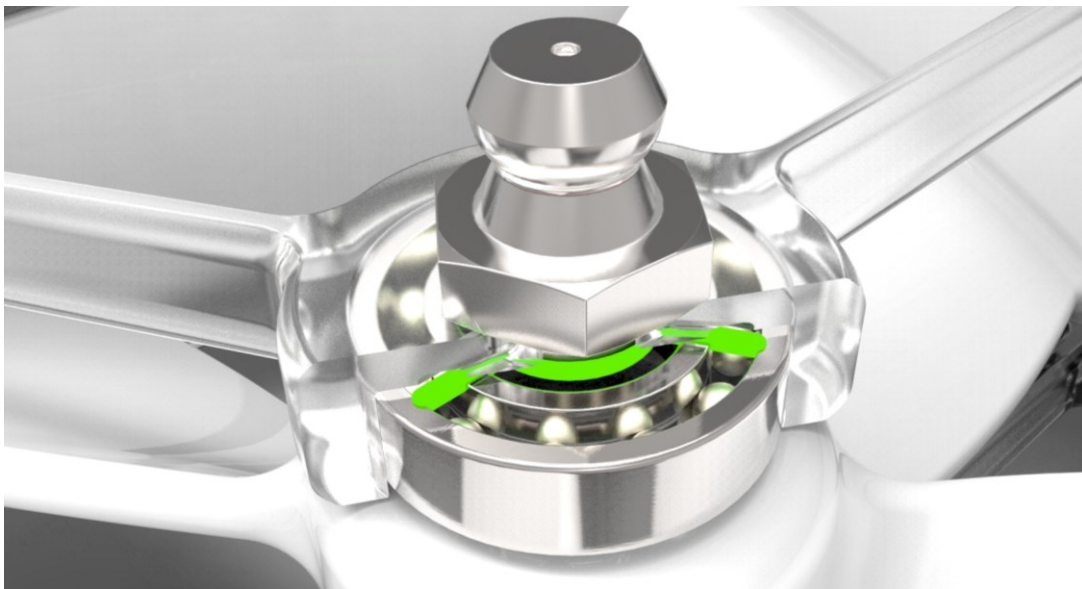


FIGURE 41: GREASE FLOW (GREEN) FROM PROPELLER HUB NIPPLE

In Figure 41, the grease flow direction is rendered green. The grease flows through small radial slots from the centre and into the ball bearings. Alternatively, closed bearings could be used, which is stated by SKF to be maintenance free within the life of the bearings [26]. The grease nipple can easily be removed from the design if found unnecessary.

The ball bearings are stainless steel **SKF W 61800** deep groove design, with dimensions of 19x10x5 mm, and they can handle 1480N radial dynamic load and 830 N radial static load. The axial load capacity is 25% of the static radial load capacity, which represents **208N**. The bearing casings and balls are made of X65Cr13 and X105CrMo17 steel respectively, these are stainless steels with good abrasion and corrosion resistance. [26] Since there are two bearings in the thruster, the load capacity will be around 400N axial and 3000N radial, which is well within the design load of the thruster, which is 200N axial and 1000N radial total.

The rotor hub is connected by three bars with a height of 8mm and a width of 3 mm, with rounded edges. The thin profile minimizes flow interruption that would affect the efficiency. The design is presented in Figure 42, where it is rendered translucent for a better view of the bearing.

The openings between the bars are a maximum of 50x100mm. This opening is potentially large enough to let salmon get hurt by the propeller. Covering the thruster opening with a mesh may therefore be required. An alternative is to increase the number of bars to the hub. The 3D-model is parametric, so doubling the number of bars and decreasing the thickness will only take seconds. Whether this will be required is not known at the time. Argus has experienced that the salmon keep a distance from the ROV, but thorough camera monitoring during the testing is required in order to verify this.

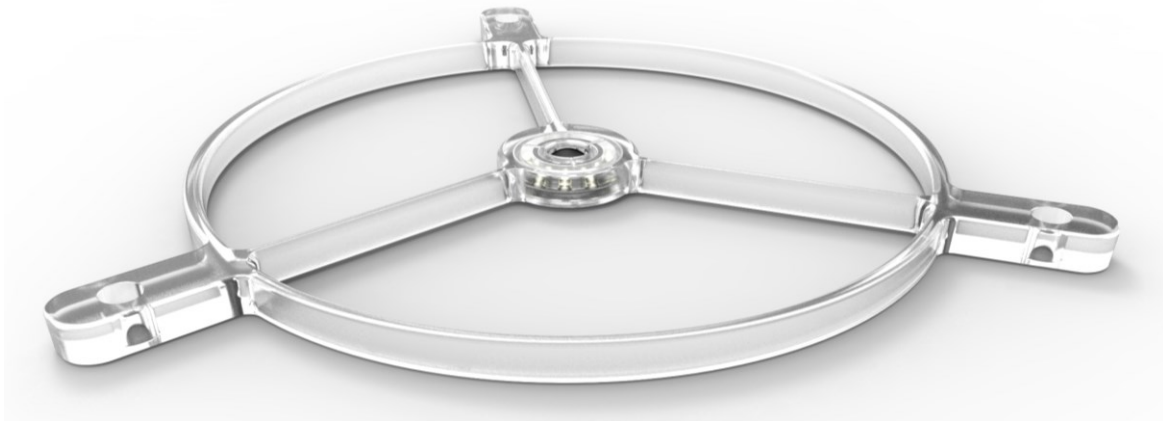


FIGURE 42: RIM-THRUSTER HUB (RENDERED TRANSLUCENT)

The highly conservative load estimate of 400N axial and 1000N radial load per hub creates stresses far below yield strength for 7075-t6 aluminium, which typical is about 450MPa [27]. This means that lower grades of aluminium also could be used. The aluminium will be hard anodized and coated for better surface properties. This will protect against corrosion and abrasion.

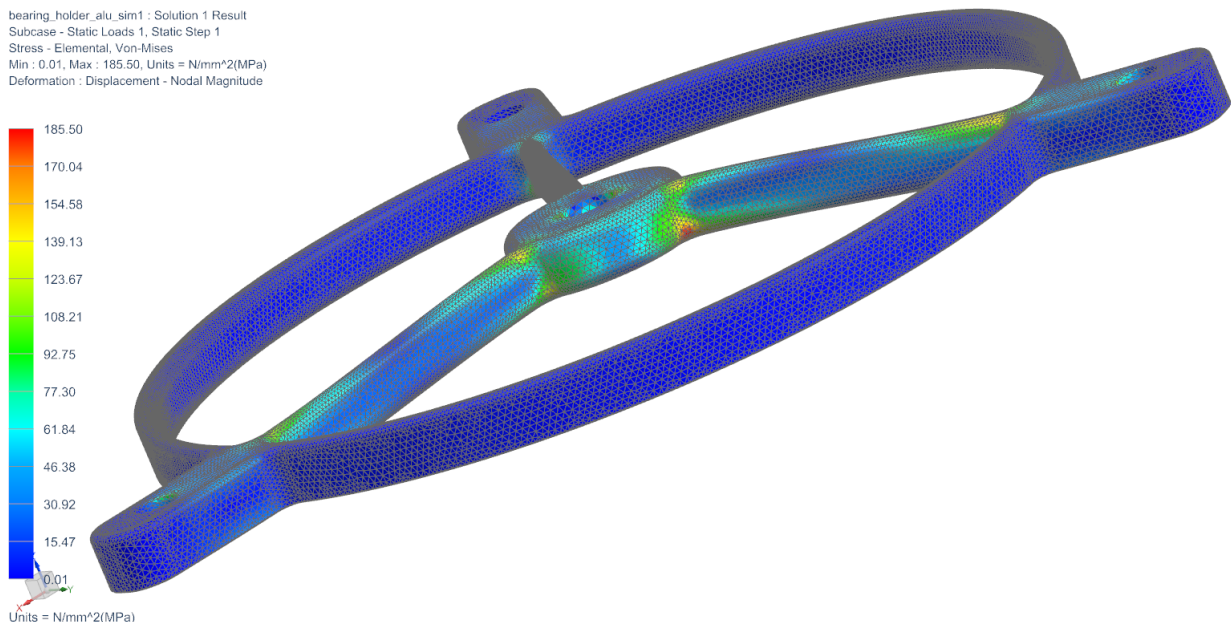


FIGURE 43: STRESS PLOT OF ROTOR HUB (MAX 185,5MPA)

The FEA-plot in Figure 43 shows stress resulting from 1000N bearing loads in radial direction and 400N upward force in axial direction. The structure is fixed in the outer bolt holes and the mesh is CTETRA(10) with element size of 1mm. Maximum displacement was **0,4mm** and stress was **186MPa**, which is acceptable. Details found in Appendix I: Rim-thruster FEA details.

On the third design, the stator is skewed like the stator on in the thruster test rig, which is presented in Figure 83 in chapter 6.2.1. The stator had to be skewed due to the extensive cogging effect found at low rpms. In that design, standard block magnets were used due to their easy accessibility and low price. More info about the prototype design can be found in chapter 6.2.

In the final design, custom made neodymium magnets will be used. Since these could be made for a relatively low price, a specially curved magnet that fits the cylinder curvature with minimal air gap could be cast, illustrated in Figure 44. During the winding of the modified Busck stator, it was found that the skewing of the stator made it more difficult to mount the copper windings. This problem is removed by casting custom magnets instead of skewing the stator.

The electromagnetic (elmag) design will be done in cooperation with Argus RS because of the knowledge and experience required for a successful and efficient motor.

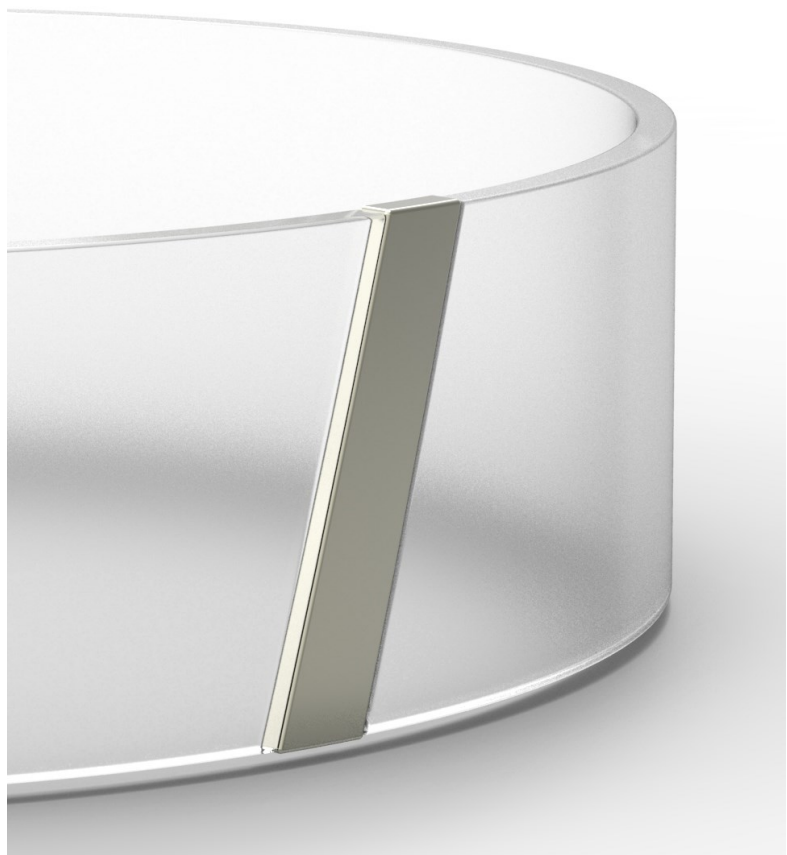


FIGURE 44: CYLINDER SECTION MAGNET

### 5.4.3 HORIZONTAL THRUSTERS

The two horizontal thrusters are the Mantas main thrusters. They propel the ROV forwards and backwards, control the yaw, and create suction to pull in the salmon. Since these thrusters are aligned with the main direction of travel, a low profile is not required. That means that conventional ROV thrusters could be used. The horizontal thrusters also have to be a lot more powerful than the vertical thrusters. In this chapter, two relevant thruster models will be compared. Several other thruster manufacturers have been considered, for instance Seamor Marine [15], but few lightweight thrusters had the required thrust force of 150-200N.

Final thruster choice will be done by Argus RS during the summer / fall 2014.

#### 5.4.3.1 RMI THRUSTER

RMI (Robot Marine Indonesia) have a series of compact but powerful thrusters. The RMI 1000 thruster is a 1000W thruster with 200N thrust force and a weight of only 2kg. The thruster has a maximum operation depth of 300m, and a magnetic propeller coupling, where no axle penetrates the casing. The magnetic coupling is stated to reduce the maintenance need and improve the robustness of the thruster. The RMI 1000 costs 3150 USD. The RMI 500 has half the thrust and power. It weighs 1,7kg and costs 2100 USD [28].

RMI has provided an exterior 3D-model of the RMI 1000 for design implementation. A Keyshot rendering is displayed in Figure 45.

The RMI 1000 thruster runs on 24V / 42A DC, and the RMI 500 use 24V / 20A DC. The exterior geometry of the RMI1000 is  $\varnothing 154 \times L 290 \text{mm}$ , and the motor cylinder casing is  $\varnothing 76 \text{mm}$ .

The RMI 1000 thruster seems to fit every need of the Manta, with light weight, compact size and sufficient thrust force.



FIGURE 45: RMI 1000 EXTERIOR 3D MODEL [28]

#### 5.4.3.2 SUBMERTEC ARS850 THRUSTER

Argus RS has good experiences with ARS850 thrusters from Submertec. They also have several thrusters of this model available, so they are highly relevant for an early prototype.

The Submertec [29] ARS850 is a powerful, but heavy thruster. It can generate a substantial thrust force of 350N, but that requires a higher current than what the Manta will use. It costs approximately 3000 USD, which is slightly less than the RMI 1000 thruster, but it is larger and heavier. The size difference can be seen in Figure 46. The stainless steel casing of this thruster could however be changed to aluminium to reduce weight, something Argus has done earlier.

The exterior geometry of the Submertec ARS850 is  $\varnothing 159 \times L 300 \text{mm}$ , and the motor cylinder casing is  $\varnothing 84 \text{mm}$ . The weight is about 5,2kg with standard casing. [12]



FIGURE 46: SUBMERTEC ARS850 (LEFT) NEXT TO A RMI 1000 (RIGHT)

A model that illustrates how the thruster could be mounted to the hull has been made. The thruster assembly in Figure 47 is mounted in the wings and the rear tubes are mounted on the hull. The thruster assembly should be easy to remove from the ROV for maintenance. Since the thruster details still are not set, the mounting system is very general at this time.

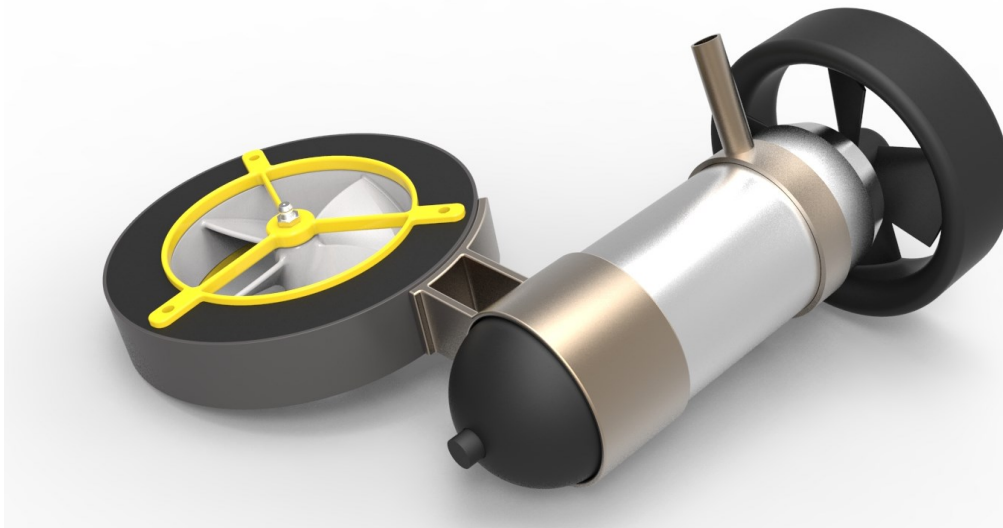


FIGURE 47: CONCEPTUAL THRUSTER ASSEMBLY

#### 5.4.3.3 HORIZONTAL THRUSTER CONCLUSION

The Submertec thrusters' weight is a limiting factor, which makes these thrusters impractical for the final ROV. They can however be used for early prototyping. The RMI 1000 thruster fills every requirement for the Manta, with its high thrust force compared to weight.

**The recommended horizontal thruster for the Manta is therefore the RMI 1000 thruster.**

## 5.5 LAMPS

Argus RS has experience with custom-made lamps on their ROVs for a long time. Existing solutions for Subsea / ROV lamps are anyway expensive, so making custom made lamps that fit the need perfectly does not have to cost more. Successful designs could also be sold separately.

For efficient net inspection and fish acquisition, the Manta requires lamps with sufficient luminous flux. In unclear water, it is important to have some distance between the light source and the camera. This will minimize light reflection from particles in the water that could compromise the visibility. Good design with respect to shape, material composition and component use is required. Several different designs have been developed, with different impacts on the Mantas cost and performance. The final concept is chosen based on how it fits the Mantas streamlined shape, how good lighting conditions it will provide for the camera, and manufacturing ease and cost.

The ability of the light to render realistic colours is quantified by the Colour Rendering Index, CRI.

*“In general terms, CRI is a measure of a light source's ability to show object colors "realistically" or "naturally" compared to a familiar reference source, either incandescent light or daylight.”* [30]

The CRI number will be an important parameter when selecting the final LEDs, and the colour of their lights. A CRI number of 100 represents perfect natural light, and a number close to this is desired.

Argus typically use a series of 200lm 3V / 0,7A light emitting diodes (LEDs) soldered to a circuit board. The circuit board is connected to a water cooled heat exchanger, as the LEDs release a lot of heat. The lamp is then enclosed in a water tight compartment. An example of this lamp is shown in Figure 48. Argus RS manufactures ROVs that can reach down to 6000m, and their lamps are therefore over-dimensioned with respect to strength compared to needs of the Manta, which will has a maximum design depth of 100m.



FIGURE 48: DEEPWATER LAMPS ON AN ARGUS ROV

A LED-board that Argus already uses has been used as basis for two designs, shown in Figure 49. The CREE XM-L2 1000 lumen LED [31] has been used for two others. The final design features a custom made LED-board with 31 Osram LCW CQAR.CC 200 lumen LEDs [32] and two single LED 10000 lumen /100W lamps.

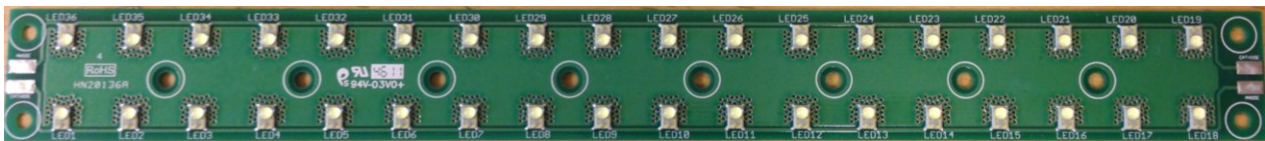


FIGURE 49: ARGUS' CUSTOM MADE RECTANGULAR LED CIRCUIT BOARD

The lamp design is done by first selecting the LED type and number. A suitable casing is then developed. The casing has to be easy to manufacture, be able to handle the pressure and provide enough heat dissipation for the LEDs.

### 5.5.1 EMBEDDED DESIGN

The first idea that occurred was to completely encapsulate the LED-board in a polymer, shown in Figure 50. Removing all the air also removes the pressure difference. The design without internal cavities was not expected to deform due to the hydrostatic pressure.

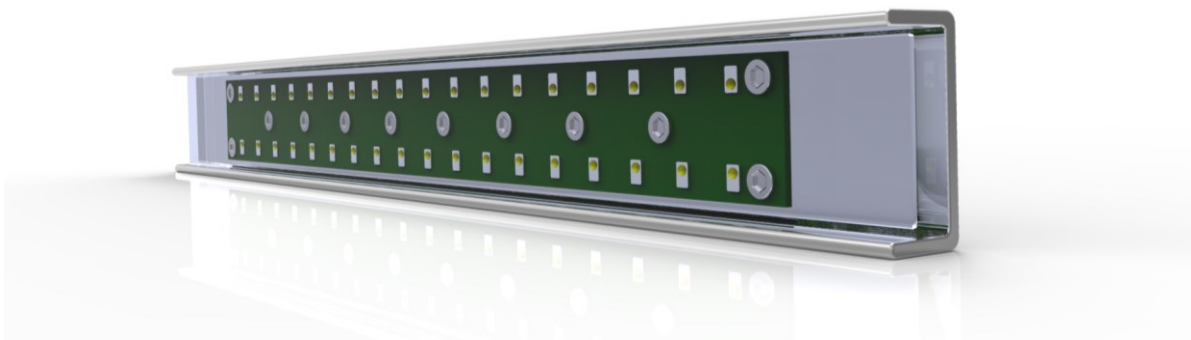


FIGURE 50: ILLUSTRATION OF *EMBEDDED DESIGN*

Two main issues with this design have been identified during the thesis. One is chemical incompatibility between the LEDs and the polymer and the second issue is thermal strains. A support document from CREE Inc. [31], one of the World’s largest LED manufacturers has addressed these issues:

The typical LED has a silicone lens to protect the LED chip and focus the light, illustrated in Figure 51. This silicone lens is easily discoloured by common chemicals that contain volatile organic compounds, an example of this is shown in Figure 52. Examples of these are Cyanoacrylates (superglue), methyl- and ethyl acetate (nail polish removers) and glycol ethers (electronic cleaners). The CREE test report also states “*Do not apply conformal coatings directly on the LED lens, as this will affect LED optical performance and reliability.*” [33]

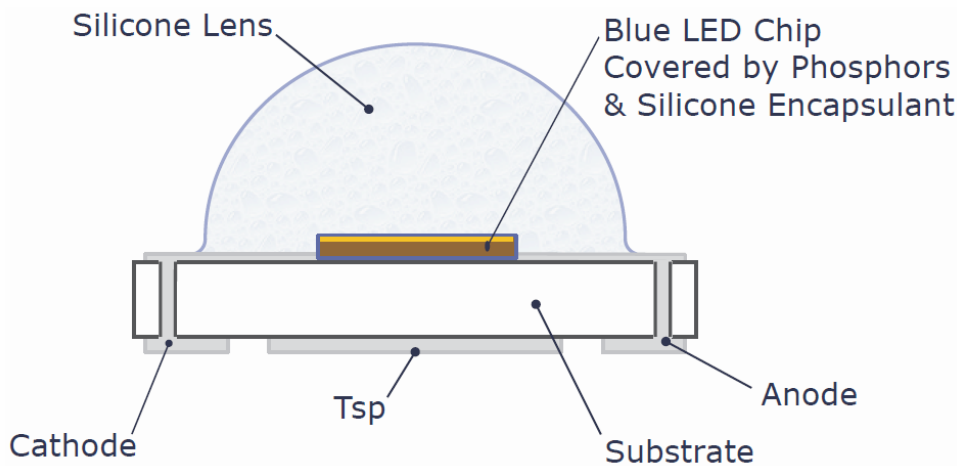


FIGURE 51: CROSS-SECTION OF TYPICAL LED [33]

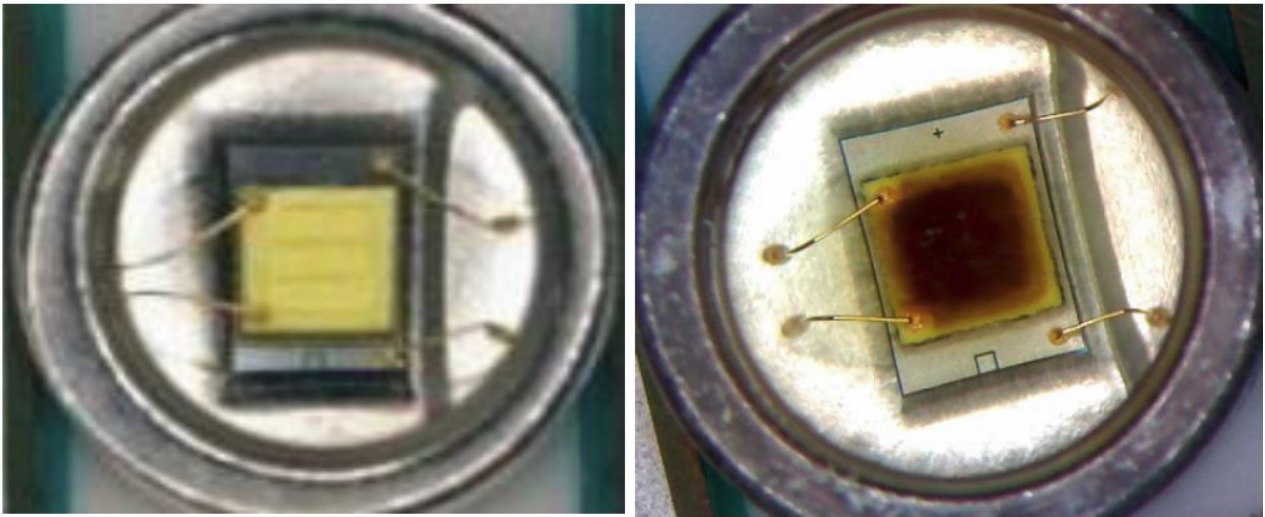


FIGURE 52: NORMAL LED (LEFT) AND A LED DISCOLORED DUE TO CHEMICAL INCOMPATIBILITY (RIGHT) [33]

The second issue is thermal strains caused by the temperature gradient between the heated LEDs and the cold water. This issue applies to all parts that are in contact with water, including aluminium housing and the polymer lens. Thermal properties of the most relevant lamp materials are displayed in Table 8.

Materials	Average coefficient of thermal expansion [( $\mu\text{m}/\text{m}/\text{K}$ )].	Ratio between coefficients of thermal expansion []	Thermal conductivity [W/(m*K)]
Copper (circuit board)	17	1	275
Aluminium (profile)	23	1,4	156
Stainless steel	17	1	18
Epoxy	88	5,2	0,3
Polycarbonate (lens)	129	7,6	0,2
PMMA (lens)	117	6,9	0,2

TABLE 8: THERMAL PROPERTIES OF RELEVANT MATERIALS FOR LAMP ASSEMBLY [7]

The ratio between the coefficients of thermal expansion of the materials can be problematic. It is likely that cracking will occur, since the materials expand very differently when the temperature is changed. Cracking could also occur in the polymer due to the large temperature gradient. The cracking can both damage the components directly or lead to leaks that will short circuit or corrode the internals.

The embedded design is therefore not recommended, and that goes for any directly encapsulating of LEDs in general as well.

## 5.5.2 DRY DESIGN

The *dry design* has a polymer sheet bolted on an aluminium casing, as illustrated in Figure 53. The idea was to use an elastomer gasket between the glass and the aluminium casing. By having air in the casing, no chemical reactions are expected.

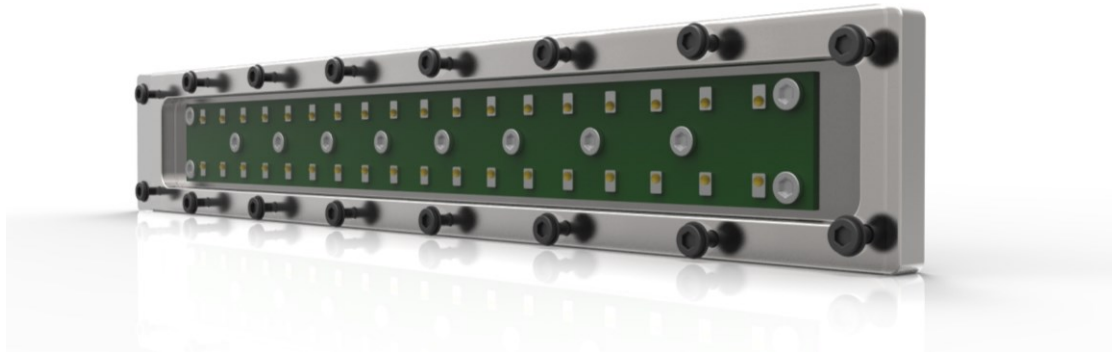


FIGURE 53: 3D-MODEL OF DRY LAMP DESIGN

A simplified analysis has been conducted with 1,5 MPa external pressure, corresponding to approximately 150m water depth. A 5mm PC plate will be sufficient to withstand this pressure, and the concentrated stresses at the contact surface would be evened out by the elastomer gasket. The simulation was conducted with 1,5mm CTETRA(10) elements, with fixed rear casing. The PC lens was connected to the casing in the FEA by surface-to-surface gluing, and no bolts were simulated. This simplification does not investigate stresses due to bolt pretension or other bolt related stresses.

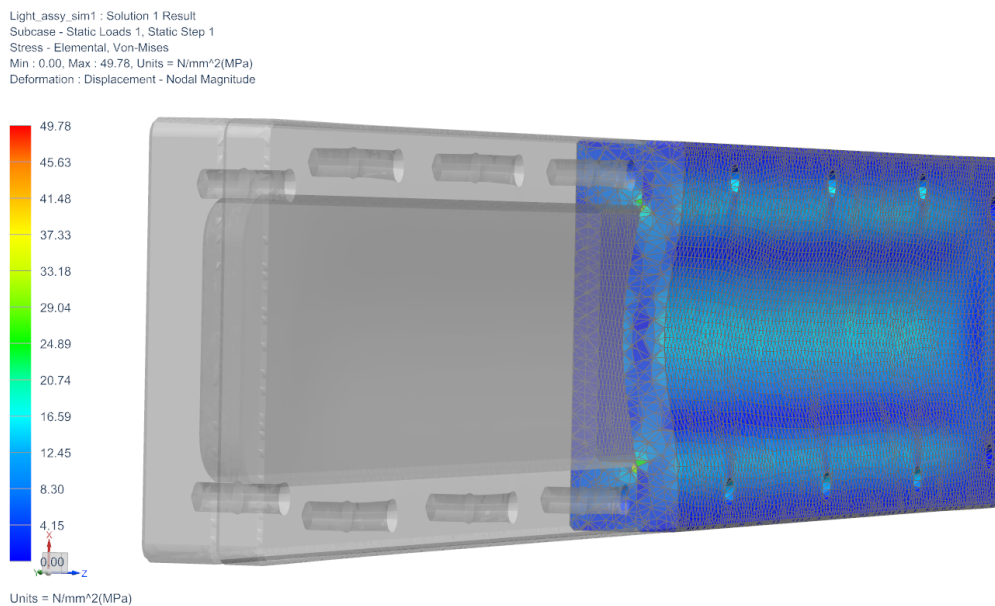


FIGURE 54: STRESS PLOT OF LAMP AT 150M DEPTH

The FEA results shown in Figure 54 are acceptable, where the maximum von Mises stress is about 63% of UTS of PC. Further FEA details are found in chapter 19.

The *dry design* costs more to manufacture than the embedded design, but is known to work well. There are challenges with different thermal expansion, so an elastic gasket is required and the bolt holes should allow for some displacement.

After revision, it was found that O-rings would provide a more reliable seal. The O-ring would require a slot and thereby a thicker sidewall. The final design would have a large front area, which is unwanted on the Manta.

### 5.5.3 CREE XML-T6 DESIGN

The Cree XML-T6 1000lm LED is one of the world's most popular LEDs at the moment. The compact design and high luminous flux makes it ideal for head lamps, torches and bike lamps. The popularity pushes the prices down, at the moment the cost of one LED is about 6 USD including shipping from Hong Kong bought on eBay. Lenses and reflectors made for this LED specifically are also commonly available and fairly priced. Several different LEDs have been purchased for investigation or prototyping in this project. Some of these components are pictured in Figure 55.



FIGURE 55: 60° LENS (UPPER LEFT), 20MM XML LED (TOP) AND 16MM (BOTTOM)

Polycarbonate (PC), acrylic (PMMA) and borosilicate glass have been evaluated as lens material for the lamps. PC has the best impact strength, but PMMA is stiffer and has better optical properties. PMMA has approximately the same tensile strength of up to 80 MPa, but it is more stiff and brittle. PMMA is up to ca. 2 times stiffer than PC, but only has 1/10<sup>th</sup> of the fracture elongation [7]. Borosilicate glass has a very low coefficient of thermal expansion and good optical properties. It is however costly to manufacture and is therefore not used for these lamp designs.

Argus AS also has positive experiences using PMMA for these applications, so the chosen material is PMMA.

### 5.5.3.1 SINGLE LED DESIGN

The design with a single CREE XML2 LED is compact and light, and can be easily be fitted anywhere on the hull. Illustrations of its design are presented in Figure 56.



FIGURE 56: SINGLE LED DESIGN

Single LED lamps could be mounted around the hull if needed. The clamp, which is orange in Figure 57, is designed to push the lens against the casing and O-ring when it is tightened with a bolt. The casing is made of aluminium, and the glass is 4mm PMMA.

The lamp weighs 50g and measures  $\varnothing 35 \times L 33 \text{mm}$ .

At this time the single LED lamp design is not used.

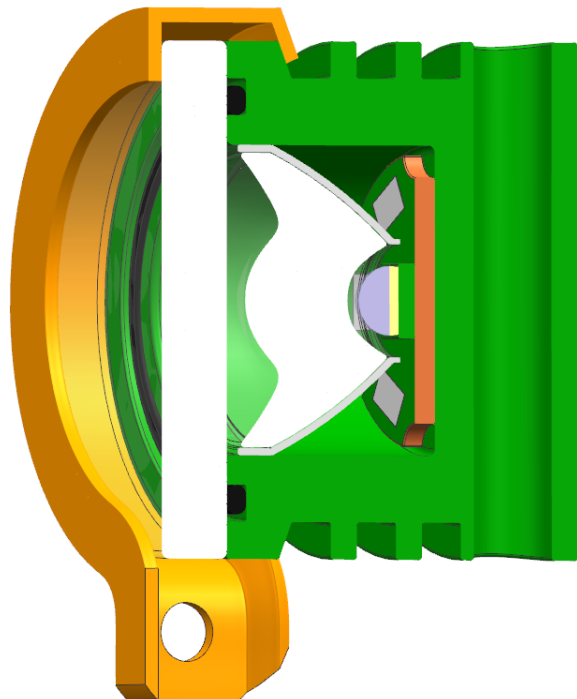


FIGURE 57: SECTION VIEW OF LAMP

### 5.5.3.2 TRIPLE LED DESIGN

The 3-LED design uses t CREE XML 1000lm LEDs with 20mm copper heat sinks and 60 degree 21mm wide lenses. A rendering of the design is displayed in Figure 58. The casing is made of aluminium so the water will provide efficient cooling. The LEDs and Lenses cost less than 20 USD in total, so the main cost will be the aluminium casing. The outer lens is made of 5mm PMMA.

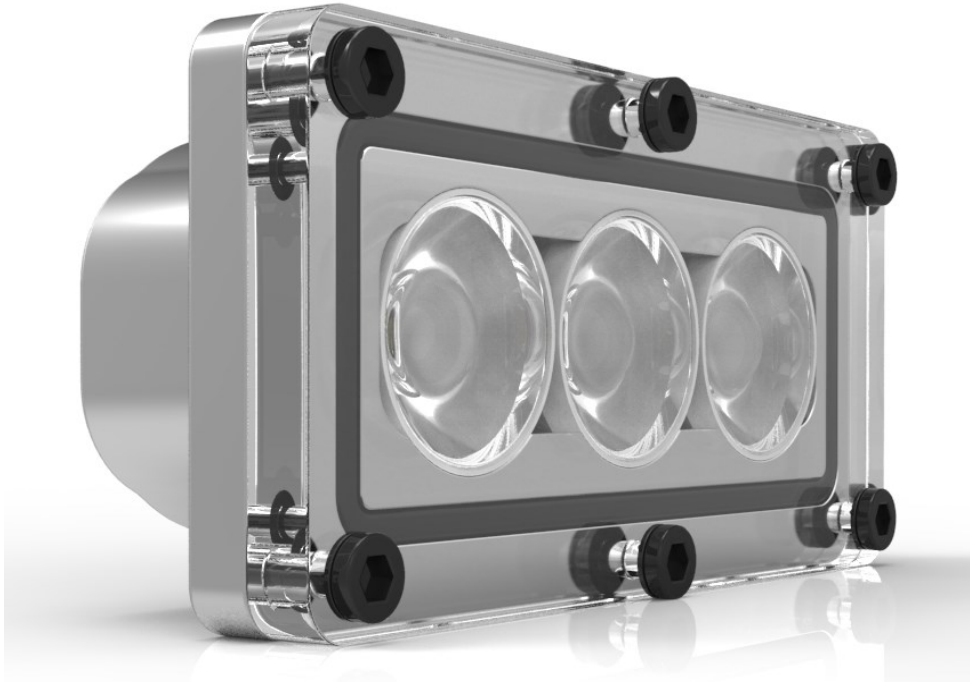


FIGURE 58: 3X CREE XML DESIGN, TOTAL OF 3000LUMEN

The LED copper boards have a good contact surface to the aluminium casing, and the casing is in direct contact with sea water (Figure 60). This provides efficient cooling of the LEDs.

The outer geometry of this lamp is W85xH42xL25mm and it weighs 126g.

This design could use different lenses, and for instance use two 60 degree lenses for wide beams and one 30 degree lens for a more focused beam.



FIGURE 59: COOLING RIBS

Cooling ribs could be added to the rear, like in Figure 59, although it is most likely not needed due to the efficient cooling by the surrounding water.

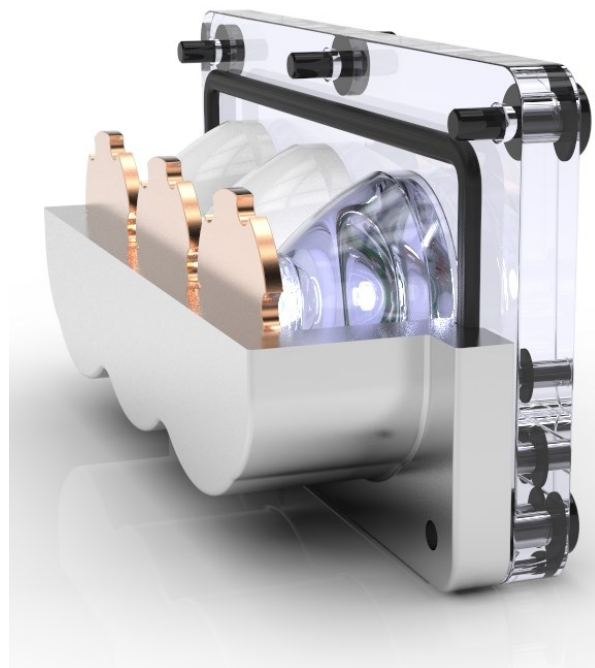


FIGURE 60: SECTION VIEW OF CASING

#### 5.5.4 CUSTOM LED RACK

The custom light bracket is based on the Osram LCWCQAR CC 180lumen LED [32]. The design is illustrated in Figure 61. This LED is Argus RS' preferred LED due to its compact size. The light from this LED is very good with respect to colour rendering index (CRI). These LEDs has a CRI of 96, where 100 is perfect natural light. The single LED in Figure 62 measures 3x3x2mm.

The lamp has a rack of 31 LEDs that provide a total of 5600 lumens. Since there are no reflectors or optics mounted, the beam will be very diffuse, which is good for close inspections.



**FIGURE 61: CUSTOM LED RACK WITH A TOTAL OF 5600 LUMENS**

The lamp has a 4mm PMMA lens that is sealed with a rubber seal (black) and glued with an elastic paste. There has to be a rubber seal closest to the LEDs to separate the LEDs from the fumes from the paste. Silicone-based glue should not be used, as damaging gas is known to diffuse from this type of glue when subjected to heat from the LEDs. The lamp dimensions are approximately 130x30x10mm and the weight is around 80g.

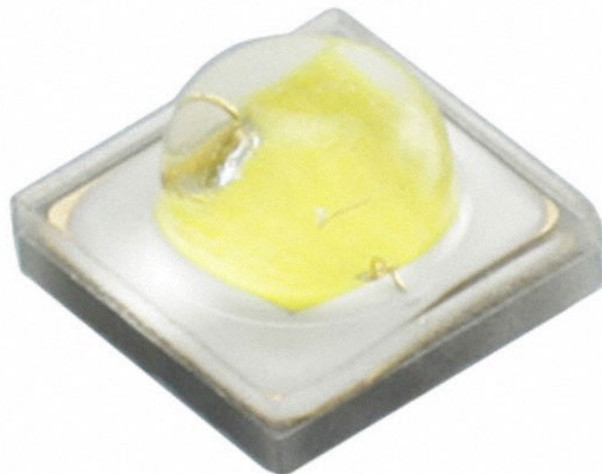


**FIGURE 62: 3 X 3 X 2 MM OSRAM LCWCQAR CC LED**

### 5.5.5 100 W SINGLE LED LAMP

High power LEDs are starting to have a very fair price. At the moment, 100W LEDs with 10 000 lumen (rated by seller) light flux only cost 13 USD [34]. Since these LEDs are so powerful, cooling ribs on the rear of the lamp are needed, see Figure 63. If this lamp is used in air, the LED will soon be damaged from the high temperature, because of the lack of cooling water.

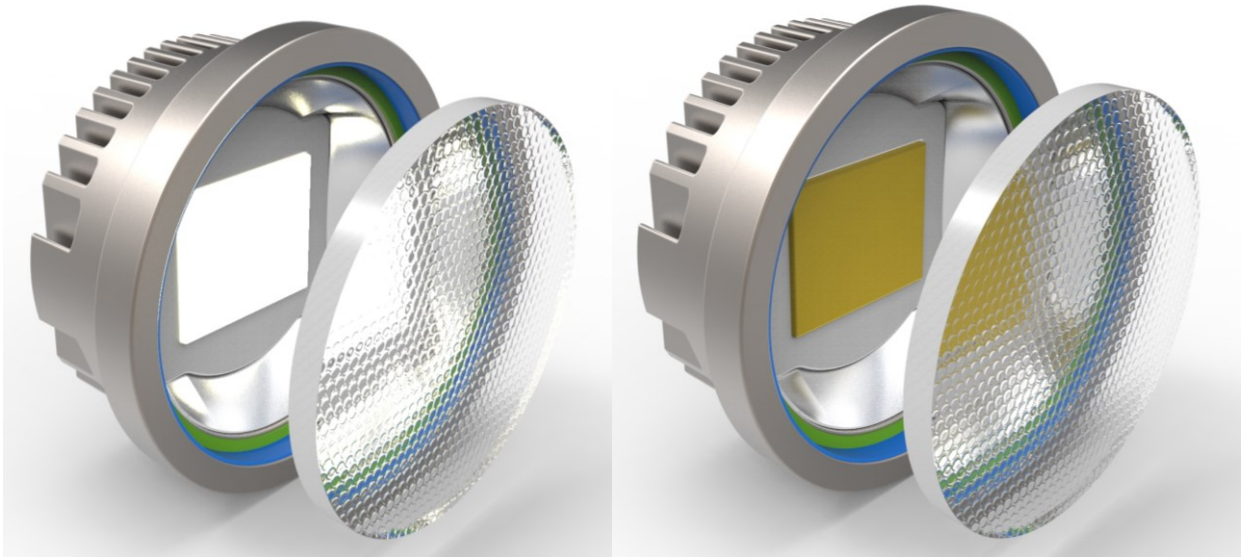


FIGURE 63: 100 W LED DESIGN

The section view in Figure 64 shows the internal design. It consists of the LED board, a reflector, seals, the casing and a lens. The weight is 145g and it measures Ø75x30mm. The different colours of the seals represent different materials. As noted earlier many sealants contain substances known to harm LEDs over time. Therefore the inner (green) seal will be of a compatible material. The exterior seal (blue) can then be made of a strong and flexible paste. The lens could be bumped for a wider beam, like in Figure 63.

This LED is sold under many brands, none of which provide any decent datasheet for the LED.

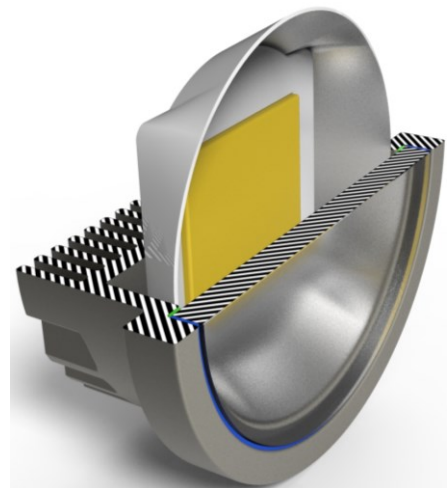


FIGURE 64: SECTION VIEW OF 100W LED

There are reflectors and lenses on the market that cost very little. The 120° glass lens and the reflector in Figure 65 were bought for 4 USD. In the final design, only the reflector is used.

**The chosen lamps are the 100W single LED design and the custom LED rack. This choice is made in dialogue with Argus RS.**

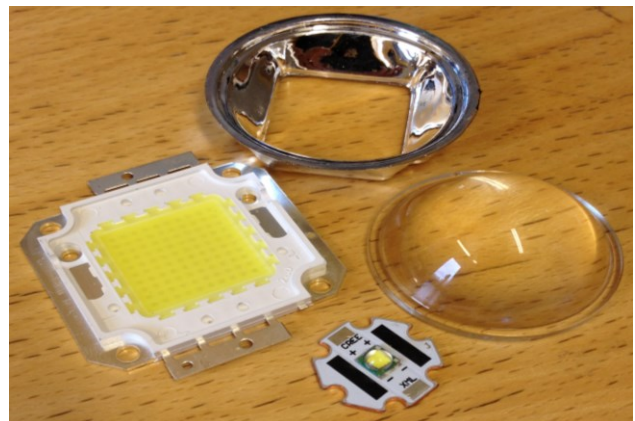


FIGURE 65: 100W LED WITH REFLECTOR, 120° LENS AND XML LED (BELOW) FOR SCALE

## 5.6 BUOYANCY UNITS

Most of the Mantas components are heavier than water, so buoyancy units are required. The ROV should have slightly positive buoyancy, so the buoyancy unit should be made after all other components have been fully designed and the buoyancy requirements have been determined. The buoyancy material that will be used is Diab Divinycell HCP30. The material is a closed cell foam especially developed as a buoyancy material, with high impact resistance, low water absorption and excellent buoyancy performance it is perfect for a lightweight ROV. The material has a density of  $200\text{kg}/\text{m}^3$ , and has a maximum operation depth of 190m and 300m crush depth [6].

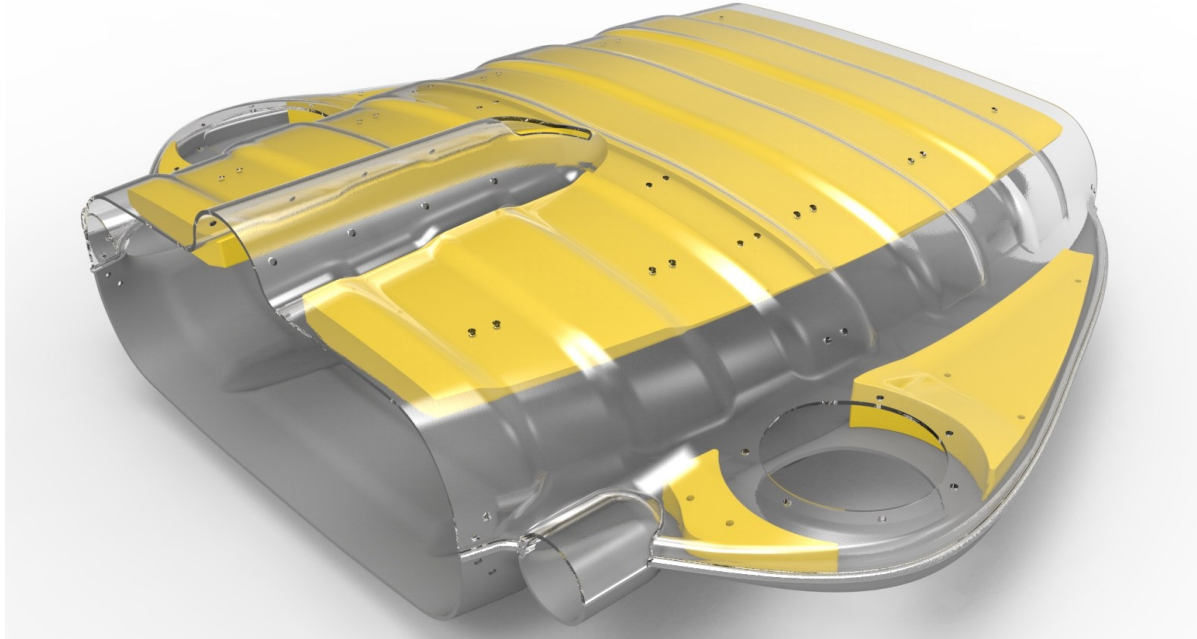


FIGURE 66: BUOYANCY UNIT LOCATIONS IN THE HULL

Buoyancy units will be mounted in the wings and at inside the top of the hull, as seen in Figure 66. The units in the wings fill up the cavity perfectly and are mounted with bolts through the hull. This will stiffen the wings and minimize trapped water. The buoyancy in the wings will be separated by the thruster, so there are two individual units in each wing. The wing units could also be mounted together with the thruster, creating one easily removable unit in each wing. This unit could consist of a horizontal and a vertical thruster mounted together with a buoyancy unit.



FIGURE 67: MAIN BUOYANCY UNIT

The current design will be machined to fit the inside of the hull, and the main unit can easily be extended downwards for increased buoyancy. The slot in front is for the electronics cylinder, and a gap provides sufficient cooling. The units will be connected to the hull by bolts and the bolt holes can be seen in Figure 66. The main unit now has a volume of  $11,4 \text{ e}6 \text{ mm}^3$  and provide buoyancy force of approximately 90N. The total buoyancy volume is  $13,2 \text{ e}6 \text{ mm}^3$ , which represents approximately **106N buoyancy. The weight of the buoyancy units in air is estimated to 2,6kg in total.**

## 5.7 UMBILICAL LIFTING POINT

The Mantas umbilical cable, which is yellow in Figure 68 and Figure 69, is a combination of electrical power- and control wires, and lifting wires. The lifting force from the umbilical is retained by a rubber sleeve that evens out the forces and hinders unwanted sharp bends to the wires.

The rubber flex sleeve is mounted in a pivot, which allows for some rotation. The umbilical will therefore lay flat against the hull while moving and it pivots up when tension is applied to the umbilical.

In Figure 68, the model of the Manta can be viewed from above without the upper hull section or main buoyancy unit. The location of the umbilical connection is just in front of the expected centre of mass.

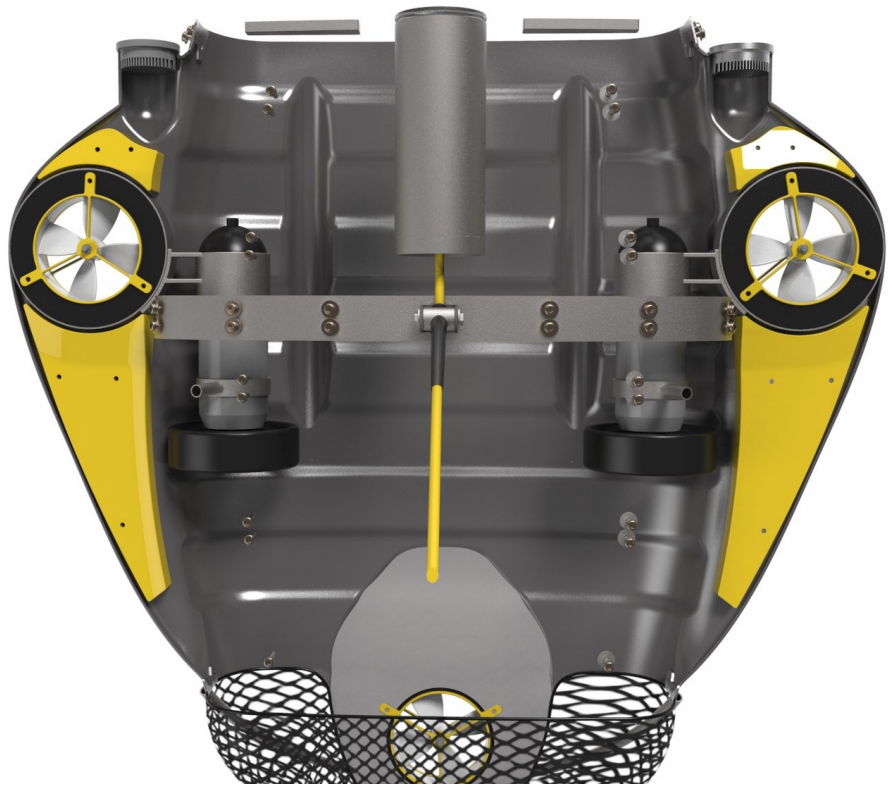


FIGURE 68: UMBILICAL CONNECTION POINT SEEN FROM ABOVE

In Figure 69, the stainless steel umbilical fixture and rubber sleeve are rendered translucent for better overview. The pivot bolt is aluminium. Note the brass bushing in the bolt hole that reduces wear. This bushing could also be made of Teflon or Nylon. The side bolts are M8x12mm stainless steel.

The pivot bolt is 25mm in diameter and 34mm long and is made of hard anodized aluminium. The 316L stainless steel fixture has a wall thickness of 3mm.

Argus RS has specified the umbilical to have 10mm diameter.

The mass of the umbilical lifting point is estimated to be 170 grams including the rubber sleeve.

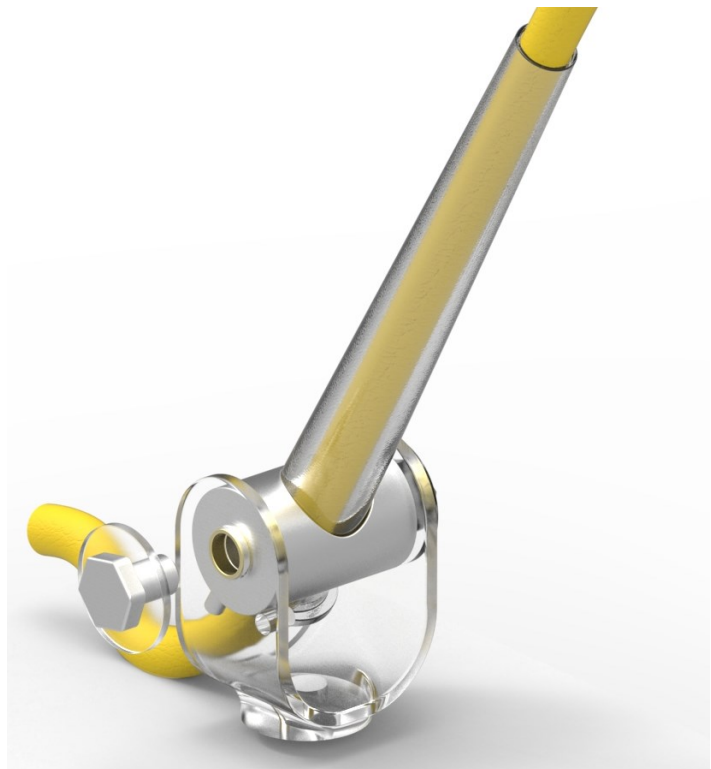


FIGURE 69: UMBILICAL LIFTING POINT

The lifting point has been simulated in Siemens NX 8,5 using 1500N force. Both upwards and forwards force. The assembly was simulated in two parts. The stainless steel bolts are fixed and the aluminium centre part is loaded with an upwards force of 1500N, shown in Figure 70. The result is shear loaded bolts.

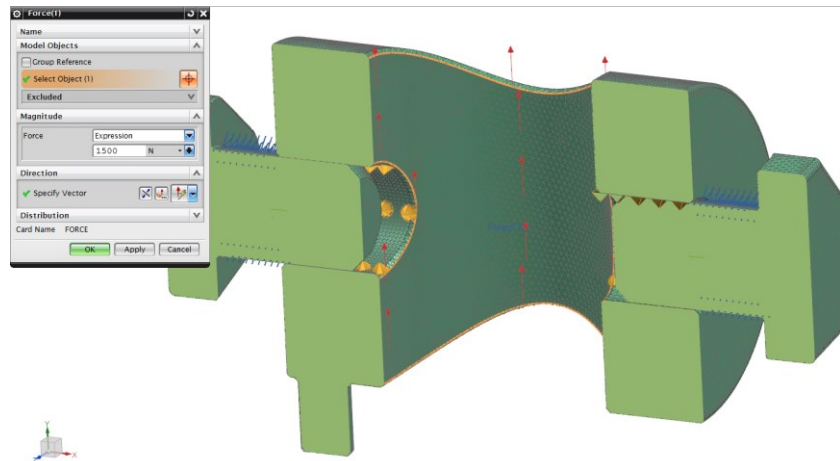


FIGURE 70: LOAD CASE ON UMBILICAL PIVOT (1500N DISTRIBUTED)

The stainless steel fixture is loaded with a bearing force of **750 N on each of the holes**. Both an upwards and a forwards force (worst scenario) have been simulated. Since the fixture is supported in side direction by the pivot body and bolts, similar support constraints have been added. Load case is displayed in Figure 71.

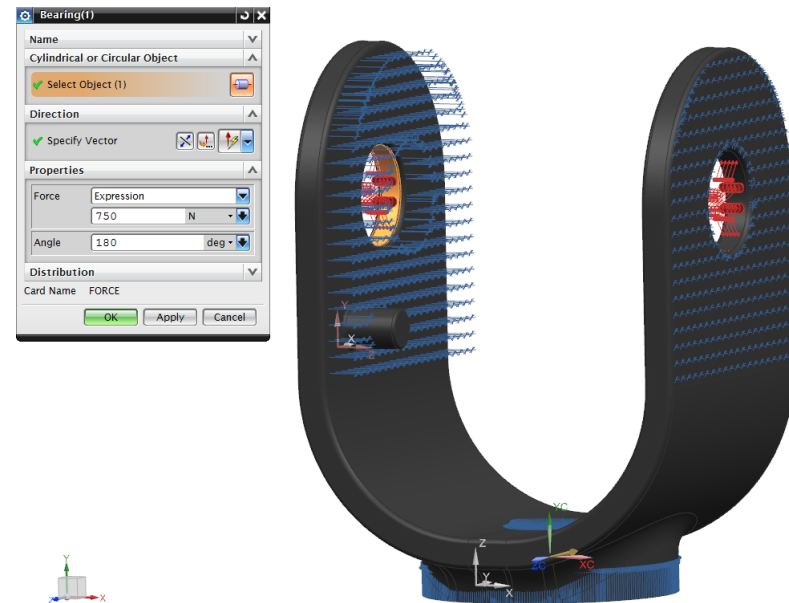


FIGURE 71: LOAD CASE ON UMBILICAL FIXTURE (2X750N BEARING FORCE)

Larger pictures with visible numbers are available in chapter 21.

umbi-assy\_sim3 : Solution 1 Result  
 Subcase - Static Loads 1, Static Step 1  
 Stress - Elemental, Von-Mises  
 Min : 0.00, Max : 245.53, Units = N/mm<sup>2</sup>(MPa)  
 Deformation : Displacement - Nodal Magnitude

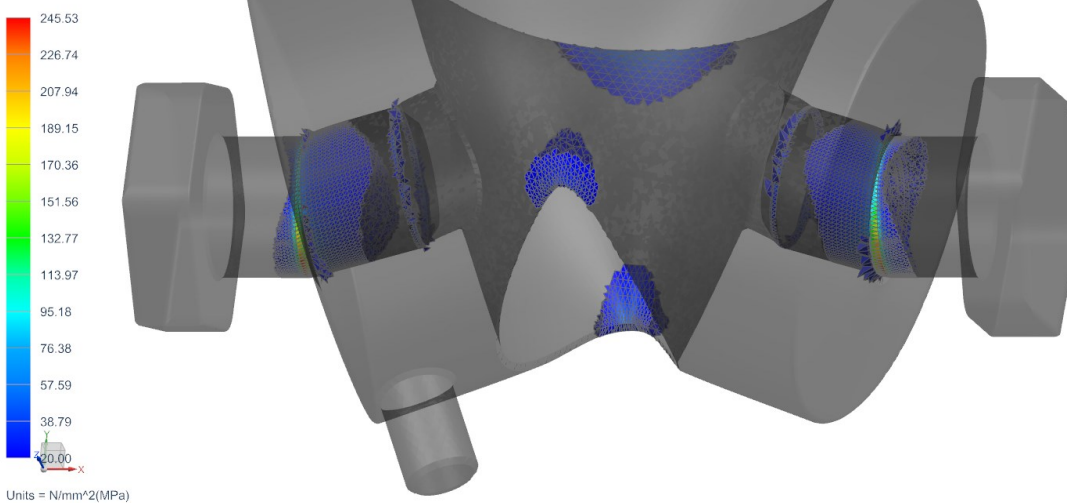
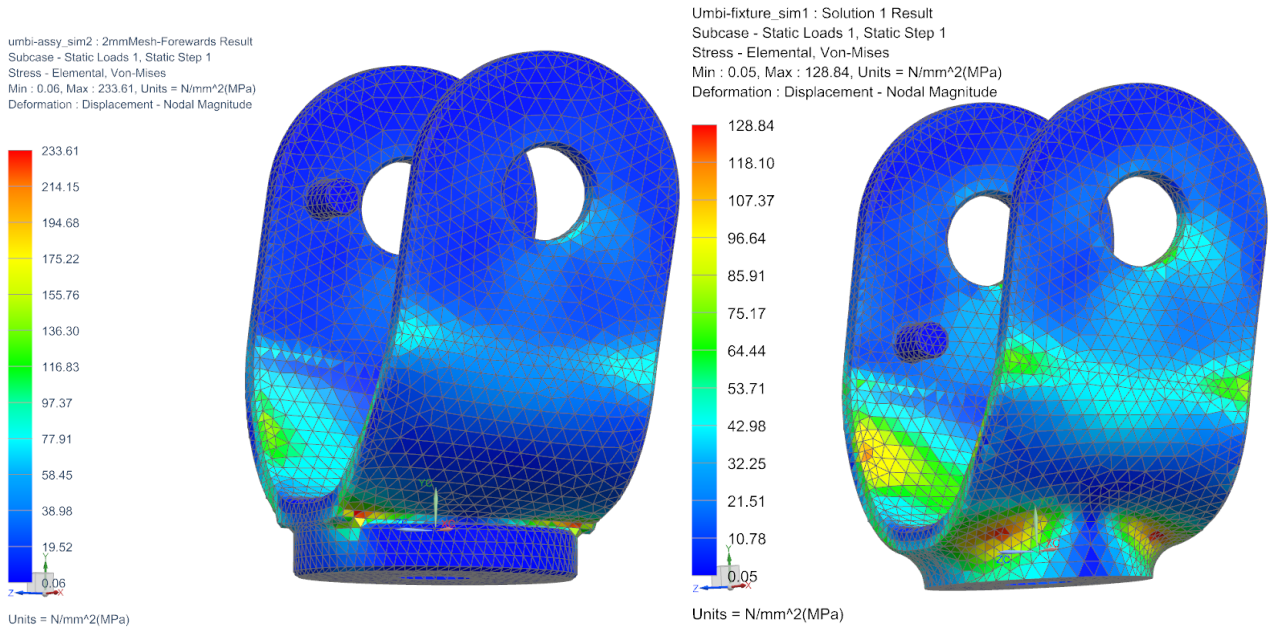


FIGURE 72: STRESS PLOT ON UMBILICAL PIVOT 1000X DEFORMATION (MAX 246MPA)

The bolts are exposed to stress concentrations in the area where they enter the holes, as can be seen in Figure 72. Since the bolts work as an axle, there has to be shear loading and the stress naturally will be concentrated at the border areas. Stress below 20MPa is rendered translucent in Figure 72. Mesh had element size of 0,5mm (CTETRA(10)). The material is AISI 310 SS steel.



**FIGURE 73: UMBILICAL FIXTURE BEFORE (LEFT) AND AFTER REDESIGN – SAME LOAD AND MESH**

The fixture has been redesigned a couple of times in order to reduce the stress concentrations. The FEA results from the two last design stages are displayed in Figure 73. After the last redesign, the maximum von Mises stress went from **234 MPa to 129 MPa**, with the same element size of 2mm and identical load conditions.

A finer mesh, with element size 0,5mm, resulted in the maximum von Mises stress of **199 MPa** in the worst load case.

The FEA results are viewed upon as satisfactory. Details about the FEA of the umbilical lifting points can be found in chapter 21 Appendix L: Umbilical lifting point.

### 5.7.1 LOAD DISTRIBUTION BRACKET

The forces from the umbilical are distributed by a bracket made of 5mm aluminium, displayed in Figure 74.



FIGURE 74: LOAD DISTRIBUTION BRACKET

The bolts that connect the bracket with the hull are M6x10 with 20mm wide shims to even out the bolt forces. The lifting point is connected to the bracket by an M8x20 bolt. The part has been simulated as an assembly with the hull in chapter 20: Appendix K: Hull simulations.

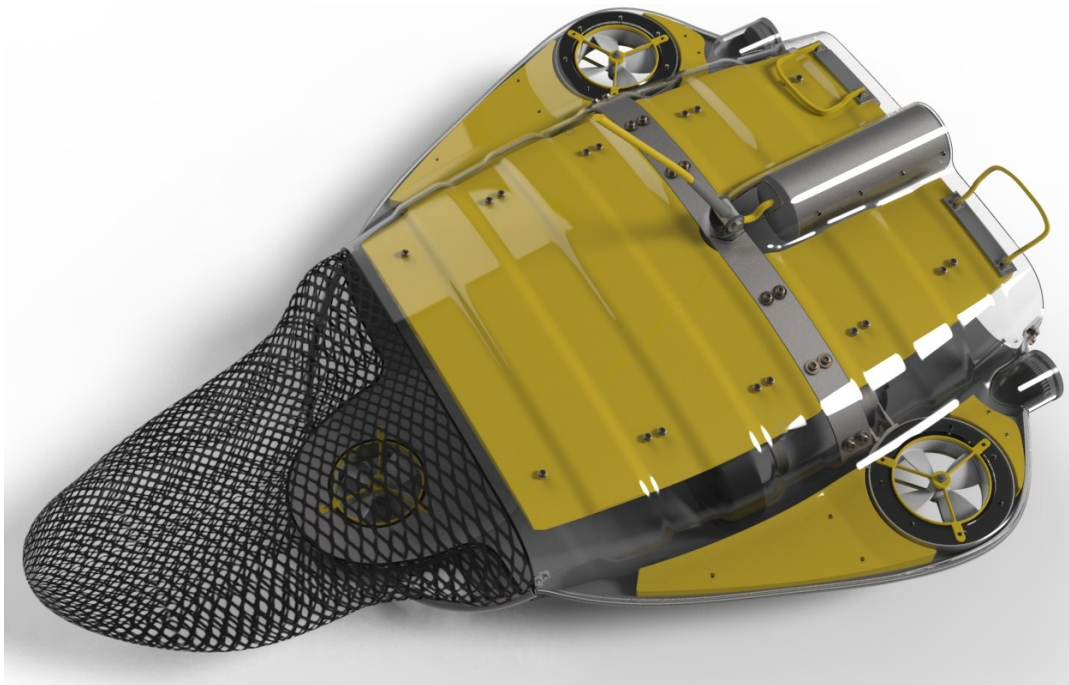


FIGURE 75: MOUNTED LOAD DISTRIBUTION BRACKET

The umbilical cable connection point, which is pictured in Figure 75, is located close to the middle of the main thrusters. This is slightly in front of the expected centre of mass. There are a couple of arguments for placing the umbilical connection point here:

- When the Manta moves through the water the umbilical will align to body backwards. If the connection was too close to the front, any force from the umbilical would destabilize the direction of travel, *trying* to force the ROV to turn around making it hard to control.
- If the umbilical was connected at the rear of the ROV, the Manta would most likely spill the caught catch when lifting it upwards by the umbilical.

A compromise is therefore found, where the umbilical is mounted on a pivot in a flexible rubber sleeve. This will ease the alignment of the umbilical when not used for lifting and protect the often problematic connection point of the wires. If lifting the ROV by crane it is positive if the ROV will align to the ground or deck correctly *on its own*, this is also maintained if the umbilical is close to the centre of mass.

## 5.8 LIFTING HANDLE

In order to lift the Manta by hand, lifting handles are mounted on the upper front of the hull, like in Figure 76. The handles are yellow to provide visibility, and they flip back when not in use. The lifting handles are just a concept at this point, because existing solutions might work just as well.



FIGURE 76: CONCEPT FLIP UP HANDLE

The surface mounted handle in Figure 77 cost 4 USD from parts-express.com, and there are several similar designs on the market. This means that there is probably no need for a custom made handle.



FIGURE 77: SURFACE MOUNTED HANDLE FROM PARTS-EXPRESS.COM

The resulting assembly is fairly detailed, see renderings in Figure 78.

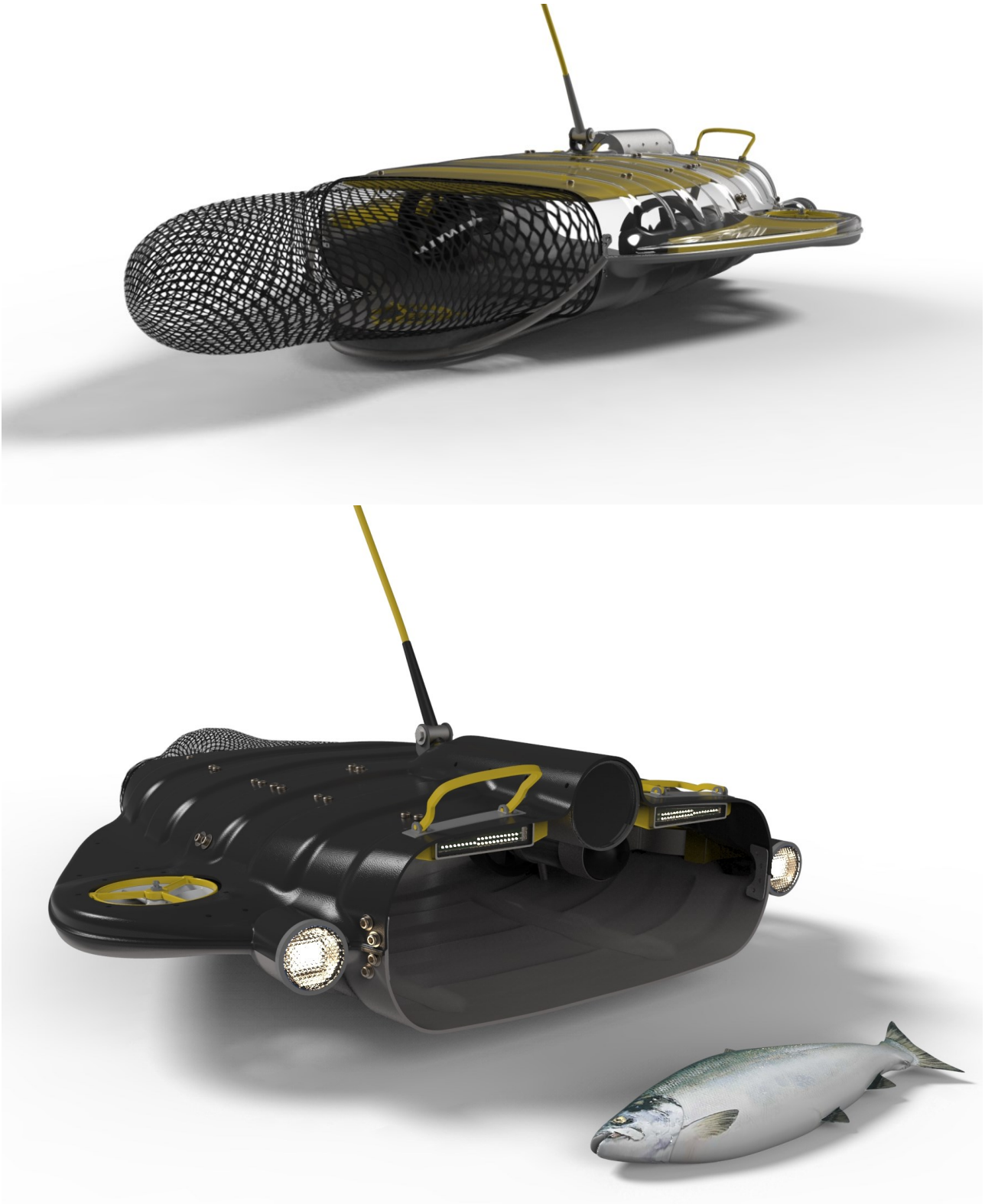


**FIGURE 78: THE MANTA (THE 3D MODEL OF THE SALMON IS COURTESY OF MAGNUS SKOGSFJORD)**

## 6 PROTOTYPING

Since the start of this project, it has been a goal to create a prototype of the Manta components. A prototype could confirm that the principles work as expected and also give an indication of how much work is needed to manufacture the product

The primary component that needed to be prototyped was the vertical thruster. In the preceding project thesis [1] the hull was designed for a thruster with outer geometry of **ø190xh40mm** and changes in the thruster geometry may require modifications to the hull design.

In order to build a successful thruster prototype, experience and knowledge about electromagnetic (elmag) design is required. The author does not have any experience with elmag design, and only possesses basic knowledge about brushless permanent magnet motors. It was therefore necessary to cooperate with Frederik Wendel at Argus RS when designing the thruster. Wendel has had the main responsibility for electromagnetic design, which includes designing the stator and winding parameters, and rotor magnet set-up. Wendel has also done the final assembly of the electromagnetic components in the thruster prototype, and done made minor improvements to the test rig.

When designing the stator it was a goal to find an already existing stator laminate that suited the geometry and motor requirements. Cutting prototype stator laminate is expensive, since it needs precision and there are many sheets in total. This process requires laser, water jet cutting, or a custom made punching tool for larger series. Because of the large investment cost of the punching tool the stator design should be verified using a completely tested thruster prototype before the tool is ordered.

It was found necessary to develop a flexible test rig to investigate what motor characteristics different electromagnetic designs will result in. The test rig could provide a solid foundation for measuring how power, torque and speed changes when the winding- or magnet parameters are altered. Argus RS will tune the parameters with a combination of FEA and trial and error.

The thruster prototype will be mounted in this rig before the final design.

**The goal for the motor is 2500 rpm and 4 Nm torque, which is estimated by Argus RS to result in approximately 100 N thrust force from the finished thruster.**

The different components will be described individually before the complete setup is presented.

There has not been made a prototype of the hull in this project due to the limited time available and the unknown details that still are present.

## 6.1 SMARTMOTOR STATOR BASED PROTOTYPE

One example of an already existing stator that could fit the needs is the 25Nm SmartMotor actuator motor in Figure 79. It is pictured with a 140x30mm 3D-printed concept rotor inside. Because the torque is many times the required value, the stator laminate stack height, and thereby weight, could be reduced significantly.

SmartMotor has offered a stator for research purposes, but there has not been time for testing this stator during this spring.



FIGURE 79: SMART MOTOR ACTUATOR STATOR

## 6.2 BUSCK STATOR BASED PROTOTYPE

### 6.2.1 STATOR

Argus RS has provided a Busck stator [35] to the project that will be used as a basis for the vertical thruster prototype. The stator was originally 140mm high and weighed approximately 20kg. The copper windings were removed from the stator stack and the stack was divided. The stator design is done by Argus RS. The laminate stack height was specified to be 20mm and the back-iron is set to 8mm. That means that the diameter would need to be reduced from  $2 \cdot ro1 = 210\text{mm}$  to  $2 \cdot ro2 = 186\text{mm}$ , illustrated in Figure 80. Argus RS had also found out that massive *cogging* occurred with the unmodified motor configuration. Cogging is the uneven torque that occurs on some motor designs when the speed is low. The magnets jump from being aligned to one set of stator teeth to the next. Since the prototype design is for the vertical thrusters, it has to have as little cogging as possible since the thrusters must be able to operate at low RPMs. There are different ways of reducing the cogging, for instance by using a different number of poles on the stator and rotor or displace the stator laminate so that the stator teeth are skewed. In the last example, the rotor magnets experience approximately the same force independent of position, which greatly reduce the cogging. This was the strategy when making the prototype.

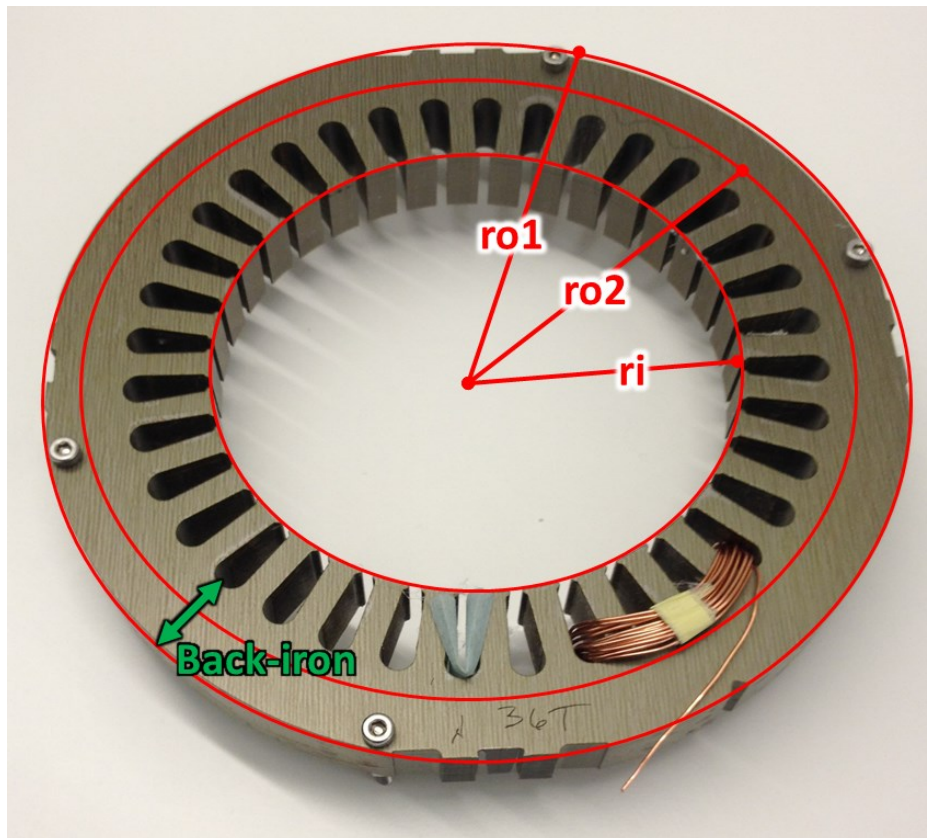


FIGURE 80: STATOR FROM BUSCK MOTOR

In order to save weight, the stator back-iron was reduced significantly in the lathe.

The stator laminate consist of individual soft steel plies with 0,4mm thickness that were only bonded together by enamel, so there was a need to design and manufacture a jig for the diameter reduction. The jig is displayed in Figure 81. It was required in order to distribute the constraining load and hold the plies together during the turning operation, and later during the separation and reorientation of the laminate. The laminate is fastened to the jig by twelve M6 bolts with wide shim



FIGURE 81: STATOR JIG BEFORE AND AFTER MOUNTING IN THE LATHE

The stator was mounted in the jig in a lathe and carefully aligned to the rotation axis with a dial gauge, both in radial and axial direction. The jig was radially aligned within 5/100 mm in the radial direction and the stator laminate was aligned to within 10/100mm. The enamel surface was somewhat rough and uneven and made better alignment difficult. Both operations were performed in the IPM workshop.

The turning was done with 0,25mm cuts (diameter reduction) with 200 RPM and cutting fluid. The cuts were small to minimize deflection of the end-layers in the laminate, and generally reduce the stress of the assembly. The diameter was reduced by 24mm, with a final back iron thickness of 8mm, a very time-consuming process. The stator is pictured before and after the diameter reduction in Figure 82 at the top and bottom respectively.



**FIGURE 82: THE STATOR IN THE JIG BEFORE (ABOVE) AND AFTER DIAMETER REDUCTION**

The next process was skewing of the stator laminate, so that the top ply was displaced one position compared to the bottom one. This corresponds to a slope of approximately 60 degrees. The skewed stator is displayed in Figure 83. After the skewing, the stator was clamped and glued together with Loctite 5 minute epoxy.

One lesson learned during the process of reducing the stator diameter is that a thicker steel sheet should be added on both sides of the stator in the jig, in order to distribute the load and pressure on the outer stator plies. This could allow deeper cuts and faster federate, which will greatly reduce the process time.



FIGURE 83: SKEWING OF THE STATOR TEETH

The process reduced the weight of the stator from 2790g to 1390g, a weight reduction of 50%.

Thruster prototype stator data		
Data	Original	Modified
Outer Diameter [mm]	210	186
Inner Diameter [mm]	130	130
Height [mm]	20	20
Weight [g]	2790	1390
Weight reduction [g]	-	<b>1400</b>
Weight reduction [%]	-	<b>50,2</b>

TABLE 9: THRUSTER STATOR DATA

The stator data are displayed in Table 9. These data only represent the “easily achieved” weight reduction. It is thought that the stator teeth are thicker than what is necessary, and when the stator teeth cross section is reduced, the back-iron could also be reduced. This will greatly reduce the stator weight

### 6.2.2 ROTOR

The rotor of the prototype is made with a combination of 3D-printing and machining. The components are an aluminium axle, a 3D-printed ABS propeller, 24 neodymium permanent block magnets, and a steel rotor ring to hold the magnets and increase the magnetic flux. The design is illustrated in Figure 84.



**FIGURE 84: THRUSTER PROTOTYPE ROTOR 3D MODEL**

The propeller of this thruster prototype is designed with focus on mechanical strength rather than hydrodynamic efficiency. The main objective for the propeller is to hold the magnets, and it might also be subjected to a simple thrust test in purified water. It is important to use purified water so the motor will not short circuit. Totally pure water does not conduct electricity, and small contamination from the motor will be unproblematic with short test times. Argus RS has tested uncoated thrusters this way before. Oil could also be used, but due to the different viscosity the results will probably be different from water. Water is also much easier to remove after the test.

The propeller features 6 blades, with a 30 degree outer slope and 60 degrees inner slope. The wall thickness is 3mm over the whole blade.

The 24 magnets will be oriented in pairs with the same polarity, resulting in 12 poles on the rotor.

FEM-analysis was conducted on the propeller in order to make sure it could handle the large magnetic forces. The load was 1000N radial bearing forces on the rim, and 300N axial geometrically distributed forces on the blades.

The rim propeller has been analysed using a 2mm CTETRA(10) mesh and ABS as material.

parametric rim-propeller\_sim2 : Solution 1 Result  
Subcase - Static Loads 1, Static Step 1  
Displacement - Nodal, Magnitude  
Min : 0.000, Max : 1.451, Units = mm  
Deformation : Displacement - Nodal Magnitude

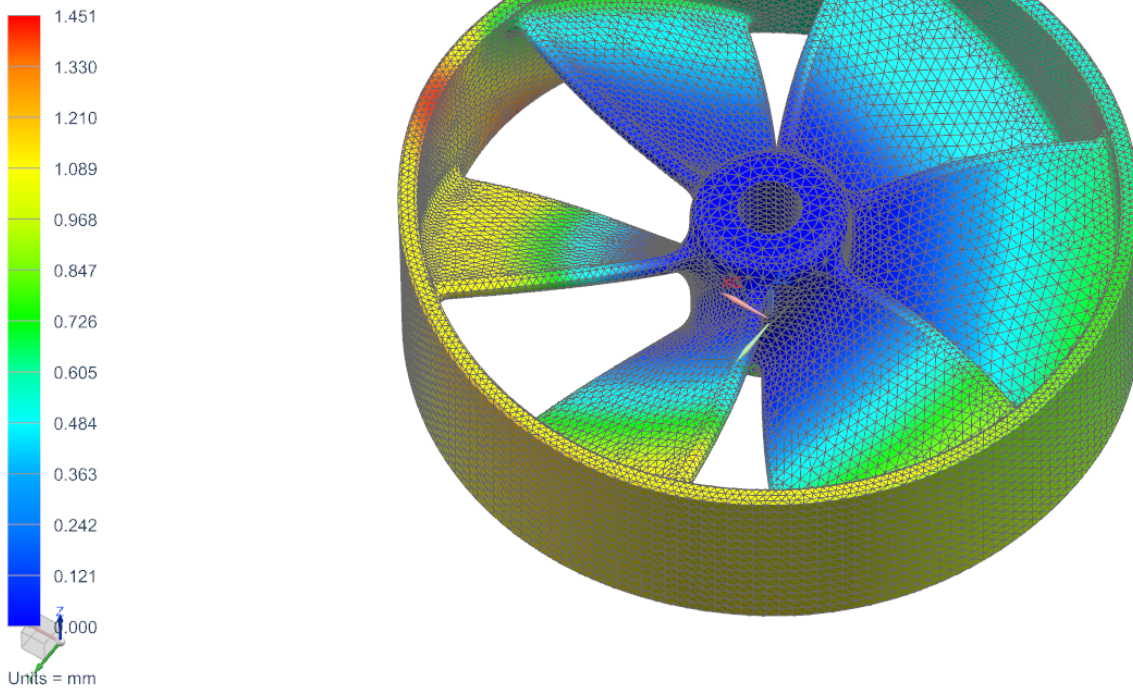


FIGURE 85: DISPLACEMENT PLOT OF RIM PROPELLER

The displacement plot in Figure 85 shows that the propeller is too compliant for the given load state and an air gap of 1mm. When the rotor was tested in the test rig it showed no visible displacement, and the rotor did not touch the stator with 1mm air gap on each side. This shows that the rotor setup is sufficiently stiff, which indicates that the load case is conservative.

parametric rim-propeller\_sim2 : Solution 1 Result  
Subcase - Static Loads 1, Static Step 1  
Stress - Elemental, Von-Mises  
Min : 0.03, Max : 46.18, Units = N/mm<sup>2</sup>(MPa)  
Deformation : Displacement - Nodal Magnitude

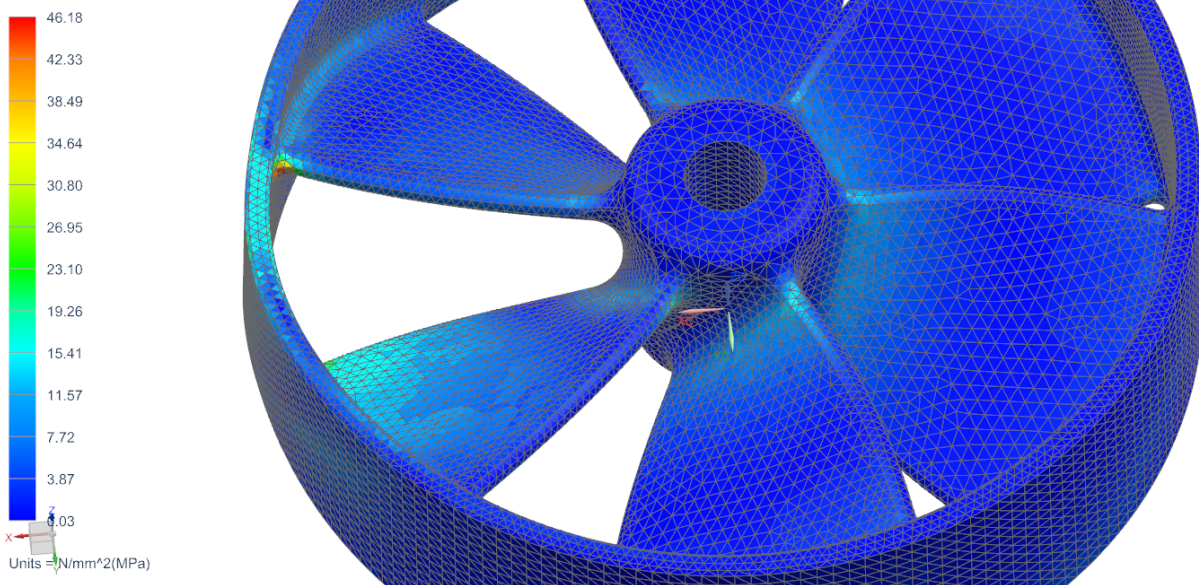
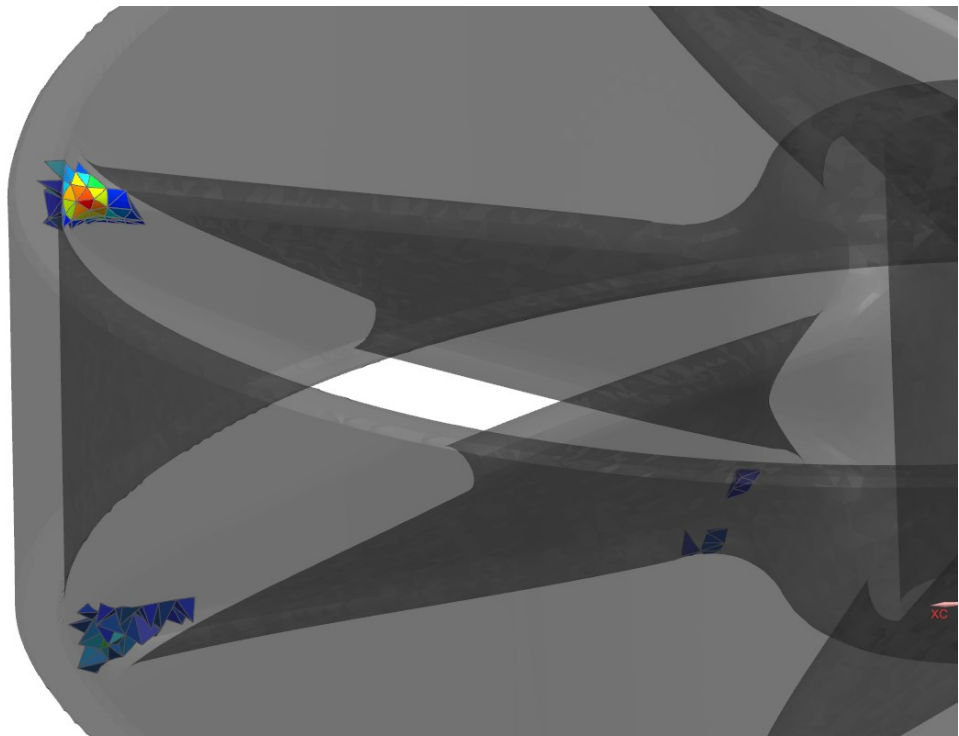
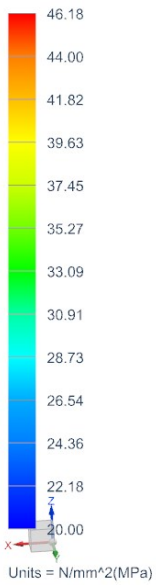


FIGURE 86: STRESS PLOT OF RIM PROPELLER

parametric rim-propeller\_sim2 : Solution 1 Result  
Subcase - Static Loads 1, Static Step 1  
Stress - Elemental, Von-Mises  
Min : 0.03, Max : 46.18, Units = N/mm<sup>2</sup>(MPa)  
Deformation : Displacement - Nodal Magnitude



**FIGURE 87: STRESS PLOT OF RIM PROPELLER,**

Elements with stress level below 20MPa are rendered translucent in Figure 87. Although some parts of the propeller have a von Mises stress above yield strength, most of the propeller has low stress levels, displayed in Figure 86. The highest stress levels are restricted a small area on the surface. Also, the load state is highly conservative. The results are therefore regarded as satisfactory

The propeller can be made a lot thinner by using stronger and stiffer materials, like ABS-CF or PC. The best method of manufacturing the propeller is probably injection moulding if the production volume is large enough to justify the tool expenses.

**Details about load state and mesh are found in chapter 17: Appendix H: Thruster prototype FEM analysis.**

The rotor iron was made from a 126x114mm steel pipe, which was turned down and 24 slots for the magnets were milled. The rotor iron is pictured in Figure 88. The slots measures 30x10x2mm, and is made so that standard N42 30x10x5mm magnets [36] will provide a 1mm air-gap between the rotor and the stator.

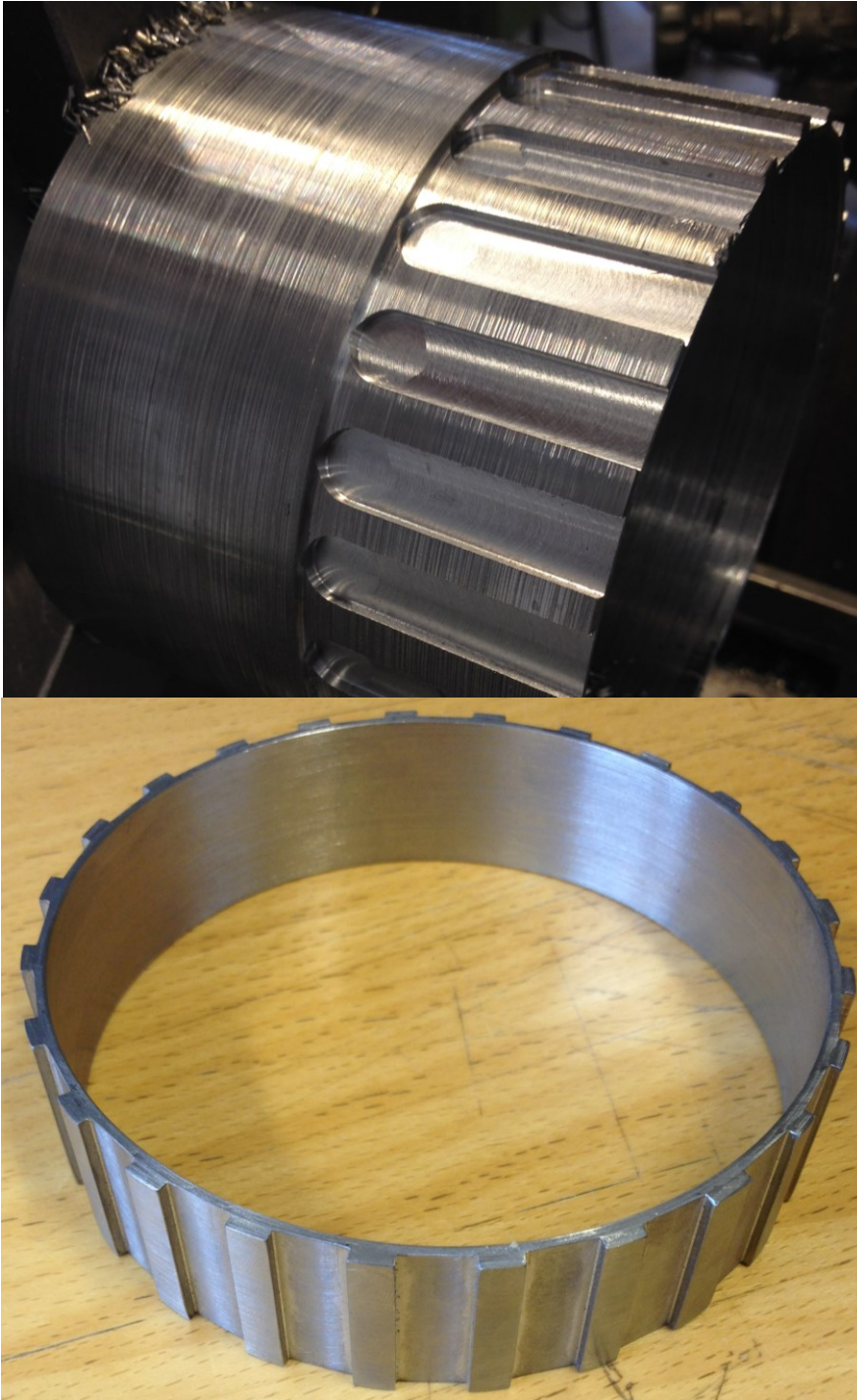


**FIGURE 88: MANUFACTURING THE ROTOR IRON**

The final rotor for the test rig weighs 545g with the current propeller design. It is shown in Figure 89. The main weight contribution is the magnets that weigh 265g and the rotor iron that weighs 175g. The magnets will get slightly lighter in the finished design, as thinner custom casted neodymium magnets with curved outer surface will be used. This will ensure a constant air-gap over the magnets, which will lead to better efficiency and thereby lower weight per output torque.



**FIGURE 89: FINISHED PROTOTYPE ROTOR**

The propeller was sanded down in order to even out the 3D-printed surface. When the roughest surface had been evened out, acetone was applied. Acetone dissolves ABS plastic, so the surface roughness was reduced further. The result is a smooth and glossy surface.

### 6.3 THRUSTER TEST RIG

In order to perform efficient and easy testing of motor characteristics, a test rig was designed and manufactured. The test rig requirements were that it should be easy to change both stator and rotor, and the rig had to be rigid enough to withstand the magnetic forces in the motor.

The test rig is designed to provide flexibility to work with different rotors and stators. The design was created after investigating what materials were available at the IPM workshop.

The design, which is illustrated in Figure 90, allows for stator diameters between 115 and 265mm and heights up to 30mm. The 12mm axle runs through a set of two standard 12x37x12mm ball bearings, which allows for removal of the rotor within seconds. The stator is removed by loosening the 4 bolts and sliding the pillars outwards. The design focuses on easy access to both stator and rotor. This way the stator could be wound and reassembled efficiently for a different test configuration.

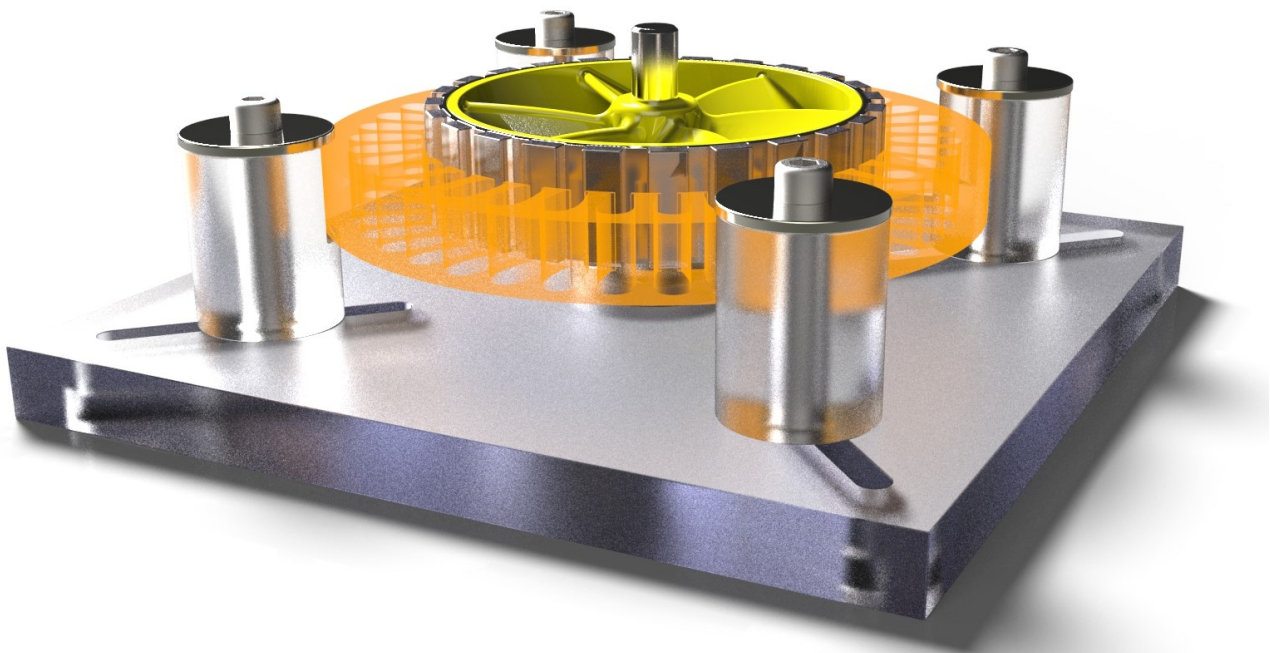


**FIGURE 90: STATOR TEST RIG ASSEMBLY**

In Figure 90, aluminium is rendered translucent while the stator position is indicated by orange.

The test rig was machined at IPMs workshop in Trondheim by the use of manual lathes and mills. Some of the machining steps are pictured in Figure 91. Documentation and machine drawings can be found in chapter 22 Appendix M: Machine drawings of thruster test rig.

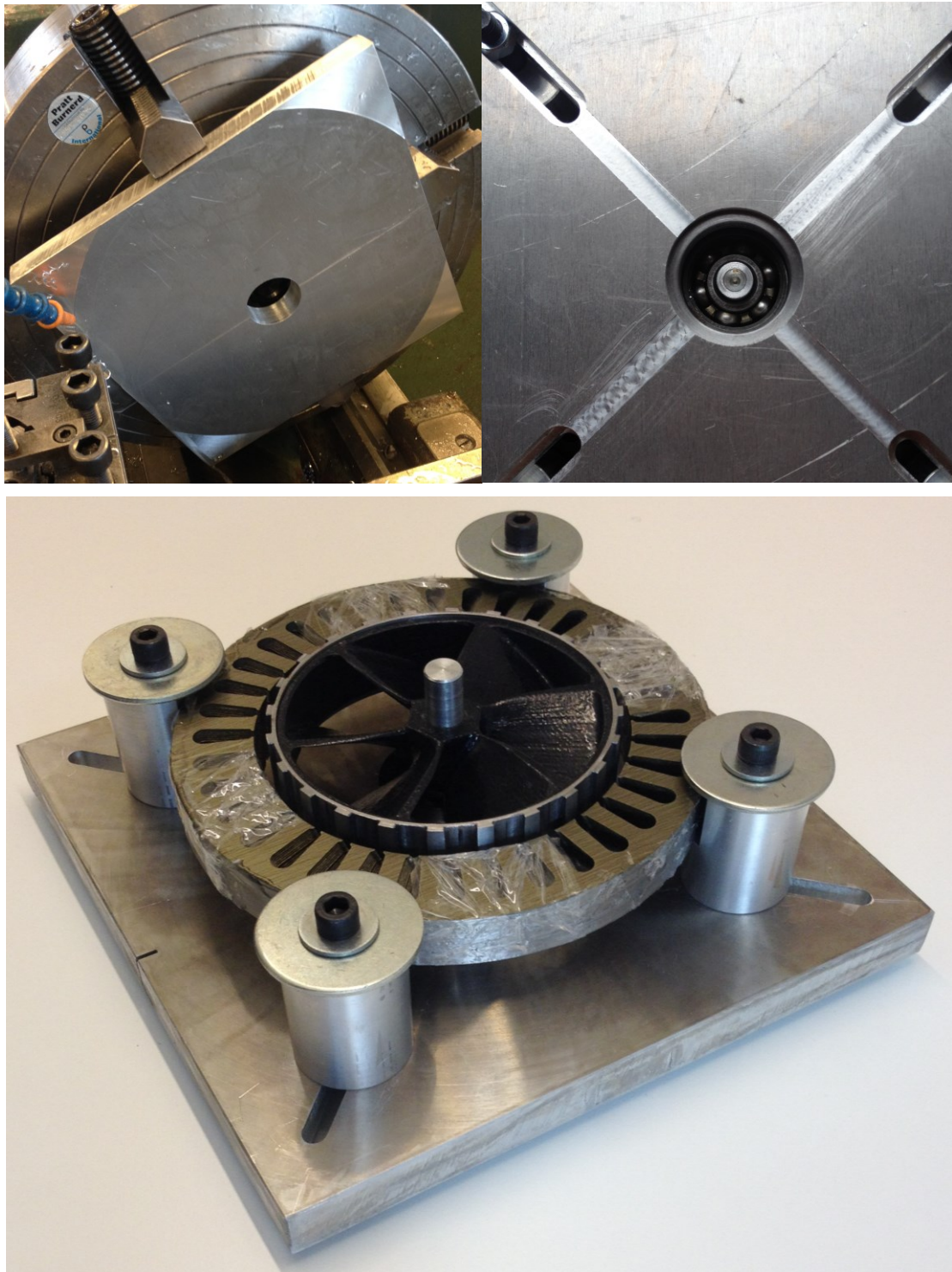


**FIGURE 91: THRUSTER IN TEST RIG WITHOUT MAGNETS AND WINDINGS**

The stator is taped in Figure 91, as it is only held together by a thin layer of epoxy on the outer cylinder surface. When the testing is complete and satisfactory results have been achieved, the whole stator will be dipped in special enamel that will penetrate the steel laminate and hold it together. The test rig was handed over to Argus RS for winding and testing 09.04.2014.

The stator was wound by Frederik Wendel at Argus RS. The test rig was also improved by adding some adjustment screws for fine tuning the concentricity of the rotor and stator, pictured in Figure 92 and Figure 93. This was needed because of the strong magnetic forces and the small air gap.

The torque cogging that was present prior to the skewing of the stator is now gone.

There are also no problems with deflection of the axle / propeller due to the large magnetic forces.

Due to some difficulties with the motor control, which is out of the scope of this thesis, no performance data are available at this time. The difficulties was caused by inaccurate readings from the Hall Effect sensors due to the fact that one rotor pole is simulated by two magnets. This problem is fixable, but it could not be done in time for the report.

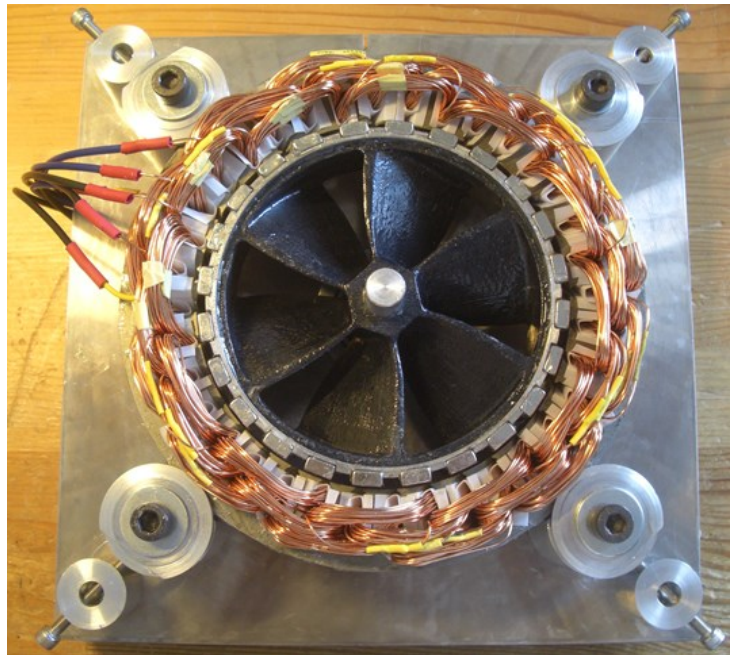


FIGURE 92: COMPLETE PROTOTYPE THRUSTER TEST RIG

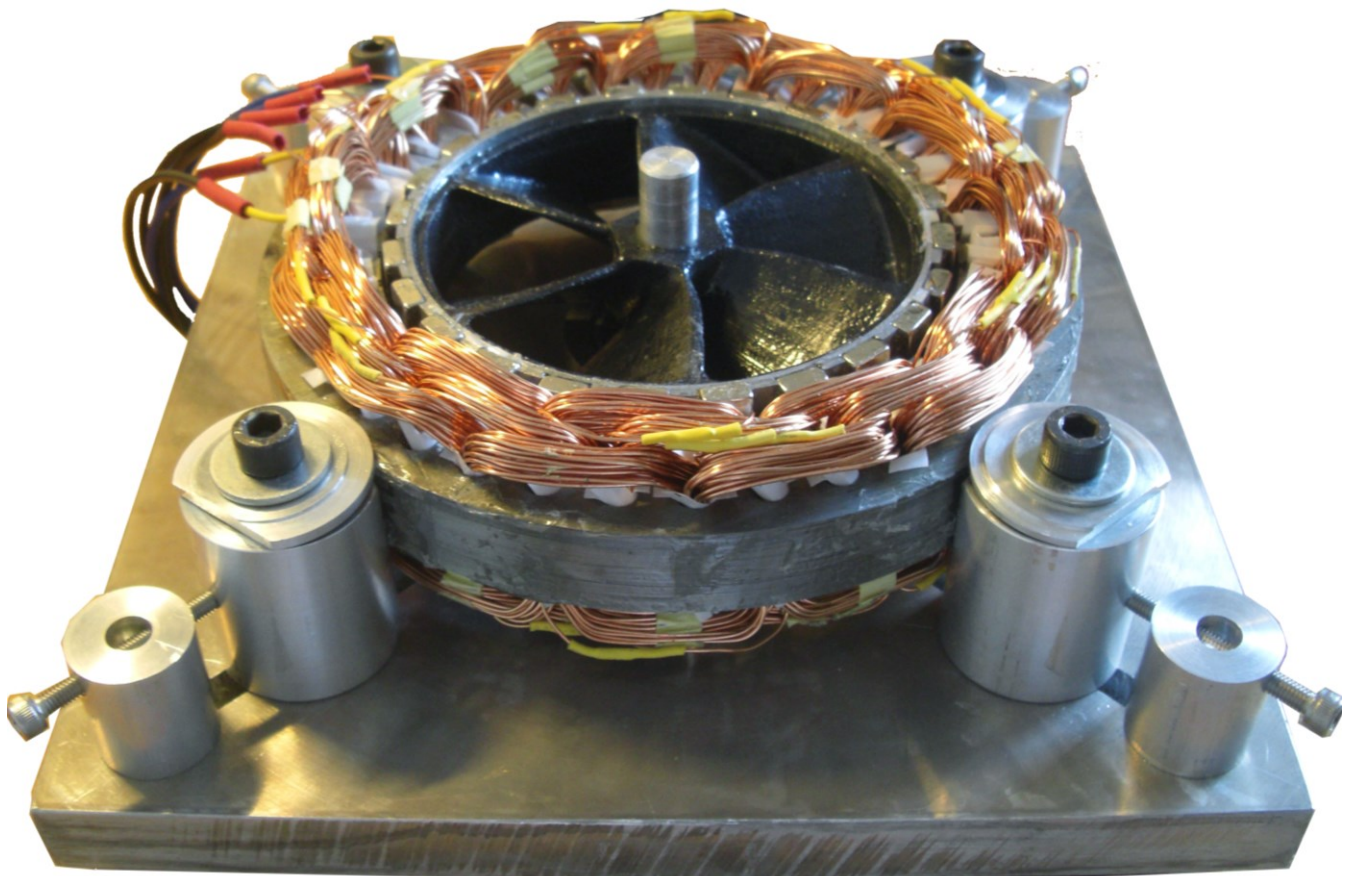


FIGURE 93: COMPLETE PROTOTYPE TEST RIG

## 7 MANUFACTURING

Part of this project is to investigate the ways to manufacture the new Manta.

### 7.1 MANUFACTURING THE HULL

As discussed in chapter 10.1, the most suitable manufacturing method for the thermoplastic hull is vacuum forming. The relative small series of units require a manufacturing method that has a reasonable investment cost.

The hull is thought to be manufactured in two pieces and then assembled together. As discussed in chapter 5.2.2.4, the chosen way of connecting the hull sections is a combination of bolts and glue. The combined process of vacuum forming and hot welding is a good alternative if the tool cost is acceptable. The only manufacturer found to provide this service in Norway is Plexx AS.

Some Norwegian and some foreign manufacturers of vacuum formed products have been contacted for a price estimate. The basis for the estimate was a set of machine drawings, which gave an overview of size and geometry, and a couple of renderings showing the final product. The cost data found is displayed in Table 10.

Estimated manufacturing cost of hull in NOK							
	Units:	20	100	500	20	100	500
Manufacturer	Tool Cost	Cost pr. hull			Cost pr. hull incl. tool investment		
Formvac AS	100 000	1 000	1 000	1 000	6 000	2 000	1 200
Unica AS	30 000	1 040	1 040	1 040	2 540	1 340	1 100
Plexx AS	132 000	800	800	800	7 400	2 120	1 064
Plexx AS TwinSheet*	240 000	700	700	700	12 700	3 100	1 180
Gyli Plast AS	120 000	1 300	720	600	7 300	1 920	840
Red numbers are not specified for the given unit number, but based on 100 hulls							
*TwinSheet welds together the hull in the forming process, eliminating the need for assembling two parts							

TABLE 10: ESTIMATED COST OF MANUFACTURING HULL

Note that Unica AS has a much lower tool cost than the competitors. Even though proper machine drawings have been provided and aluminium moulds were specified, there can have been a misunderstanding. Argus RS has been in contact with a Chinese supplier, and their tool cost corresponds to that of Unica AS. Unica AS is therefore the recommended manufacturer of the hull.

Before making an expensive aluminium forming tool, a foam mould will be used for the prototype. This will be done to verify accuracy of manufacturing method, and the mould parameters could be changed if needed.

## 8 CONCLUSIONS AND FUTURE WORK

A concept for a lightweight Remotely Operated Vehicle (ROV) named the Manta was designed for inspection of the net cages and collection of dead fish at aquaculture facilities. The current thesis has presented the initial development and engineering design of the product, including requirements and need findings, material selection, technical solutions and design verification by the finite element method.

The hull of the Manta has been designed and engineered based on the currently chosen components, which may be changed in the future. The Manta's hull features a large internal cavity, and the two horizontal thrusters are located inside of it. The thrust force created by the horizontal thrusters results in an internal flow through the hull, which is used to collect salmon in a rear-mounted net while the ROV is propelled forward. The three vertical thrusters are mounted into thin wings on the exterior of the hull. These are designed to provide control of vertical movement, as well as pitch and roll. The wings protect the thrusters from accidental loading. Streamlined body results in less water resistance and a lower risk of entanglement or damage to the net cage.

The hull design is based on 4 mm thick ABS plastic sheets manufactured by vacuum forming, with a total component weight equal to 6,6 kg. ABS was selected due to the combination of easy manufacturing, good impact properties, low density and low cost. The hull will be formed as two parts, an upper and a lower section, which are joined together by adhesives and bolts. The shape of the hull is geometry stiffened by double curvature and corrugation, which is required due to the compliant hull material. The corrugation has proven to increase the stiffness of a simplified hull with 45% with respect to lifting, without any considerable increase in mass.

The 3D model and material specification has been considered as sufficient for manufacturing based on dialogues with the Norwegian manufacturers contacted. The estimated cost of the hull is approximately 1000 NOK per unit excluding tool cost. The cost per unit is about 2000 NOK including tool cost for 100 units. The lowest tool cost estimate from Norwegian suppliers was 30 000 NOK while the highest cost estimate was 240 000 NOK. For the latter, however, the suggested tooling enables subsequent in-line hot welding of the joints and therefore reduced overall cost.

The vertical thrusters' centre axes are perpendicular to the main direction of travel, so a low profile is required. No commercially available thruster designs that satisfy the requirements were found. A conceptual design of the rim-thruster is complete, with a weight less than expected. The current design has an estimated weight equal to 1,7 kg compared to expected 2,0 kg. According to the problem description, prototyping has been conducted, emphasizing the critical design of the vertical rim-thruster. The thruster prototype is mounted in a special designed test rig, which is believed to resemble the critical functions and conditions for the components. Data from the testing could provide vital information about electromagnetic design and simulation accuracy.

The final weight of the Manta is estimated to be approximately 29 kg with the specified materials and components. The final weight may differ to some extent, especially regarding the design of vertical thrusters and the selected horizontal thruster model. The final design is illustrated with a large salmon for scale in Figure 94.

A list of remaining subjects has been made.

The project will be completed by Argus and Inventas during the fall of 2014.

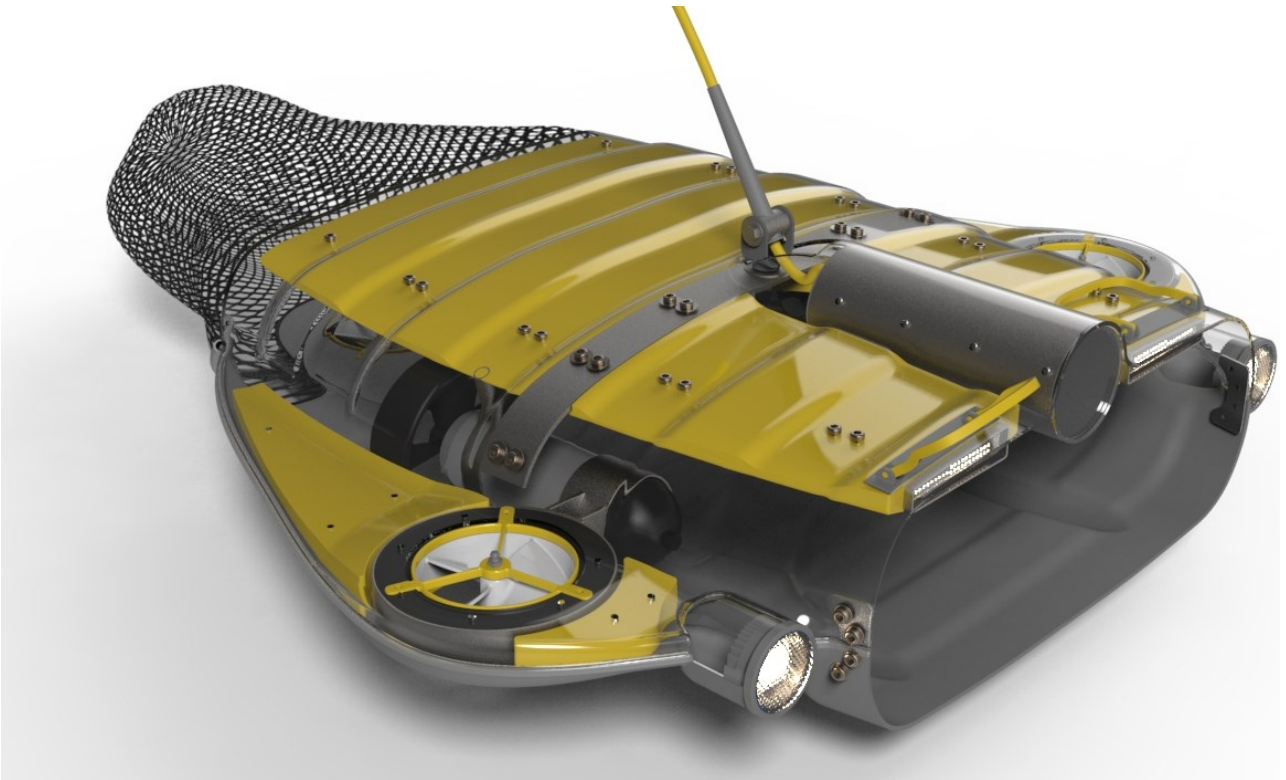


FIGURE 94: FINAL DESIGN

More illustrations of the final design are found in Appendix C: Illustrations of final design.

## 8.1 FUTURE DESIGN TASKS

- Rim-thrusters must be fully developed
  - This will be an important part of the total project. Mechanical design is almost complete and awaits the stator geometry for finalization. The design is dependent on the specific electromagnetic design to be developed by Argus RS.
- Horizontal thrusters must be specified and connections have to be fully designed.
- All electronic components must be specified.
  - Argus RS has already some solutions for motor control, sensors, cameras and lighting etc. that could be used. When the thrusters are designed, more detailed specifications of electrical system could be completed. There could also be other relevant thrusters on the market that needs to be explored.
  - The electronics and sensors will be specified by Argus based on their experience with ROV development, and the size and shape of these components are unknown at this time. The types of sensors include depth, temperature, compass and oxygen levels.
- Design of a simple launch and recovery ramp with floaters.
  - This ramp could be mounted on the deck and tilted into the water. This ramp would make it much easier to launch and recover the Manta.
- Net and quick release net locks.
  - The net should be easy to disconnect and to empty. The net should be possible to lift by hand and by the use of a winch. Different net sizes may also be required.
- A custom-made trolley that will ease the transportation could be designed.

## 8.2 FUTURE SIMULATION REQUIREMENTS

- Realistic lifting with all the weights and components included.
  - Both with umbilical and lifting handles.
- Centre of mass and buoyancy requirements must be calculated.

## 8.3 FUTURE PROTOTYPING

- Rim thrusters
  - After Argus RS has finalized the electromagnetic design based on the results from the thruster test rig, prototypes of the complete design has to be made for testing.
- Electronic assembly
  - When all internal components are specified and the geometry is set, a prototype will be made in order to verify the design by lab- and field tests. Important parameters are fail pressure and internal temperature during operation.
- Hull
  - Make a low cost vacuum forming mould from a cheaper foam material. As aluminium moulds are expensive, a prototype will be made using a low cost foam mould. The foam mould is less durable and efficient, so larger series manufacturing would be uneconomical.

## 8.4 FUTURE TESTING

- Thrusters must be tested
  - In distilled water to test rotational speeds and thrust.
  - After embedding, the thrusters must be tested in particle-filled water to verify bearing- and coating durability, and the heat dissipation (cooling) of the motor must be verified.
- Pilot project(s) at an aquaculture facility.

## 9 REFERENCES

1. **Myklebost, Magnus Rogne.** *Project Thesis: Lightweight ROV design.* IPM, NTNU. 2013.
2. **Finnmark Fylkeskommune - fiskeri og havbruk.** <http://www.ffk.no/emner-og-tjenester/naring/fiskeri-og-havbruk/havbruksforvaltning.aspx>. [Online]
3. **Hal F. Brinson and L. Catherine Brinson.** *Polymer Engineering Science and Viscoelasticity - An introduction.* s.l. : Springer, 2008.
4. **Azom.com.** <http://www.azom.com/article.aspx?ArticleID=83>. [Online]
5. **Petras, Achilles.** *Design of Sandwich Structures, PhD thesis.* Cambridge : s.n., 1998.
6. **DIAB group.** *Divinylcell HCP data sheet.*
7. **Granta Design.** CES Selector 4.6. 2005.
8. **Eurapipe.** Sydenyhvac.net. [Online]  
<http://www.sydneyhvac.net/Files/hydronicdesign/ABSdata.pdf>.
9. **Troughton, Michael J.** *Handbook of Plastics Joining - A Practical Guide (2nd Edition).* s.l. : William Andrew Publishing, 2008.
10. **Siemens.** *NX 8 CAST.*
11. **Plexx AS.** <http://www.plexx.no/>. [Online]
12. **Argus Remote Systems.** <http://www.argus-rs.no/products/electrical-rovs/rover>. [Online]
13. **Ø. Krøvel, R. Nilssen, S. E. Skaar, E. Løvli, N. Sandøy.** *Design of an Integrated 100kW Permanent Magnet Synchronous Machine.* s.l. : Department of Electrical Power Engineering, NTNU, Trondheim, Norway.
14. **Brunvoll Thrusters AS.** *Brunvoll presents a "Rim driven thruster" (RDT) .* 2005.
15. **Seamore Marine.** <http://www.seamor.com/>. [Online]
16. **Schottel.** <http://www.schottel.de/>. [Online]
17. **Hanselman, Dr. Duane.** *Brushless Permanent Magnet Motor Design - 2. edt.* s.l. : Magna Physics Publishing, 2006.
18. **Colton, Shane W.** *Design and Prototyping Methods for Brushless Motors and Motor Control.* s.l. : Massachusetts Institute of Technology, 2010.
19. **Thin Gap.** <http://www.thingap.com/technology/>. [Online]
20. **Leibniz Institute for Solid State and Material Research.** <http://www.ifw-dresden.de/de/institute/institut-fuer-komplexe-materialien/abteilungen/chemie-funktioneller-materialien/corrosion/corrosion-of-permanent-magnet-materials/corrosion-properties-of-ndfeb-permanent-magnets/>. [Online]
21. **Fraden, Jacob.** *Handbook of Modern Sensors: Physics, Designs, and Applications.* s.l. : Springer, 2010.
22. **Schottel.** <http://shipbuildingtribune.com/2012/06/06/germany-schottel-rim-thruster-srt-for-osvs-superyachts-and-inland-water-vessels/>. [Online]
23. **Brunvoll AS.** *Brunvoll presents a "Rim driven thruster".* 2005.
24. **Voith Rim-Drive Technology Brochure. Voith Turbo Advanced Propeller GmbH & Co.**
25. **Craftech Industries inc.** <http://info.craftechind.com/blog/bid/259158/Top-5-Materials-for-Plastic-Bearings-Used-on-Metal-Surfaces>. [Online]

26. **SKF.** *SKF stainless steel deep groove ball bearings data sheet.*
27. **Alcoa Mill Products.** *ALLOY 7075 datasheet.*
28. **PT. Robo Marine Indonesia.** <http://robomarine.com/thrusters.html>. [Online]
29. **Submertec Limited.** <http://submertec.co.uk/>. [Online]
30. **Lighting Research Center.** <http://www.lrc.rpi.edu/programs/nlpip/lightinganswers/lightsources/whatisColorRenderingIndex.aspx>. [Online]
31. **CREE inc.** <http://www.cree.com/>. [Online]
32. **Osram Opto Semiconductors.** *OSLON Square® Datasheet v1.2.* 2013.
33. **CREE inc.** *Cree® XLamp® LEDs.* 2013.
34. **LCK LED.** <http://www.lck-led.com/zxpower-z100-100w-high-power-p-478.html>. [Online]
35. **Busck.** <http://www.busck.se/no>. [Online]
36. **SuperMagnete.** <http://www.supermagnete.de/eng/Q-30-10-05-N>. [Online]
37. **MachineDesign.** <http://machinedesign.com/plastics-and-composites/putting-right-spin-rotational-molding-designs>. [Online]
38. **XINYI mould.** <http://www.prettypmould.com/index.php/history-of-blow-molding/>. [Online]
39. **SubsTech.** [http://www.substech.com/dokuwiki/doku.php?id=injection\\_molding\\_of\\_polymers](http://www.substech.com/dokuwiki/doku.php?id=injection_molding_of_polymers). [Online]
40. **Sinotech.** <http://www.sinotech.com/thermoforming.html>. [Online]
41. **Advanced Lightweight Engineering.** <http://www.ale.nl/?portfolio=manufacturing-processes>. [Online]
42. **J&J Mechanic.** <http://www.jjmechanic.com/process/handlayup.htm>. [Online]
43. **Trygavac.** <http://www.tygavac.co.uk/process/resin-infusion.html>. [Online]
44. **Vedvik, Nils Petter.** *Essential Mechanics of Composites.* 2013.
45. **RTP co.** <http://www.sintef.no/project/ffs/dokumenter/seminar-april2011/Long-Fiber-Composites-April2011.pdf>. [Online]
46. **Simulia Corp.** Abaqus 6.12 Documentation Collection.
47. **Encyclopedia Britannica.** <http://global.britannica.com/EBchecked/topic/271336/Hookes-law>. [Online]
48. **Anderson, T. L.** *Fracture Mechanics: Fundamentals and Applications.* s.l. : CRC Press, 2005.
49. **Composites World.** <HTTP://WWW.COMPOSITESWORLD.COM/ARTICLES/HOLE-AMBITIONS-OPTIMIZE-CUSTOMIZE>. [Online]
50. **Kollar, Springer &.** *Mechainics of composite structures.* s.l. : Cambridge University Press, 2003.
51. **Irgens, Fridtjov.** *Formulas mechanics.* s.l. : Tapir Academic Press, 2008.
52. **Torayca.** *T300 Data Sheet.*
53. **AK Steel Corporation.** *316 / 316 L steel data sheet.*
54. **SM Remote Systems.** *Manta 505 Brochure.* 1993.

55. **Northvale Korting.** <http://www.northvalekorting.co.uk/prod-fluidjet.asp>. [Online]

56. **Formvac AS.** <http://formvac.no/index.php?sideID=286&ledd1=270>. [Online]

## 10 APPENDIX A: MANUFACTURING COMPONENTS

The acquisition cost of a structure is a combination of material cost and cost of manufacturing. One can also argue that the maintenance cost is an important cost aspect. Some materials will need production methods that are unfeasible in this case, while other materials are so easy and low cost to shape that they become relevant even though they score low on other properties. For instance forming of aluminium sheets will require expensive equipment that most likely will be uneconomical for small series manufacturing. Both ABS plastic (and other thermoplastic sheet materials) and fibre composites can be manufactured using relative inexpensive moulds and equipment. Prototyping moulds can be made even less costly. The most relevant materials are therefore the inexpensive heavier solution with thermoplastic or the lightweight but costly solution with carbon fibres from their manufacturing properties alone.

### 10.1 THERMOPLASTICS

Examples of thermoplastic component manufacturing are machining, extrusion, blowtrusion, blow moulding, injection moulding, rotation moulding and vacuum forming. The Manta's hull has a thin wall compared to its size, so only a few methods are practically relevant. These will be explained below.

*Rotational moulding* uses a mould that is filled with thermoplastic pellets and heated while rotating the mould. The melted plastic is then cooled while the mould still rotates. This can create a product with a complex shape and closed cavities [37], illustrated in Figure 95. The machinery is represents a substantial cost and sufficient tolerances have proven to be challenging.

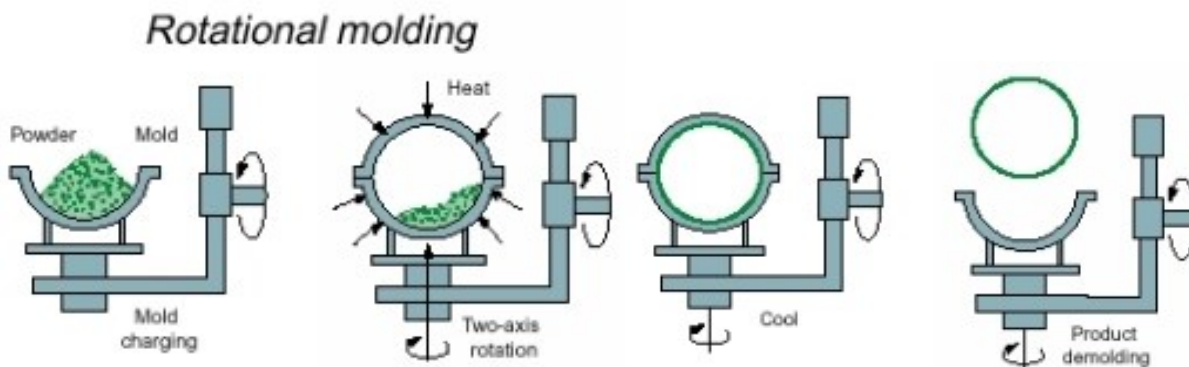


FIGURE 95: ROTATIONAL MOULDING PROCESS

*Blow moulding* use pressurized air in combination with a mould to shape a softened plastic from an extruder like in Figure 96. The process is efficient, but is typically used for mass production like plastic bottles etc. because of the somewhat complex machinery. [38]

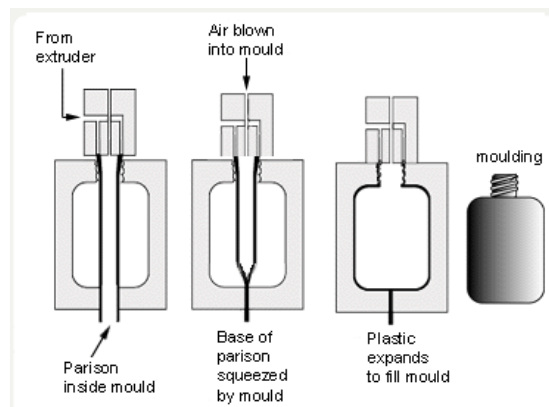


FIGURE 96: BLOW MOULDING PROCESS

With Injection moulding the extruder directly injects molten plastic into a mould under high pressure. The required machinery is illustrated in Figure 97. The process is typically used for mass production because of the requirement of expensive moulds and machinery. The process itself is however highly efficient. [39]

### Injection Molding

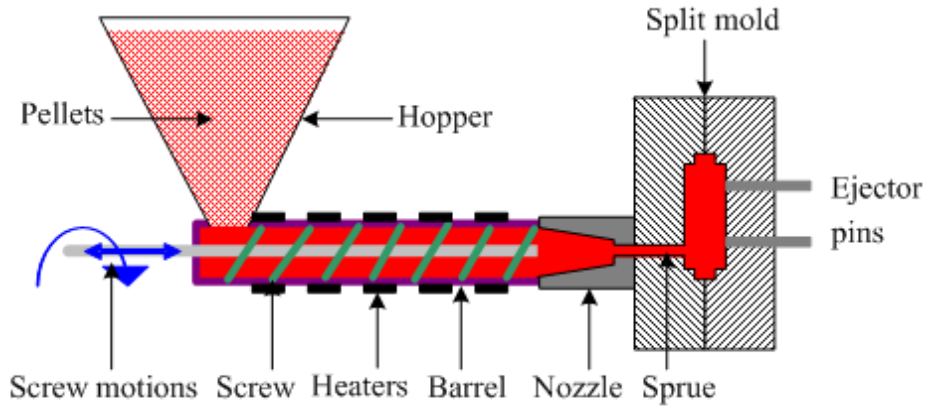


FIGURE 97: INJECTION MOULDING PROCESS

Thermoplastic sheets can easily be shaped by *vacuum forming*, where a preheated sheet is placed on top of a mould. The air underneath is sucked out, and the softened plastic fills the mould, like the process in Figure 98. This process is designed for sheet material, and can both be done manually or in an automated process. The process is efficient and the moulds are fairly priced. This manufacturing method is therefore feasible for the small series manufacturing of the Mantas hull. [40].

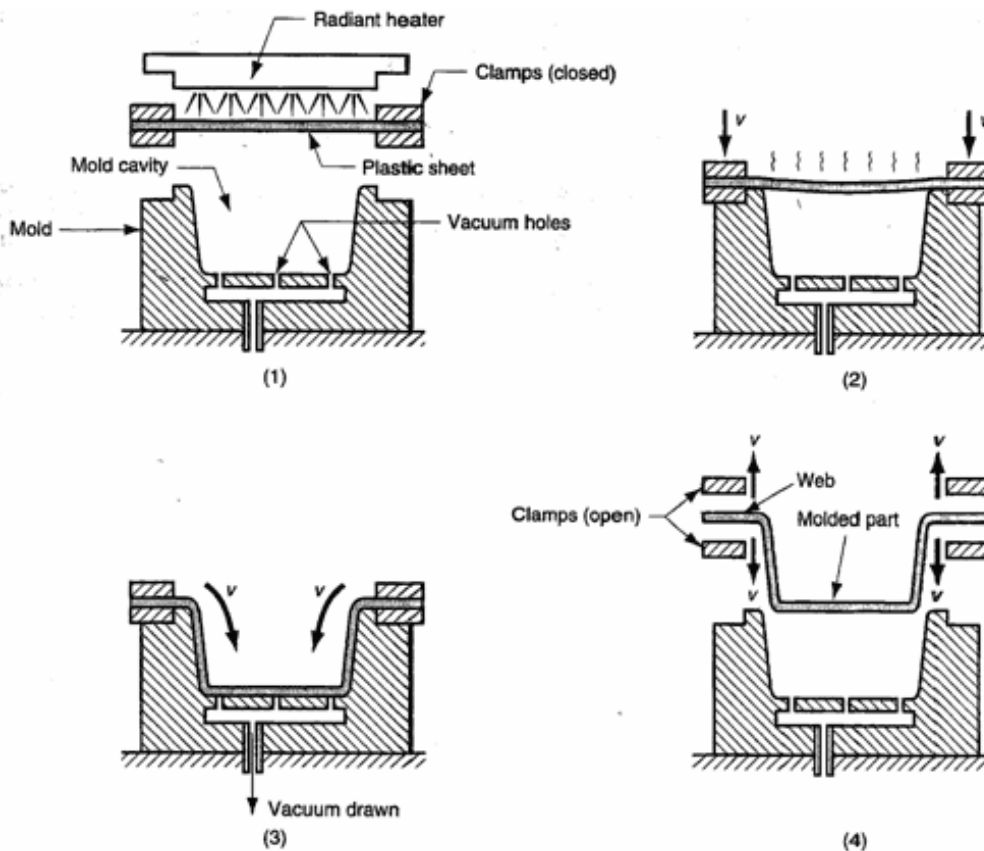


FIGURE 98: VACUUM FORMING PROCESS [40]

## 10.2 FIBRE COMPOSITE LAMINATE

The manufacturing of a fibre composite can be done in many ways, where the most relevant will be introduced. Manufacturing composite parts is expensive even though some of the manufacturing methods require little equipment. The materials are often costly and small-scale manufacturing may require a lot of man-hours.

*Resin transfer moulding (RTM)*, is a method where the resin is injected into a mould containing the fibres, illustrated in Figure 99. This process requires expensive machinery, but is very efficient and the resulting laminate is typically high quality with high fibre fraction (fibre weight pr. total composite weight) and low void content. This method is therefore typically used for smaller high quality fibre composite parts. However the costly moulds and complex machinery makes this method relatively expensive for the manufacturing of some hundred hulls. If the production volume is increased, it can still be relevant. [41]

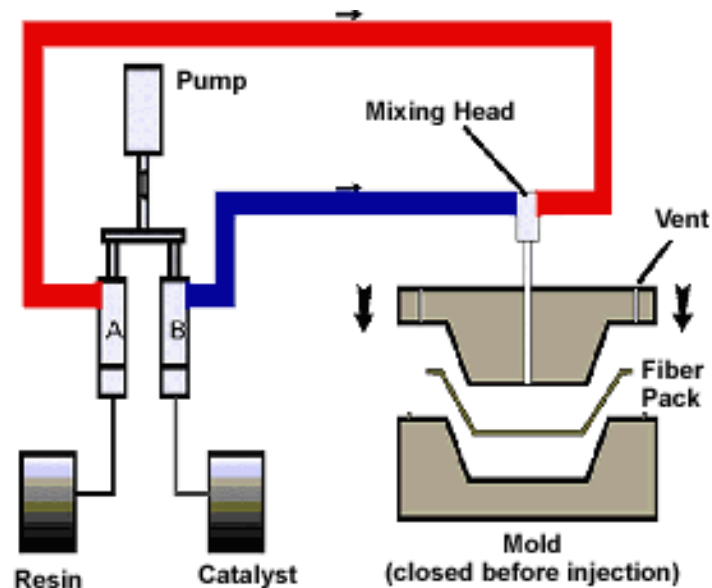


FIGURE 99: RESIN TRANSER MOULDING PROCESS

With *hand layup*, the fibres are wetted by hand, and a roller is used to consolidate the plies, shown in Figure 100. This method is time-consuming but fairly easy. The resulting laminate does however have a lower fibre fraction because of the lack of pressure, and there are typically some air bubbles / voids in the material. [42]

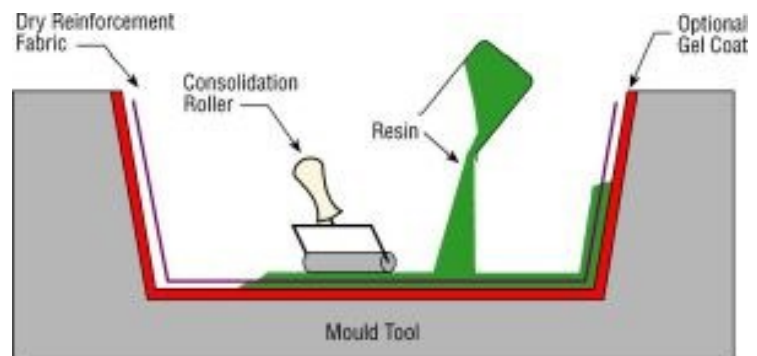


FIGURE 100: HAND LAYUP OF COMPOSITES

*Spray up* utilizes a chopper gun that combines pressurized resin with chopped up fibres, and sprays these into the mould, like in Figure 101. The process is fast and fits large component manufacturing, like boat hulls. The result is a randomly oriented fibre composite, which has a relative low fibre fraction and a high void content. Randomly oriented fibres also create a weaker composite than weaved fabrics. [41]

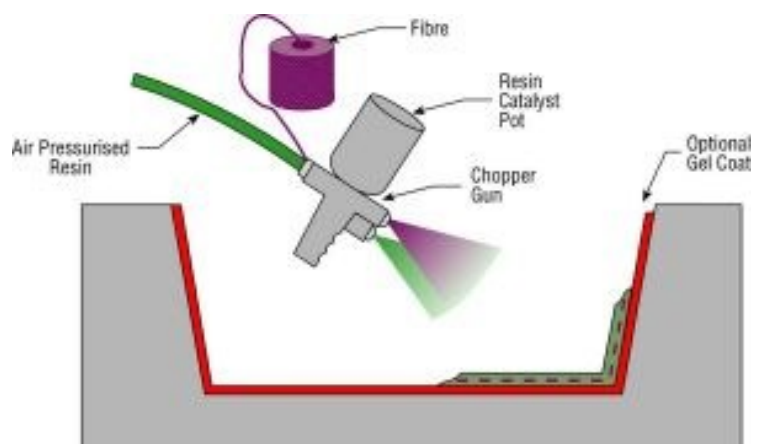


FIGURE 101: SPRAY UP PROCESS

In the *vacuum infusion* process, the fibre weaves are laid into a mould and covered by a vacuum bag. Vacuum is applied in order to suck the resin, for instance epoxy, through the fibre laminate. An even larger pressure difference could be applied by using an autoclave (pressure vessel). The result is a high quality laminate with low void content and a high fibre fraction. The equipment needed is also low cost. Some of the different components of a vacuum infusion are presented in Figure 102.

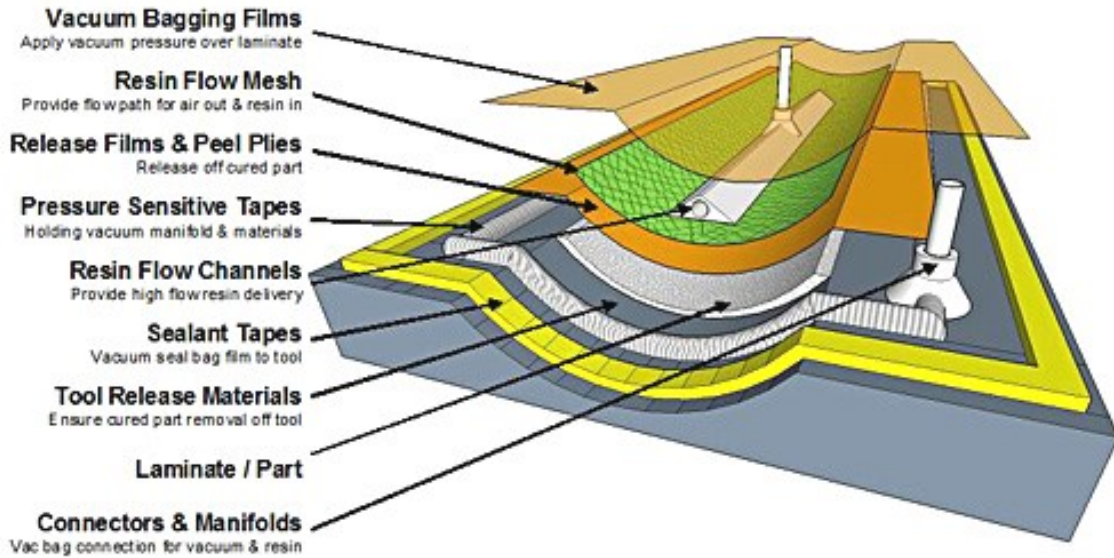


FIGURE 102: VACUUM INFUSION LAYUP [43]

The best way of manufacturing geometry like the Mantas hull is probably vacuum infusion moulding, because of the combination of low cost equipment and high quality results. The process is however time consuming and a complex product like the Mantas hull is probably going to take up to five to six work hours, based on experience. This time could be shortened considerably by practice, using pre-cut fibre cloths and reuse vacuum bagging. Pre-impregnated fibre can also be used in the vacuum mould, which will save some time, but the material itself is more expensive. A composite structure should therefore only be used if strictly necessary.

# 11 APPENDIX B: MATERIAL COMPARISON

## 11.1 COMPOSITE MATERIAL THEORY

Composite materials combine features of different materials that often are useless on their own. There are many kinds of composite materials, but in this thesis only fibre composites will be discussed. These consist of strong and stiff fibres, bonded together in a polymer matrix, creating a lightweight and strong material. Composite materials with oriented continuous fibres are typically orthotropic or transversely isotropic. Orthotropic means that the material has three mutually perpendicular planes of material symmetry and if an orthotropic material has an isotropic plane it is called transversely isotropic [44]. This is illustrated in Figure 103. Material orientation in combination with modifying the thickness can be used to focus strength at the most exposed areas, but it also adds complexity to the simulation and manufacturing. Typically, composites are very strong in the fibre direction and considerably weaker in the other directions. This has to be taken into account when designing the structure and specifying material orientation.

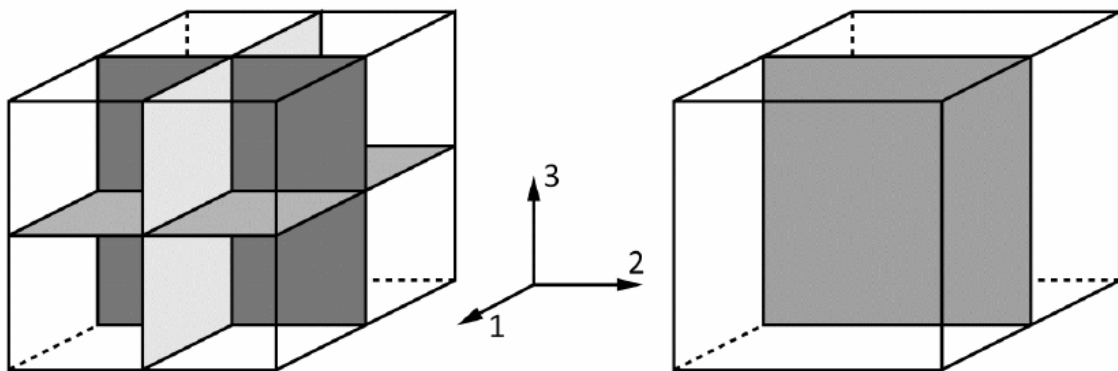


FIGURE 103: PLANES OF SYMMETRY IN AN ORTHOTROPIC MATERIAL (LEFT) AND PLANE OF ISOTROPY IN A TRANSVERSELY ISOTROPIC MATERIAL (RIGHT) [44]

Composite materials can have different fibre orientations, which is illustrated in Figure 104. The fibre weave is most relevant when used in a laminated carbon fibre hull and randomly oriented short (ca. 1-2mm) or long fibres (ca. 10-15mm) [45] are most relevant as ABS-CF fibre sheets or as in injection moulded components.



FIGURE 104: FIBRE ORIENTATION IN COMPOSITES - FROM LEFT: UNIDIRECTIONAL CONTINUOUS AND DISCONTINUOUS, RANDOMLY ORIENTED LONG AND SHORT FIBRE AND WEAVED FABRIC [44]

### 11.1.1 LAMINATE

The most sensible way of creating a strong and stiff thin-walled structure of fibre-reinforced polymers is by using a laminate. A laminate is made from two or more plies bonded together. The plies could have different orientations, thicknesses and compositions, shown in Figure 105.

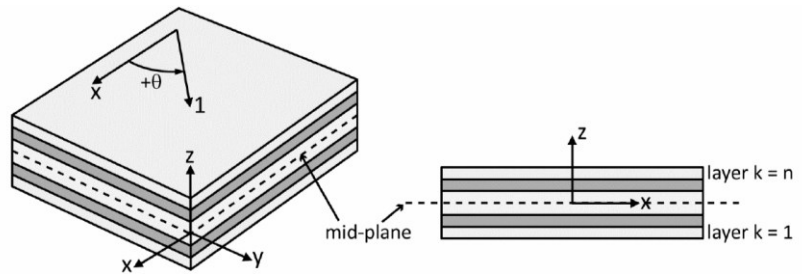


FIGURE 105: ILLUSTRATION OF A LAMINATE [44]

Standard laminate theory, which is used by S4R elements in Abaqus [46], uses some assumptions, which for the Mantas hull is thought to be valid. These are: Plane stress, strains vary linearly through thickness, Hooke's Law [47] apply, displacements and strains are small compared to thickness. Also out-of-plane normal strains and shear strains are neglected and normal distance from any point to the middle surface is constant. [44]

### 11.1.2 SANDWICH STRUCTURE

When an even higher stiffness and strength to weight ratio is needed, a low density core material can be added to the centre of the laminate. The structure is now defined as a sandwich structure.

			
Relative Bending Stiffness	1	7.0	37
Relative Bending Strength	1	3.5	9.2
Relative Weight	1	1.03	1.06

FIGURE 106: SANDWICH STRUCTURE PROPERTIES [5]

This design uses a low density core to increase the second moment of inertia per weight significantly, by increasing the distance between the load carrying skins of the structure as displayed in Figure 106. The bending stiffness is linearly related to the second moment of inertia. The core could be made of closed cell foam, which will provide buoyancy to the hull.

It could also be required to use stronger and stiffer foam (higher HCP value) even though the hydrostatic pressure from the water depth itself does not require so. There can also be challenges with water entering the sandwich and degrading the material and structure, for instance by freezing and expanding.

### 11.1.3 MATERIAL UTILIZATION

The material utilization is a parameter that describes how close the load state is to failure, in other words how much of the strength that is utilized. FEM analysis is done in order to investigate what kind of behaviour a given external load creates inside the structure. When the utilization exceeds 100% it is assumed that the structure will fail. How this is found out varies with respect to what kind of failure criterion that is used. In this thesis it will be focused on Maximum stress criterion for composites and von Mises yield criterion for isotropic materials. It is important to utilize the material strength, as more material adds weight. On the other hand it is wise to have some safety margin in case of unexpected loads, wrong assumptions, material imperfections or other errors.

#### 11.1.4 FAILURE IN COMPOSITES

It is challenging to predict failure in fibre-reinforced composites, as there are so many failure modes dependent on the local loading of the material. The load state typically changes over the structure and this has to be accounted for. Some of the most important failure modes in composites are illustrated in Figure 107.

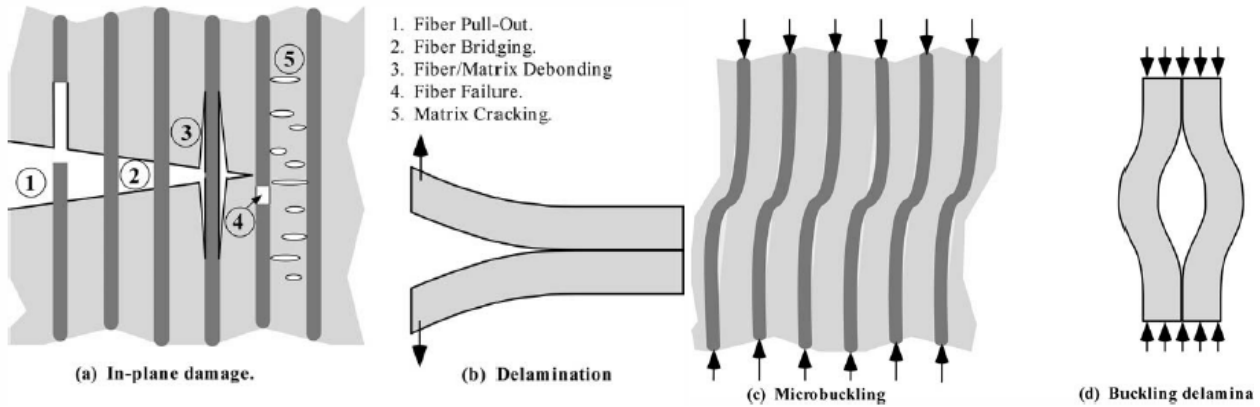


FIGURE 107: FAILURE IN COMPOSITES (FIG 6.15 [48])

**Matrix cracking** is the cracking of the polymer (resin) that holds the fibres together. In the case of the hull, this is not critical as the hull does not need to be water proof (there is water on both sides). However, cracks in the matrix can create voids large enough for water to get trapped. This can both be an issue with contamination and when the ROV is used in cold climate the entrapped water will freeze and expand, which might be problematic over time when the cracks propagates.

Matrix cracking is devastating in the electronic pressure vessel, as this has to be totally waterproof. The solution here can be to coat the outside with an elastic and waterproof material.

**Fibre fracture** is one of the most critical failure modes in composite materials. Typically it is the fibres that represent most of the strength of the material, so a large scale fibre fracture will most likely lead to failure of the component. In the ROV hull a fibre fracture can be caused by general overloading of the hull or local overload caused by impacts, concentrated loads or stress concentrations.

**Delamination** is also a failure mode that can create major problems with the Mantas structure. Delamination is the separation of the different plies of the composite. This can come from shear stress of bended lamina or tensile stress perpendicular to the plies. When the plies separate, the sheet will lose much of its stiffness, which again will lead to a larger deformation. Delamination can be a result of overload or impacts. The laminate is especially vulnerable to impacts on the edges. The delamination will most likely propagate when subjected to repeated freezing and thawing. Local delamination can also happen during machining. [49].

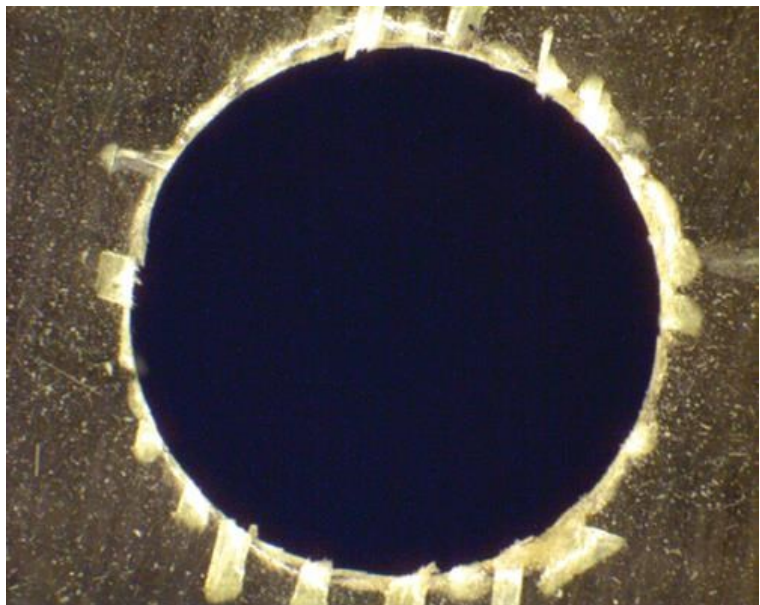


FIGURE 108: LOCAL DELAMINATION AROUND A DRILLED HOLE. [10]

### 11.1.5 MAXIMUM STRESS THEORY FOR COMPOSITES

The maximum stress theory is one of the most intuitive and easy to apply failure criterions for composites [50]. The maximum stress criterion compares each stress component directly with its respective material strength parameter. Since orthotropic materials have three planes of material symmetry, the criterion checks the stresses in each of the three material directions with the respective strength.

$$f = \max \left( \frac{\sigma_1}{X_T}, \frac{-\sigma_1}{X_C}, \frac{\sigma_2}{Y_T}, \frac{-\sigma_2}{Y_C}, \frac{\sigma_3}{Z_T}, \frac{-\sigma_3}{Z_C}, \frac{|\tau_{12}|}{S_{12}}, \frac{|\tau_{13}|}{S_{13}}, \frac{|\tau_{23}|}{S_{23}} \right) = 1$$

FIGURE 109: MAXIMUM STRESS CRITERION

In the equation in Figure 109,  $\sigma_i$  represents normal stress in  $i$ -direction,  $\tau_{ij}$  represents shear stress in the  $ij$ -plane. The Latin letters represent material strength in given direction. T stands for tensile load state and C is compressive. Typically the composite is stronger in tensile than compression in the fibre direction, and the opposite in the direction perpendicular to the fibres.

According to maximum stress theory failure occurs when the value  $f = 1$  (utilization 100%). As can be seen from the formula, there is no interaction between the different components. This is not conservative, as it is safe to assume that failure can happen as a result of a combination of loads that individually are below the failure limit. This requires a safety margin. Failure in laminated structure is very hard to predict, as the failure mode can vary much from different load cases and geometry.

### 11.2 INITIAL MATERIAL COMPARISON

To do a fast review of the relevant materials, an initial material comparison has been performed. The main objective was to get some quantitative data on strength and stiffness relative to weight (specific strength and stiffness). These numbers are calculated by dividing strength and stiffness on the material density. The main focus is on fibre composites, but a couple of other widely used engineering materials have been taken into account.

Three types of ply materials (fibres) have been considered; Aramid- (Kevlar), Glass- and Carbon fibre. These combinations represent some of the most common groups of fibres used in composites. The numbers represent the material data for unidirectional fibres, i.e. all the fibres go in one direction. This is not the kind of fabric that is most reasonable to use for the hull of the ROV. Here, a fibre weave is most practical, where bundles of fibres are woven together, typically in 0/90 degrees or +45/-45 degrees orientation. Data are displayed in Table 11.

Material	Stiffness (GPa)	Strength (MPa)	Density (g/cm <sup>3</sup> )	Specific strength MPa/(g/cm <sup>3</sup> )	Specific stiffness GPa/(g/cm <sup>3</sup> )	Specific bending stiffness relative to steel ()
Carbon fiber (T300/5208 uni)	181	1500	1,6	937,5	113,1	104,9
Glass fiber (Scotchply 1002 uni)	39	1062	2,0	531,0	19,5	11,6
Aramid fiber(Kevlar 49 uni)	76	1400	1,5	933,3	50,7	53,4
Steel 316L	200	485	7,8	62,2	25,6	1,0
Aluminium 6061-T6	70	300	2,7	111,1	25,9	8,4
ABS-20%CF	13	110	1,1	100,0	11,8	23,2
ABS-plastic	4	42	1,1	38,2	3,6	7,1

TABLE 11: MATERIAL COMPARISON [50]

The specific strength and stiffness is the material strength and stiffness divided by the density of that material. We can see that the fibre composites rank high (green colour in Table 11), whereas the metals and thermoplastics are at the bottom (red colour in Table 11). Note that even though 316L steel is more than ten times stronger than ABS, its specific strength is only about 60% more than ABS. If we look at the ABS plastic that is added 20% carbon fibres (CF), it has very good properties compared to steel.

One very relevant parameter for material selection in the Manta is the specific bending stiffness. As specific stiffness only describes how stiff the material is, the specific bending stiffness takes geometry into account.

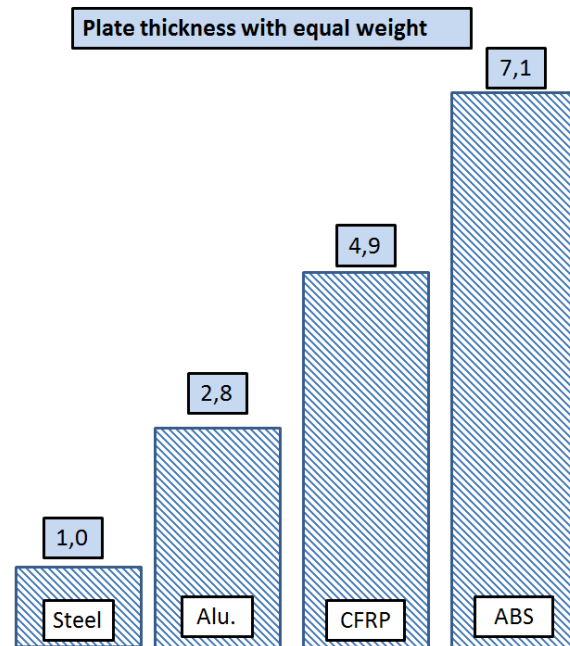


FIGURE 110: PLATE THICKNESSES WITH EQUAL WEIGHT

$$Bending\ stiffness = E * I_{xx} = E * \frac{width * thickness^3}{12} \quad [51]$$

E is the Young's modulus (material stiffness).

When using a lighter material one can create a larger geometry with the same weight. The bending stiffness is heavily influenced by the second moment of inertia. For a plate the second moment of inertia is related to the thickness cubed. In other words if the plate thickness is doubled, its stiffness is multiplied by eight. A comparison of how thick plates one can get with the same mass can be seen in Figure 110. This is a direct comparison of densities, in this case relative to steel. As a result of this, an ABS plate will be about seven times stiffer with respect to bending compared to steel, given the same mass. From Table 11, one can see that a carbon fibre reinforced composite is best with respect to specific strength and (bending) stiffness. These parameters are important in order to create a rigid, strong and yet light structure. However a carbon fibre composite (500 NOK/kg) is about five times as expensive as glass fibre or ABS-20%CF (100NOK/kg), and over thirty times more expensive than unfilled ABS plastic (15NOK/kg) [7]. There are also other downsides of using CFRP in the hull.

Note that there are several versions of all fibres families listed above, and that the ones listed are some of the most common. Especially carbon fibres exist in many variations, some are far stronger than the listed in the table. For instance H-IM6/epoxy composite has a tensile strength of 3500 MPa (app. C [50]), more than twice that of the T300-composite. The final material decision has to be made on the basis of durability, toughness, price, availability and other engineering parameters (like failure strain, compressive strength and - stiffness.)

### 11.3 MATERIAL COMPARISON BY FEM ANALYSIS

The initial FEM analysis was conducted using Abaqus 6.12 software because of its good reputation of composite simulations. The model was made in Siemens NX 8,5 and the geometry was imported to Abaqus for the simulations. It was split into sections for better load distribution control.

An early FEA comparison of a couple of alternative engineering materials was done in order to investigate if the use of a fibre composite was required. The hull is a simplified monocoque, where the skin of the structure carries the load. This design has been chosen for the comparison, even though other designs might prove more sensible for the different materials. S4R 2D are elements, and the element size is listed at the different simulation plots.

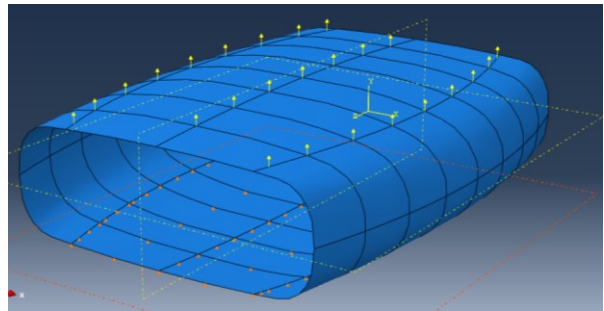


FIGURE 111: LOAD DISTRIBUTION USED FOR FEM MATERIAL COMPARISON

The most relevant load state for this test was a lifting simulation, where 1500N was applied on 25 nodes distributed over the top of the hull, illustrated in Figure 111. Lifting the ROV with a full net is most likely the toughest load state. The details around the connection between the umbilical and the monocoque were not determined at this point, so the simulated load state is for material comparison only.

It is likely the manufacturing process of the composite that represents the largest part of the structural cost. In other words if it is decided to use a fibre composite the price difference between glass- and carbon fibre is small compared to the cost of the work done. This is why only carbon fibre reinforced polymer (CFRP) is analysed in this comparison.

#### 11.3.1 STRUCTURAL RESPONSE CRITERIA

When defining minimum weight in this case, the required structural behaviour had two criteria: Material utilization had to be equal to or less than 70% and the maximum deflection had to be less than or equal to 5 cm. Note that these requirements are only for this material comparison and not for the actual structure.

Comparison of material groups by FEM analysis - Typical values								
Material	E (GPa)	Re (MPa)	Density (g/cm <sup>3</sup> )	Thickness (mm)	Smises (MPa)	Utilization	Failure theory	Weight (kg)
Aluminium	70	300	2,7	1,5	210,5	0,70	Von Mises	4,86
ABS plastic	4	30	1,05	5,5	18,3	0,61	Von Mises	6,93
CFRP-weave	70	800*	1,6	1,5	0,28**	0,28	Max Stress Criterion	2,88
		*UTS			**MSTRS			

TABLE 12: MATERIAL COMPARISON BASED ON FEM ANALYSIS (GEOMETRY DEPENDANT).

From Table 12, one can see that the carbon fibre composite is the lightest alternative, and it is expected that a hull made of CFRP will weigh approximately half of a hull made of ABS.

Some simulations with sandwich structures have also been performed. The idea was to utilize the core foam both to stiffen the structure and for buoyancy. With the thickest core, the result was about 7 kg of buoyancy from the hull, which helps significantly.

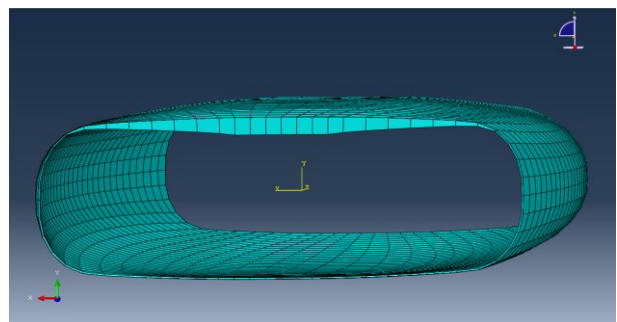


FIGURE 112: EXAMPLE OF SANDWICH DISTRIBUTION

If the final decision is to use CFRP in the hull it is recommended to use sandwich structure in the upper part of the hull. The details around the sandwich analysis are found later in this chapter.

Total CF thickness [mm]	Tot Core thickness [mm]	Buoyancy [kg]	mass [kg]	disp [mm]	MSTRS [J]
1,5	none	-1,08	2,88	172	0,42
2	none	-1,44	3,84	104	0,26
3	none	-2,16	5,76	42	0,13
2	distr. 20-5mm	2,86	5,68	17	0,16
2	distr. 30-7,5mm	5	6,60	14	0,16
2	distr. 40-10mm	7,17	7,53	14	0,16

TABLE 13: EFFECT OF SANDWICH CORE THICKNESS

Distr. means that the sandwich is distributed with a maximum thickness on the centre section and a minimum thickness at the exterior edge.

## 11.4 FEA BASED MATERIAL COMPARISON ON SIMPLIFIED HULL

The simulations in this chapter is conducted in Abaqus 6.12 with the use of S4R elements.

### 11.4.1 MATERIAL DATA USED IN THE FEA

E denotes the Young's modulus (stiffness) and  $\nu$  denotes the Poisson ratio.

CFRP-weave [50]:

$E_1=E_2= 70 \text{ GPa}$ ,  $E_3= 8\text{GPa}$ ,  $\nu_{12}=\nu_{13}=0,05$ ,  $\nu_{23}=0,55$   $G_{12}=G_{13}=4\text{GPa}$   $G_{23}=5\text{GPa}$

Fail stress: Fibre tension: 800 MPa, Fibre compressive: 800MPa, Shear: 75MPa. This is an estimate based on unidirectional data of fibre tension fail stress 1860MPa and compressive 1470MPa. [52]

ABS-plastic [7]:

$E=2,2\text{GPa}$ ,  $\nu=0,35$ , density= $1,05 \text{ g/cm}^3$ , Yield stress 30 MPa

ABS-20% CF [7]:

$E=12\text{GPa}$   $\nu=0,34$ , density= $1,12 \text{ g/cm}^3$ , Yield stress 110 MPa

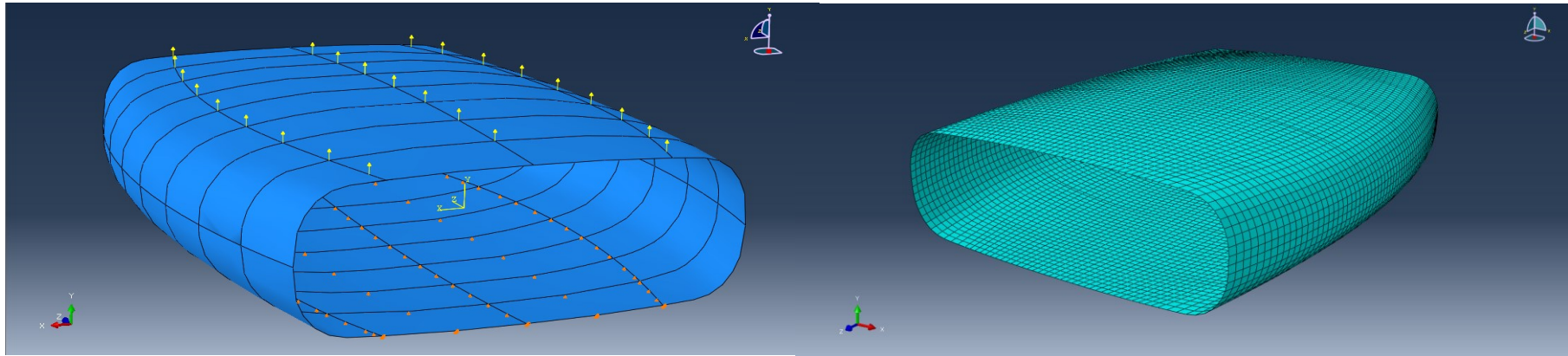
s

6061 Aluminium [7]:

$E= 70 \text{ GPa}$ ,  $\nu=0,33$ , density  $2,7\text{g/cm}^3$

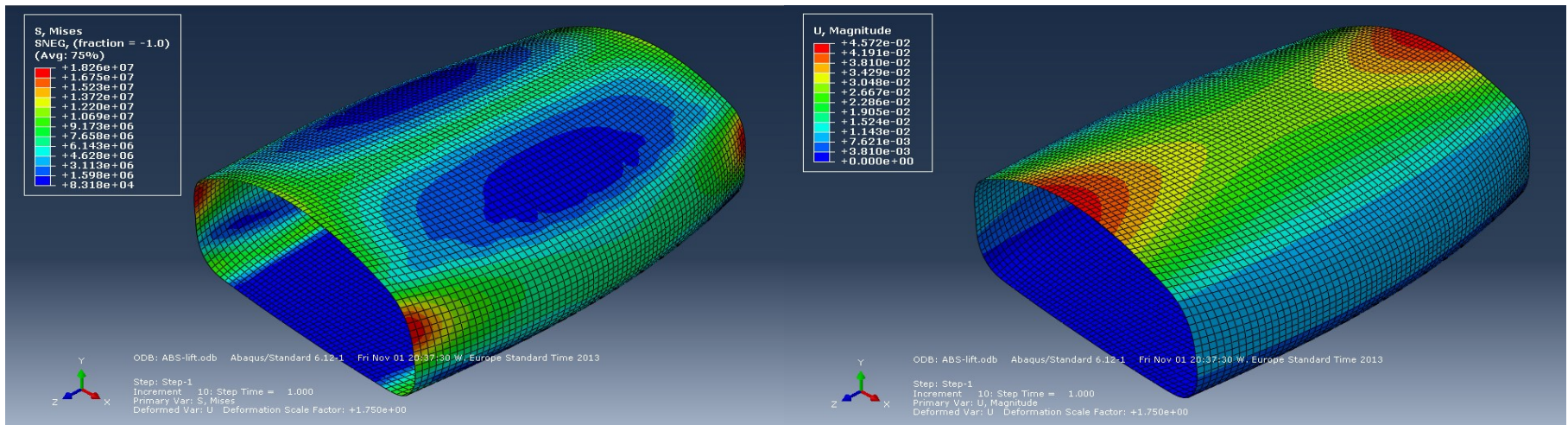
Divinylcell HCP50 [6]:

$E=0,4\text{GPa}$ ,  $\nu=0,32$ , density  $0,25\text{g/cm}^3$



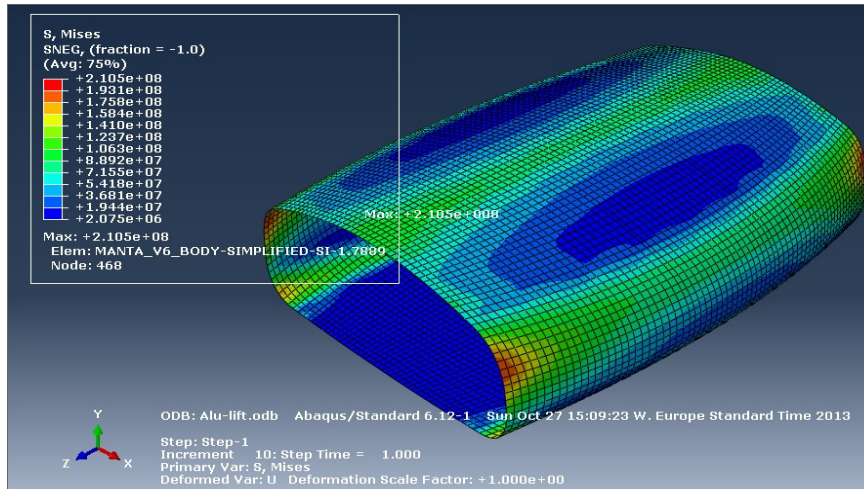
**Load case:** 1500N upward force divided on 25 points.  
**Constraint:** Fixed vertical movement on bottom plate and horizontal movement on front edge

**Mesh:** 12,5mm structured mesh with quadratic S4R-elements.

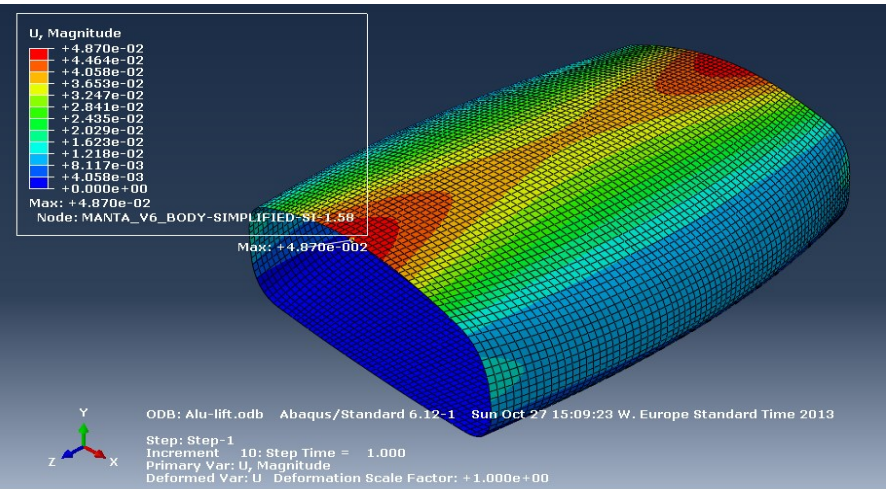


**5,5mm ABS plastic:** Maximum von Mises stress: 18,7MPa

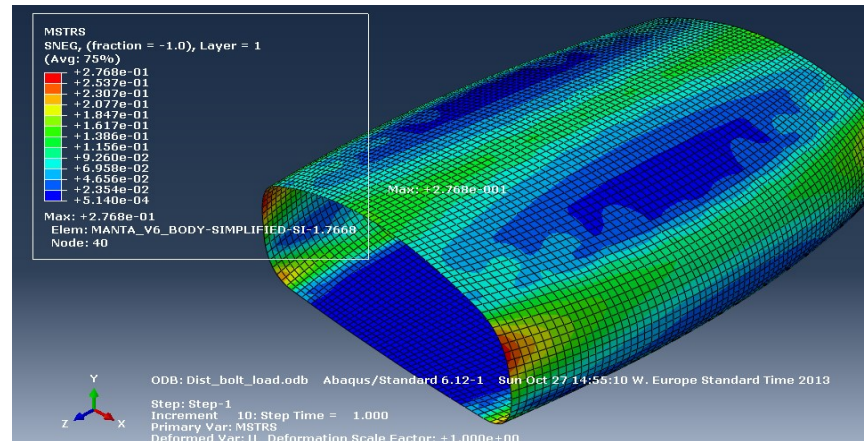
**5,5mm ABS plastic:** Maximum displacement: 46mm



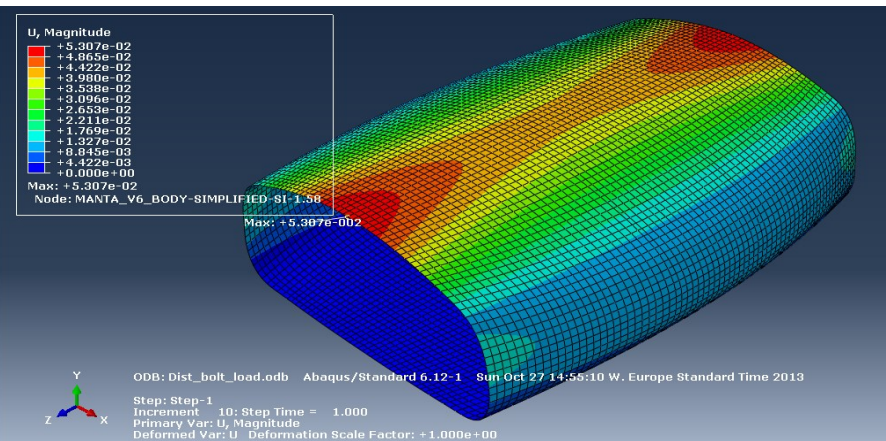
**1,5mm Aluminum: Max von Mises stress: 211 MPa**



**1,5mm Aluminum: Max displacement: 49mm**

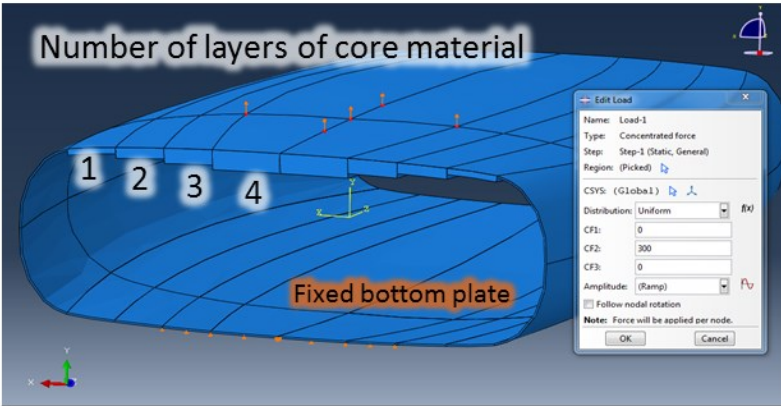


**1,5mm CFRP: Maximum stress criterion: 28%**



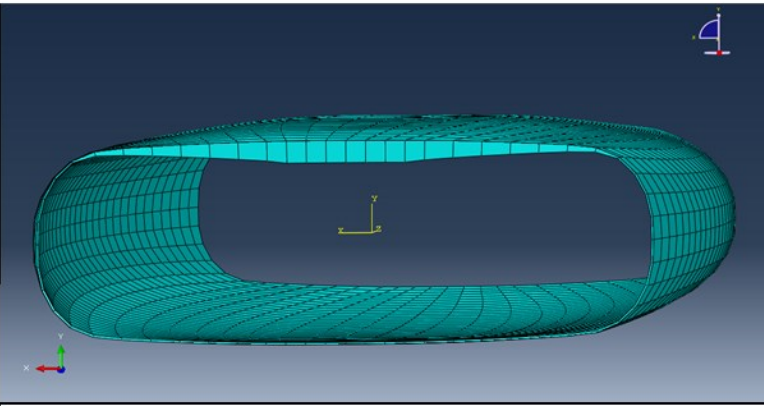
**1,5mm CFRP: Maximum displacement 53mm**

# Sandwich comparison



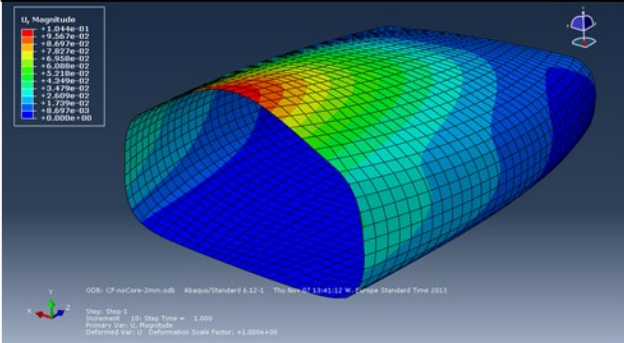
Load case: 1500 N total on 5 points. Vertically fixed bottom plate and horizontally fixed front point. CFRP skin and HCP50 Core

The deformation scale is 1 (no amplification).

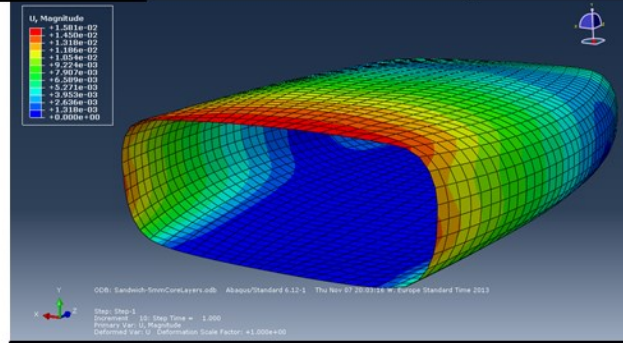


Sandwich core distribution and load case

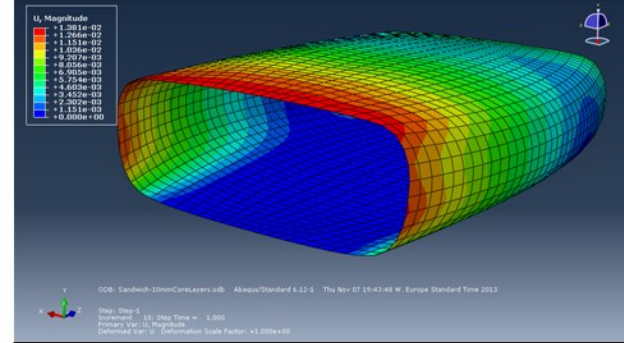
25mm S4R quad mesh with rendered shell thickness



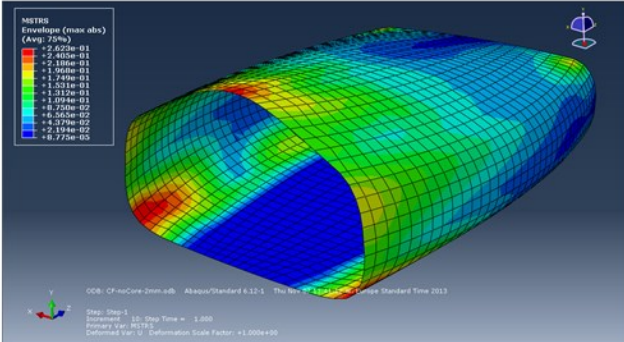
2mm CFRP only: Max displacement 104mm



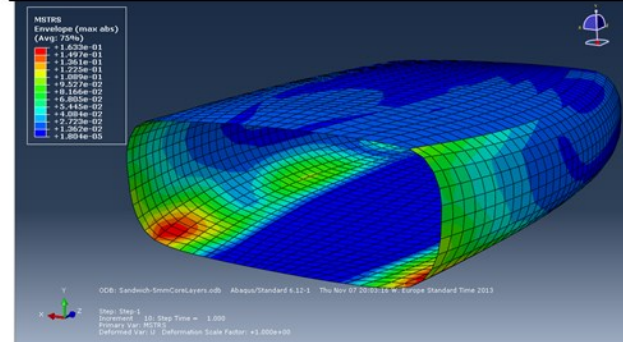
Sandwich of 2mm CFRP and 5-20mm core: Max displacement 16mm



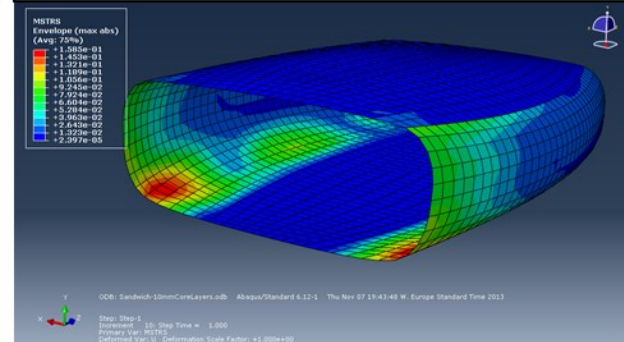
Sandwich of 2mm CFRP and 10-40mm core: Max displacement 14mm



No core: MSTRS max 0,26

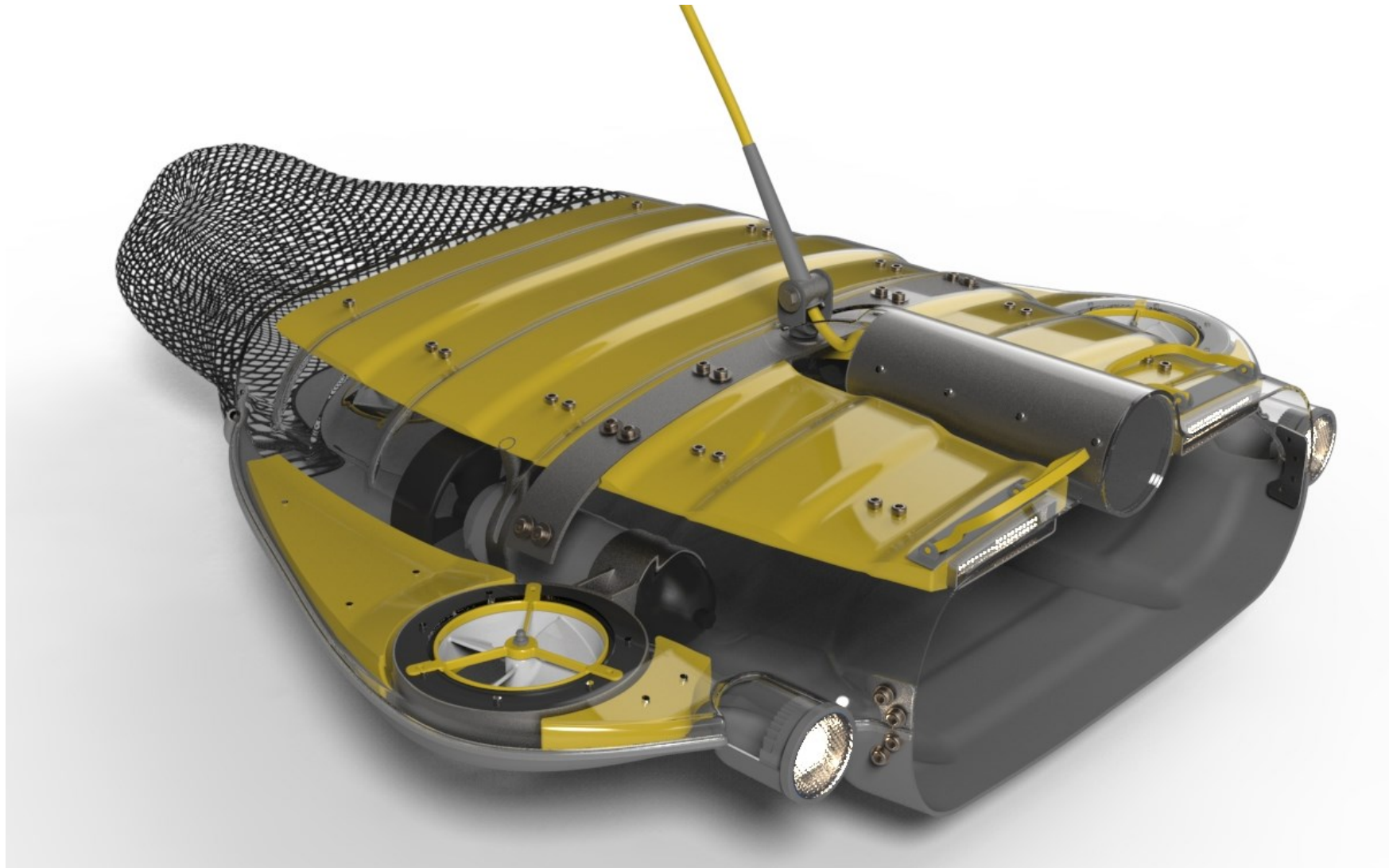


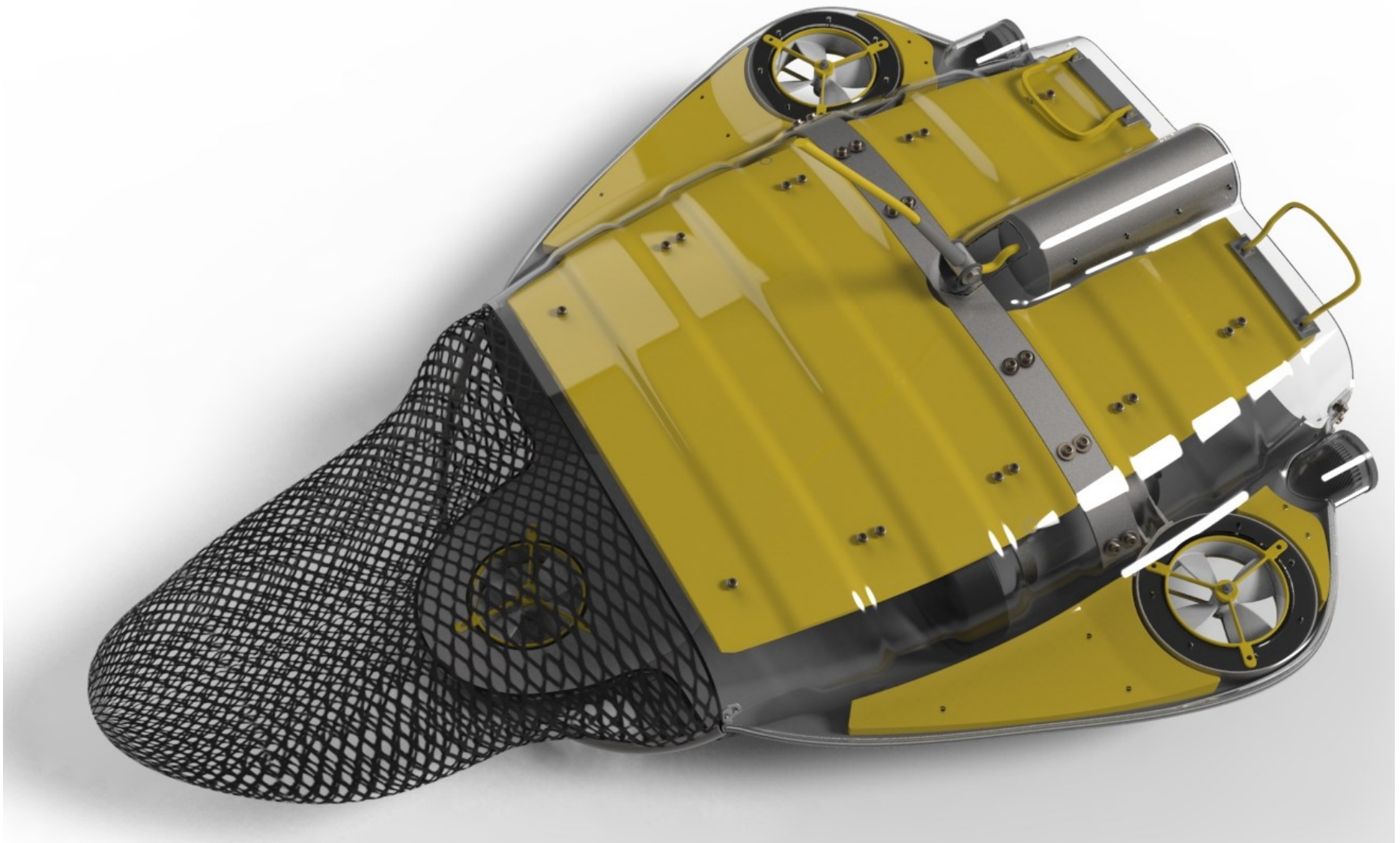
Sandwich 5-20mm core: MSTRS max 0,16



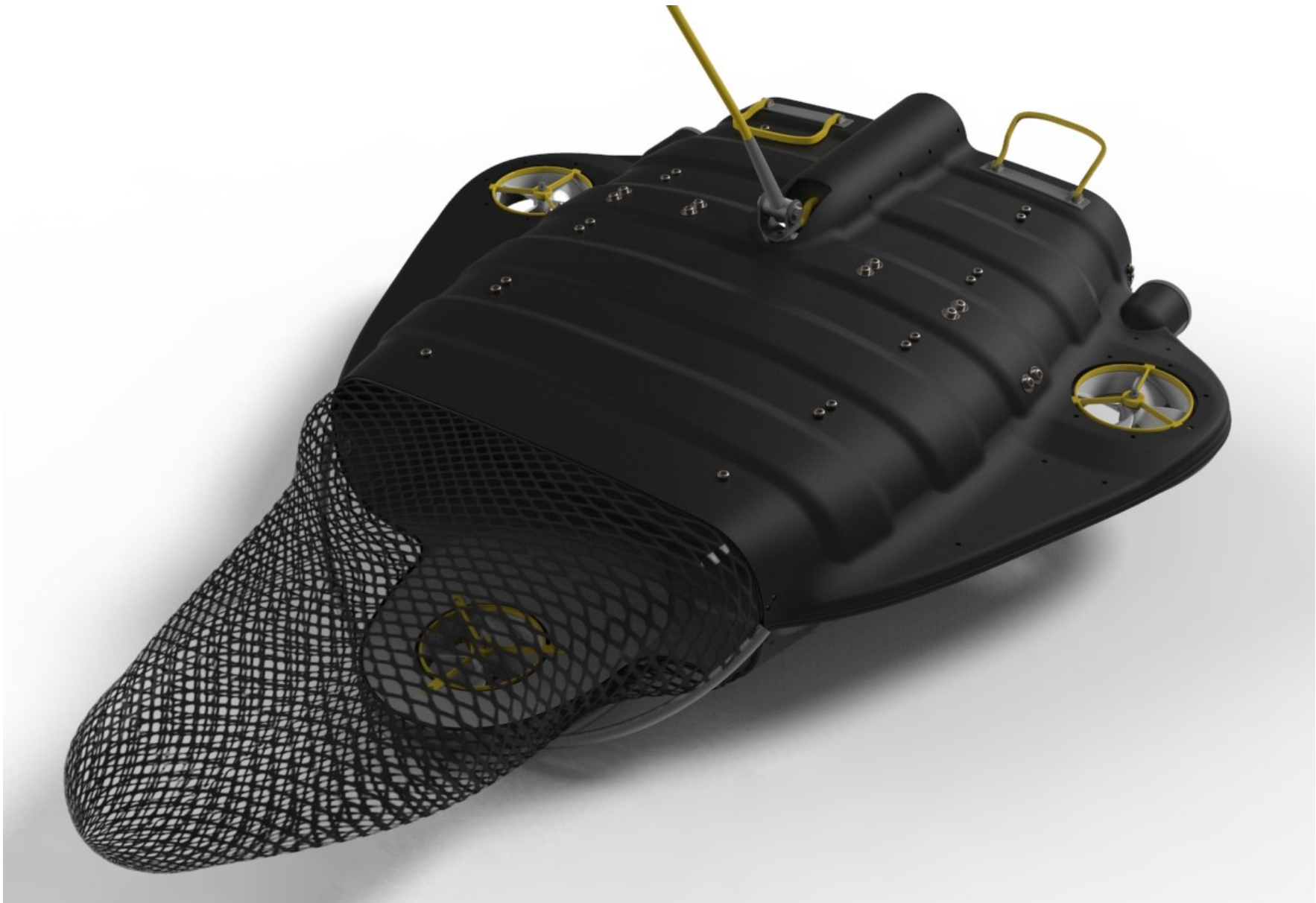
## 12 APPENDIX C: ILLUSTRATIONS OF FINAL DESIGN

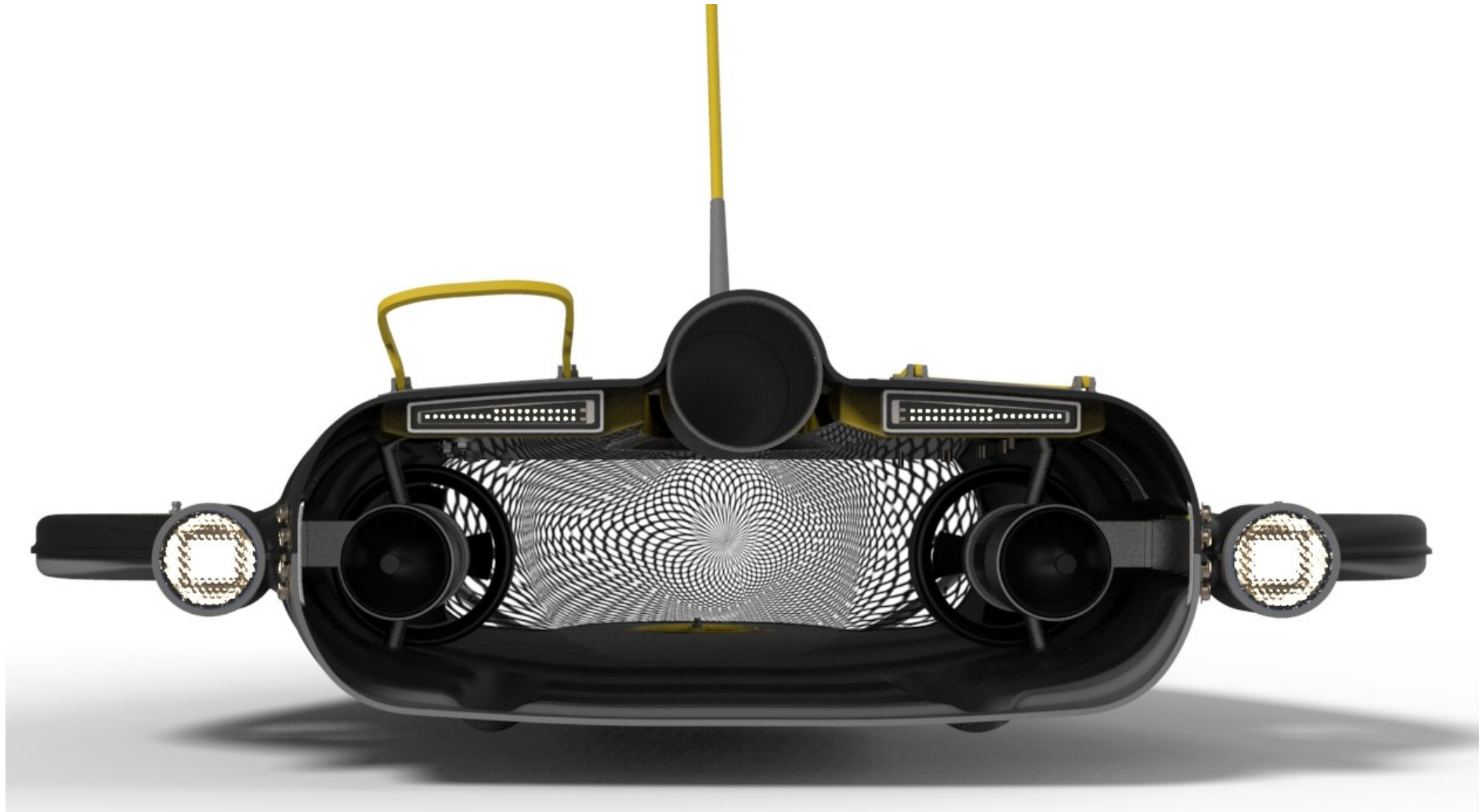
Upper part is rendered as transparent for better view of internal components.



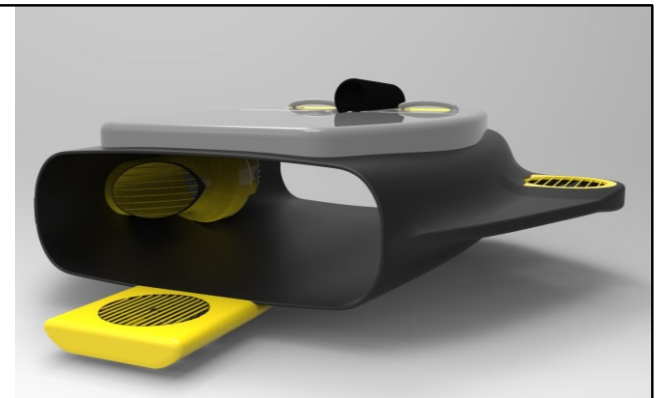
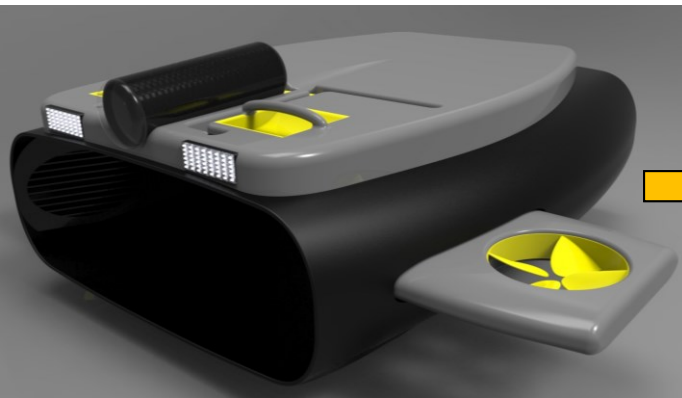
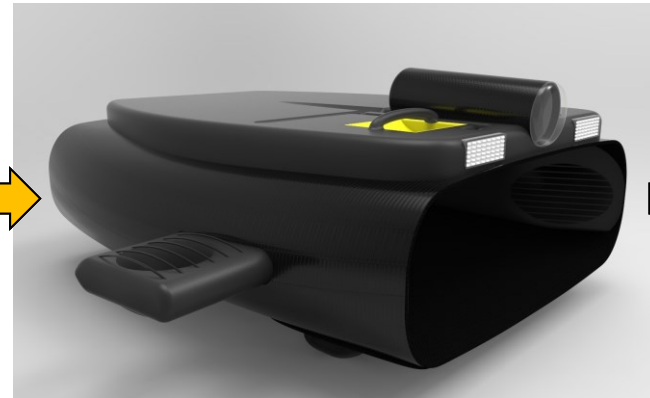
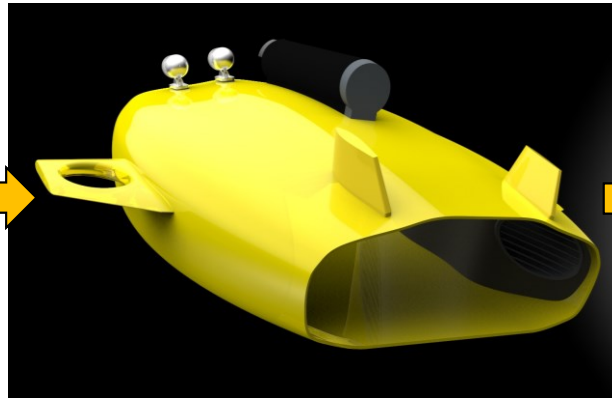
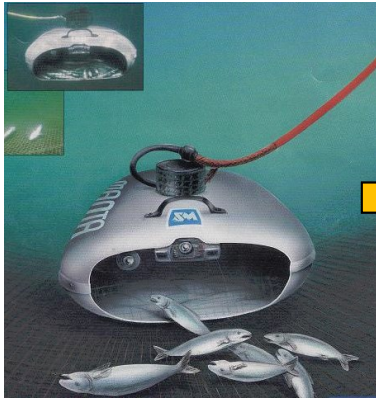




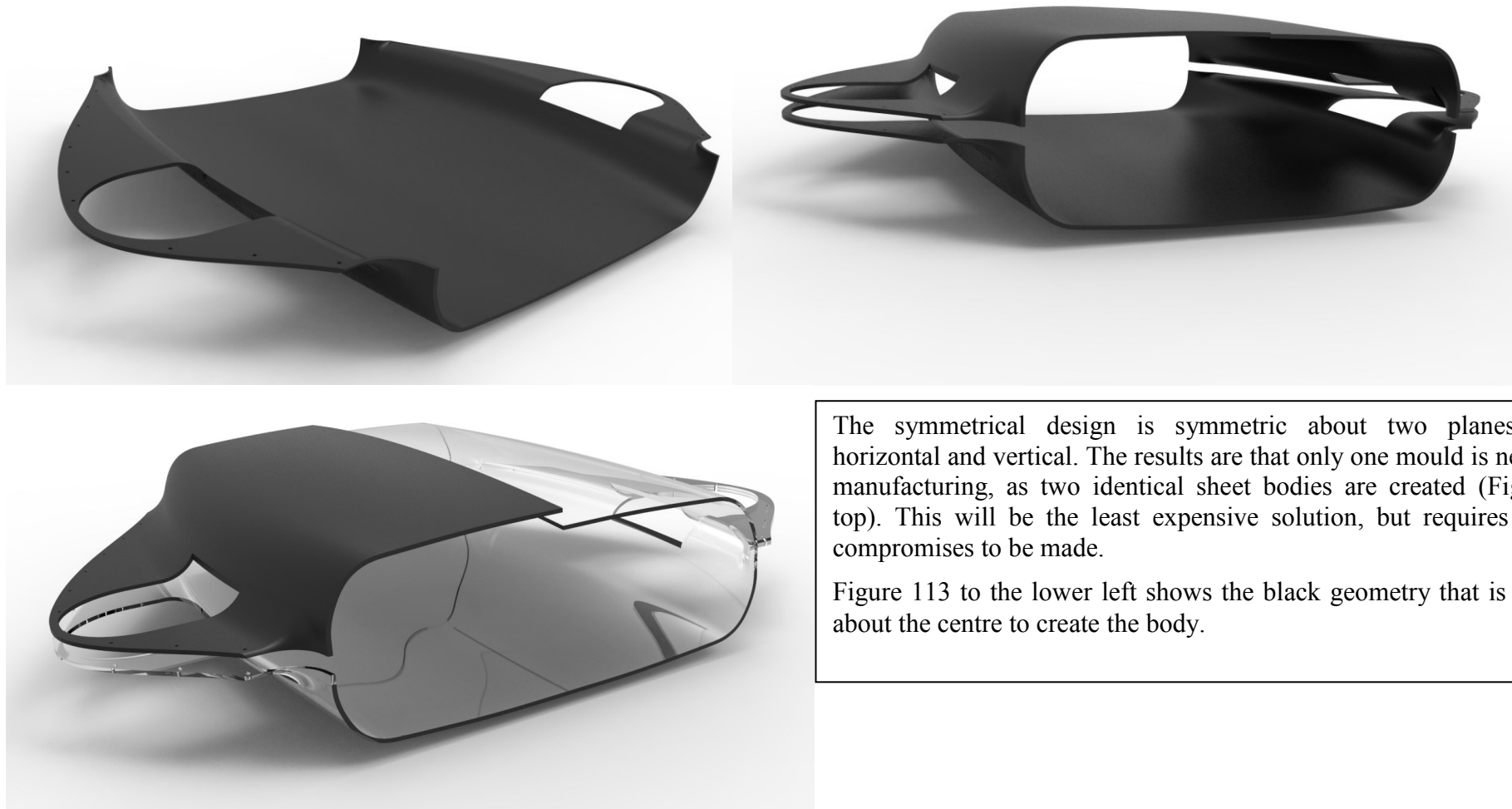




# 13 APPENDIX D: EVOLUTION OF HULL DESIGN



## 14 APPENDIX E: ALTERNATIVE SYMMETRICAL HULL DESIGN



The symmetrical design is symmetric about two planes, centre horizontal and vertical. The results are that only one mould is needed for manufacturing, as two identical sheet bodies are created (Figure 113 top). This will be the least expensive solution, but requires a lot of compromises to be made.

Figure 113 to the lower left shows the black geometry that is mirrored about the centre to create the body.

FIGURE 113: ALTERNATIVE SYMMETRICAL HULL

## 15 APPENDIX F: CORRUGATED VS SMOOTH HULL

This analysis was done on a simplified hull to minimize end effects and simplify the analysis. The hull section that was analysed does not have any wings or holes, and it is only half of the general geometry that has been analysed. The hull is 4mm thick and has been meshed by a 2,5mm CTETRA(10) elements. The model was sectioned so there was a 200mm wide upper and lower face that could be loaded and fixed respectively. The load was 500N geometrically distributed over the upper centre section, directed upwards (simulating lifting). Material is ABS from NX material library. **Mesh convergence is discussed in chapter 5.2.1.**

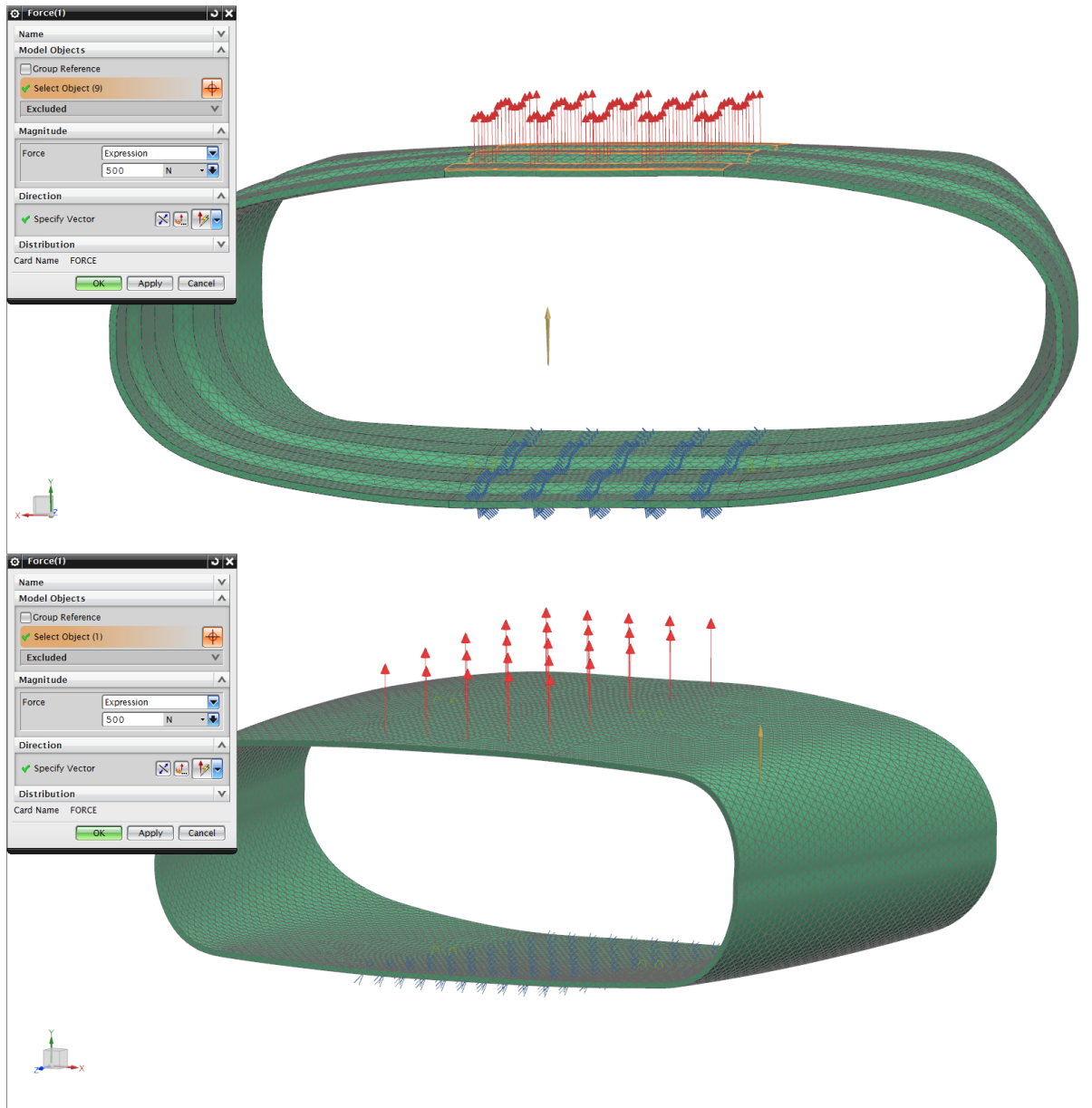
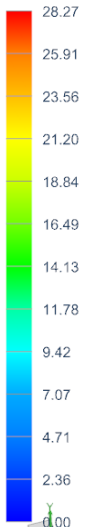
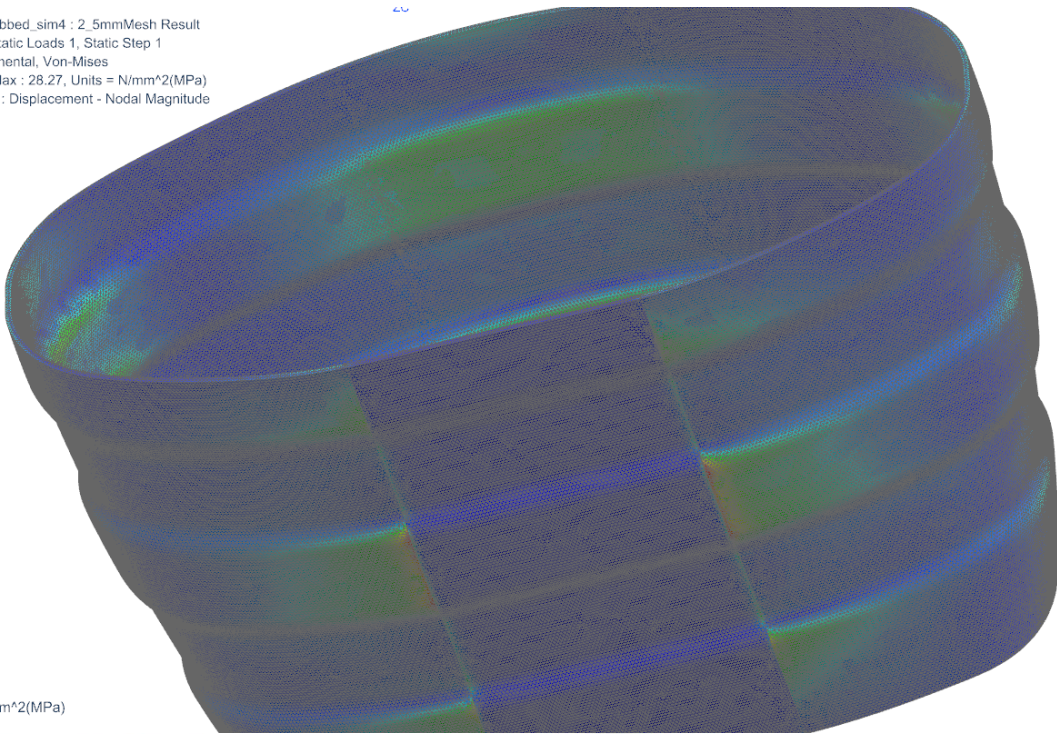


FIGURE 114: CORRUGATED (UPPER) AND PLANE (LOWER) HULL LOAD STATE (SHOWN ON 10MM MESH)

Hull\_v9.1 - ribbed\_sim4 : 2\_5mmMesh Result  
Subcase - Static Loads 1, Static Step 1  
Stress - Elemental, Von-Mises  
Min : 0.00, Max : 28.27, Units = N/mm<sup>2</sup>(MPa)  
Deformation : Displacement - Nodal Magnitude



Units = N/mm<sup>2</sup>(MPa)



Hull\_v9.1 - ribbed\_sim2 : 2\_5mmMesh Result  
Subcase - Static Loads 1, Static Step 1  
Stress - Elemental, Von-Mises  
Min : 0.00, Max : 19.35, Units = N/mm<sup>2</sup>(MPa)  
Deformation : Displacement - Nodal Magnitude



Units = N/mm<sup>2</sup>(MPa)

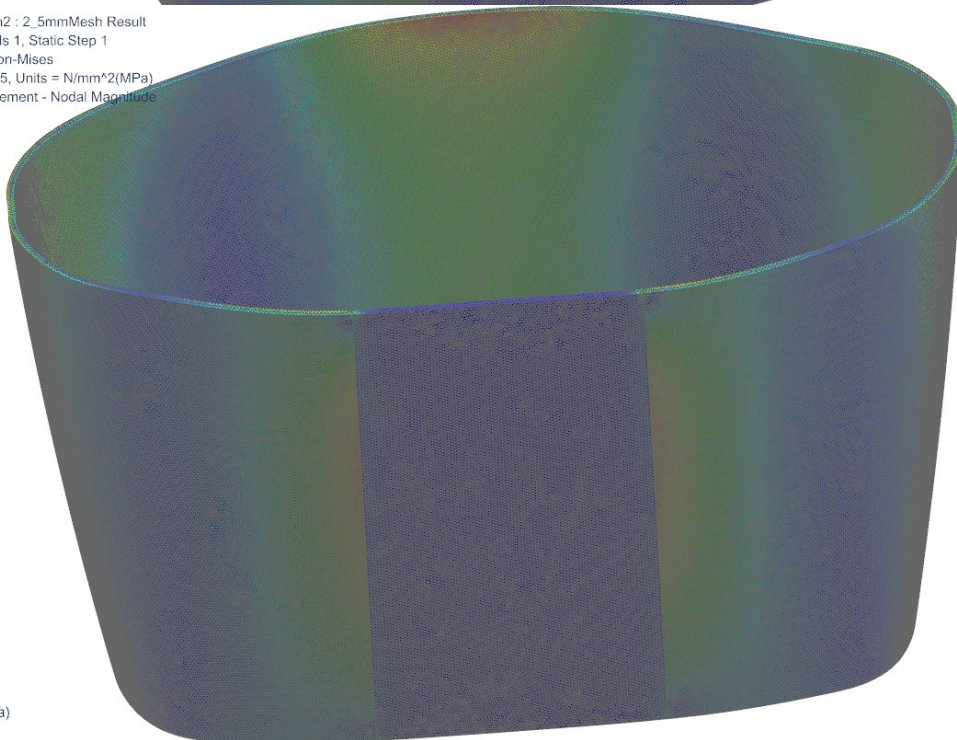
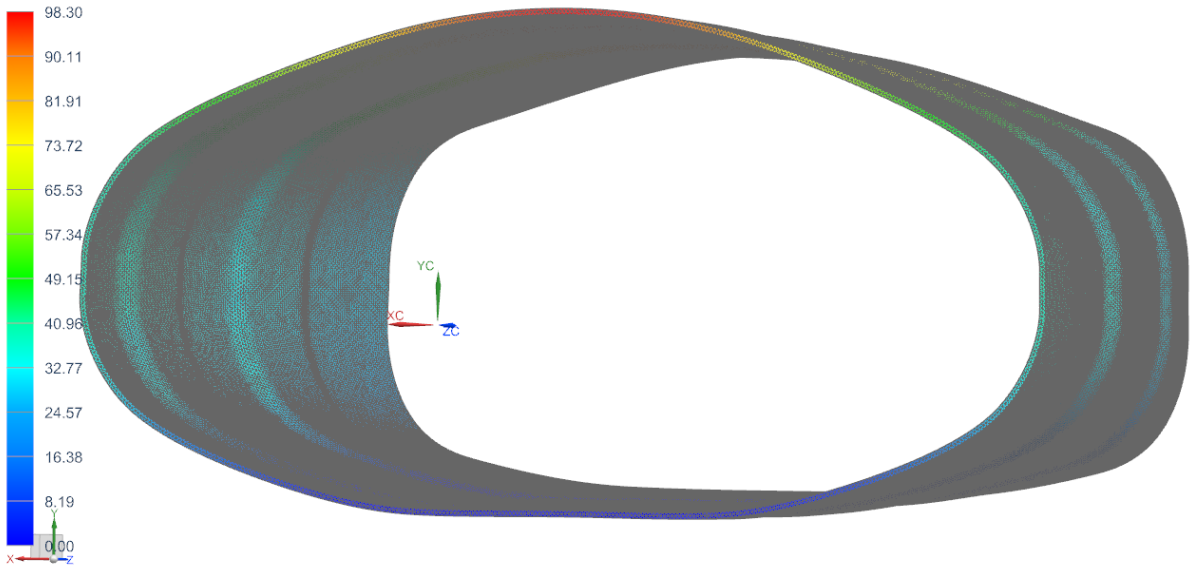


**FIGURE 115: RESULTING STRESS PLOT ON CORRUGATED (UPPER) AND PLANE(LOWER) SIMPLIFIED HULL**  
2,5mm Mesh is used

Hull\_v9.1 - ribbed\_sim4 : 2.5mmMesh Result  
Subcase - Static Loads 1, Static Step 1  
Displacement - Nodal, Magnitude  
Min : 0.00, Max : 98.30, Units = mm  
Deformation : Displacement - Nodal Magnitude



Units = mm  
Hull\_v9.1 - ribbed\_sim2 : 2.5mmMesh Result  
Subcase - Static Loads 1, Static Step 1  
Displacement - Nodal, Magnitude  
Min : 0.00, Max : 141.51, Units = mm  
Deformation : Displacement - Nodal Magnitude

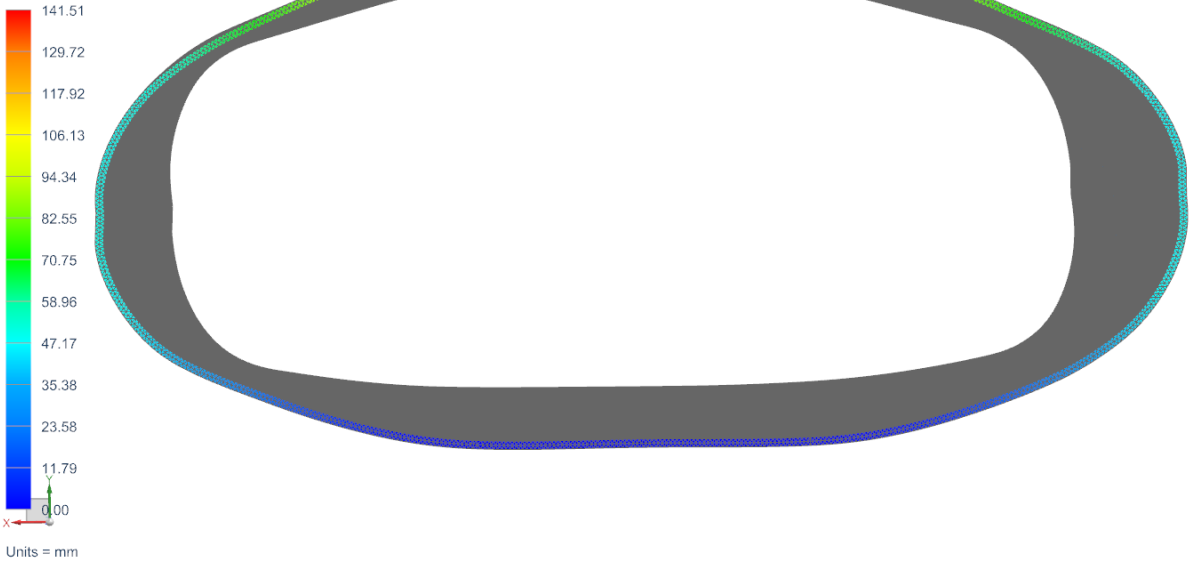
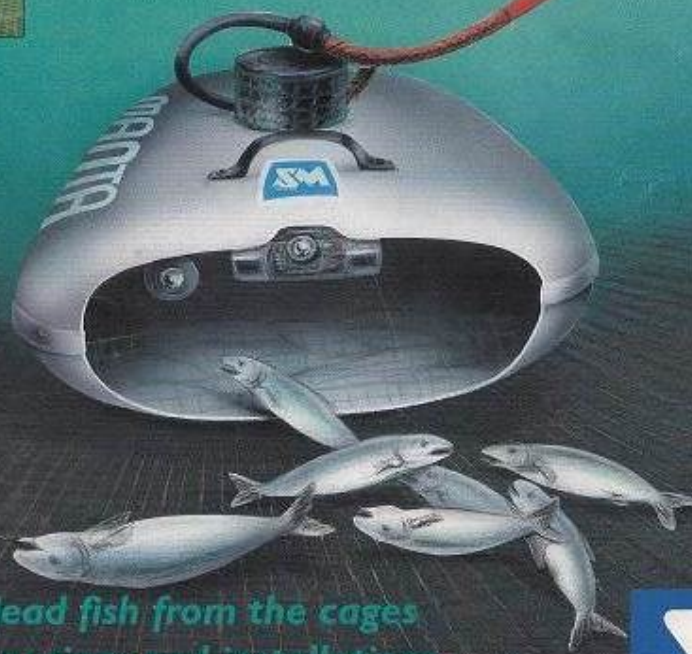


**FIGURE 116: RESULTING DISPLACEMENT ON HULL. (CORRUGATED ON TOP)**

**MANTA 505**

# MANTA 505

Easily operated  
submersible vessel for the fish  
farming industry



- Removes dead fish from the cages
- Inspects moorings and installations
- Cleans the net using high pressure jets
- Measures environmental pollution inside and outside the installation



**SM Remote  
Systems**

# 17 APPENDIX H: THRUSTER PROTOTYPE FEM ANALYSIS

## 17.1 RIM PROPELLER FEA DETAILS

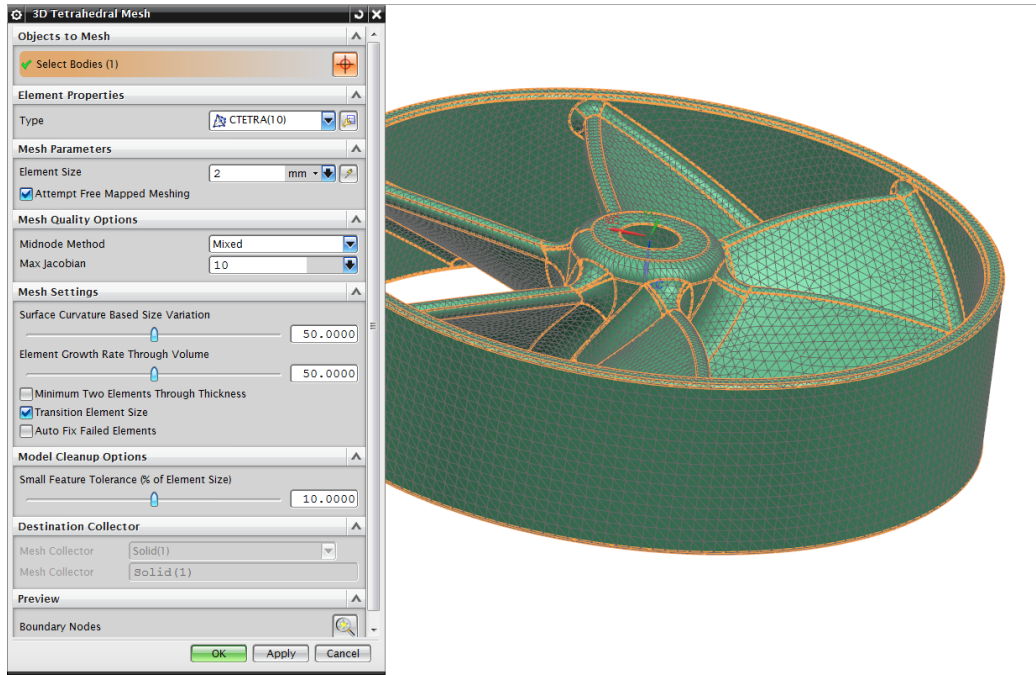


FIGURE 117: 2MM CTETRA(10) MESH

Figure 117 shows the 2mm CTETRA(10) mesh. The material used in FEA is ABS from NX material library. Automatic element size was suggested to be 5,5mm.

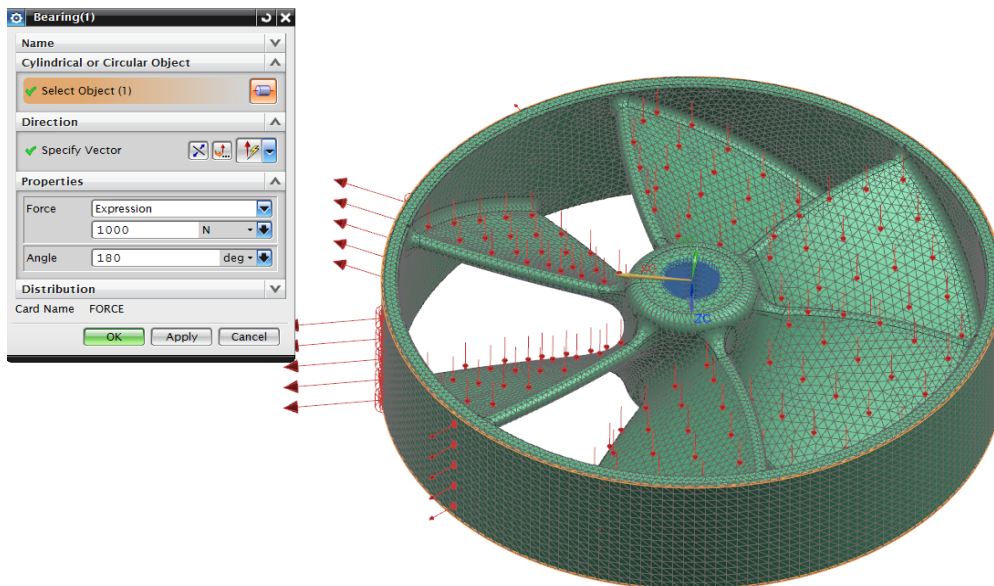
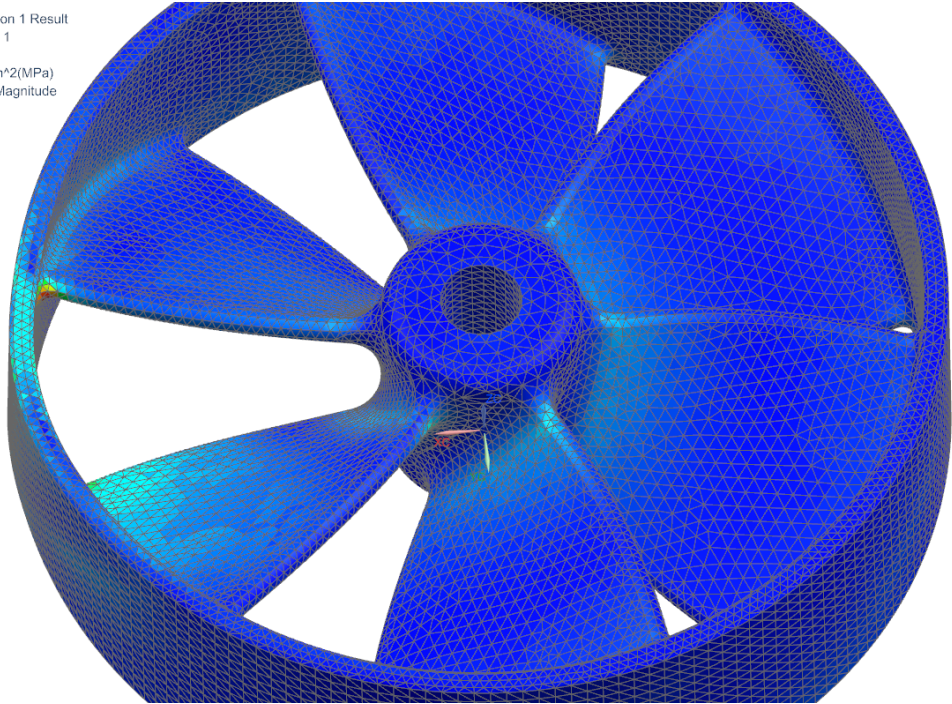
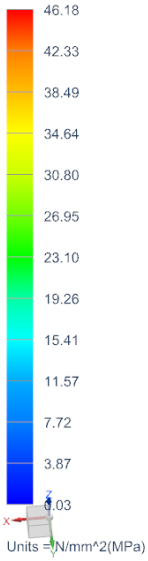


FIGURE 118: PROPELLER LOAD.

Figure 118 displays the load case of the propeller analysis. The loads are combined from 1000N Bearing force on the rim in the x-direction, and 300N thrust force at the blades in the -Y direction. Fixed in centre hole. The bearing force is a simplification of the magnetic force that works when the rotor is not concentric to the stator. The air-gap on the left side is smaller, which leads to much more powerful magnetic forces.

parametric rim-propeller\_sim2 : Solution 1 Result  
Subcase - Static Loads 1, Static Step 1  
Stress - Elemental, Von-Mises  
Min : 0.03, Max : 46.18, Units = N/mm<sup>2</sup>(MPa)  
Deformation : Displacement - Nodal Magnitude



**FIGURE 119: STRESS PLOT OF THE ROTOR**

parametric rim-propeller\_sim2 : Solution 1 Result  
Subcase - Static Loads 1, Static Step 1  
Displacement - Nodal, Magnitude  
Min : 0.000, Max : 1.451, Units = mm  
Deformation : Displacement - Nodal Magnitude

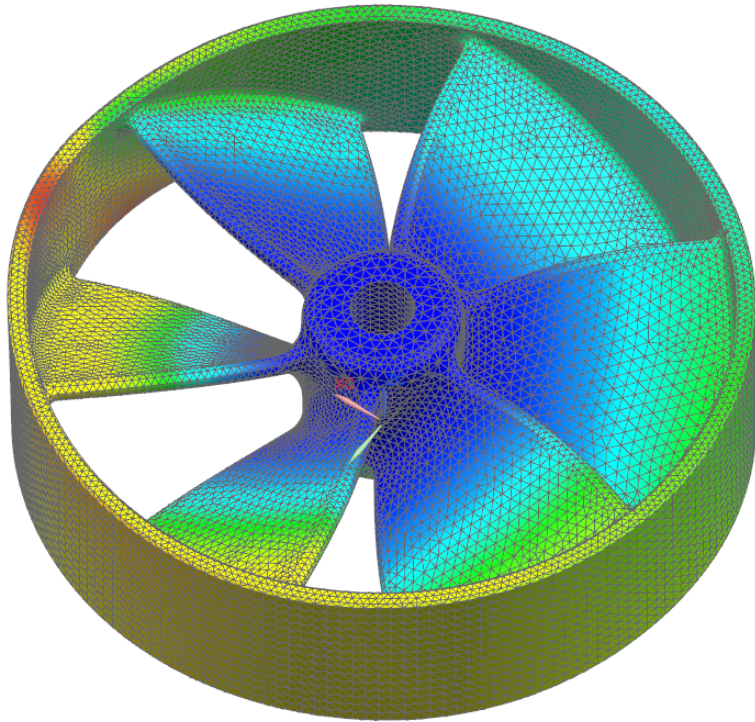


**FIGURE 120: DISPLACEMENT PLOT OF THE ROTOR**

## 17.2 PROPELLER AXLE FEA DETAILS

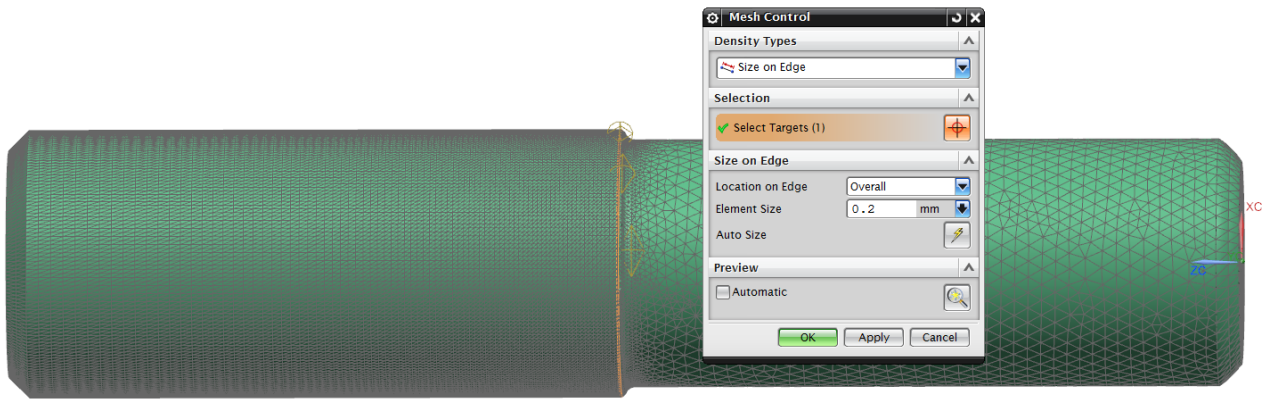


FIGURE 121: AXLE MESH:

Material used is 6061 Aluminium from NX Material Library. 1mm CTETRA(10) mesh was used, with a 0,2mm mesh refinement along critical edges.

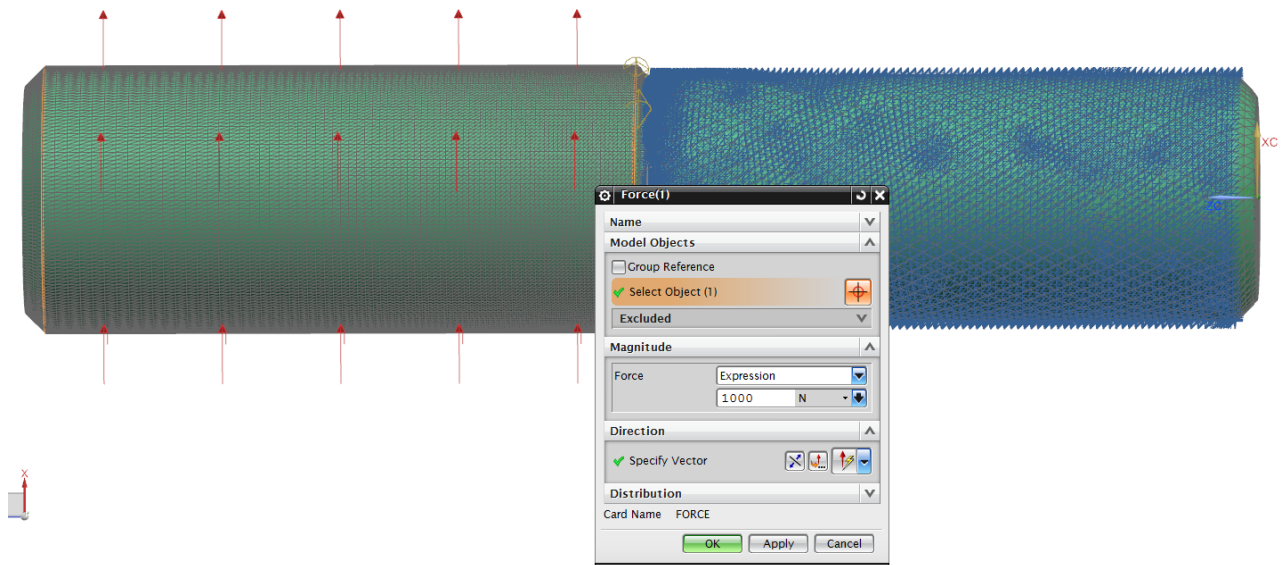
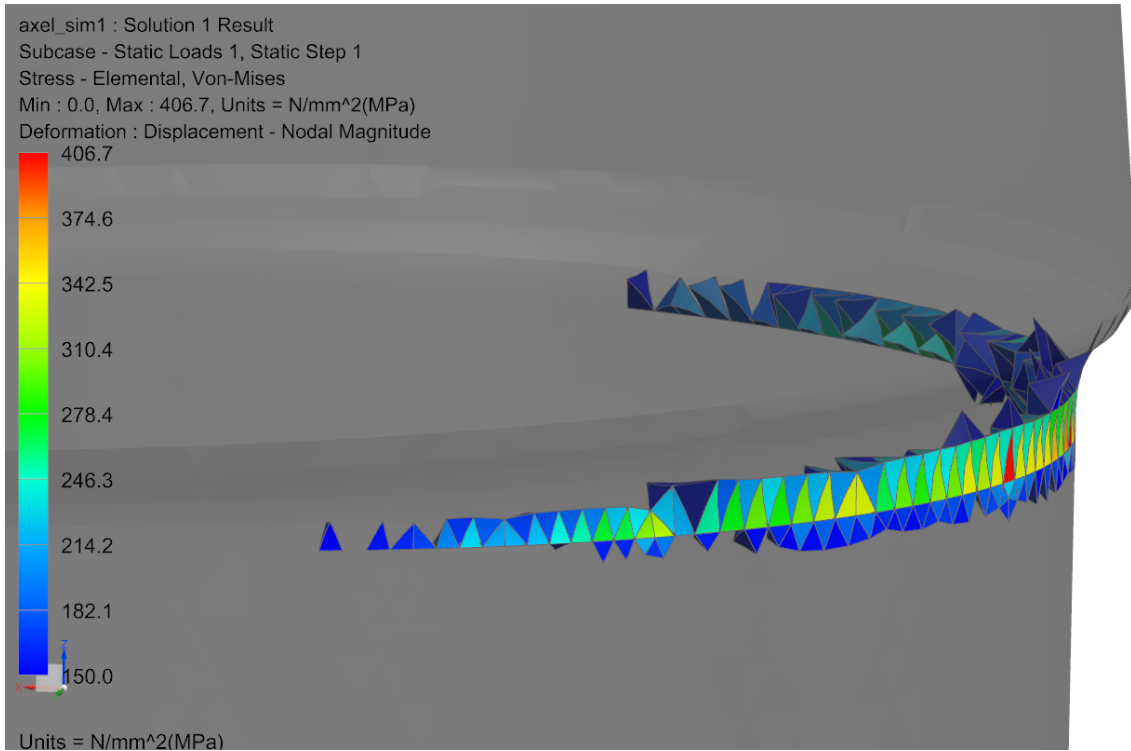


FIGURE 122: AXLE LOAD STATE

The axle is fixed on the 12mm part (right) and a 1000N force in the X-dir is applied on the 13mm part (left).



**FIGURE 123: AXLE STRESS PLOT: MAX STRESS 407MPA**

Elements with stress levels below 150MPa are translucent. Only the surface is subjected to high stress. Also note that this load state is the worst case and the load magnitude is highly conservative, as the magnetic forces will be balanced once the rotor is centered in the stator.

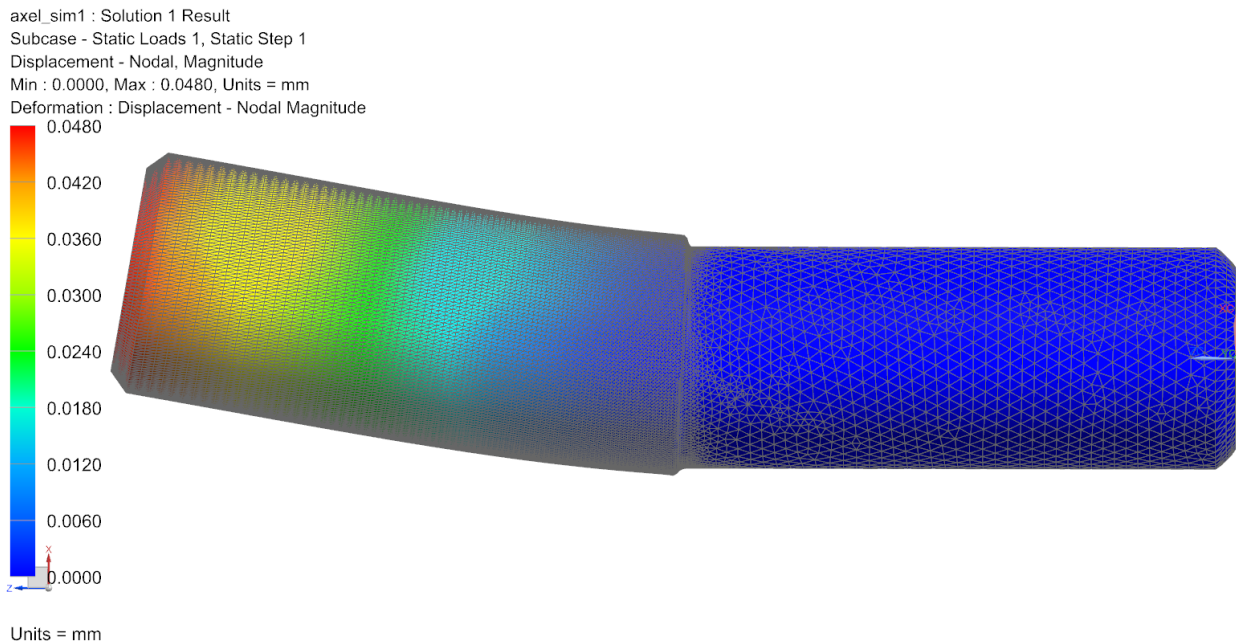


**FIGURE 124: DISPLACEMENT PLOT AXLE - 100X DEFORMATION – MAX DISPLACEMENT 0,048MM**

## 18 APPENDIX I: RIM-THRUSTER FEA DETAILS

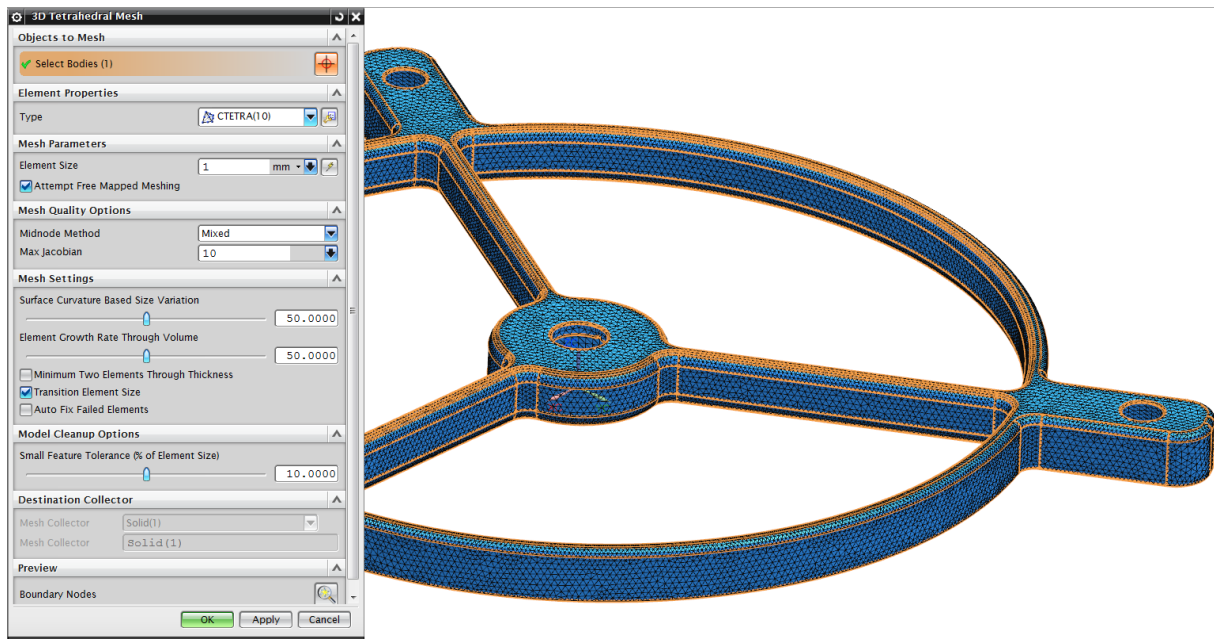


FIGURE 125: THRUSTER HUB MESH (1MM CTETRA(10))

Material used is 6061 aluminium from NX 8,5 material library.

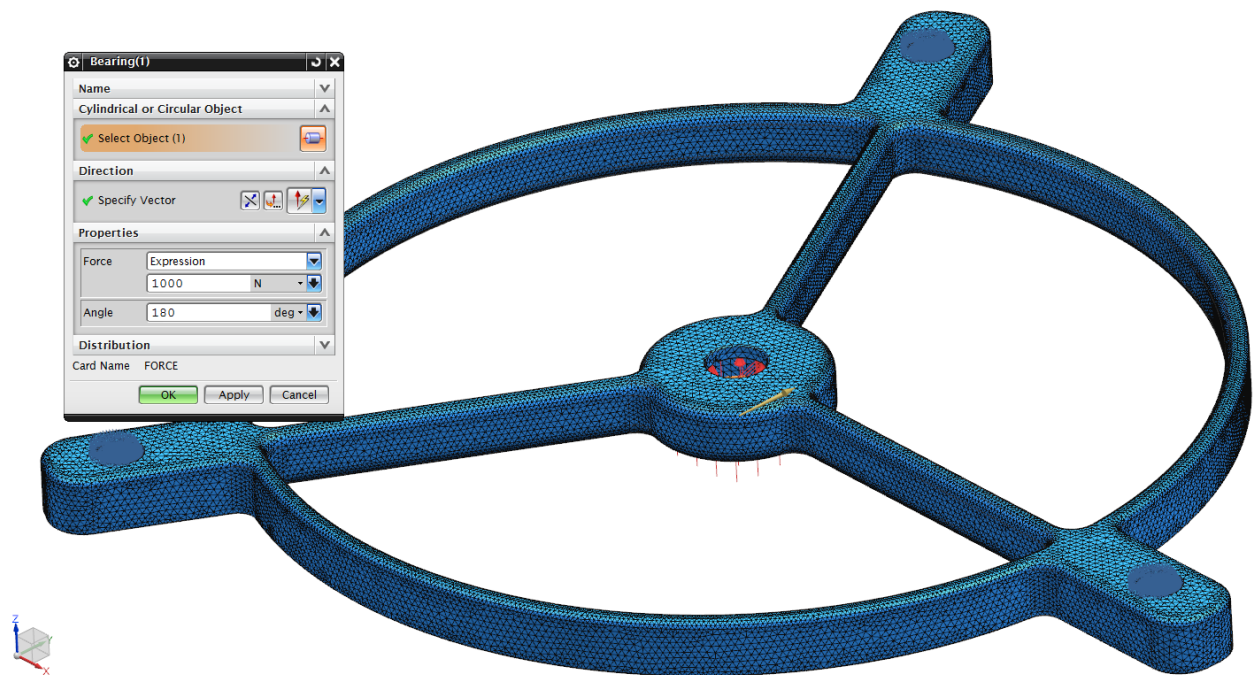
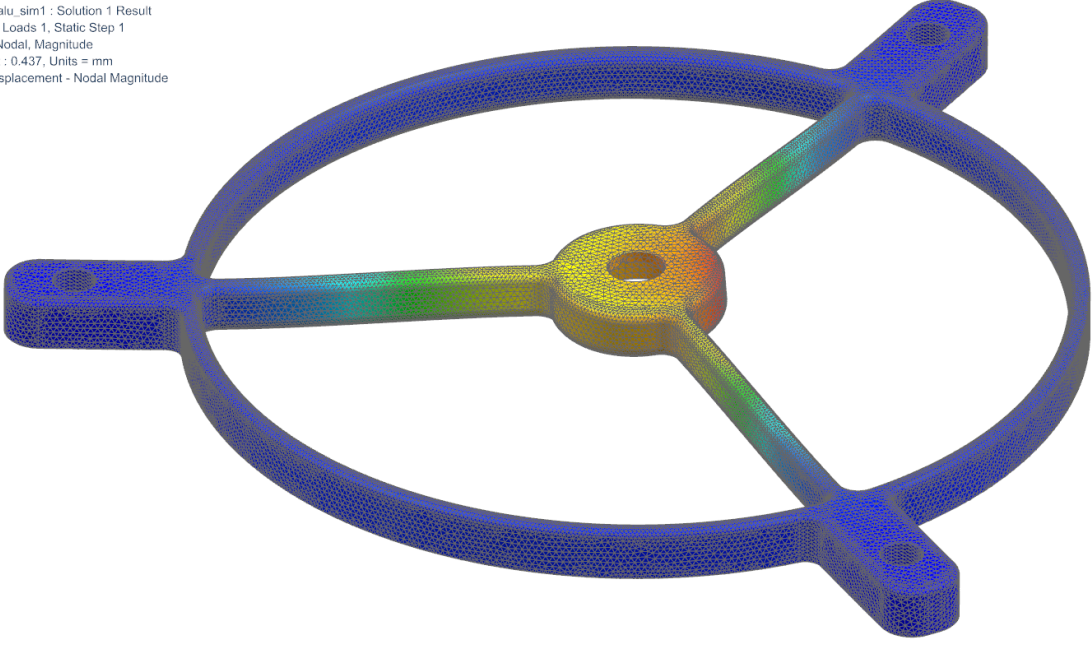


FIGURE 126: THRUSTER HUB LOAD

The hub is loaded by 1000N bearing force in Y-dir (radial) and 400N Z-dir (axial). This is a very conservative load case, since the typical load per hub probably will be below 200N radial and 100N axial during operation. However, due to the uncertainties the simulation loads has been set high.

bearing\_holder\_alu\_sim1 : Solution 1 Result  
Subcase - Static Loads 1, Static Step 1  
Displacement - Nodal, Magnitude  
Min : 0.000, Max : 0.437, Units = mm  
Deformation : Displacement - Nodal Magnitude



**FIGURE 127: THRUSTER HUB DISPLACEMENT PLOT (MAX 0,437MM)**

bearing\_holder\_alu\_sim1 : Solution 1 Result  
Subcase - Static Loads 1, Static Step 1  
Stress - Elemental, Von-Mises  
Min : 0.01, Max : 185.50, Units = N/mm<sup>2</sup>(MPa)  
Deformation : Displacement - Nodal Magnitude

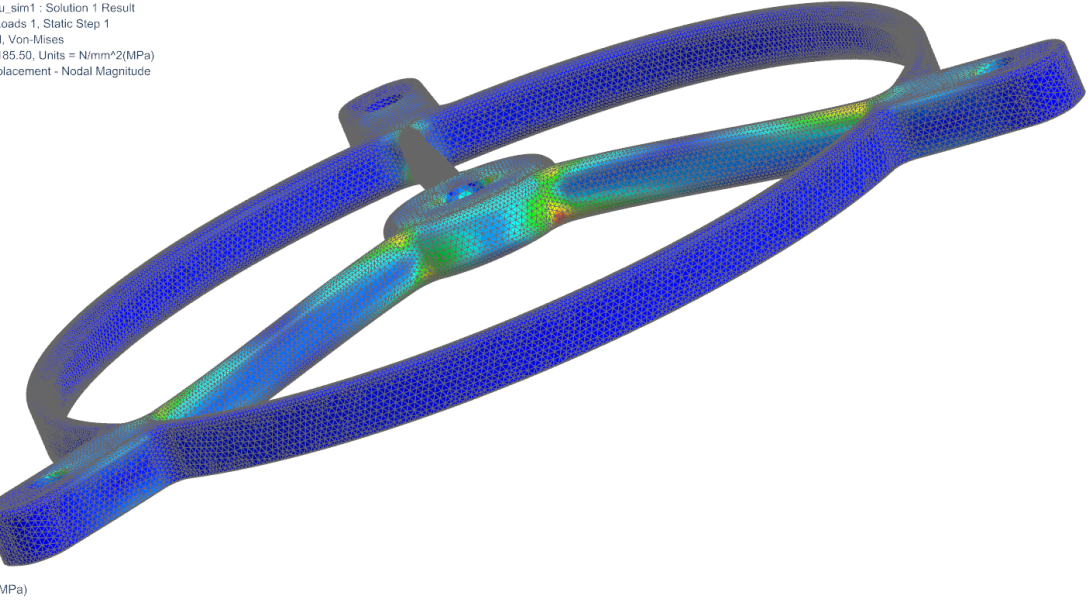
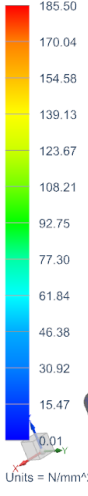


**FIGURE 128: THRUSTER HUB STRESS PLOT (MAX 185,5 MPA VON MISES)**

The results are satisfactory, and further reduction of bar thickness could be done.

## 19 APPENDIX J: ROV LIGHT FEA DETAILS

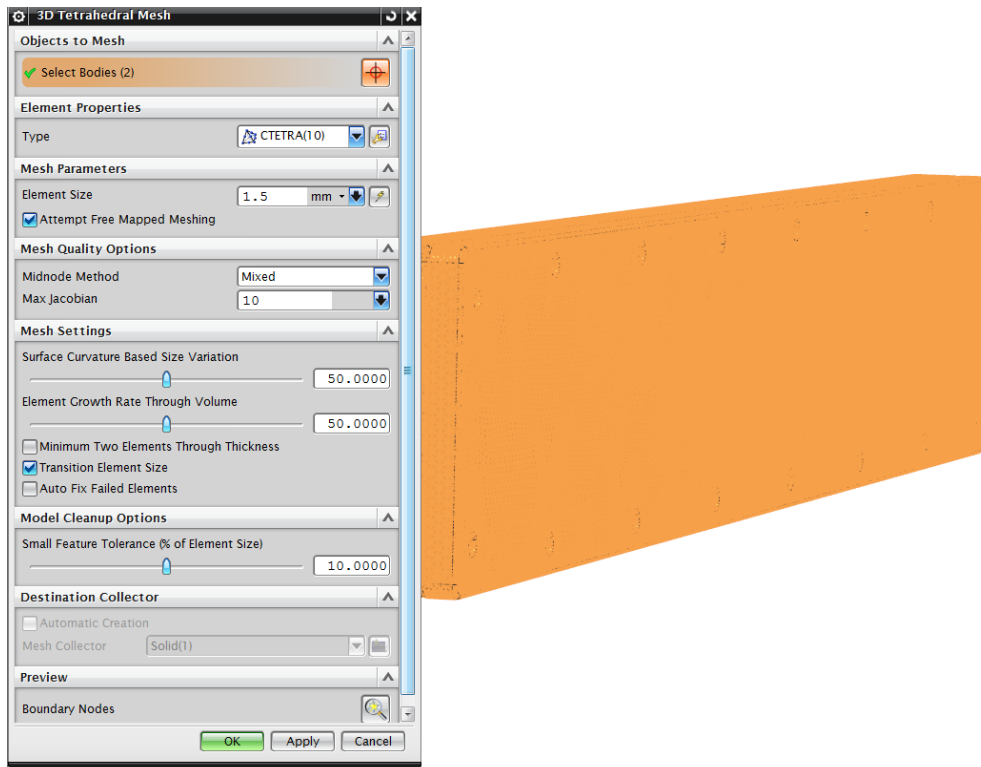


FIGURE 129: LIGHT ASSEMBLY FEA MESH DETAILS

The mesh of the assembly was mated using the “Mesh mating condition”.

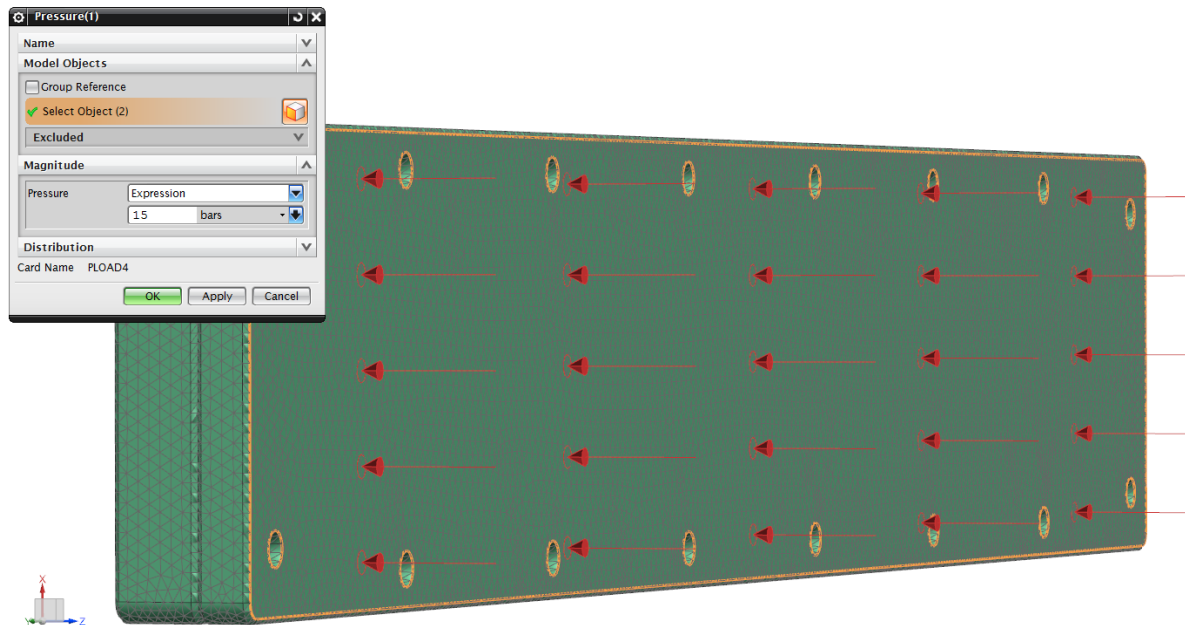
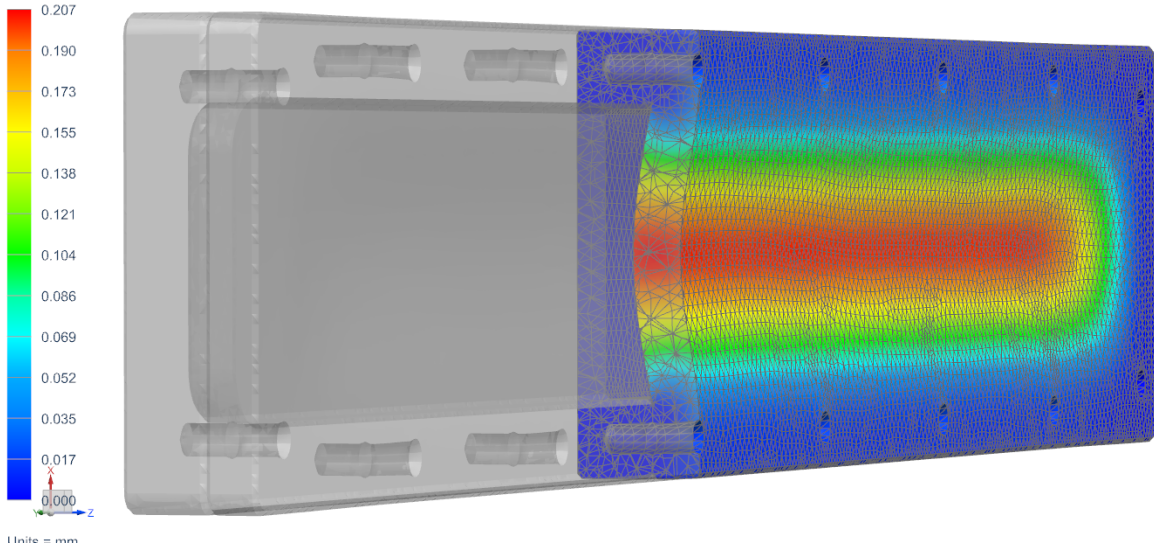


FIGURE 130: LIGHT ASSEMBLU FEA LOAD DETAILS

Materials used are 6061 aluminium for the rear casing and PC for the lens.

Light\_assy\_sim1 : Solution 1 Result  
Subcase - Static Loads 1, Static Step 1  
Displacement - Nodal, Magnitude  
Min : 0.000, Max : 0.207, Units = mm  
Deformation : Displacement - Nodal Magnitude



**FIGURE 131: LIGHT ASSEMBLY FEA DISPLACEMENT PLOT**

Light\_assy\_sim1 : Solution 1 Result  
Subcase - Static Loads 1, Static Step 1  
Stress - Elemental, Von-Mises  
Min : 0.00, Max : 49.78, Units = N/mm<sup>2</sup>(MPa)  
Deformation : Displacement - Nodal Magnitude

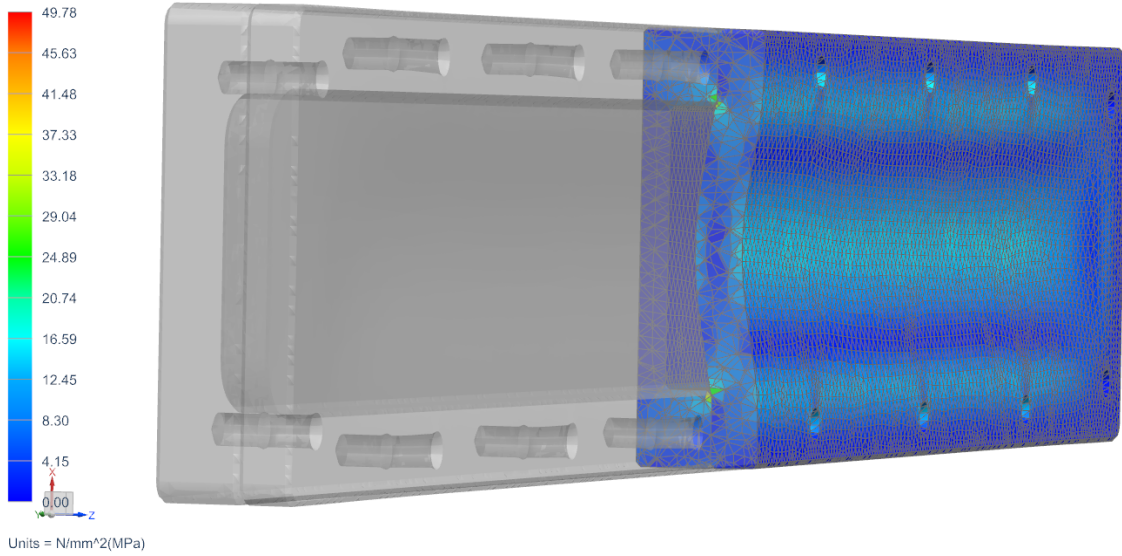


**FIGURE 132: LIGHT ASSEMBLY FEA STRESS PLOT**

## 20 APPENDIX K: HULL SIMULATIONS

The hull was simulated using ABS from NX material library and the lifting bracket glued in place. The lifting bracket is 5mm 6061 Aluminium. From the results it can be seen that the stress levels are higher than what 6061 Aluminium could handle. Material in the bracket will therefore have to be higher grade aluminium like 7075 T6.

The 6mm CTETRA(10) mesh gave a total number of 387 076 elements. The geometry was also analysed using 11,5mm mesh (interfered by NX) which gave slightly lower stress levels.

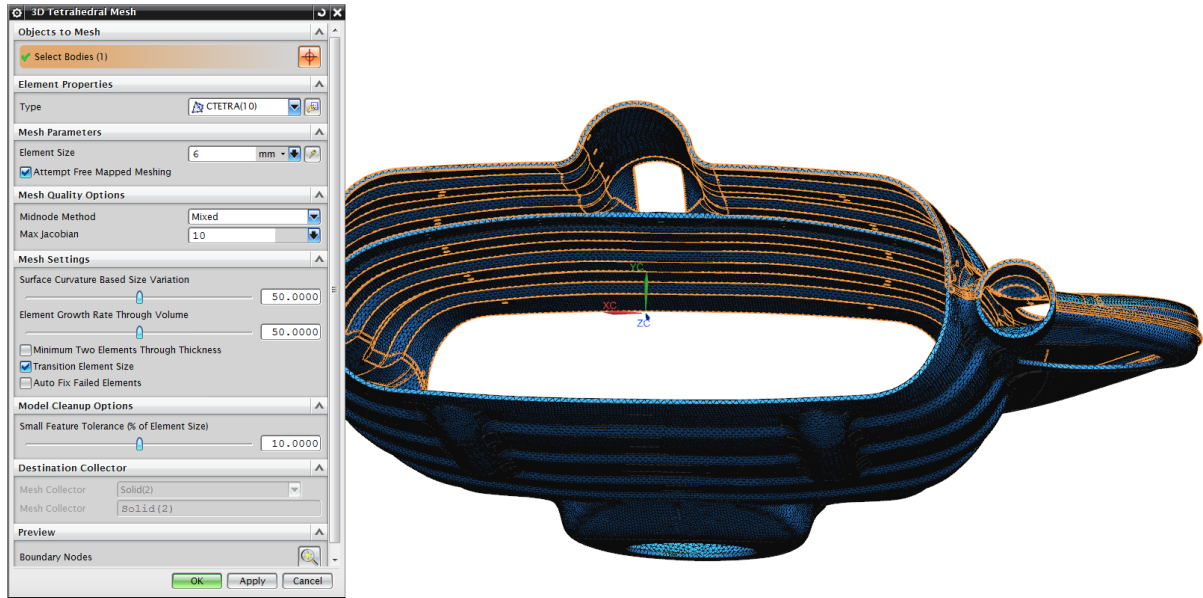


FIGURE 133: HULL FEA 6MM CTETRA(10) MESH

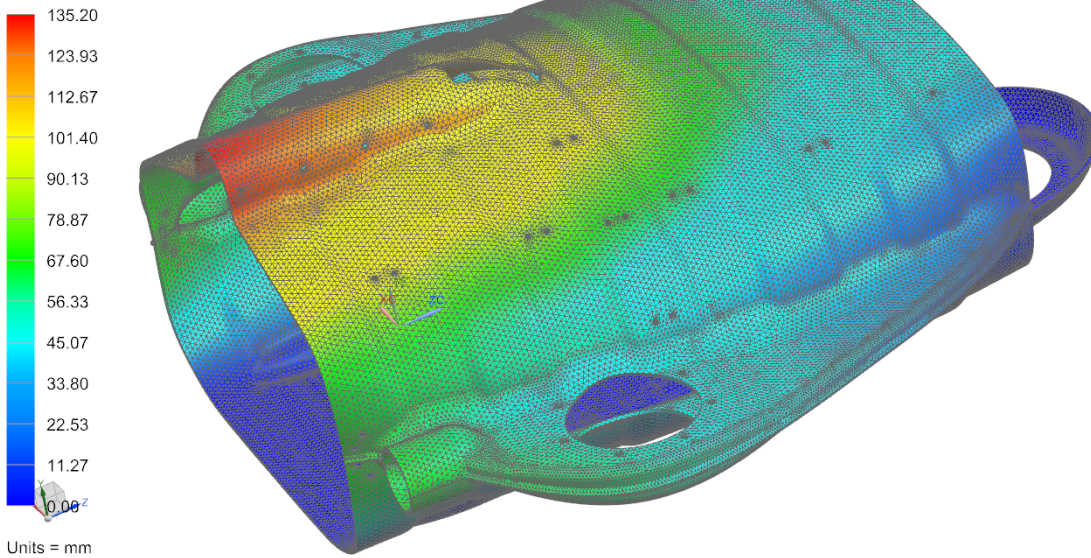
The aluminium bracket is glued to the hull and the hull is glued together using standard surface-to-surface gluing. The load is 1500N force distributed on the centre area of the bracket, which represent a realistic distribution but conservative magnitude.



FIGURE 134: HULL LOAD STATE

The displacement of the hull is severe with this load state and assembly. The complete assembly will be supported by the buoyancy units, so a considerably lower displacement is expected. The complete assembly analysis has not been conducted due to its complexity.

Hull\_v12\_ribbed\_sim1 : Copy of Solution 1 Result  
Subcase - Static Loads 1, Static Step 1  
Displacement - Nodal, Magnitude  
Min : 0.00, Max : 135.20, Units = mm  
Deformation : Displacement - Nodal Magnitude



**FIGURE 135: HULL DISPLACEMENT (MAX 135MM)**

Max strain in Figure 136 occurs at the rear of the hole for the umbilical.

Hull\_v12\_ribbed\_sim1 : Copy of Solution 1 Result  
Subcase - Static Loads 1, Static Step 1  
Strain - Elemental, Von-Mises  
Min : 0.0000, Max : 0.0219, Units = mm/mm  
Deformation : Displacement - Nodal Magnitude

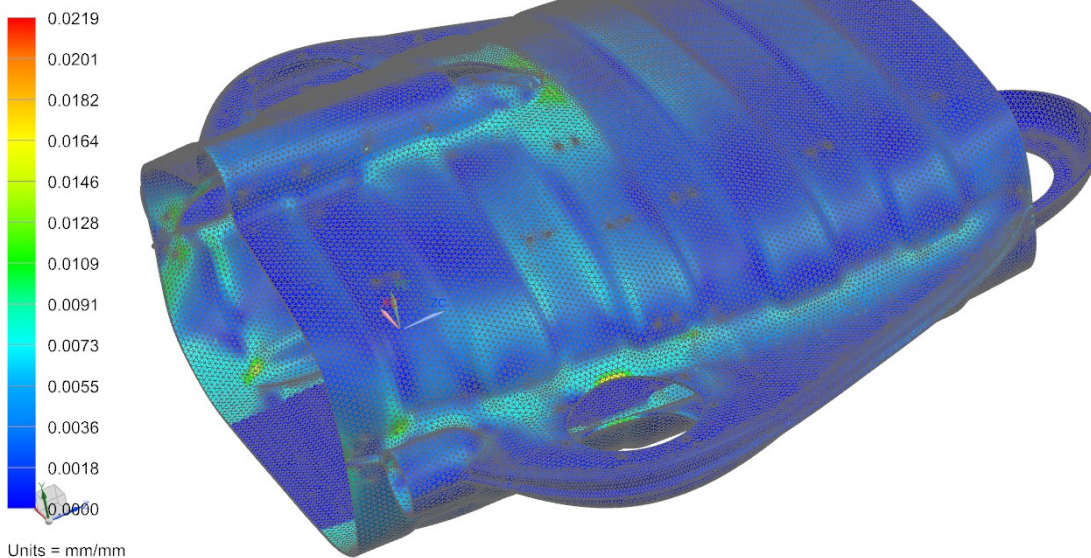


**FIGURE 136: HULL STRAIN (MAX 0,022)**

The low level stress plot renders elements with stress below 10MPa transparent. The scale goes to 35 that represents typical yield stress of standard grade ABS, although there are ABS grades that can have a yield stress of up to 51MPa [7]. Since the bracket is higher loaded this plot does not describe its stress levels well.

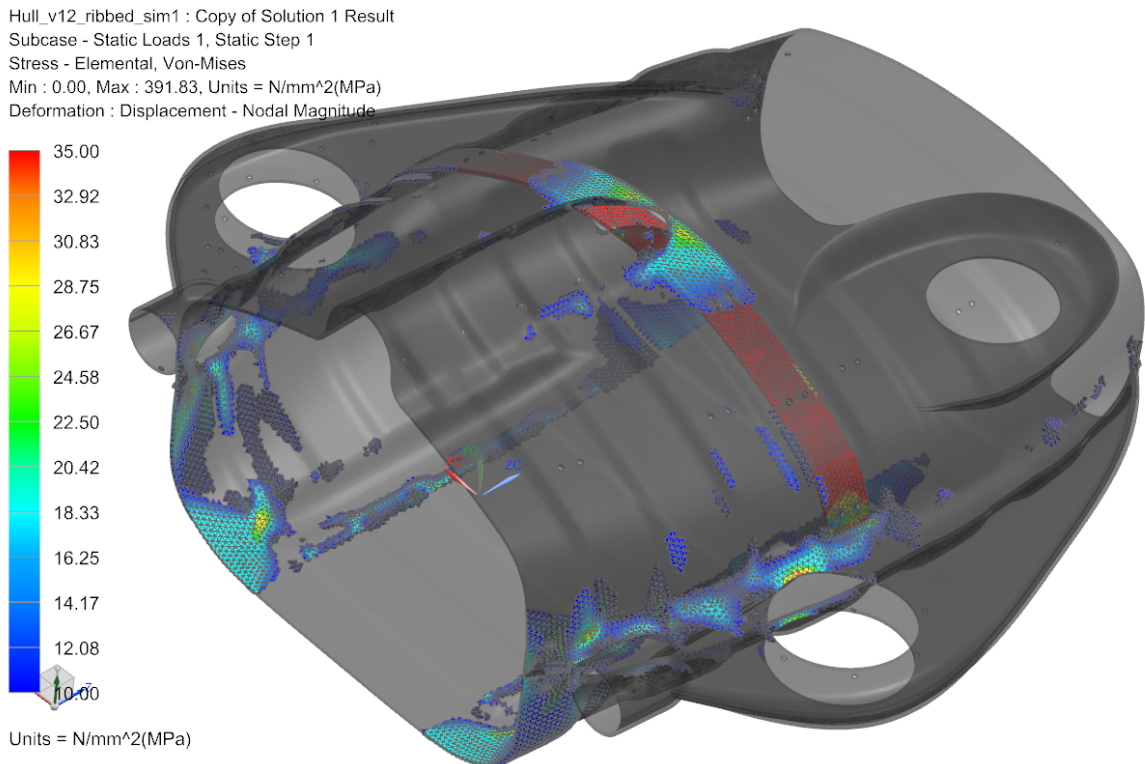


FIGURE 137: HULL LOW LEVEL STRESS

The high level stress plot goes from 25MPa to 392 MPa, which is the maximum stress in this analysis. Elements with stress below 25MPa are transparent, and from this it can be seen that the hull generally experiences low stress. The aluminium bracket has high stress at the point where it is connected to the umbilical. This stress could be lowered by adding material at this area,

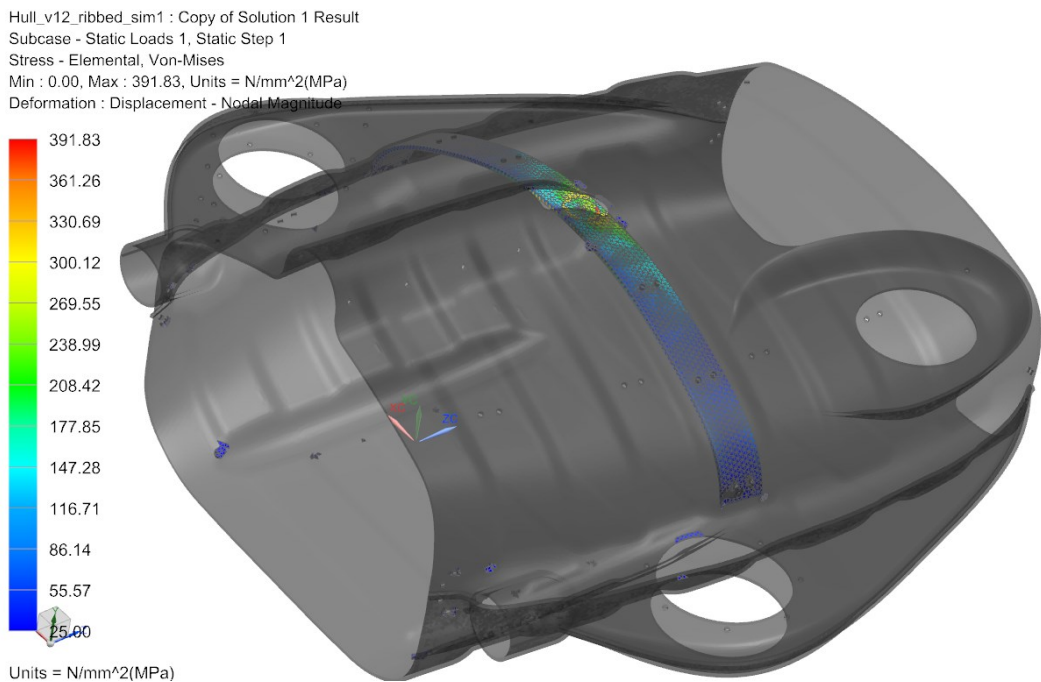


FIGURE 138: HULL HIGH LEVEL STRESS

## 20.1 REAR THRUSTER WING LOADING

The rear thruster wing is a very exposed part of the hull. Some analyses have been done concerning loads acting on this part of the hull in order to investigate the need for extra support. The lower hull section were meshed using 5mm CTETRA(10) mesh for both the load cases. This mesh is somewhat coarse with respect to the mesh convergence test results in chapter 5.2.1. The results must therefore be considered with this in mind Material used is ABS from NX material library.

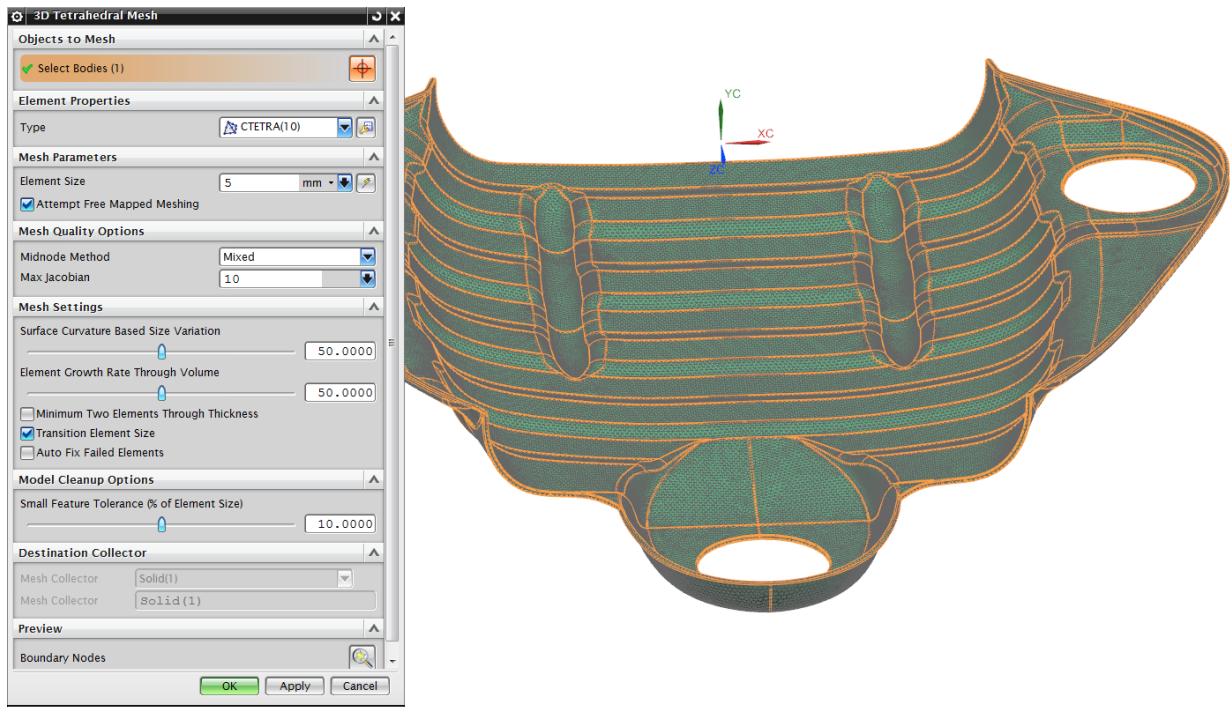


FIGURE 139: 5MM CTETRA(10) MESH ON LOWER HULL

The upwards bump load is thought to be the toughest, and it could happen if the Manta is put down unevenly on the deck. The Manta will weigh approximately 30kg, so a force of 500N is thought to be sufficient, although putting it down hard will probably result in even larger forces. The lower hull section is fully fixed where it is connected to the upper hull section.

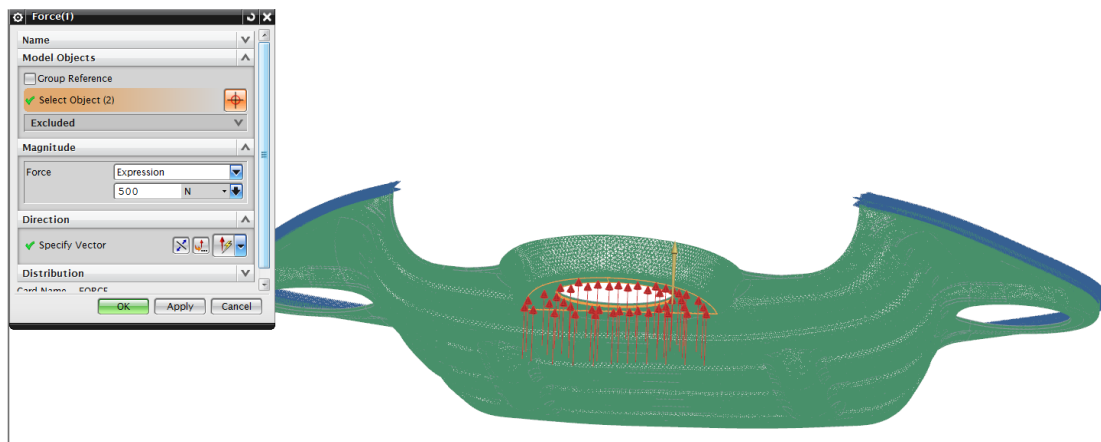
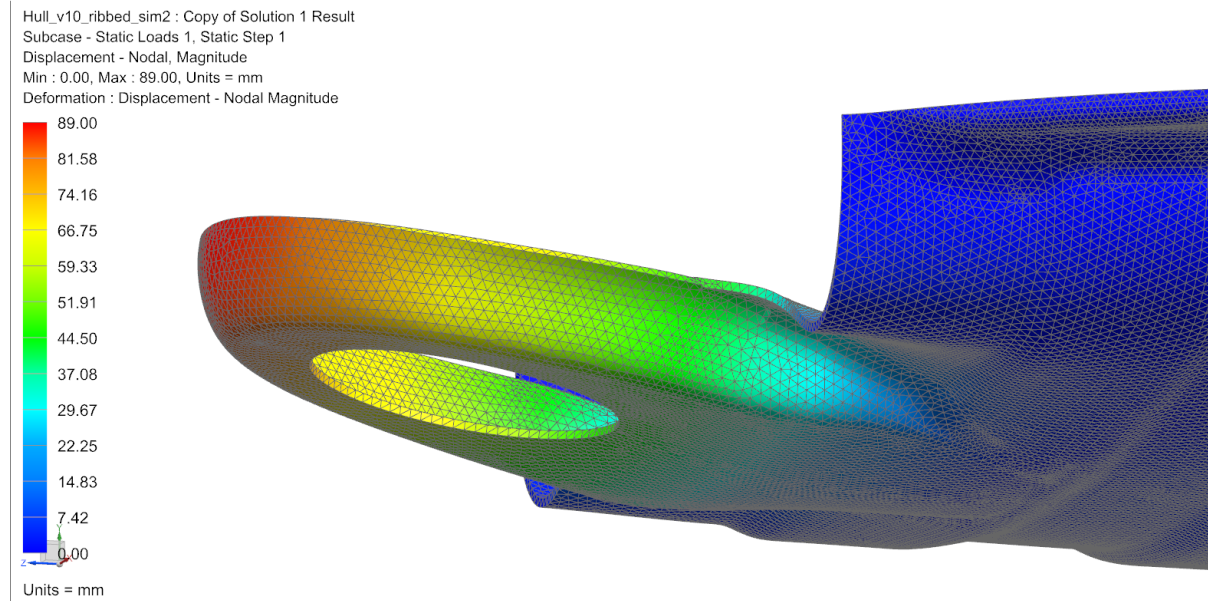


FIGURE 140: UPWARDS 500N FORCE LOAD CASE

The resulting displacement of 89mm is severe, but the deformation mostly occurs at parts of the hull without any mounted components. The area where the rear thruster is mounted does not flex much.



**FIGURE 141: REAR THRUSTER WING DISPLACEMENT PLOT (1X DEFORMATION)**

The stress plot shows stresses above yield strength, which is typical about 35 MPa for ABS, at the outer surface of the rear wing. Since this is an elastic analysis, the material will yield and experience plastic deformation. This will most likely damage the rear wing, especially over time. Although the rear wing will be considerably supported by the upper lid and the thruster the results indicates a need for a rear thruster bumper or other sort of support.

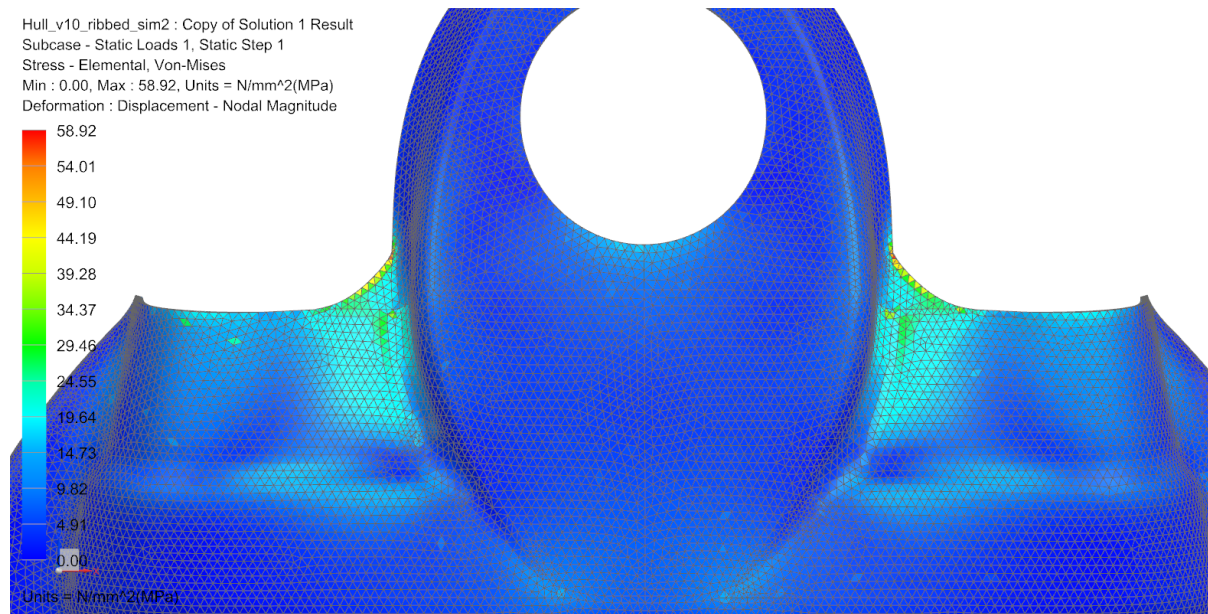


**FIGURE 142: REAR THRUSTER WING STRESS PLOT**

At the inwards bump load case, a force of similar magnitude is applied to the rear of the thruster wing in the inward direction. Mesh and material is the same as the upwards bump case. This load case is considerably less problematic for the structure, due to a lower bending moment created.

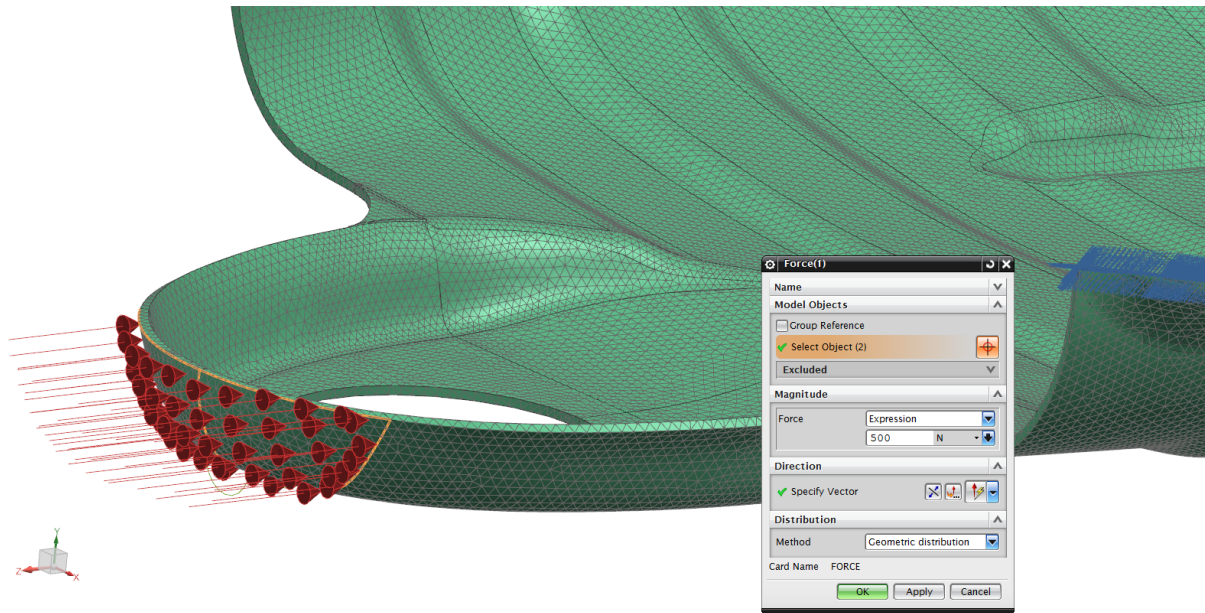


FIGURE 143: INWARDS FORCE LOAD CASE (500N)

From the stress plot in Figure 144, we can see that this load case is unproblematic for the structure. The maximum occurring stress of 14 MPa is far below the yield stress of ABS (ca. 35MPa).

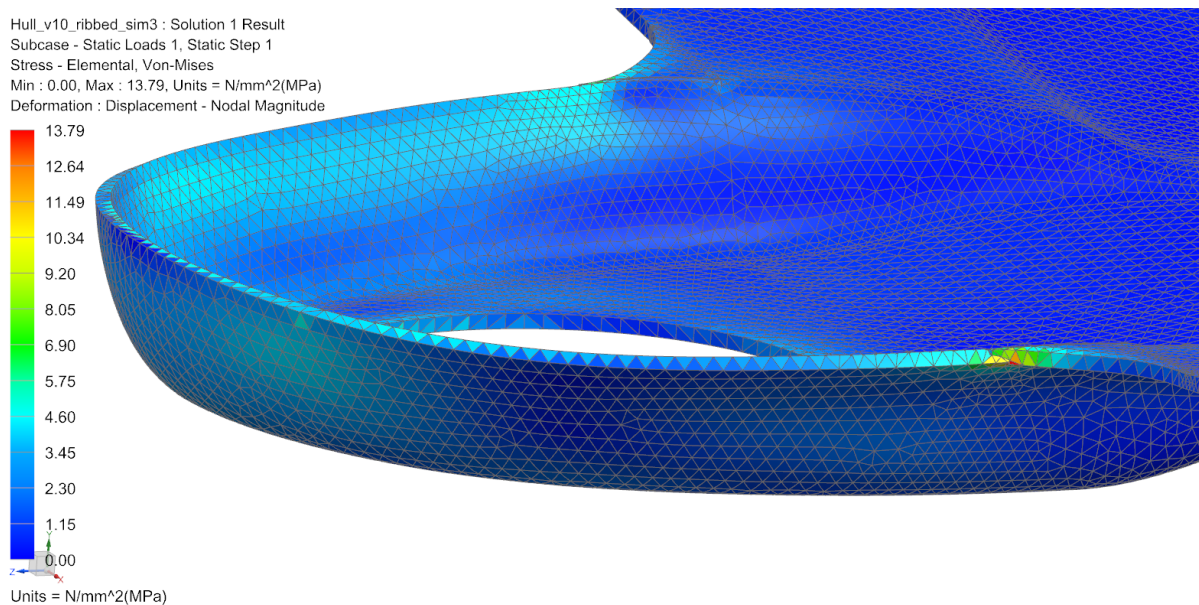


FIGURE 144: INWARDS LOAD CASE STRESS PLOT

Maximum displacement is 7mm.

## 21 APPENDIX L: UMBILICAL LIFTING POINT

### 21.1 UMBILICAL FIXTURE FEA RESULTS

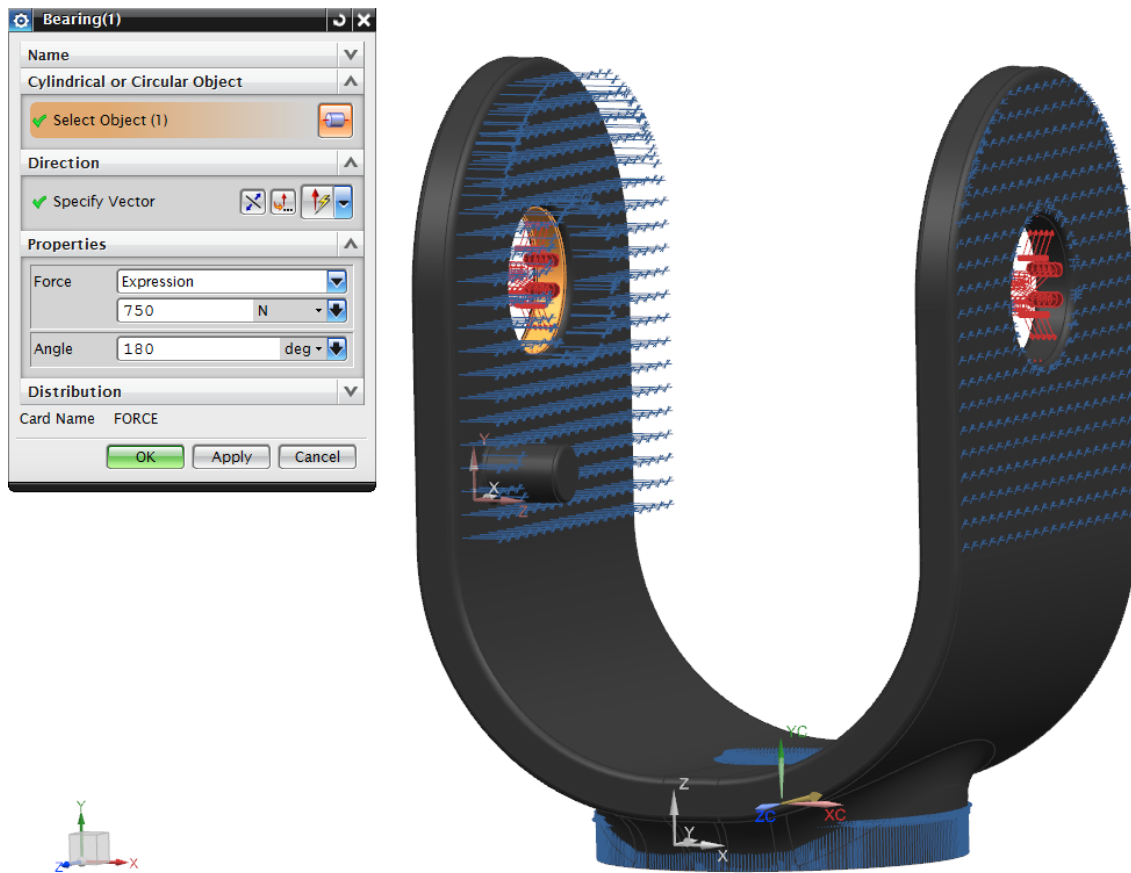


FIGURE 145: UMBILICAL FIXTURE LOAD CASE.

The umbilical fixture is supported in the Y direction (upwards), and totally fixed in the centre to simulate a bolt load, as illustrated in Figure 145. The bolt pretension is not simulated, which will result in lower stress around the bolt hole. The plates are supported in X direction (sideward), as the centre umbilical holder and bolts would support the plates. The 1500N total bearing force has been simulated both in Y direction (upwards) and Z direction (forwards). This load condition is 50% more than the winch will be limited to (design load 1000N). Even though the Manta including dead fish only will weigh a maximum of around 80kg, added mass from water and fast acceleration could create high loads when pulling the Manta up. **Note that the main way of getting the ROV to the surface is by use of the motors, not by pulling it up by the umbilical.** This is only a back-up solution for getting the ROV up if it has malfunctioned.

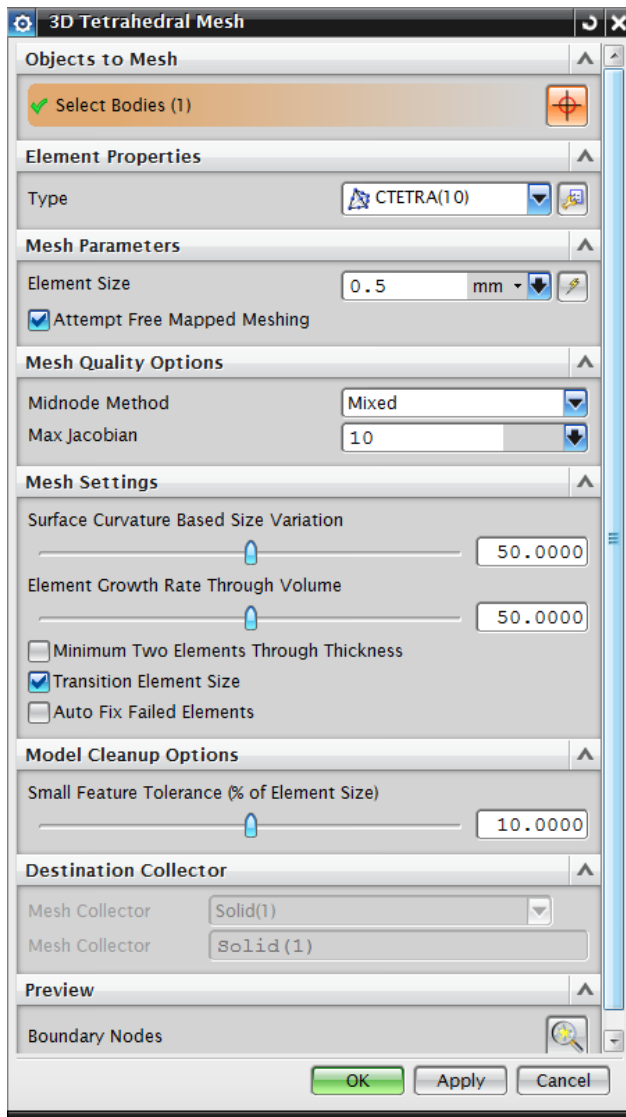
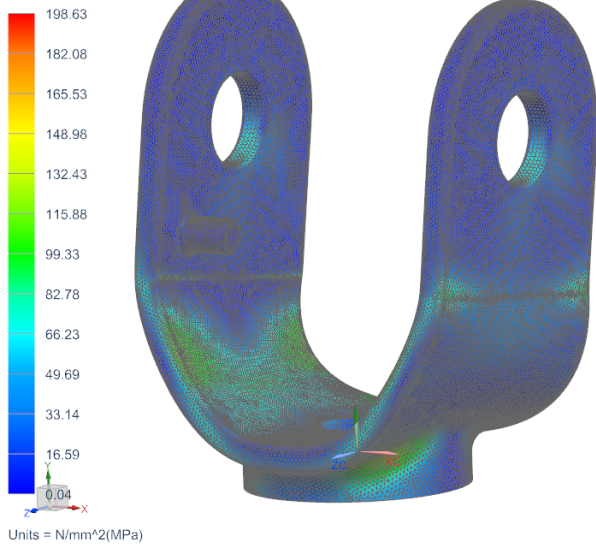


FIGURE 146: UMBILICAL FIXTURE MESH - 0,5MM CTETRA(10) ELEMENTS

0,5mm element size gave a total number of 474624 elements. The fixture has also been analysed with 2mm elements. Material used is for FEA is AISI 310 SS (stainless steel).

Umbi-fixture\_sim1 : Copy of Solution 1 Result  
 Subcase - Static Loads 1, Static Step 1  
 Stress - Elemental, Von-Mises  
 Min : 0.04, Max : 198.63, Units = N/mm<sup>2</sup>(MPa)  
 Deformation : Displacement - Nodal Magnitude



Umbi-fixture\_sim1 : Copy of Copy of Solution 1 Result  
 Subcase - Static Loads 1, Static Step 1  
 Stress - Elemental, Von-Mises  
 Min : 0.03, Max : 56.60, Units = N/mm<sup>2</sup>(MPa)  
 Deformation : Displacement - Nodal Magnitude

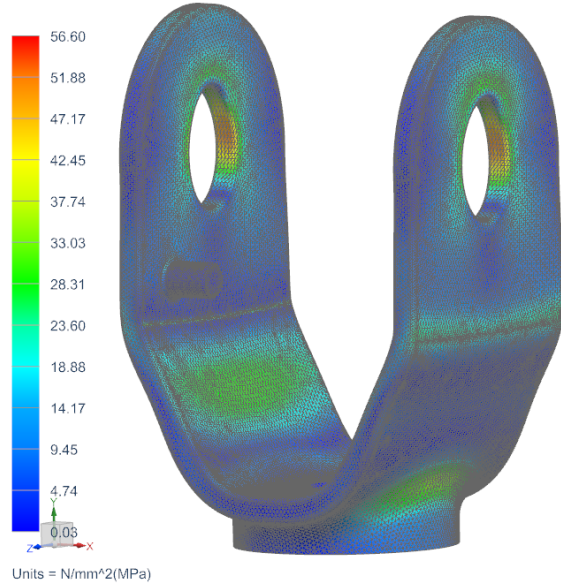
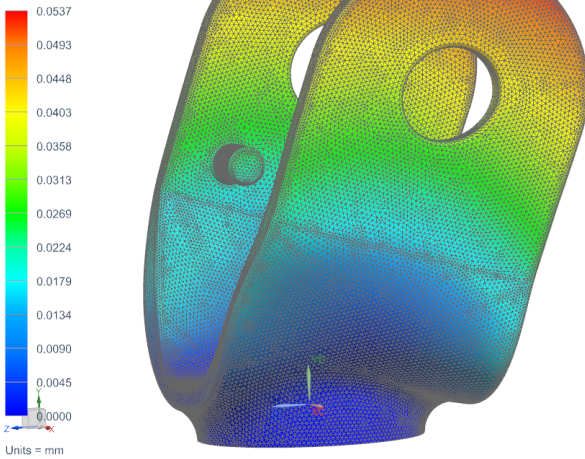


**FIGURE 147: STRESS PLOT FROM STRAIGHT FORWARDS FORCE (LEFT) AND STRAIGHT UPWARDS FORCE (RIGHT)**

Umbi-fixture\_sim1 : Copy of Solution 1 Result  
 Subcase - Static Loads 1, Static Step 1  
 Displacement - Nodal, Magnitude  
 Min : 0.0000, Max : 0.0537, Units = mm  
 Deformation : Displacement - Nodal Magnitude



Umbi-fixture\_sim1 : Copy of Copy of Solution 1 Result  
 Subcase - Static Loads 1, Static Step 1  
 Displacement - Nodal, Magnitude  
 Min : 0.000E+000, Max : 5.326E-003, Units = mm  
 Deformation : Displacement - Nodal Magnitude

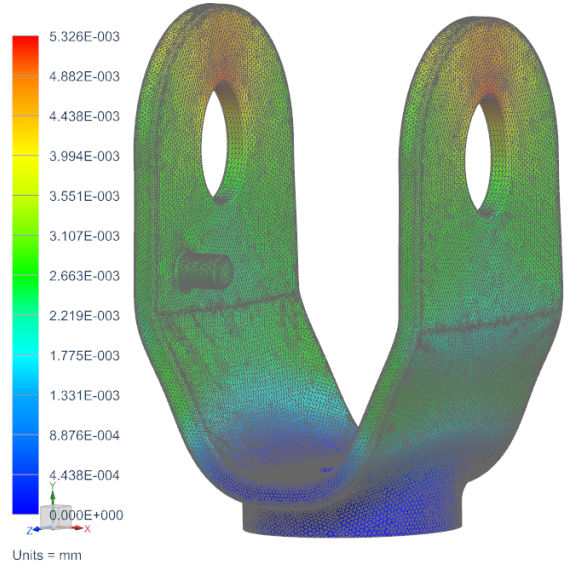


**FIGURE 148: DISPLACEMENT PLOT FROM STRAIGHT FORWARDS FORCE (LEFT) AND STRAIGHT UPWARDS FORCE (RIGHT)**

The maximum von Mises stress is well below the yield strength of for instance 316L stainless steel, about 290 MPa [53]. The results are therefore satisfactory. If a larger safety factor is wanted, 4mm sheet steel could be used instead of 3mm as it is in this case. Stronger steel could alternatively be used.

## 21.2 UMBILICAL PIVOT FEA RESULTS

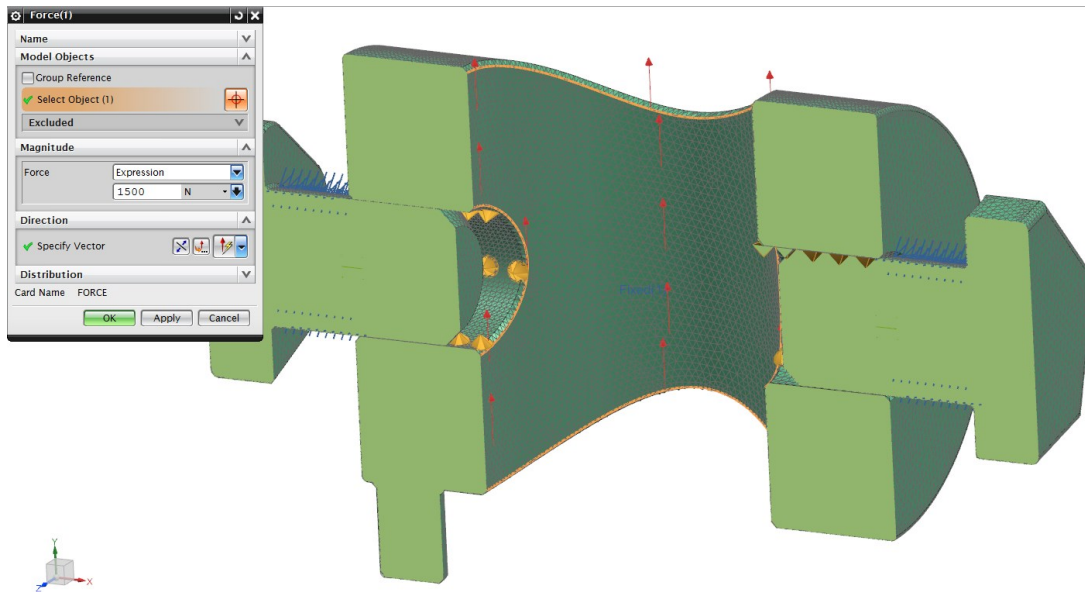


FIGURE 149: UMBILICAL PIVOT LOAD DATA

The pivot is loaded through its cylindrical inner face with a 1500 N geometrically distributed force. The bolts are fixed just outside the hole, and constrained to the hole by surface-to-surface gluing (orange cones). In real reality the bolts would not be completely fixed, as the bushing allows for some movement and elastic deformation. Fixing the bolts is therefore seen upon as conservative.

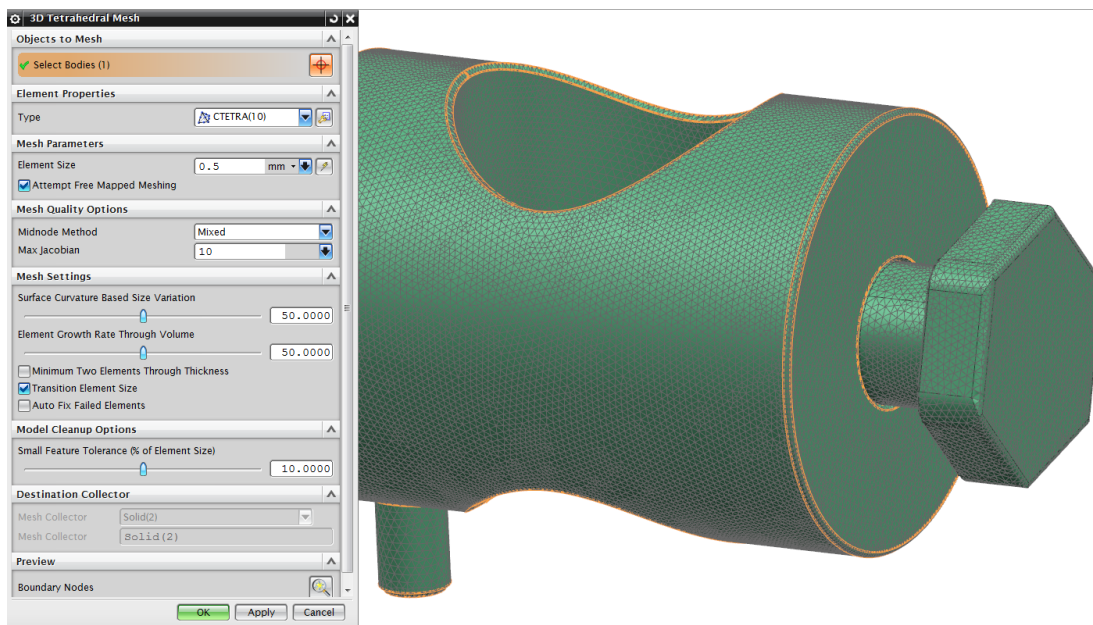
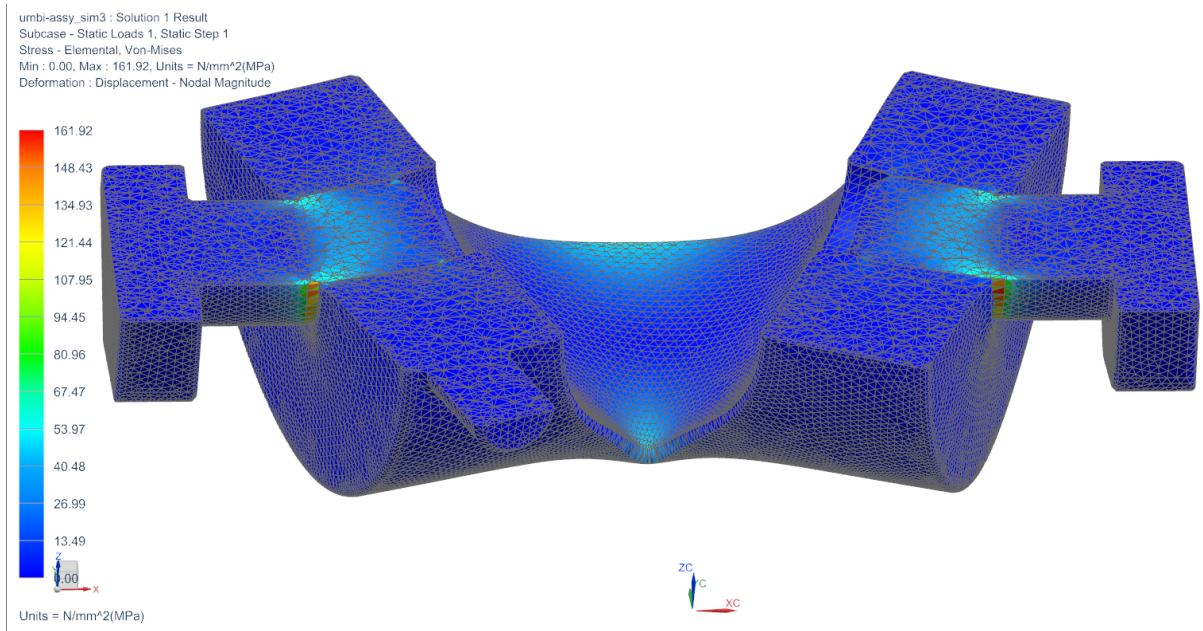


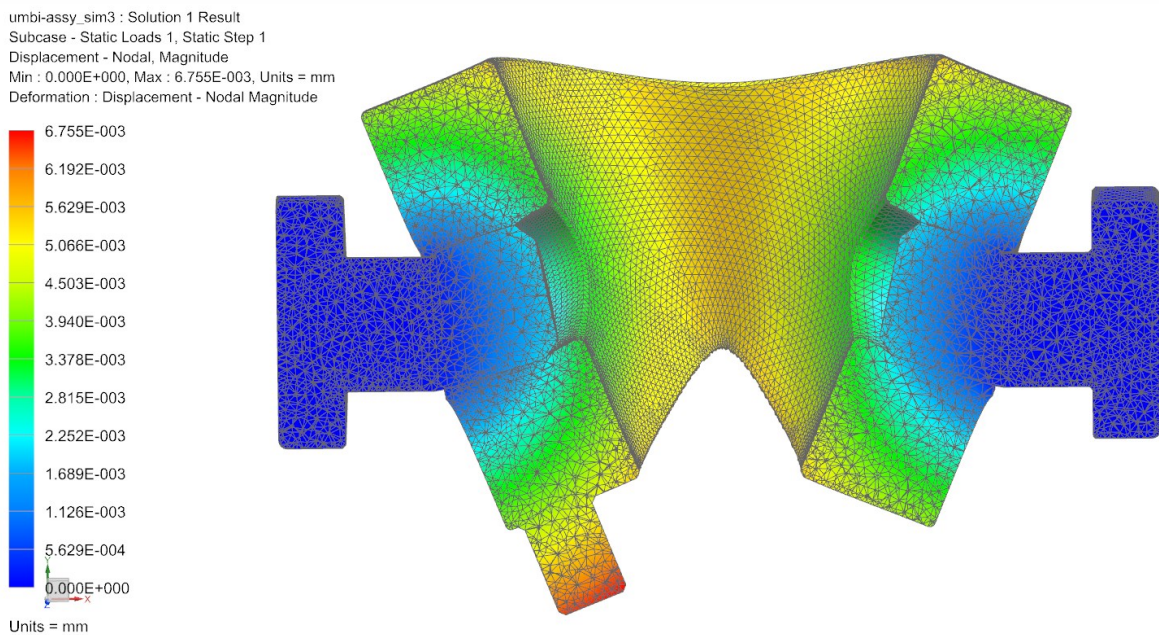
FIGURE 150: UMBILICAL PIVOT MESH DATA – 0,5MM CTETRA(10) ELEMENTS

Material used in FEA is 6061 aluminium for the pivot (centre) and AISI 310 SS stainless steel for the hex bolts.



**FIGURE 151: UMBILICAL PIVOT STRESS PLOT (HALF SECTION VIEW)**

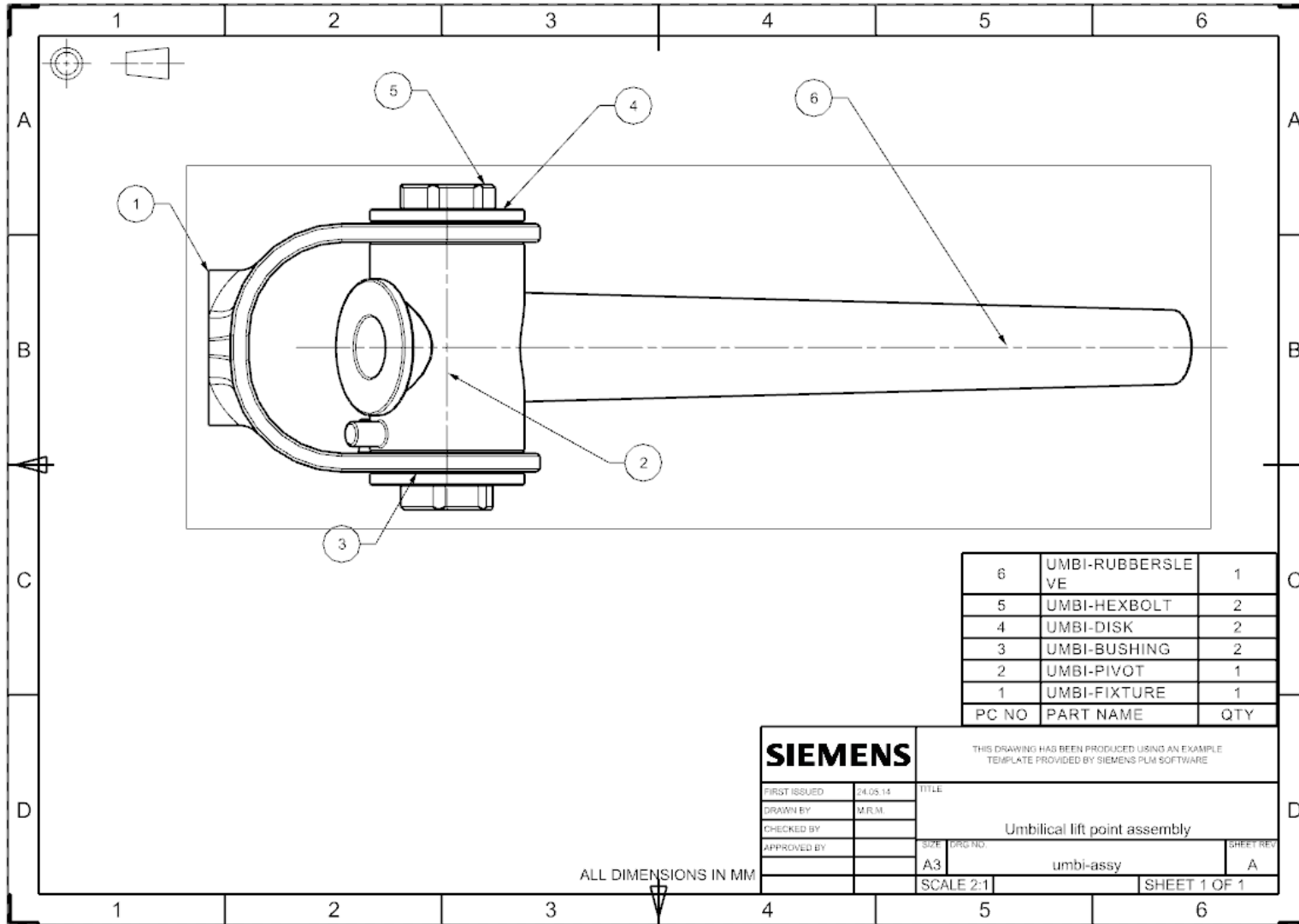
The stress plot in Figure 151 shows the von Mises stress to reach the maximum value of 162MPa at upper and lower part of the bolts where they enter the pivot body. Since this is both a conservative load case and the load has a safety factor of 1,5, the results are seen upon as satisfactory.

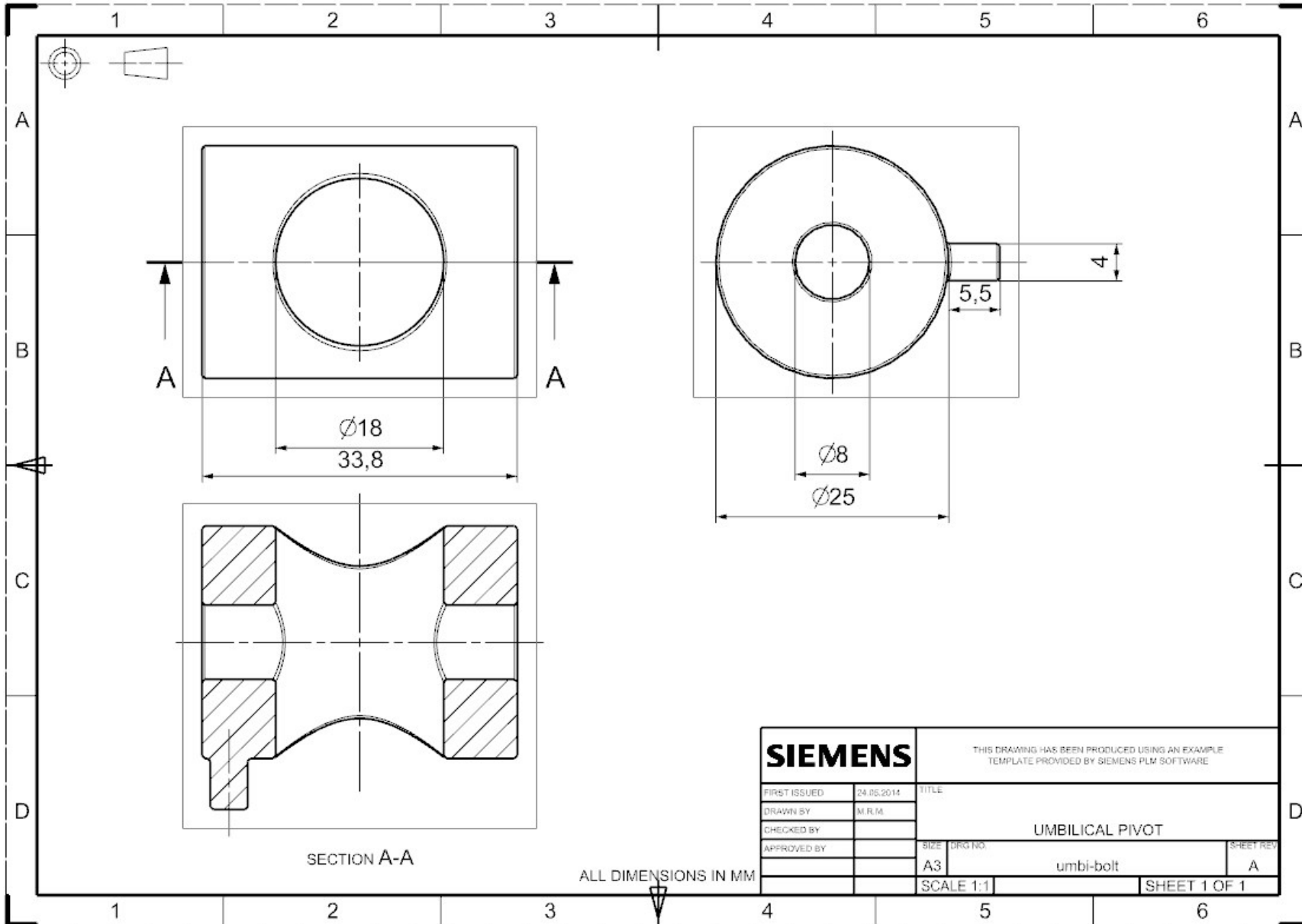


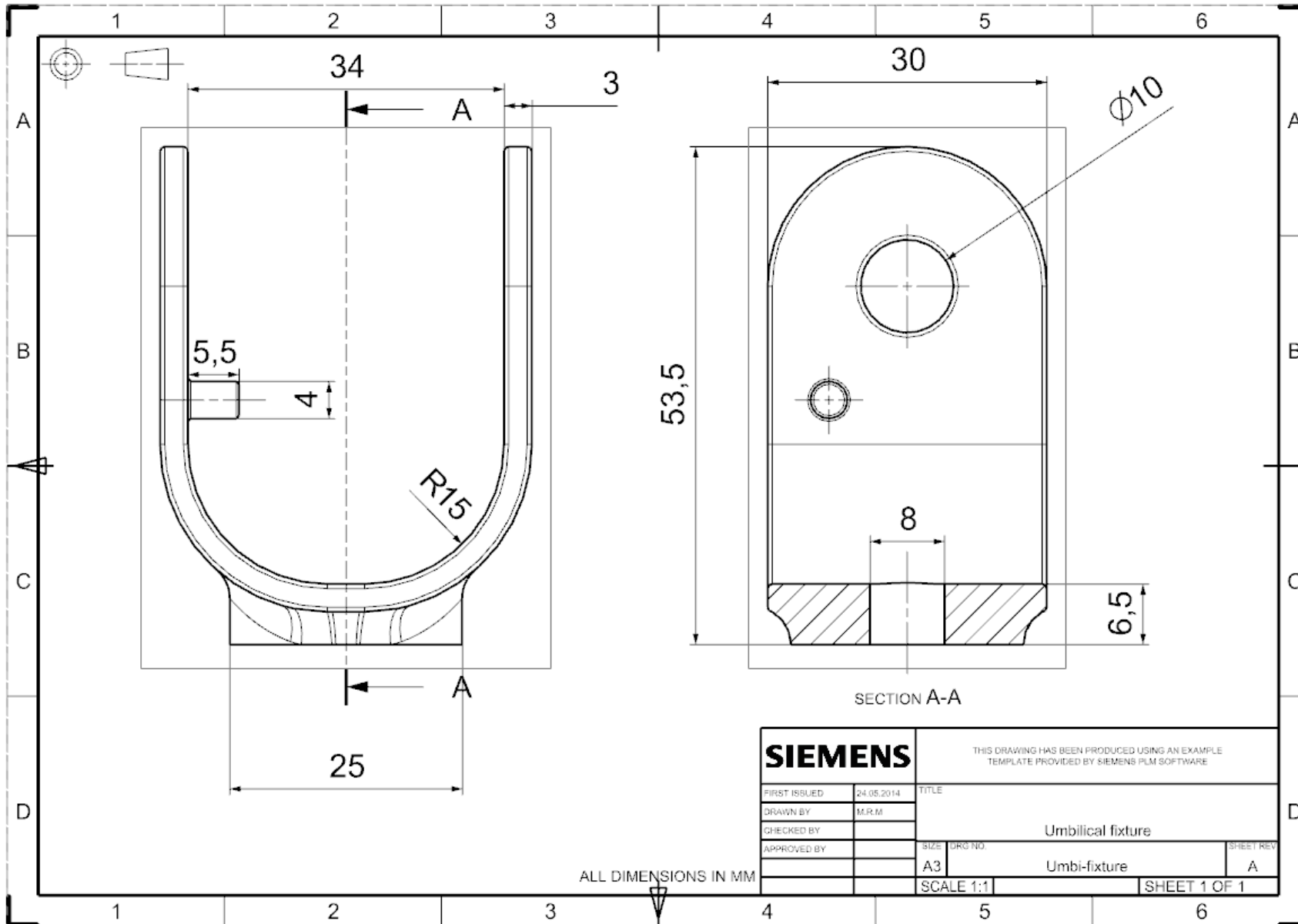
**FIGURE 152: UMBILICAL PIVOT DISPLACEMENT PLOT 100X DEFORMATION (HALF SECTION VIEW)**

The displacement plot in Figure 152 shows a very small deflection that is of no concern to the function of the pivot. The pivot body will have plastic shims to minimize wear and a small air gap (0,5mm).

### 21.3 UMBILICAL LIFTING POINT MACHINE DRAWINGS (ORIGINALLY A3 SIZE)







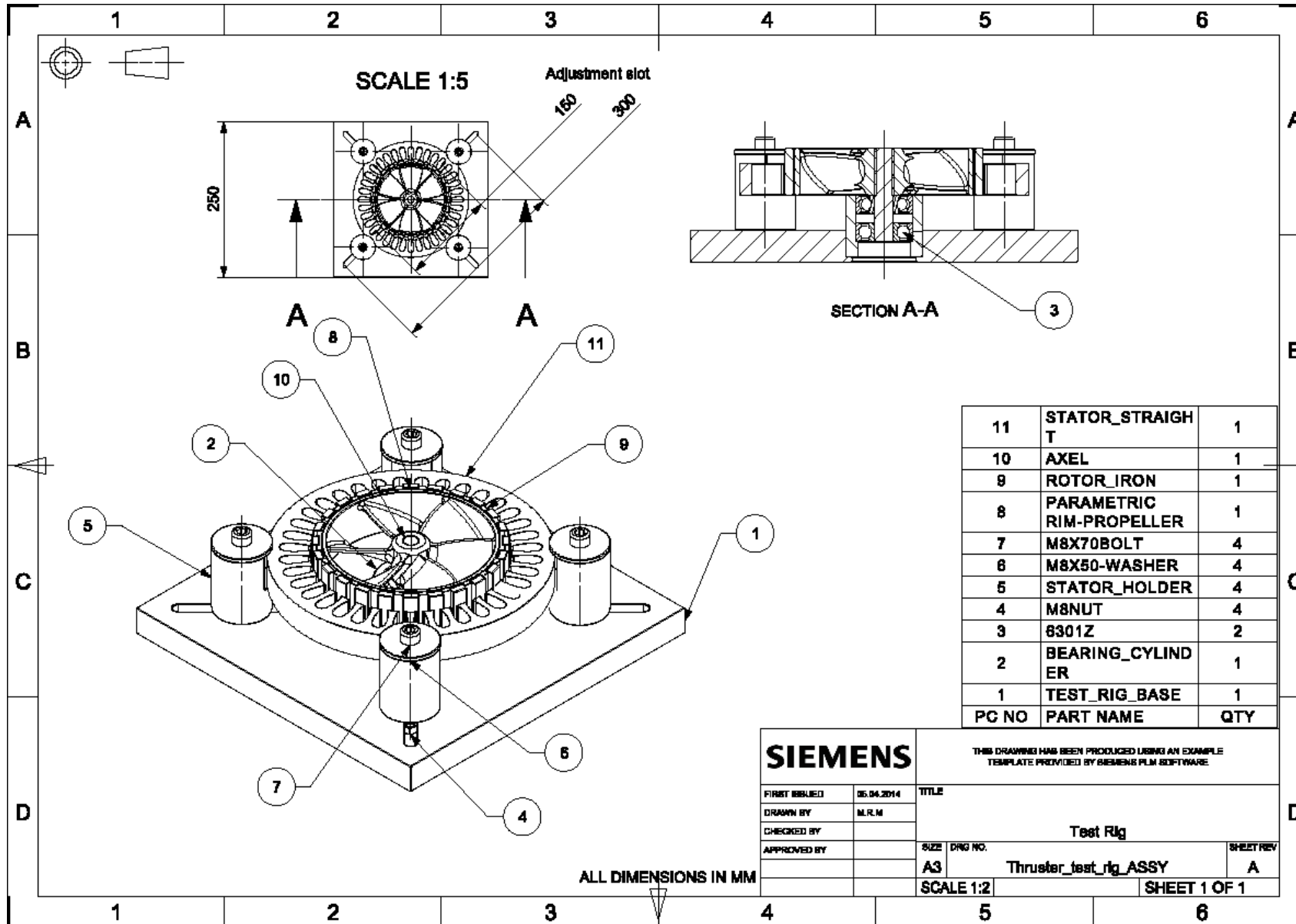
<b>SIEMENS</b>		THIS DRAWING HAS BEEN PRODUCED USING AN EXAMPLE TEMPLATE PROVIDED BY SIEMENS PLM SOFTWARE	
FIRST ISSUED	24.05.2014	TITLE	
DRAWN BY	M.R.M	Umbilical fixture	
CHECKED BY		SIZE	DRG NO.
APPROVED BY		A3	Umbi-fixture
		SCALE 1:1	SHEET 1 OF 1

ALL DIMENSIONS IN MM

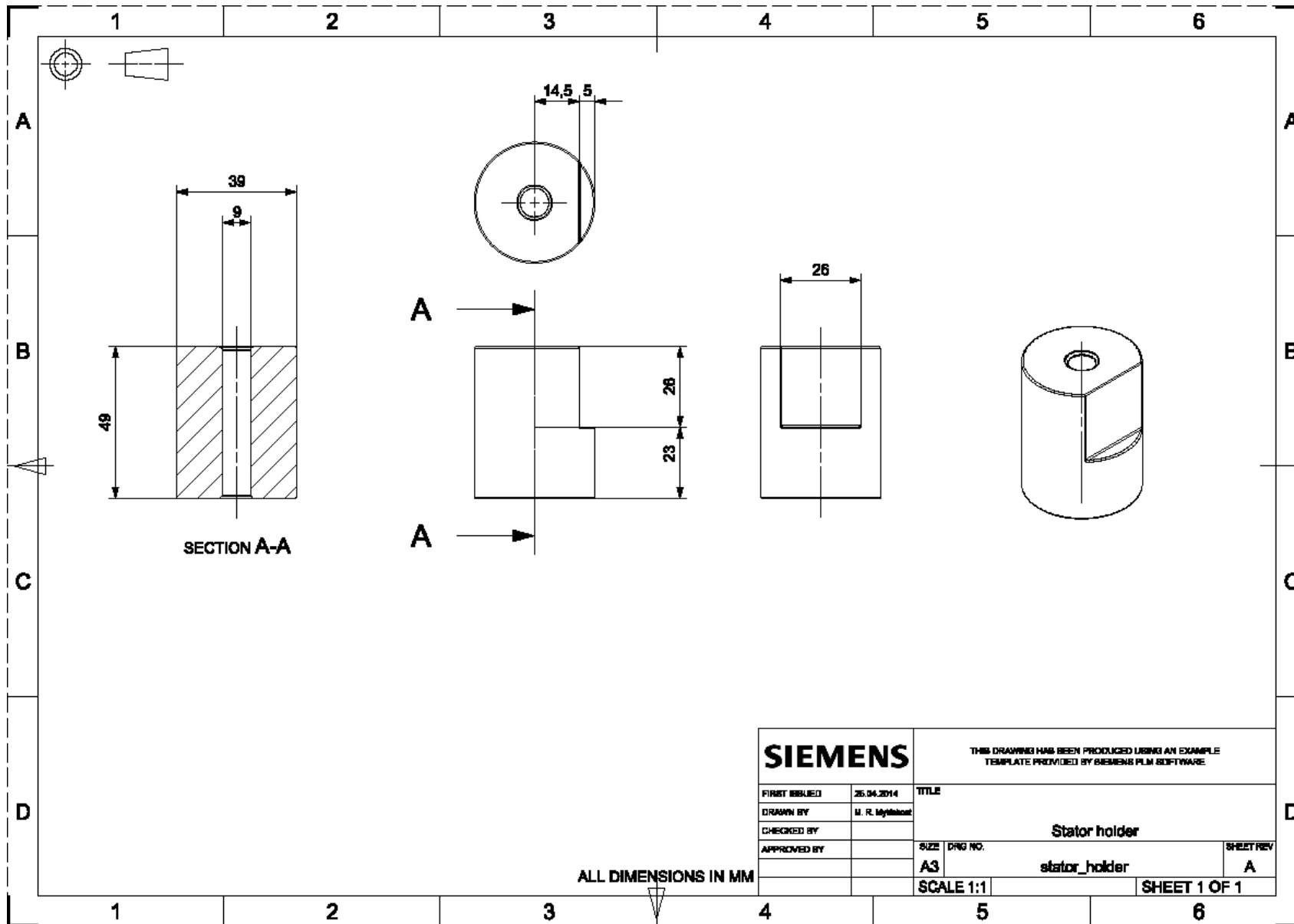
## 22 APPENDIX M: MACHINE DRAWINGS OF THRUSTER TEST RIG

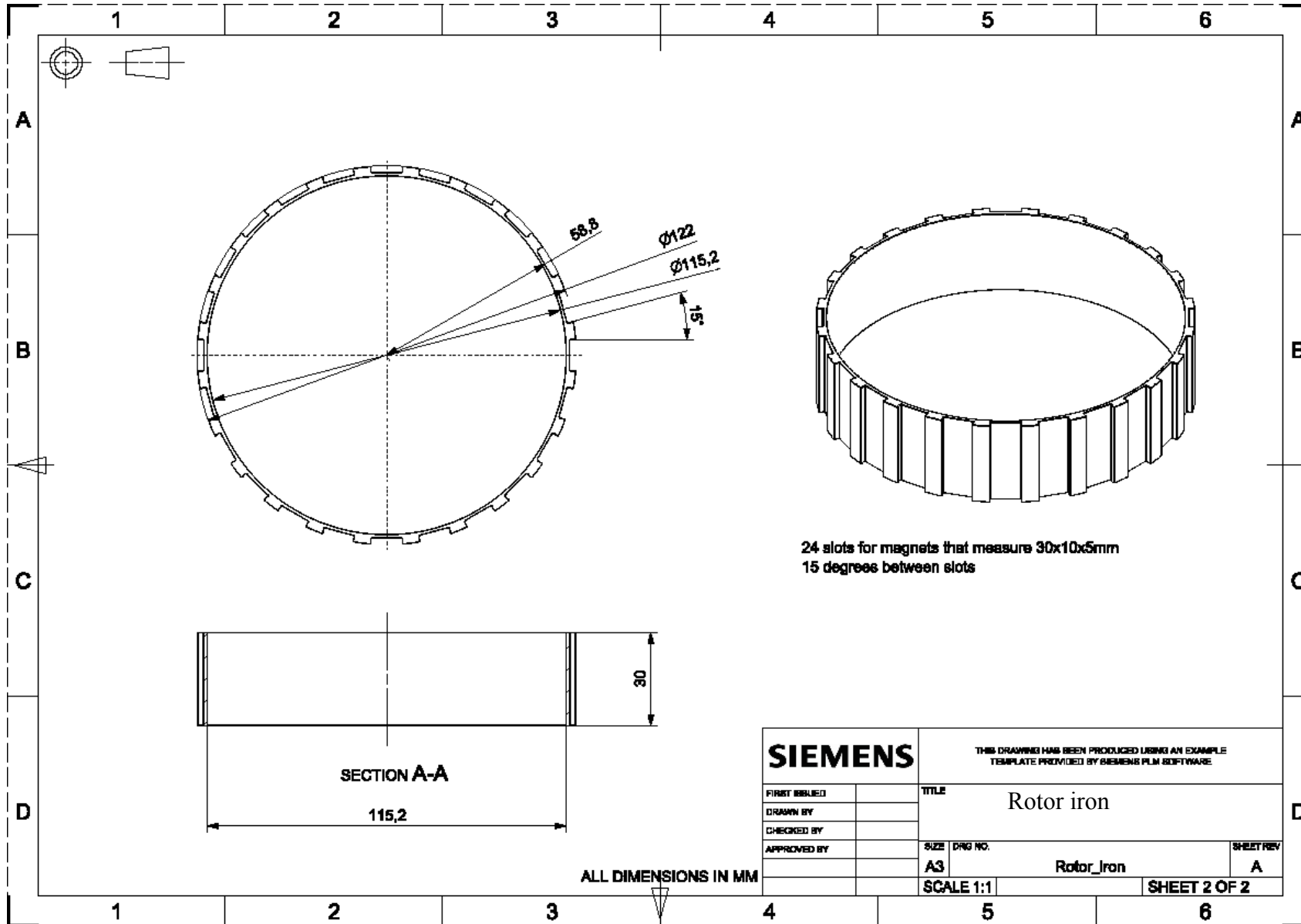
The test rig was made from what materials were available in the workshop, and that is the reason for some of the odd measurements. If for instance the work piece started as 50mm diameter, it was turned down to 49mm in order to ensure a circular cross section.

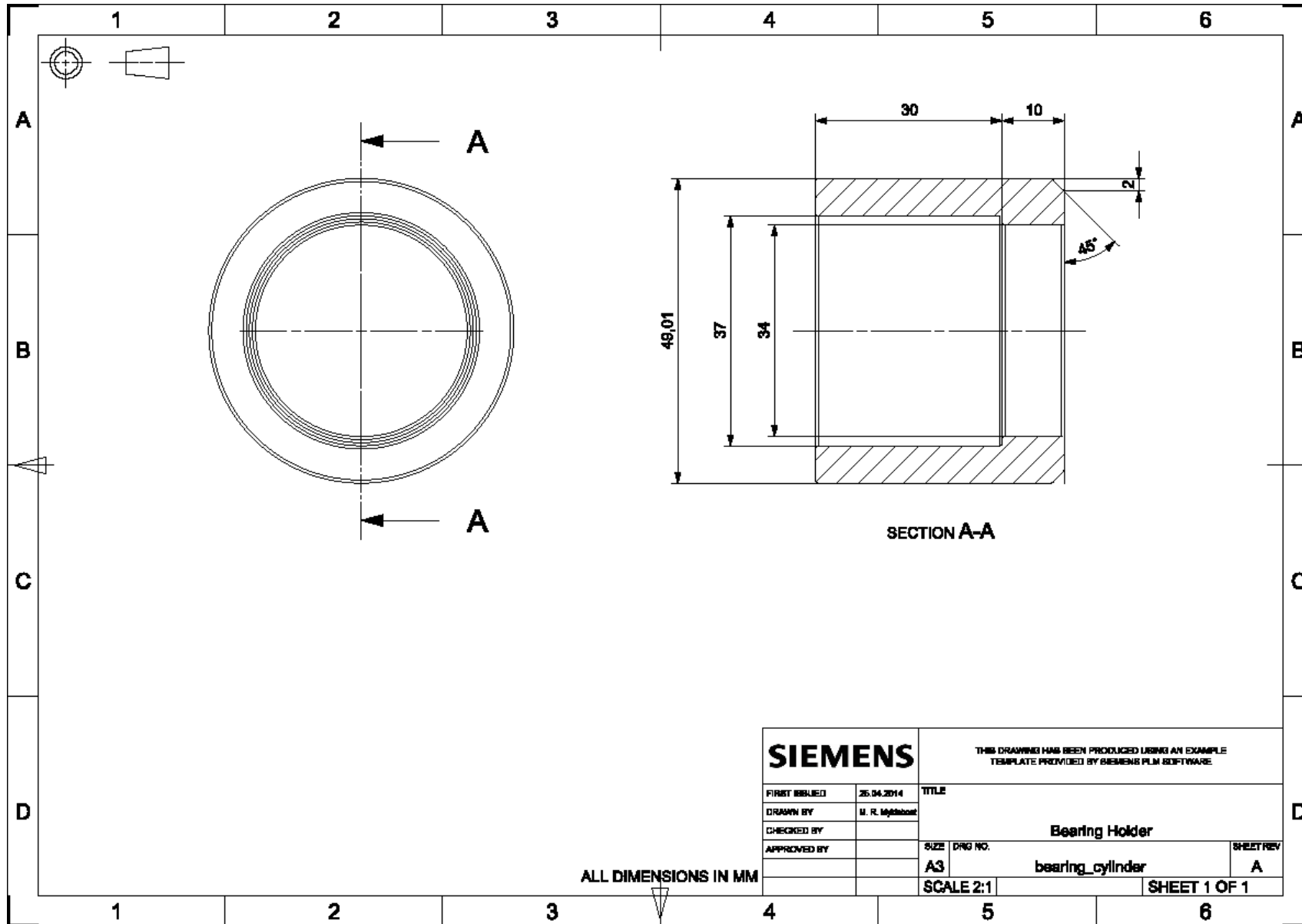
**All machine drawings are originally in A3 format, so the scale is not correct in this report.**





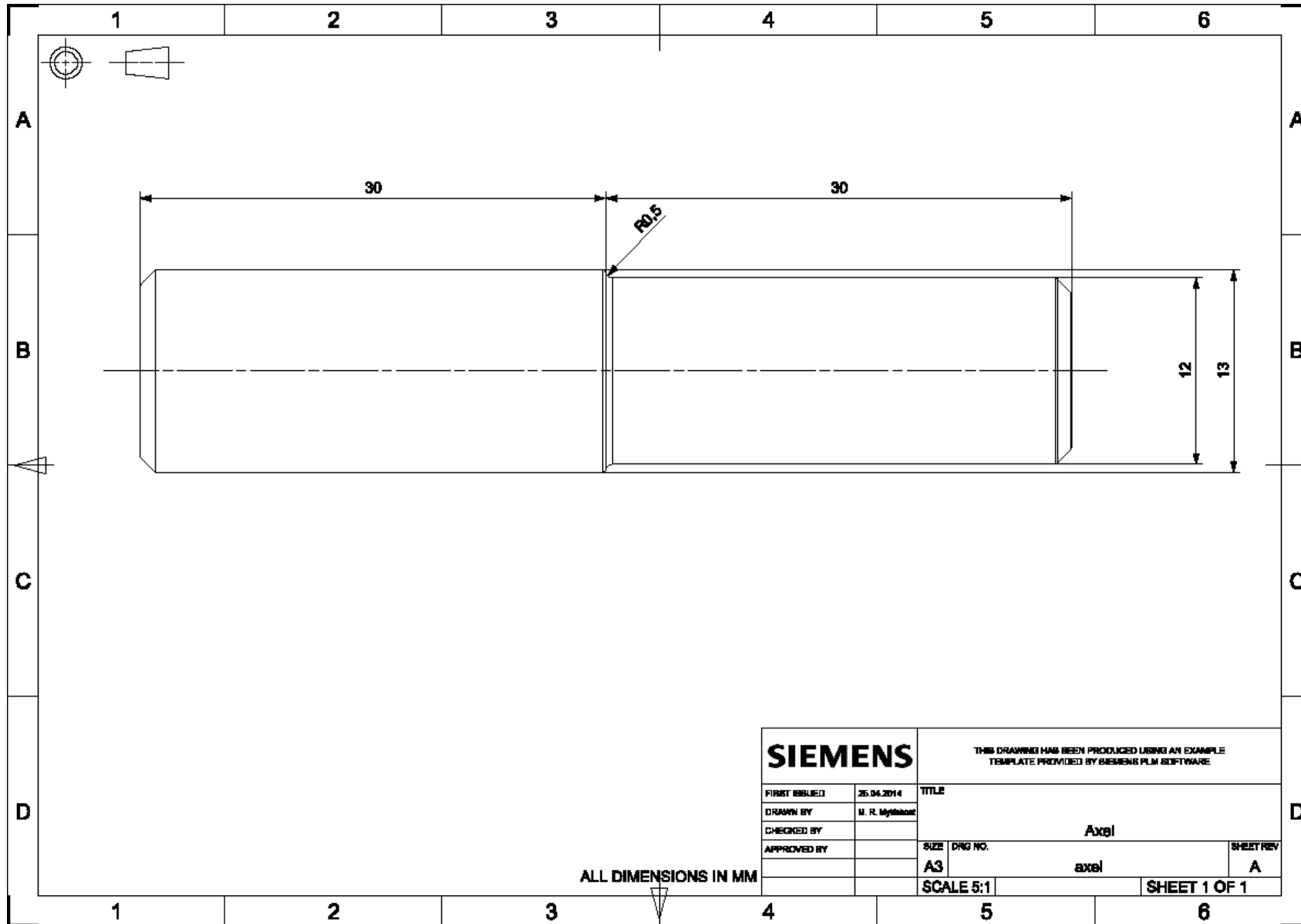


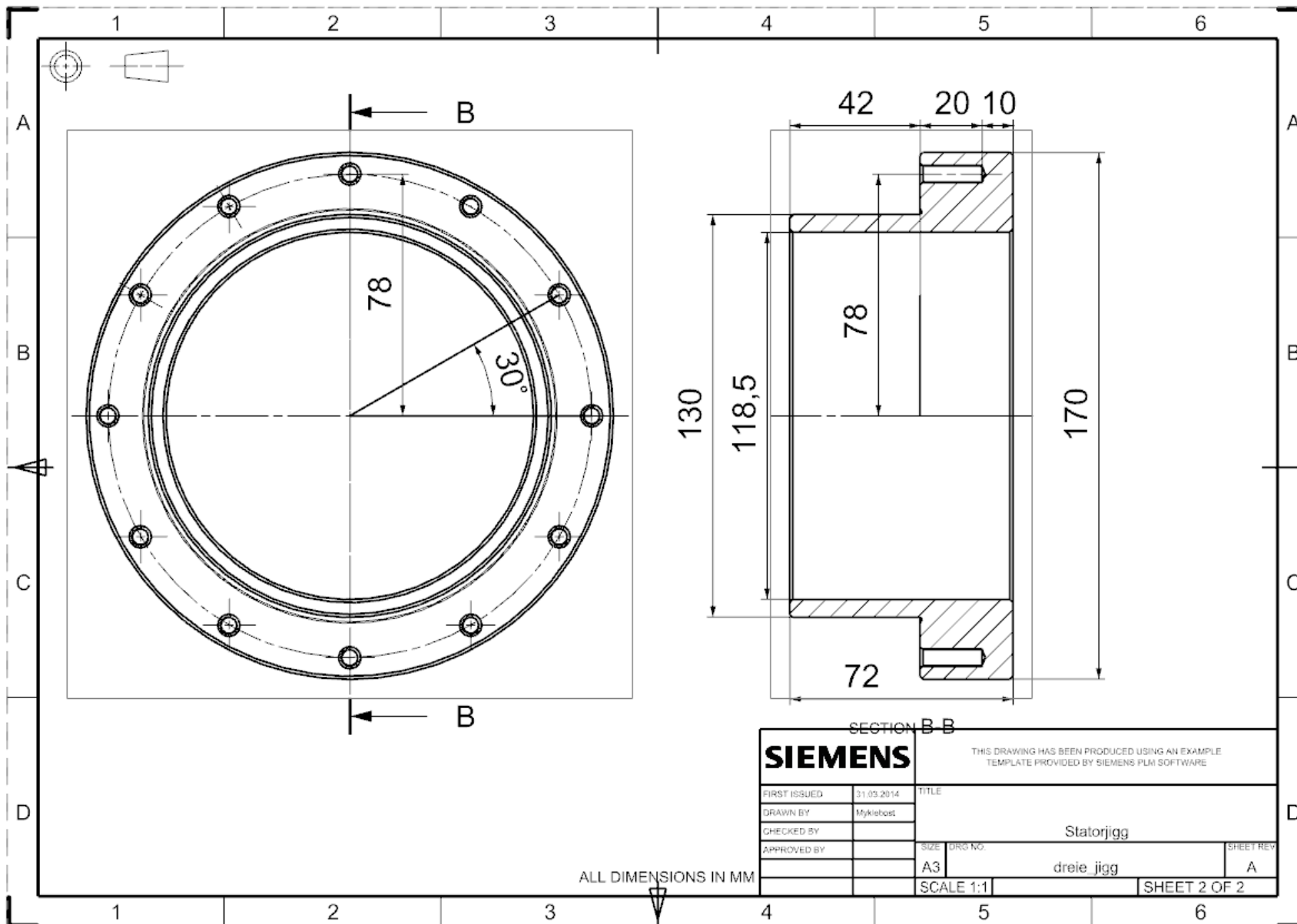




<b>SIEMENS</b>		THIS DRAWING HAS BEEN PRODUCED USING AN EXAMPLE TEMPLATE PROVIDED BY SIEMENS PLM SOFTWARE	
FIRST ISSUED	25.04.2014	TITLE	
DRAWN BY	M. R. M... ..	Bearing Holder	
CHECKED BY		SIZE	DWG NO.
APPROVED BY		A3	bearing_cylinder
		SCALE 2:1	SHEET REV
			A
			SHEET 1 OF 1

ALL DIMENSIONS IN MM

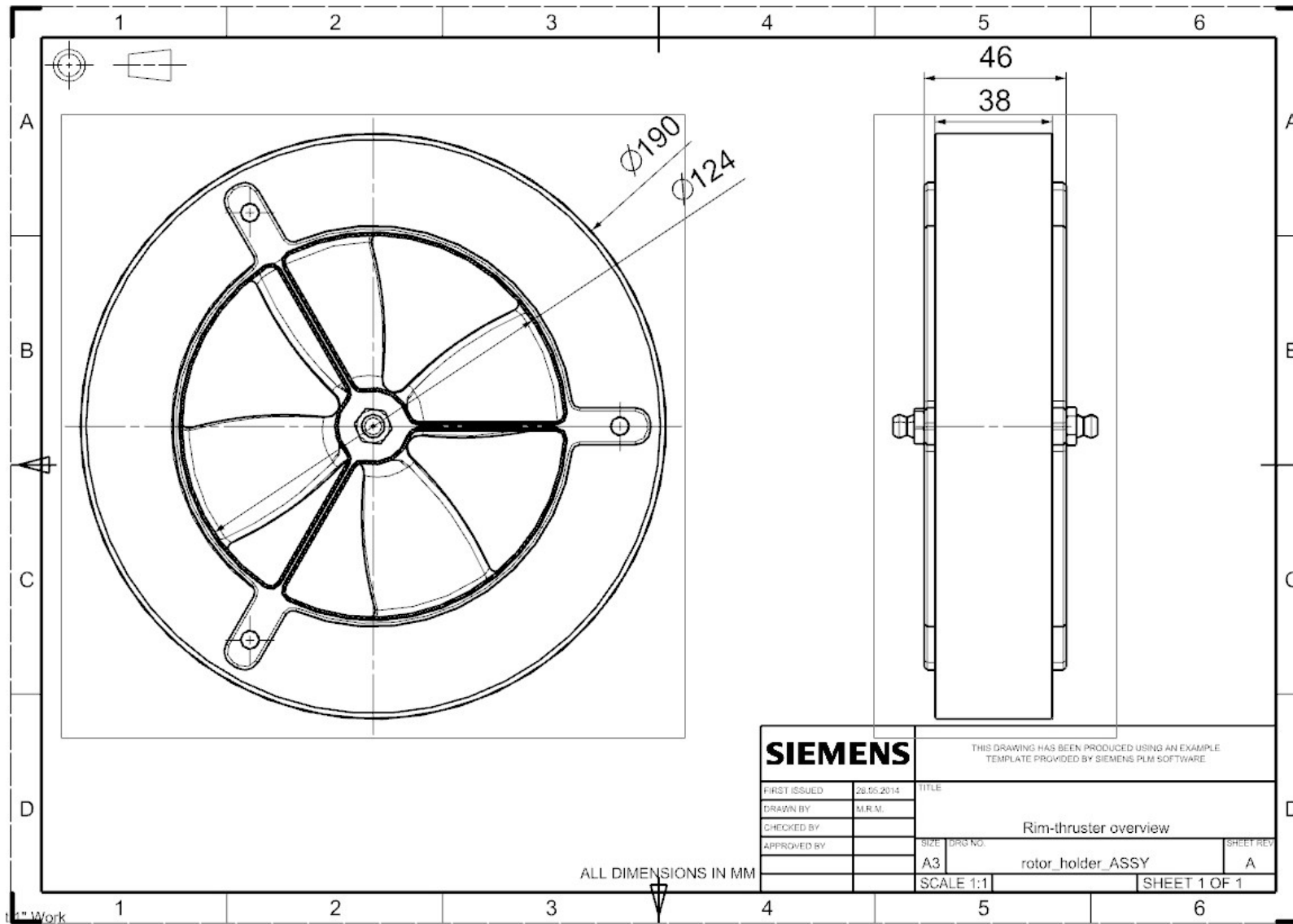


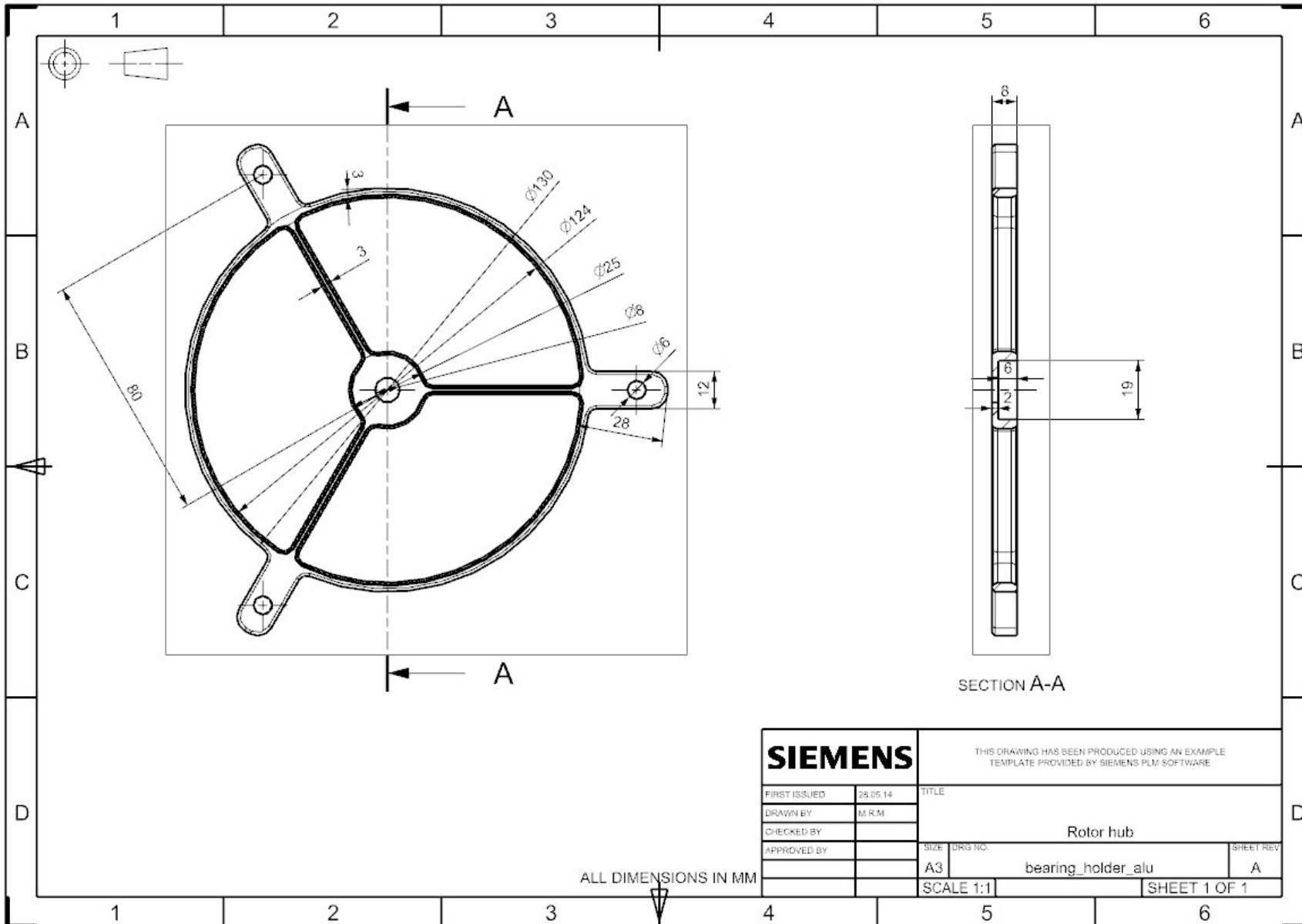


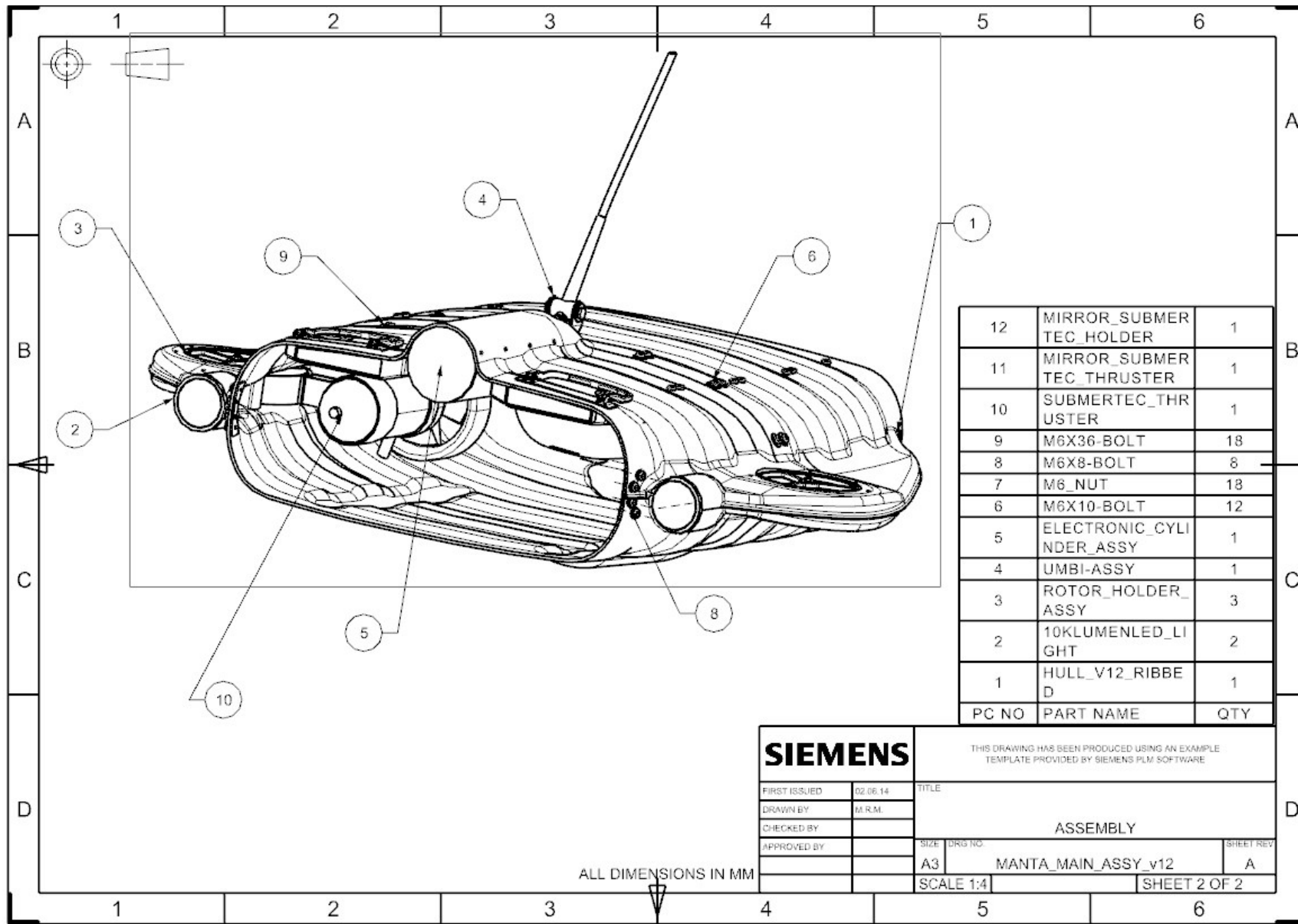
SECTION B-B

<b>SIEMENS</b>		THIS DRAWING HAS BEEN PRODUCED USING AN EXAMPLE TEMPLATE PROVIDED BY SIEMENS PLM SOFTWARE	
FIRST ISSUED	31.05.2014	TITLE	
DRAWN BY	Myklebost	Statorjigg	
CHECKED BY		SIZE	DRG NO.
APPROVED BY		A3	dreie_jigg
ALL DIMENSIONS IN MM		SCALE 1:1	SHEET 2 OF 2

## 23 APPENDIX N: MACHINE DRAWINGS OF COMPONENTS



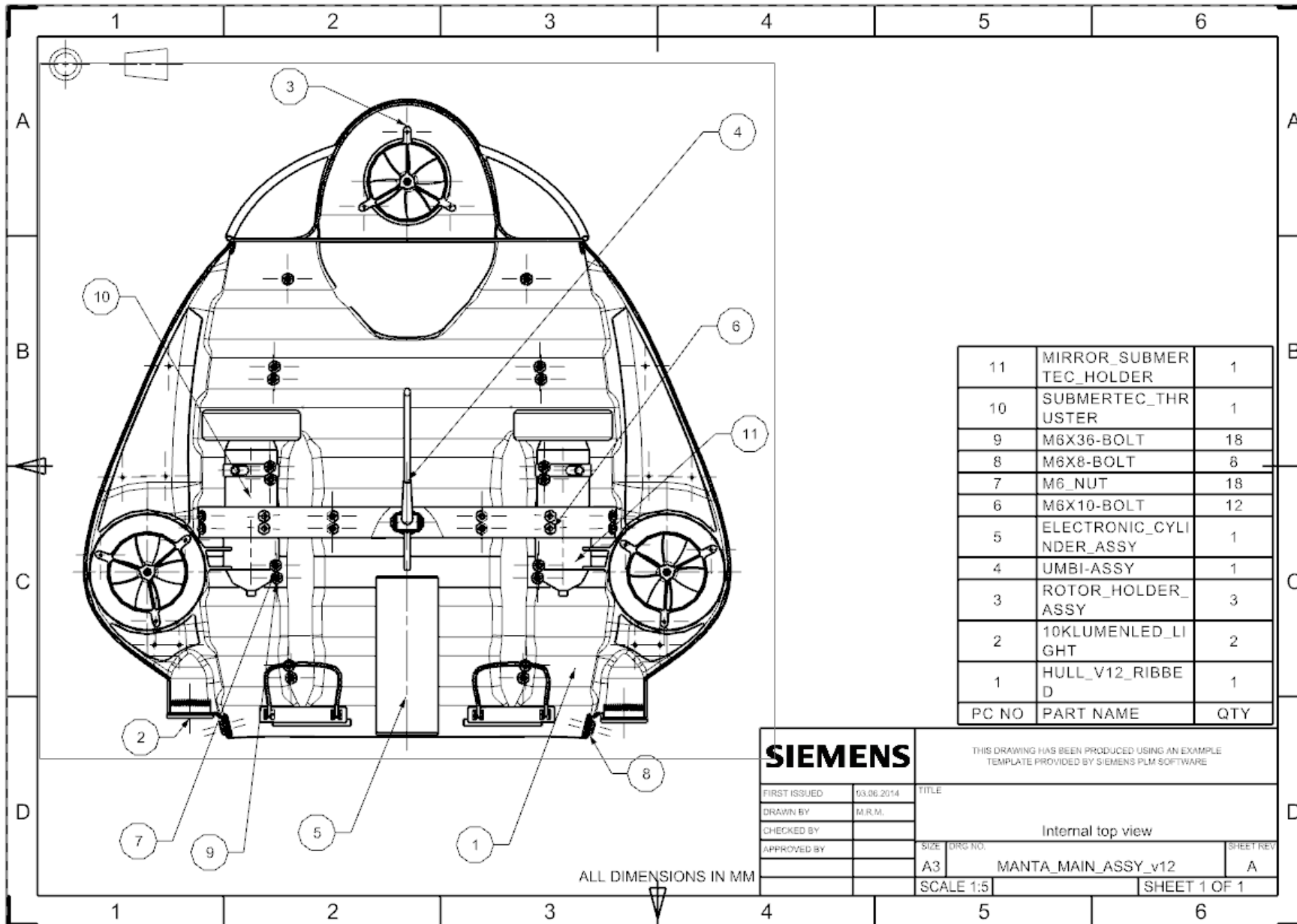


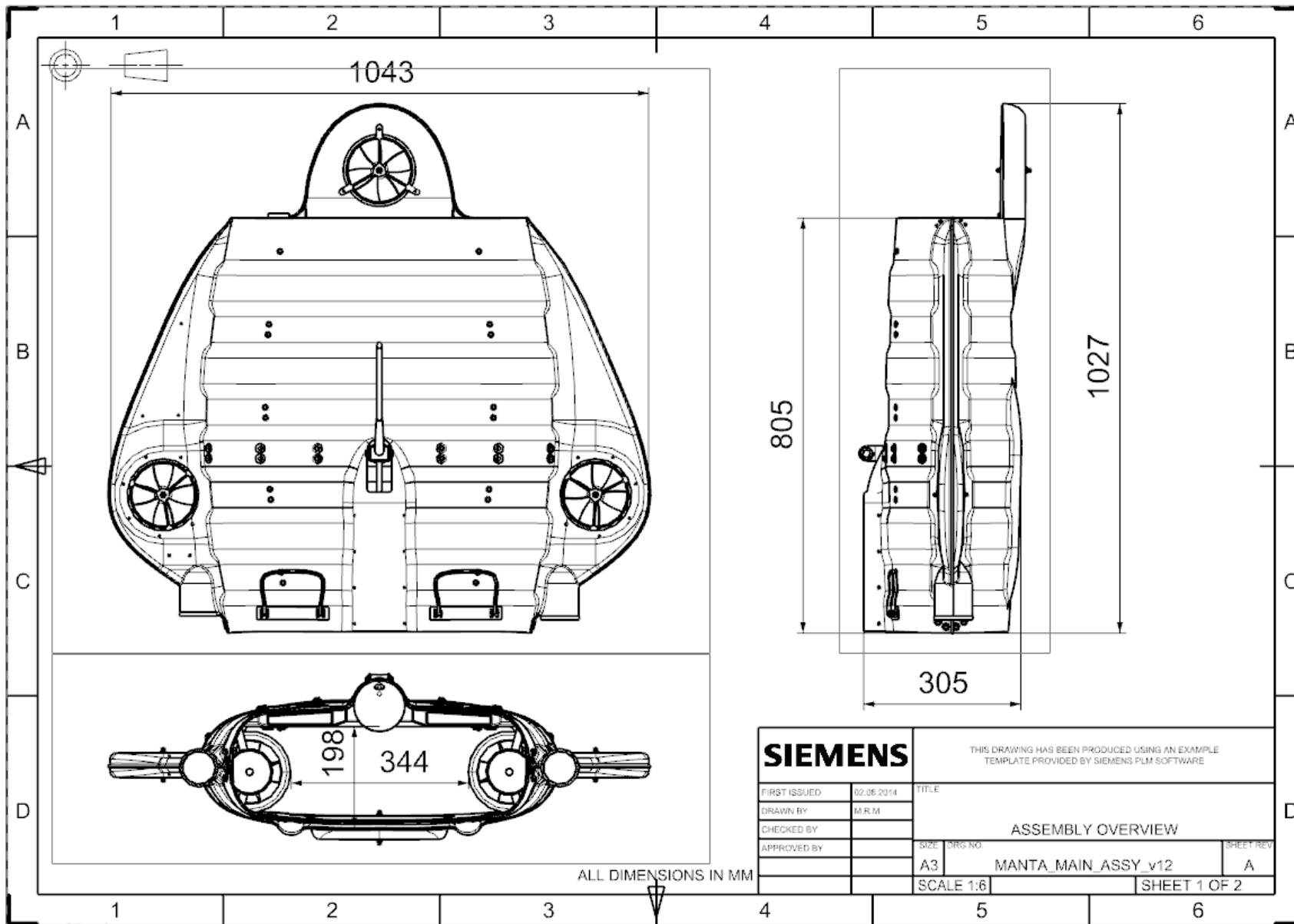


12	MIRROR_SUBMER TEC HOLDER	1
11	MIRROR_SUBMER TEC THRUSTER	1
10	SUBMERTEC_THR USTER	1
9	M6X36-BOLT	18
8	M6X8-BOLT	8
7	M6_NUT	18
6	M6X10-BOLT	12
5	ELECTRONIC_CYLI NDER_ASSY	1
4	UMBI-ASSY	1
3	ROTOR HOLDER_ ASSY	3
2	10KLUMENLED_LI GHT	2
1	HULL_V12_RIBBE D	1
PC NO	PART NAME	QTY

<b>SIEMENS</b>		THIS DRAWING HAS BEEN PRODUCED USING AN EXAMPLE TEMPLATE PROVIDED BY SIEMENS PLM SOFTWARE	
FIRST ISSUED	02.06.14	TITLE	
DRAWN BY	M.R.M.	ASSEMBLY	
CHECKED BY		SIZE	DRG NO.
APPROVED BY		A3	MANTA_MAIN_ASSY_v12
		SCALE 1:4	SHEET REV A
			SHEET 2 OF 2

ALL DIMENSIONS IN MM





## 24 APPENDIX O: RISK ASSESSMENT SHEET (NORWEGIAN)

NTNU	<b>Kartlegging av risikofylt aktivitet</b>	Utarbeidet av	Nummer	Dato	
		HMS-avd.	HMSRV2601	22.03.2011	
HMS		Godkjent av	Side	Erstatter	
		Rektor		01.12.2006	

Enhet: IPM Dato: 31.01.2014

Linjeleder: \_\_\_\_\_

Deltakere ved kartleggingen (m/ funksjon):

(Ansv. veileder, student, evt. medveiledere, evt. andre m. kompetanse)

Nils Petter Vedvik og Magnus Rogne Myklebost

Kort beskrivelse av hovedaktivitet/hovedprosess:

Masteroppgave student Magnus Rogne Myklebost. DEVELOPMENT OF ROV

Er oppgaven er rent teoretisk? (JA/NEI)

Nei

"JA" betyr at veileder Innestår for at oppgaven ikke inneholder noen aktiviteter som krever risikovurdering.

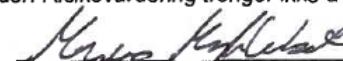
Dersom "JA": Beskriv kort aktiviteten i kartleggingskjemaet under. Risikovurdering trenger ikke å fylles ut.

Signaturer:

Ansvarlig veileder:



Student:



ID nr.	Aktivitet/prosess	Ansvarlig	Eksisterende dokumentasjon	Eksisterende sikringstiltak	Lov, forskrift o.l.	Kommentar
1	Maskinering i IPM verksted	MRM	HMS-runde	IPMs interne HMS prosedyrer	Arbeidsmiljøloven, Arbeidsplassforskriften, Forskrift om utførelse av arbeid, Forskrift om tiltaks- og grenseverdier	Alle deltagere gjør seg kjent med gjeldene HMS prosedyrer, lover og forskrifter
2	Funksjonstest av prototype	MRM	Argus interne HMS dokumentasjon	Argus interne HMS prosedyrer	Arbeidsmiljøloven, Arbeidsplassforskriften, Forskrift om utførelse av arbeid, Forskrift om tiltaks- og grenseverdier	Alle deltagere gjør seg kjent med gjeldene HMS prosedyrer, lover og forskrifter
3	Sammenstilling av prototype	MRM	Argus interne HMS dokumentasjon	Argus interne HMS prosedyrer	Arbeidsmiljøloven, Arbeidsplassforskriften, Forskrift om utførelse av arbeid, Forskrift om tiltaks- og grenseverdier	Alle deltagere gjør seg kjent med gjeldene HMS prosedyrer, lover og forskrifter

NTNU	<b>Risikovurdering</b>	Utarbeidet av	Nummer	Dato	
		HMS-avd.	HMSRV2603	04.02.2011	
HMS /KS		Godkjent av	Side	Erstatter	
		Rektor		09.02.2010	

ID nr.	Aktivitet/prosess fra kartleggingskjemaet	Mulig uønsket hendelse	Vurdering av sannsynlighet (1-5)	Vurdering av konsekvens				Risiko-verdi (menneske)	Kommentarer/ status Forslag til tiltak
				Menneske (A-E)	Ytre miljø (A-E)	Øk./ materiell (A-E)	Om-dømme (A-E)		
1a	Arbeid i verksted i forbindelse med funksjonstest	Kuttskader	2	D	A	B	B	D2	Grundig opplæring og gjennomgang av faremomenter ved bruk av maskiner
1b	Arbeid i verksted i forbindelse med motorprototyping	Elektrisk skade	2	C	A	B	B	C2	Grundig opplæring og gjennomgang av faremomenter ved bruk av maskiner
2a	Arbeid i verksted i forbindelse med maskinering / produksjon	Alvorlige kuttskader, avrivningsskader og knusskader	2	E	A	B	B	E2	Grundig opplæring og gjennomgang av faremomenter ved bruk av maskiner
2b	Arbeid i verksted i forbindelse med maskinering / produksjon	Øyeskader fra metallspen o.l	3	D	A	A	B	D3	Bruk av vernebriller
2c	Arbeid i verksted i forbindelse med maskinering / produksjon	Små kutt- eller brannskader	3	B	A	B	B	B3	Grundig opplæring og gjennomgang av faremomenter ved bruk av maskiner
3a	Arbeid i verksted i forbindelse med bygging av prototype	Kuttskader, avrivningsskader og knusskader	3	D	A	B	B	D3	Grundig opplæring og gjennomgang av faremomenter ved bruk av maskiner
3b	Arbeid i verksted i forbindelse med bygging av funksjonsmodell	Elektrisk skade	2	C	A	B	B	C2	Grundig opplæring og gjennomgang av faremomenter ved bruk av maskiner

